STRINGQFT

String-Theoretic Construction
of Quantum Field Theory

VOLUME XIII

M-Theory Geometric Engineering

Xingyang Yu

StringQFT v1.0 / Source build candidate

Drafted with AI assistance under the supervision of the author.
Manuscript free to read. All rights reserved.

Contents

XIII.1 Seven-dimensional gauge theory from ALE **1**
XIII.1.1 Photons and the missing charged vectors . . . 1
XIII.1.2 Gauge fields that stay near the singularity . . . 1
XIII.1.3 Electric charges of the wrapped membranes . . . 4
XIII.1.4 Mass from calibrated area . . . 5
XIII.1.5 The seven-dimensional vector multiplet . . . 8
XIII.1.6 The gauge coupling and the Planck scale . . . 10
XIII.1.7 An external circle and the IIA description . . . 12
XIII.1.8 Exercises . . . 16

XIII.2 Curves, surfaces, and the 5D prepotential **19**
XIII.2.1 A particle and a string ask for different volumes . . . 19
XIII.2.2 What a triple-intersection tensor can measure . . . 20
XIII.2.3 The compact cube from adjunction . . . 22
XIII.2.4 A positive Kähler class and a signed divisor coordinate . . . 24
XIII.2.5 The cubic, effective metric, and magnetic string . . . 26
XIII.2.6 Changing a background while watching the chamber . . . 28
XIII.2.7 Can the observables reconstruct the two curve periods? . . . 32
XIII.2.8 What changes with a divisor basis? . . . 33
XIII.2.9 Exercises . . . 35
Status and sources . . . 37

XIII.3 Matter and masses from blown-up surfaces **39**
XIII.3.1 Adding matter without adding a gauge scalar . . . 39
XIII.3.2 A ruled surface with one split fiber . . . 39
XIII.3.3 Coulomb charge and real mass . . . 42
XIII.3.4 The massive cubic from curves and weights . . . 44
XIII.3.5 Crossing a matter wall . . . 47
XIII.3.6 Decoupling a heavy flavor . . . 51
XIII.3.7 Exercises . . . 53

XIII.4 Flops, thresholds, and gauge-theory chambers **57**
XIII.4.1 A charged particle reaches zero mass . . . 57
XIII.4.2 The curve at the wall . . . 57
XIII.4.3 How triple intersections change . . . 60

XIII.4.4 The hypermultiplet threshold . . . 63
XIII.4.5 Five Kähler chambers . . . 65
XIII.4.6 Flop or end of a chamber? . . . 71
XIII.4.7 Exercises . . . 75

XIII.5 Rank-one SCFT limits and their counterexamples 78
XIII.5.1 What shrinks at strong coupling? . . . 78
XIII.5.2 The three tests along a contraction path . . . 78
XIII.5.3 The local projective plane and the E0 limit . . . 81
XIII.5.4 Two ruled surfaces with the same prepotential . . . 83
XIII.5.5 What distinguishes the two pure gauge theories? . . . 87
XIII.5.6 Positive metric, forbidden period . . . 89
XIII.5.7 Exercises . . . 93

XIII.6 Several compact surfaces and the canonical-singularity program 97
XIII.6.1 Two surfaces and a shared curve . . . 97
XIII.6.2 The fan and its compact curves . . . 98
XIII.6.3 The common section and the intersection tensor . . . 100
XIII.6.4 The signed cubic and the gauge chamber . . . 102
XIII.6.5 Curve positivity and the point contraction . . . 104
XIII.6.6 Crossing the flop wall . . . 107
XIII.6.7 What a canonical singularity can add . . . 109
XIII.6.8 Exercises . . . 111

XIII.7 Flavor data from the noncompact geometry 114
XIII.7.1 One modulus and six masses . . . 114
XIII.7.2 Compact support and boundary periods . . . 115
XIII.7.3 The lattice orthogonal to the canonical class . . . 117
XIII.7.4 A weak gauge frame for the six masses . . . 119
XIII.7.5 A zero root period and a shrinking curve . . . 124
XIII.7.6 The currents missing at weak coupling . . . 128
XIII.7.7 What the root lattice leaves undetermined . . . 130
XIII.7.8 Exercises . . . 132

XIII.8 Wrapped particles, partition functions, and the IIA circle limit 136
XIII.8.1 What changes when the circle shrinks? . . . 136
XIII.8.2 Wrapped particles and circle parameters . . . 136
XIII.8.3 One box in the square vertex . . . 140
XIII.8.4 The two fixed points on the gauge side . . . 144
XIII.8.5 From four finite factors to the SW term . . . 147
XIII.8.6 What the index remembers . . . 151
XIII.8.7 Exercises . . . 153

XIII.9 Five-dimensional fixed points and six-dimensional KK origins 157
XIII.9.1 A circle introduces a scale . . . 157
XIII.9.2 A pencil whose fibers are elliptic . . . 157

XIII.9.3 The period that measures the KK gap . . . 161
XIII.9.4 The flop moves the exceptional curve . . . 163
XIII.9.5 A limit that leaves the daughter at finite scale . . . 166
XIII.9.6 Which parameters survive? . . . 170
XIII.9.7 The same threefold on external circles . . . 172
XIII.9.8 Exercises . . . 173

XIII.10 Frozen singularities and discrete background data 177
XIII.10.1 Returning to the ALE singularity . . . 177
XIII.10.2 Measuring the three-form on the link . . . 177
XIII.10.3 Gauge algebra and allowed deformations . . . 179
XIII.10.4 From a link period to a circle identification . . . 182
XIII.10.5 Two different lifts over the same type IV fiber . . . 185
XIII.10.6 The same monodromy with two orientifold signs . . . 188
XIII.10.7 Exercises . . . 190

XIII.11 Atlas of M-theory engineering backgrounds 193
XIII.11.1 What an atlas entry specifies . . . 193
XIII.11.2 Equal cubics on different ruled surfaces . . . 194
XIII.11.3 A flop followed by a mass flow . . . 196
XIII.11.4 A KK scale and a five-dimensional point . . . 198
XIII.11.5 A protected coefficient on an external circle . . . 201
XIII.11.6 A frozen phase needs a background . . . 203
XIII.11.7 What the other ordinary lattices measure . . . 205
XIII.11.8 Read the entries with their relations . . . 209
XIII.11.9 Exercises . . . 211

Chapter XIII.1

Seven-dimensional gauge theory from ALE

XIII.1.1 Photons and the missing charged vectors

Resolve an A_2 surface singularity and two compact spheres appear. The eleven-dimensional three-form can put two of its indices on either sphere and leave a vector in the seven extended dimensions. This accounts for two photons. At the singularity, however, the gauge algebra is $\mathfrak{su}(3)$. Where are its six charged vectors on the resolved side? They are particles made from membranes wrapped on oriented two-cycles. As the cycles shrink, these particles become light enough that the photon description must be enlarged.

We work on the unwarped product of seven-dimensional Minkowski space and a complete hyperkähler ALE space X, with an end asymptotic to $\mathbb{R}^4/\Gamma$, $\Gamma \subset SU(2)$. Set the background four-form flux to zero and use trivial C-field holonomy on the link S^3/Γ of the singularity. This choice of background allows the ordinary ADE enhancement; the dynamical three-form still fluctuates. Some ADE singularities admit other supersymmetric link data, as Chapter 10 explains. We use the surface geometry from Volume IV and recall the relevant form reduction and membrane action as they enter. An external circle at the end of the chapter will let us compare this sector with the six-dimensional type IIA gauge theory.

XIII.1.2 Gauge fields that stay near the singularity

Which internal profiles give a seven-dimensional field with finite kinetic energy? The answer depends on the norm of the profile over the *whole* surface, including its noncompact end. Let E_1, E_2 be the ordered exceptional spheres on the complex resolution of A_2. Each has self-intersection -2; they meet once, with positive complex intersection

sign. Their matrix Q is the negative of the Cartan matrix C:

$$Q_{ij} = E_i \cdot E_j, \qquad Q = \begin{pmatrix} -2 & 1 \\ 1 & -2 \end{pmatrix}, \qquad C = -Q. \tag{XIII.1.1}$$

A two-form ω_i of unit period on E_i and zero period on the other sphere will measure the coefficient of E_i in an oriented cycle. To find its norm, start from the compactly supported Poincaré duals ξ_i, which have periods given by intersections:

$$\int_{E_j} \xi_i = Q_{ij}, \qquad \int_X \xi_i \wedge \xi_j = Q_{ij}. \tag{XIII.1.2}$$

In particular, ξ_1 does not have unit period on E_1. The classes of the unit-period forms are obtained by inverting Q:

$$[\omega_i] = (Q^{-1})_{ij}[\xi_j], \qquad \int_{E_j} \omega_i = \delta_{ij}. \tag{XIII.1.3}$$

Here and below repeated cycle indices are summed.

For this example the inversion can be done before using any Hodge theory. Multiplying the two matrices gives

$$Q^{-1} = -\frac{1}{3}\begin{pmatrix} 2 & 1 \\ 1 & 2 \end{pmatrix}, \qquad [\omega_1] = -\frac{2[\xi_1] + [\xi_2]}{3}, \qquad [\omega_2] = -\frac{[\xi_1] + 2[\xi_2]}{3}. \tag{XIII.1.4}$$

For example, the first of these classes has periods

$$\int_{E_1} \omega_1 = -\frac{2(-2)+1}{3} = 1, \qquad \int_{E_2} \omega_1 = -\frac{2(1)-2}{3} = 0. \tag{XIII.1.5}$$

The fractions belong to the change of cohomology basis. A membrane on E_1 still has an integral wrapping number. We are choosing forms that measure that number, rather than declaring a fractional membrane. The compactly supported representatives ξ_i are useful for computing the intersection pairing; the kinetic calculation needs their harmonic representatives, which need not have compact support.

The L^2 Hodge result for a complete ALE metric identifies the square-integrable harmonic two-forms with the real image of compactly supported cohomology in ordinary cohomology, with the inherited middle-degree pairing. Since Q is nondegenerate this image is the full real two-dimensional space here. This identification does not say that the integral map is an isomorphism: its index for A_2 is $|\det Q| = 3$. Its real version is what we need to choose the harmonic representatives in (XIII.1.3). The pairing is negative definite. A nonzero self-dual L^2 harmonic form would have positive wedge square, so the harmonic forms in this space are anti-self-dual. Consequently their kinetic pairing is positive:

$$\begin{gathered} *_4 \omega_i = -\omega_i, \\ G_{ij} := \int_X \omega_i \wedge *_4 \omega_j = -(Q^{-1} Q Q^{-1})_{ij} = \frac{1}{3}\begin{pmatrix} 2 & 1 \\ 1 & 2 \end{pmatrix}_{ij}. \end{gathered} \tag{XIII.1.6}$$

The symmetric and antisymmetric combinations have norms determined by eigenvalues 1 and 1/3, respectively, when their coefficient vectors have Euclidean norm one. Thus the two fields are independent and both have a positive kinetic term.

It is useful to test positivity for an arbitrary real coefficient vector $f = (f_1, f_2)^T$, not only for a form in the chosen basis. The norm is

$$\|f_i\omega_i\|_{L^2}^2 = \frac{2}{3}(f_1^2 + f_1 f_2 + f_2^2) = \frac{1}{2}(f_1 + f_2)^2 + \frac{1}{6}(f_1 - f_2)^2. \tag{XIII.1.7}$$

Thus the apparent mixing in G is ordinary kinetic mixing between finite-norm profiles. The modes $(\omega_1 + \omega_2)/\sqrt{2}$ and $(\omega_1 - \omega_2)/\sqrt{2}$ diagonalize it. They are convenient for measuring norms, whereas unit-period forms are convenient for measuring integral wrapped-cycle charges. Diagonalizing a positive quadratic form is not the same operation as choosing an integral charge basis.

Write $T = T_{\mathrm{M2}}$ for the minimal membrane tension and normalize the three-form by $\widehat{C}_3 = TC_3$. The positive membrane coupling is then $+\int \widehat{C}_3$. With A^i one-forms in the extended directions, the relevant linearized terms are

$$\widehat{C}_3 = A^i \wedge \omega_i + \cdots, \qquad \mathrm{d}\widehat{C}_3 = F^i \wedge \omega_i + \cdots, \qquad F^i = \mathrm{d}A^i. \tag{XIII.1.8}$$

The second identity uses $\mathrm{d}\omega_i = 0$. In particular a shift $A^i \mapsto A^i + \mathrm{d}\lambda^i$ descends from the three-form gauge symmetry. Integration over X multiplies the seven-dimensional kinetic term by the finite matrix G.

Contrast these profiles with a constant internal wavefunction. Writing ρ for the four-dimensional radial distance on the end, its norm contains

$$\int_{\rho_0}^{\infty} \rho^3 \,\mathrm{d}\rho = \lim_{\rho_1 \to \infty} \frac{\rho_1^4 - \rho_0^4}{4} = \infty. \tag{XIII.1.9}$$

The constant profile for the graviton, or for a three-form with only external legs, therefore gives no localized seven-dimensional zero mode. There are still bulk waves; finite norm selects the localized photons without discarding the bulk continuum. The same finite profiles that enter the kinetic term also determine how a membrane couples to each photon, as Fig. XIII.1.1 illustrates.

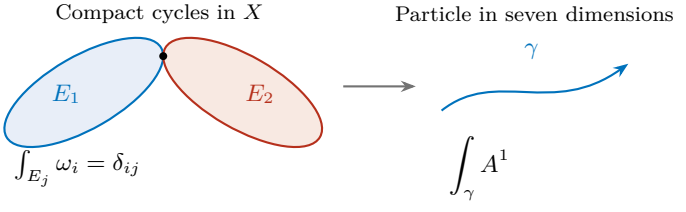


Figure XIII.1.1: The exceptional A_2 spheres and the two periods that select the photons. A membrane worldvolume $\gamma \times E_1$ has an external worldline γ and couples to A^1. The sphere drawing shows their intersection, not the pointwise support of the harmonic two-forms.

XIII.1.3 Electric charges of the wrapped membranes

Which integer charges can supply the missing vectors? First measure a charge without assuming the enhanced algebra. For the class $E_q = q_i E_i$, orient the membrane worldvolume as the external worldline γ followed by the internal surface. Then its Wess–Zumino coupling factors:

$$\int_{\gamma\times E_q} \widehat{C}_3 = \int_\gamma A^i \int_{E_q} \omega_i = \int_\gamma q_i A^i. \tag{XIII.1.10}$$

The two coefficients q_i are the electric charges in the unit-period basis used in Fig. XIII.1.1. Reversing the internal orientation reverses both charges.

The positive inner product on compact classes is minus their intersection pairing. Identify the classes of E_1, E_2 with the simple roots $\alpha_1 = e_1 - e_2, \alpha_2 = e_2 - e_3$, where e_i are orthonormal vectors in $\mathbb{R}^3$. The norm of a general class then satisfies

$$\begin{aligned} |q_1\alpha_1 + q_2\alpha_2|^2 &= q^T C q = 2(q_1^2 - q_1 q_2 + q_2^2), \\ 4(q_1^2 - q_1 q_2 + q_2^2) &= (2q_1 - q_2)^2 + 3q_2^2. \end{aligned} \tag{XIII.1.11}$$

For a root, the left side of the second line is 4, so $q_2 = -1, 0, 1$. For $q_2 = 0$, $q_1 = \pm 1$. For $q_2 = 1$, $(2q_1 - 1)^2 = 1$ gives $q_1 = 0, 1$, and the negative of this pair gives the last two solutions. The six charges can also be read off directly in the ambient coordinates:

$$q_1\alpha_1 + q_2\alpha_2 = (q_1, q_2 - q_1, -q_2). \tag{XIII.1.12}$$

An integer triple of sum zero and length squared two must have one entry $+1$ and one entry -1.

This length condition filters a lattice of possible oriented wrapping classes down to the root classes relevant to ordinary enhancement. For example, the class $E_1 - E_2$ has integral charges but gives

$$(1, -1) C \begin{pmatrix} 1 \\ -1 \end{pmatrix} = 6, \qquad \alpha_1 - \alpha_2 = (1, -2, 1). \tag{XIII.1.13}$$

It therefore cannot supply another length-two root of this algebra. The Wess–Zumino coupling measures a charge for any oriented wrapping class; the root condition and the existence of the appropriate light multiplet are additional statements. In particular, an integral charge vector alone does not identify a new gauge generator.

A second basis is often useful. If the diagonal gauge generators are the simple coroots $h_1 = \mathrm{diag}(1, -1, 0)$ and $h_2 = \mathrm{diag}(0, 1, -1)$, the charge entries are the root pairings with those coroots. For example, the 12 entry measures the first diagonal entry minus the second: these differences are 2 for h_1 and -1 for h_2. For the general charge, the same differences give

$$(q_1\alpha_1 + q_2\alpha_2)(h_j) = q_i C_{ij} = (Cq)_j. \tag{XIII.1.14}$$

The change of charge coordinates has a corresponding change of gauge fields. Denote by a^j the photons multiplying h_j. Requiring that the same charged worldline have the same coupling in either description fixes

$$A^i = C_{ij} a^j, \qquad q_i A^i = (Cq)_j a^j, \qquad F^i = C_{ij} f^j, \quad f^j = \mathrm{d}a^j. \tag{XIII.1.15}$$

For a membrane on E_1, for instance, $\int A^1 = \int (2a^1 - a^2)$. This explains why its coroot charges are $(2, -1)$ while its two wrapping coefficients are $(1, 0)$. Changing just the charge entries and leaving the fields fixed would change the physical source coupling.

The two columns of the table describe the same charge, measured by different gauge fields.

Oriented class	Charge q	Coroot charge Cq	Root generator
E_1	$(1, 0)$	$(2, -1)$	e_{12}
E_2	$(0, 1)$	$(-1, 2)$	e_{23}
$E_1 + E_2$	$(1, 1)$	$(1, 1)$	e_{13}
$-E_1$	$(-1, 0)$	$(-2, 1)$	e_{21}
$-E_2$	$(0, -1)$	$(1, -2)$	e_{32}
$-E_1 - E_2$	$(-1, -1)$	$(-1, -1)$	e_{31}

The e_{ij} here are matrix units in the complexified algebra. They make the sum of root charges visible in the commutator:

$$[e_{12}, e_{23}] = e_{13}, \qquad [e_{12}, e_{21}] = \operatorname{diag}(1, -1, 0). \tag{XIII.1.16}$$

The first bracket adds charges and the second returns a Cartan generator. This is an algebraic statement. It does not show that a sum of membrane classes contains an isolated quantum state. To understand when the particles can become light, we next calculate a mass from an actual surface representing a root.

XIII.1.4 Mass from calibrated area

How does the geometry determine the mass of a charged particle? In a static product configuration a membrane wrapped on a smooth surface Σ has a time direction in Minkowski space and two spatial directions tangent to Σ. The induced volume splits into elapsed proper time times physical area. With no external background field acting on the particle, the membrane volume term gives

$$S_{\mathrm{vol}} = -T \int_{\gamma} \mathrm{d}\tau \, \mathcal{A}(\Sigma), \qquad M_{\Sigma} = T\mathcal{A}(\Sigma), \qquad T = \frac{1}{(2\pi)^2 \ell_p^3}. \tag{XIII.1.17}$$

Here ℓ_p is the eleven-dimensional Planck length and $\mathcal{A}$ has units of length squared.

Let $\mathbf{\Omega}$ be the triplet of hyperkähler forms, with $\Omega_3 = J$ on a chosen complex slice. The oriented period vector of the class E_q is

$$\mathbf{P}_q = \int_{E_q} \mathbf{\Omega} = q_1 \mathbf{P}_1 + q_2 \mathbf{P}_2, \qquad \mathbf{m}_q = T\mathbf{P}_q. \tag{XIII.1.18}$$

For each unit $\mathbf{n}$, the form $\mathbf{n} \cdot \mathbf{\Omega}$ is the Kähler form of a rotated complex structure. Its value on an oriented unit tangent plane is at most one, with equality on a positively oriented complex plane in that structure. Integrating and choosing $\mathbf{n}$ along $\mathbf{P}_q$ gives

$$\mathcal{A}(\Sigma) \;\geq\; \mathbf{n} \cdot \mathbf{P}_q, \qquad \mathcal{A}(\Sigma) \;\geq\; |\mathbf{P}_q|. \tag{XIII.1.19}$$

A representative calibrated in that direction gives $M_q = |\mathbf{m}_q|$ in the smooth wrapped-brane calculation. The vector periods add with orientation; their norms need not add.

We can see the representative explicitly in the cyclic Gibbons–Hawking description. Take distinct centers $\mathbf{x}_a$ and no constant term in the harmonic function. The metric and the connection one-form are

$$\begin{aligned} \mathrm{d}s_X^2 &= V\,\mathrm{d}\mathbf{x}^2 + V^{-1}\eta^2, \qquad V = \sum_{a=1}^{3} \frac{1}{2|\mathbf{x}-\mathbf{x}_a|}, \\ \eta &= \mathrm{d}\chi + \mathcal{A}_{\mathrm{GH}}, \qquad \mathrm{d}\eta = -*_3\,\mathrm{d}V, \qquad \chi \sim \chi + 2\pi. \end{aligned} \tag{XIII.1.20}$$

The $\mathbf{x}_a$ have units of length squared, while χ is an angle. The coefficient $1/2$ at a center gives $\int_{S^2} \mathrm{d}\eta = 2\pi$ on a small positively oriented linking sphere in the base, so each center has the unit circle fibration and the circle caps off there. With orientation $\eta \wedge \mathrm{d}x^1 \wedge \mathrm{d}x^2 \wedge \mathrm{d}x^3 > 0$ the three self-dual forms are

$$\Omega_a = \eta \wedge \mathrm{d}x^a + V *_3 \mathrm{d}x^a, \qquad \mathrm{d}\Omega_a = 0. \tag{XIII.1.21}$$

Indeed the two terms in $\mathrm{d}\Omega_a$ cancel by $\mathrm{d}\eta = -*_3\,\mathrm{d}V$. The absence of a constant in V is what gives the ALE end. The χ-circle is internal to X.

Over a path $\mathbf{x}(s)$, pull back η to $\mathrm{d}\chi + a(s)\mathrm{d}s$. In the order (χ, s), the determinant of the induced metric is

$$\det \begin{pmatrix} V^{-1} & V^{-1}a \\ V^{-1}a & V|\dot{\mathbf{x}}|^2 + V^{-1}a^2 \end{pmatrix} = |\dot{\mathbf{x}}|^2. \tag{XIII.1.22}$$

The connection changes the off-diagonal metric but drops out of the area. On a straight segment from i to j with no center in its interior, the circle collapses only at its two endpoints and the lift is a sphere E_{ij}. The base two-form term in (XIII.1.21) vanishes on the lifted path, so its area and oriented period are

$$\mathcal{A}_{ij} = 2\pi|\mathbf{x}_j - \mathbf{x}_i|, \qquad \mathbf{P}_{ij} = 2\pi(\mathbf{x}_j - \mathbf{x}_i). \tag{XIII.1.23}$$

More generally, before choosing a straight path, integrate the square root of (XIII.1.22) over the fiber and path. The result is

$$\mathcal{A}[\mathbf{x}] = 2\pi \int_{s_i}^{s_j} |\dot{\mathbf{x}}(s)|\,\mathrm{d}s, \qquad \int_{E[\mathbf{x}]} \boldsymbol{\Omega} = 2\pi \int_{s_i}^{s_j} \dot{\mathbf{x}}(s)\,\mathrm{d}s = 2\pi(\mathbf{x}_j - \mathbf{x}_i). \tag{XIII.1.24}$$

In the second calculation the pullback of each base two-form to the one-dimensional path vanishes. The remaining term is integrated over the full circle fiber; its period supplies the factor 2π. The two integrals in (XIII.1.24) perform different jobs. The first measures path length and depends on how the path bends. The second measures an oriented period and depends only on its endpoints within this construction. Their comparison gives

$$\int |\dot{\mathbf{x}}|\,\mathrm{d}s \;\geq\; \left| \int \dot{\mathbf{x}}\,\mathrm{d}s \right|, \qquad M[\mathbf{x}] \geq 2\pi T|\mathbf{x}_j - \mathbf{x}_i|. \tag{XIII.1.25}$$

A straight segment traversed in one direction attains this minimum. The condition that no other center lie in its interior ensures that its lift is the smooth sphere used in the membrane calculation. The local cancellation of the connection in the area element does not remove the circle fibration; that fibration is what turns the path into a compact surface.

With fiber-first orientation, the sign of the period points from i to j; reversing the path changes the charge while preserving the mass. Equation (XIII.1.23) saturates the calibration bound with $\mathbf{n}$ along that path.

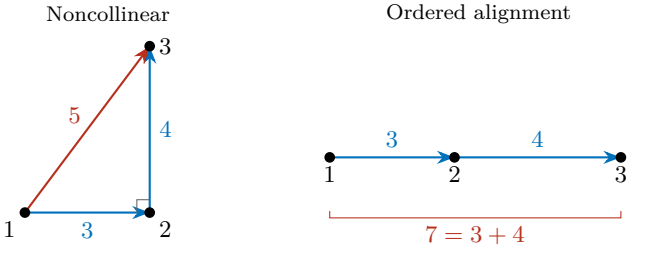


Figure XIII.1.2: Base paths whose circle lifts give the A_2 root cycles. Left: a right triangle with a direct segment for E_{13}. Right: the ordered alignment, where the outer segment passes through center 2 and its lift splits there. Lengths are shown in units of u^2; the circle caps at each dot.

Mark $E_1 = E_{12}$, $E_2 = E_{23}$ using the ordering inherited from the collinear resolution. For three noncollinear centers, the circle over the triangle provides a three-chain with boundary the three lifted edges. Their orientations give $E_{13} = E_{12} + E_{23}$ in homology. Put the centers at $(0,0,0)u^2, (3,0,0)u^2, (3,4,0)u^2$ as in Fig. XIII.1.2. The direct outer segment gives

$$\frac{(M_{12}, M_{23}, M_{13})}{2\pi T u^2} = (3,4,5), \qquad 5 < 3 + 4. \tag{XIII.1.26}$$

The outer membrane has smaller classical mass than two membranes on the adjacent edges. If the adjacent differences are aligned without changing their lengths, the outer period has norm 7 in units $2\pi u^2$. The lift now passes through the middle center and is a union of the two spheres. Equality with the two-particle threshold in this case does not establish an isolated bound state. The way the mass changes on alignment can be computed without choosing a new coordinate system. Write $\mathbf{d}_1 = \mathbf{x}_2 - \mathbf{x}_1$, $\mathbf{d}_2 = \mathbf{x}_3 - \mathbf{x}_2$, and let θ be their angle when both are nonzero. Then

$$\begin{aligned} \left(\frac{M_{13}}{2\pi T}\right)^2 &= |\mathbf{d}_1 + \mathbf{d}_2|^2 \\ &= |\mathbf{d}_1|^2 + |\mathbf{d}_2|^2 + 2|\mathbf{d}_1||\mathbf{d}_2| \cos\theta. \end{aligned} \tag{XIII.1.27}$$

This formula compares the smooth segment representatives where they exist. It also computes the period norm in the aligned limit. For fixed adjacent lengths, the two simple-root masses stay fixed while the outer-root mass changes with the relative

direction of their periods. The scalar expectation values are triplets, so two masses do not fix that direction.

For a second example, change the third center and the first separation so that the centers are

$$(\mathbf{x}_1,\mathbf{x}_2,\mathbf{x}_3)=\big((0,0,0),(2,0,0),(3,2,0)\big)u^2,\qquad (\mathbf{d}_1,\mathbf{d}_2)=\big((2,0,0),(1,2,0)\big)u^2. \tag{XIII.1.28}$$

The adjacent paths now meet at an oblique angle rather than a right angle. Their dot product and mass squares are

$$\cos\theta=\frac{1}{\sqrt{5}},\qquad \frac{(M_{12}^2,M_{23}^2,M_{13}^2)}{(2\pi T u^2)^2}=(4,5,13),\qquad \sqrt{13}<2+\sqrt{5}. \tag{XIII.1.29}$$

The cross term is essential: summing the squared simple-root masses would give 9, and summing their masses before squaring would give $(2+\sqrt{5})^2$. Neither computes the direct segment. If the same adjacent lengths are aligned in their marked order, the outer period instead has length $2\pi(2+\sqrt{5})u^2$. The root charge remains $(1,1)$ throughout this change; it is the geometry of the period vectors that changes the mass.

This distinction will matter when we use the smooth masses as coordinates for the light gauge theory.

XIII.1.5 The seven-dimensional vector multiplet

Why are the charged particles candidates for gauge vectors? The background fixes the amount of supersymmetry and therefore the multiplets of the localized fields. A nonflat hyperkähler ALE space has $SU(2)$ holonomy inside $\mathrm{Spin}(4)=SU(2)\times SU(2)$. The two internal chiral spinor spaces transform as $(\mathbf{2},\mathbf{1})$ and $(\mathbf{1},\mathbf{2})$. If the first factor is the holonomy, it fixes the second space and has no invariant vector in the first. Before imposing reality, the eleven-dimensional spinor decomposes under the product spin group as

$$S_{11}^{\mathbb{C}}=S_7^{\mathbb{C}}\otimes(S_4^+\oplus S_4^-),\qquad \dim_{\mathbb{C}} S_7^{\mathbb{C}}=8,\qquad \dim_{\mathbb{C}}(S_4^+\oplus S_4^-)^{SU(2)}=2. \tag{XIII.1.30}$$

The eleven-dimensional Majorana reality condition gives a real invariant space of dimension $8\cdot 2=16$. No projection from a separately added brane enters this count.

On the resolved side each localized photon has five physical polarizations in seven dimensions. Its three real scalar partners vary the three hyperkähler periods on the corresponding compact cycle. In the cyclic example, fix the frame of the hyperkähler triple at infinity and the common center of mass; then the two independent scalar triplets are proportional to

$$\delta\mathbf{P}_{12}=2\pi(\delta\mathbf{x}_2-\delta\mathbf{x}_1),\qquad \delta\mathbf{P}_{23}=2\pi(\delta\mathbf{x}_3-\delta\mathbf{x}_2),\qquad \sum_i\delta\mathbf{x}_i=0. \tag{XIII.1.31}$$

Both periods would stay fixed only if all three centers moved by the same vector, which the last equation forbids. These are localized variations. For instance, at fixed center of mass the variation of the $1/r$ monopole and the $1/r^2$ dipole of V vanishes, with $r=|\mathbf{x}|$.

The leading δV is of order r^{-3}, so its relative contribution is $O(r^{-2}) = O(\rho^{-4})$ in the ALE radial coordinate. With the corresponding connection variation and smooth charts at the centers, the norm converges at infinity:

$$\int^{\infty} \rho^{3}\big(O(\rho^{-4})\big)^{2}\,\mathrm{d}\rho < \infty. \tag{XIII.1.32}$$

Rotating all the period vectors rotates the fixed frame; it is not a step in the count of local scalar fields. The resulting multiplet has $5 + 3 = 8$ bosonic and eight fermionic on-shell degrees of freedom, as in the reduction of the ten-dimensional supersymmetric gauge multiplet.

For the ordinary background, the protected light wrapped-root multiplets are the charged vectors. The semiclassical area calculation gives their mass dependence on the resolved side; using them at the singularity uses their supersymmetric continuation. The classical membrane action alone does not control the regime where the cycles are smaller than the Planck scale. With this physical input, we can match the periods directly to the scalar coordinates of the gauge theory. Write the three commuting adjoint scalars as diagonal matrices with eigenvalue triplets $\boldsymbol{\phi}_i$. Expanding the covariant scalar kinetic term gives the vector mass:

$$[\Phi_a, e_{ij}] = (\phi_i^a - \phi_j^a)e_{ij}, \qquad M_{ij}^2 = \sum_{a=1}^{3}(\phi_i^a - \phi_j^a)^2. \tag{XIII.1.33}$$

The relative sign of the eigenvalues is fixed by matching the *oriented* periods to the root charges. A traceless choice is

$$\boldsymbol{\phi}_i = 2\pi T(\overline{\mathbf{x}} - \mathbf{x}_i), \qquad \overline{\mathbf{x}} = \tfrac{1}{3}\sum_i \mathbf{x}_i, \qquad \boldsymbol{\phi}_i - \boldsymbol{\phi}_j = T\mathbf{P}_{ij}. \tag{XIII.1.34}$$

We can also construct the scalar matrices directly from periods, without retaining the center coordinates. Let $\mathbf{m}_1 = T\mathbf{P}_{12}$ and $\mathbf{m}_2 = T\mathbf{P}_{23}$. The two oriented differences and the absence of a common trace mode give three linear equations:

$$\boldsymbol{\phi}_1 - \boldsymbol{\phi}_2 = \mathbf{m}_1, \qquad \boldsymbol{\phi}_2 - \boldsymbol{\phi}_3 = \mathbf{m}_2, \qquad \boldsymbol{\phi}_1 + \boldsymbol{\phi}_2 + \boldsymbol{\phi}_3 = 0. \tag{XIII.1.35}$$

Solving component by component yields

$$\boldsymbol{\phi}_1 = \frac{2\mathbf{m}_1 + \mathbf{m}_2}{3}, \qquad \boldsymbol{\phi}_2 = \frac{-\mathbf{m}_1 + \mathbf{m}_2}{3}, \qquad \boldsymbol{\phi}_3 = -\frac{\mathbf{m}_1 + 2\mathbf{m}_2}{3}. \tag{XIII.1.36}$$

The sum-root difference is consequently $\boldsymbol{\phi}_1 - \boldsymbol{\phi}_3 = \mathbf{m}_1 + \mathbf{m}_2$. Its norm reproduces (XIII.1.27). This inversion makes explicit that there are two independent scalar triplets rather than three center-position triplets in the localized gauge sector. For the oblique example (XIII.1.28), it gives

$$\frac{(\boldsymbol{\phi}_1, \boldsymbol{\phi}_2, \boldsymbol{\phi}_3)}{2\pi T u^2} = \big((5/3, 2/3, 0),\, (-1/3, 2/3, 0),\, (-4/3, -4/3, 0)\big). \tag{XIII.1.37}$$

Subtracting consecutive entries gives $(2, 0, 0)$ and $(1, 2, 0)$ in these units, so both the direction and the magnitude of each simple-root period are recovered.

The opposite sign of every $\boldsymbol{\phi}_i$ would give the same squared masses, but would reverse this period identification. In the triangle of Fig. XIII.1.2, the scalar eigenvalue triplets and the differences along the two marked roots are

$$\begin{aligned} \frac{(\boldsymbol{\phi}_1,\boldsymbol{\phi}_2,\boldsymbol{\phi}_3)}{2\pi T u^2} &= \big((2,4/3,0),\,(-1,4/3,0),\,(-1,-8/3,0)\big), \\ \frac{\boldsymbol{\phi}_1-\boldsymbol{\phi}_2}{2\pi T u^2} &= (3,0,0), \qquad \frac{\boldsymbol{\phi}_2-\boldsymbol{\phi}_3}{2\pi T u^2} = (0,4,0). \end{aligned} \tag{XIII.1.38}$$

Their differences have norms $3,4,5$, including the sum of the two adjacent differences for the outer root.

The same variables describe approaching a partial enhancement while keeping the other period nonzero. Set $\mathbf{m}_1 = \varepsilon\mathbf{v}$ and $\mathbf{m}_2 = \mathbf{w}$, where $\mathbf{w} \neq 0$ is fixed and $\varepsilon \to 0^+$. The three positive-root masses in the identified gauge EFT obey

$$M_{12} = \varepsilon|\mathbf{v}|, \qquad M_{23} = |\mathbf{w}|, \qquad M_{13} = |\mathbf{w}+\varepsilon\mathbf{v}| \longrightarrow |\mathbf{w}|. \tag{XIII.1.39}$$

Only one opposite pair becomes massless on this path. The two other positive-root masses meet each other, but remain separated from zero. This provides a useful distinction between degeneracy of massive particles and enhancement of the massless gauge algebra.

If only centers 1 and 2 coincide, only the two opposite roots e_{12} and e_{21} become massless in this example. They join one Cartan vector to give an $\mathfrak{su}(2)$ sector; the other Cartan vector supplies a relative $\mathfrak{u}(1)$. If all three centers coincide, all six root vectors become massless. Together with the two Cartan vectors they complete the adjoint of $\mathfrak{su}(3)$. The localized count has no extra photon for the common center. The local root spectrum identifies the Lie algebra; determining a global gauge group would also require the allowed line charges. We now use the same root-charge normalization to measure the kinetic coefficient.

XIII.1.6 The gauge coupling and the Planck scale

What sets the strength of interactions between these vectors? First measure the coefficient of a photon whose electric charges are fixed by (XIII.1.10). In the leading eleven-dimensional form action write $K_{11} = 2\kappa_{11}^2 = (2\pi)^8\ell_p^9$. The quadratic term, with $G_4 = \mathrm{d}C_3$, is

$$S_{G_4} = -\frac{1}{2K_{11}}\int G_4 \wedge *_{11} G_4. \tag{XIII.1.40}$$

Inserting $\widehat{C}_3 = TC_3$ and (XIII.1.8) puts T^{-2} in front of the seven-dimensional action. The product Hodge pairing separates the external and internal two-forms, giving

$$S_{\mathrm{Cartan}} = -\frac{1}{2K_{11}T^2}G_{ij}\int F^i \wedge *_7 F^j. \tag{XIII.1.41}$$

Here G_{ij} is the positive pairing measured by the unit periods in Fig. XIII.1.1.

To compare with the nonabelian trace, let h_i be the diagonal simple coroots. The vectors A^i with unit root charges multiply their *dual* generators $H^i = (C^{-1})_{ij} h_j$, not h_i themselves. In the A_2 example,

$$\begin{aligned} H^1 &= \tfrac{1}{3}\,\mathrm{diag}(2,-1,-1), & H^2 &= \tfrac{1}{3}\,\mathrm{diag}(1,1,-2), \\ \alpha_i(H^j) &= \delta_i^j, & \mathrm{Tr_f}(H^i H^j) &= (C^{-1})_{ij}. \end{aligned} \tag{XIII.1.42}$$

For example the 12 entry has charge one under H^1 and zero under H^2, and the mixed trace is $1/3$. The simple coroots would instead have trace Gram C. Thus the trace of $F = F^i H^i$ uses exactly the same matrix as the form reduction.

The field transformation (XIII.1.15) gives a second way to check the normalization. Since $G = C^{-1}$, its effect on the quadratic form is

$$F^T G F = f^T C^T C^{-1} C f = f^T C f, \qquad \mathrm{Tr_f}(h_i h_j) = C_{ij}. \tag{XIII.1.43}$$

Here the products denote the symmetric coefficient pairing of external field strengths in the action. Both the source charges and the trace Gram change when passing to coroot photons. They change together, so the coefficient extracted from the action is independent of this choice of coordinates on the Cartan subalgebra. The inverse Cartan matrix in (XIII.1.41) is therefore a consequence of unit periods, not a change in the underlying Lie algebra.

Use the action $-g_7^{-2} \int \mathrm{Tr_f}\, F \wedge {*F}$ with $\mathrm{Tr_f}(T^a T^b) = \delta^{ab}/2$ for orthogonally normalized generators. Since $F^a \wedge {*F^b} = \frac{1}{2} F^a_{\mu\nu} F^{b\mu\nu}\, \mathrm{d}^7x$, the component coefficient is $-1/(4g_7^2)$. The matching in the unit charge basis gives the leading coupling

$$g_7^2 = 2K_{11} T^2 = 2(2\pi)^4 \ell_p^3. \tag{XIII.1.44}$$

A check is A_1, where $Q = (-2)$ and the photon generator is $H^1 = \frac{1}{2}\,\mathrm{diag}(1,-1)$. The difference of its two diagonal entries is one and $\mathrm{Tr_f}[(H^1)^2] = 1/2 = G_{11}$. Using the simple coroot instead would change the charge and the kinetic pairing simultaneously. If the matrix-trace action for the *same* F and trace is written $-\frac{1}{2g_{\mathrm{alt}}^2} \int \mathrm{Tr_f}\, F \wedge {*F}$, then $g_{\mathrm{alt}}^2 = g_7^2/2$. This convention change does not alter a physical coupling. Equation (XIII.1.44) is a two-derivative matching coefficient.

The connection in $\mathrm{d} - iA$ has mass dimension one, so its curvature has dimension two. The action density has mass dimension seven, which gives

$$[A]_{\mathrm{mass}} = 1, \qquad [F]_{\mathrm{mass}} = 2, \qquad [g_7^2]_{\mathrm{mass}} = 4 - 7 = -3. \tag{XIII.1.45}$$

At fixed rank the interaction parameter at energy E scales as $g_7^2 E^3$, up to numerical group and loop factors. Work below the completion scales, and include the root particles if their masses enter the energy range of interest.

Consider taking ℓ_p to zero with E fixed. For a fixed positive area, $T\mathcal{A}$ grows as ℓ_p^{-3}, so that root is not retained at finite energy. To keep a root of nonzero mass m in the protected comparison, one can tune

$$\mathcal{A} = (2\pi)^2 \ell_p^3 m, \qquad \frac{\mathcal{A}}{\ell_p^2} = (2\pi)^2 \ell_p m \longrightarrow 0, \qquad g_7^2 E^3 \longrightarrow 0. \tag{XIII.1.46}$$

The tuned cycle leaves the smooth semiclassical regime, even though the protected mass stays finite. Keeping $g_7^2 E^3$ nonzero by scaling $E \propto \ell_p^{-1}$ would instead remove the separation from the Planck scale. A single scaling variable displays the conflict between a smooth membrane calculation and a finite-mass Planck limit. Take $\ell_p = \varepsilon \ell_{p,0}$ and $\mathcal{A} = \varepsilon^p \mathcal{A}_0$, with fixed positive $\ell_{p,0}, \mathcal{A}_0$. Then

$$M_W = \frac{\mathcal{A}_0}{(2\pi)^2 \ell_{p,0}^3} \varepsilon^{p-3}, \qquad \frac{\mathcal{A}}{\ell_p^2} = \frac{\mathcal{A}_0}{\ell_{p,0}^2} \varepsilon^{p-2}, \qquad g_7^2 E^3 = 2(2\pi)^4 \ell_{p,0}^3 E^3 \varepsilon^3. \quad \text{(XIII.1.47)}$$

For $p < 3$ the formal wrapped mass diverges, for $p = 3$ it remains finite, and for $p > 3$ it tends to zero. A parametrically large area in Planck units instead requires $p < 2$. Thus no power in this family keeps both a nonzero finite mass and a parametrically smooth cycle. For $p = 3$, supersymmetric continuation supplies the light-state interpretation after the large-area approximation is lost. At every fixed E in these paths, the seven-dimensional interaction parameter tends to zero, regardless of the area exponent. Tuning a charged mass and preserving a nonzero interaction strength are different conditions.

In this construction the seven-dimensional gauge fields form a local effective sector coupled to bulk physics. The absence of a normalizable bulk graviton zero mode does not by itself establish an autonomous interacting ultraviolet theory.

XIII.1.7 An external circle and the IIA description

Which six-dimensional data follow from compactifying this same gauge theory? Take a periodic, untwisted circle $y \sim y + 2\pi R$ in the external spacetime. Its radius R is a physical radius in a common unwarped length convention for the constant-dilaton background. It is independent of the internal GH circle. The relevant M/IIA units are

$$R = g_s \ell_s, \qquad \ell_p^3 = R\alpha', \qquad \ell_s^2 = \alpha', \qquad M_s = \ell_s^{-1}. \quad \text{(XIII.1.48)}$$

Circle-independent vectors have the same electric normalization as in seven dimensions. Integrating their action over the *circumference*, not the radius, gives

$$\frac{1}{g_6^2} = \frac{2\pi R}{g_7^2}, \qquad g_6^2 = \frac{2(2\pi)^4 \ell_p^3}{2\pi R} = 2(2\pi)^3 \alpha'. \quad \text{(XIII.1.49)}$$

At low enough energy to keep just the light modes, the vector has four transverse polarizations in six dimensions. The circle component A_y supplies the fourth adjoint scalar. The seven-dimensional spinors have opposite six-dimensional chiralities with eight real supercharges of each chirality. This is the $(1,1)$ gauge multiplet of the type IIA effective theory.

The IIA coefficient can also be obtained without reducing the seven-dimensional Yang–Mills action. Write the RR three-form kinetic term as $-\frac{\alpha_2}{2} \int F_4^{\mathrm{RR}} \wedge *F_4^{\mathrm{RR}}$ and the D2 electric source as $+\mu_2 \int C_3^{\mathrm{RR}}$. The RR exchange amplitude fixes the ratio

$$e_2^2 := \frac{\mu_2^2}{\alpha_2} = 2\pi(4\pi^2\alpha') = (2\pi)^3 \alpha'. \quad \text{(XIII.1.50)}$$

This ratio is invariant under rescaling the RR potential. In the unit source potential $\widehat{C}_3^{\mathrm{RR}} = \mu_2 C_3^{\mathrm{RR}}$, the kinetic coefficient is $-1/(2e_2^2)$. Reducing on the same ω_i therefore gives

$$S_{\mathrm{Cartan}}^{\mathrm{IIA}} = -\frac{G_{ij}}{2e_2^2}\int F^i \wedge *_6 F^j, \qquad g_6^2 = 2e_2^2. \tag{XIII.1.51}$$

The factor of two comes from matching the same form action and trace, not from a second copy of the photon. The D2 source and circle computations thus agree in their absolute leading units.

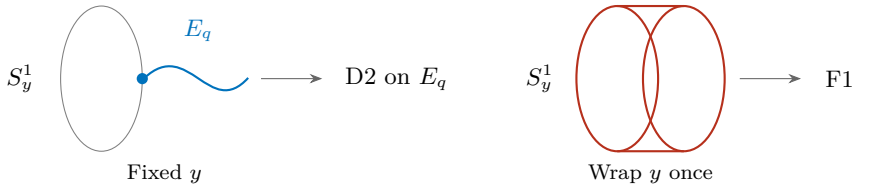


Figure XIII.1.3: Two uses of the external y-circle. The membrane on E_q at a fixed circle position reduces to a D2 on E_q; it is a particle in the extended dimensions. A membrane with one spatial direction along S^1_y and another along an extended direction reduces to a fundamental string. The internal GH circle remains part of X in both cases.

The masses and tensions make the distinction in Fig. XIII.1.3 precise. An M2 wrapped on E_q but not on the external circle becomes a D2 on the same cycle. On the zero-B, zero-flux branch its mass is still $T\mathcal{A}_q$, since

$$T = \frac{1}{(2\pi)^2 g_s \ell_s^3} = \tau_2. \tag{XIII.1.52}$$

For a membrane wrapping y, that direction multiplies the tension by $2\pi R$. A pure unit KK mode, by contrast, has momentum along the circle but does not wrap it:

$$2\pi R\, T = \frac{1}{2\pi\alpha'} = T_{\mathrm{F1}}, \qquad \frac{1}{R} = \frac{1}{g_s \ell_s} = M_{\mathrm{D0}}. \tag{XIII.1.53}$$

For the RR component without a circle leg, the WZ matching is $TC_3^{(10)} = \mu_2 C_3^{\mathrm{RR}}$, an equality of normalized source potentials in this local frame.

The field A_y also shifts the spectrum. Let b_q be the Wilson period in the charge-q sector. With $C_3 = C_3^{(10)} + B \wedge \mathrm{d}y$ in the local product frame, the same Wilson period is the type IIA B period:

$$b_q = \frac{1}{2\pi}\oint q_i A^i = \frac{T}{2\pi}\int_{E_q \times S^1_y} C_3 = \frac{1}{4\pi^2\alpha'}\int_{E_q} B. \tag{XIII.1.54}$$

Use $D_y = \partial_y - i q_i A_y^i$. In a local gauge with constant A_y, a Fourier mode $\exp(iky/R)$, $k \in \mathbb{Z}$, has D_y-eigenvalue $i(k - b_q)/R$. On the holomorphic slice write $j_q = \mathcal{A}_q/(4\pi^2\alpha')$

for the positive physical area in dimensionless units. Since $j_q/R = T\mathcal{A}_q$, the parent mass and the shifted circle momentum give

$$R^2 M_{6,k}^2 = j_q^2 + (k - b_q)^2. \tag{XIII.1.55}$$

The momentum shift follows by acting with the covariant derivative, so its sign is fixed before comparing with a D2. In the constant local gauge, $q_i A_y^i = b_q/R$. Acting on the mode gives

$$-D_y^2 \exp(iky/R) = \frac{(k - b_q)^2}{R^2} \exp(iky/R), \qquad M_{6,k}^2 = M_7^2 + \frac{(k - b_q)^2}{R^2}. \tag{XIII.1.56}$$

This is the dispersion relation of the declared charged parent field on a product circle. A Fourier label is a coordinate on that description; under an integer change of the Wilson lift the same physical state can have a different label. Light modes should be selected by the shifted momentum, rather than by the integer k alone.

On a smooth calibrated spin sphere in the type IIA description, the D2 mass uses $B + 2\pi\alpha' F_{\mathrm{wv}}$ with $n = \int F_{\mathrm{wv}}/(2\pi) \in \mathbb{Z}$. At the static DBI minimum on the smooth sphere the ratio of $\mathcal{F} = B + 2\pi\alpha' F_{\mathrm{wv}}$ to the area form is constant. If this ratio is f, the spatial determinant multiplies the area element by $\sqrt{1 + f^2}$, and $f\mathcal{A}_q = \int_{E_q} \mathcal{F} = 4\pi^2\alpha'(b_q + n)$. Using the tension τ_2 in (XIII.1.52) gives

$$R^2 M_{\mathrm{D2,n}}^2 = j_q^2 + (b_q + n)^2. \tag{XIII.1.57}$$

One can see the normalization in the determinant before squaring the mass. In an oriented orthonormal spatial frame on the sphere the antisymmetric field is $\mathcal{F}_{12} = f$, so

$$\det(\delta_{ab} + \mathcal{F}_{ab}) = \det \begin{pmatrix} 1 & f \\ -f & 1 \end{pmatrix} = 1 + f^2, \qquad M_{\mathrm{D2,n}} = \tau_2 \sqrt{\mathcal{A}_q^2 + \big(4\pi^2\alpha'(b_q + n)\big)^2}. \tag{XIII.1.58}$$

Using $\tau_2 = 1/(4\pi^2 R\alpha')$ and $\mathcal{A}_q = 4\pi^2\alpha' j_q$ gives $M_{\mathrm{D2,n}} = R^{-1}\sqrt{j_q^2 + (b_q + n)^2}$, as required. The square root combines physical area and flux energy; adding their absolute values would describe a different energy expression. This calculation uses the smooth static representative and its stated flux minimum.

Equations (XIII.1.55) and (XIII.1.57) agree for the labels $n = -k$. This compares the mass squares in the stated conventions; it does not assign an oriented ten-dimensional Page charge. A change $b_q \mapsto b_q + s$, with $s \in \mathbb{Z}$, requires $k \mapsto k + s$, $n \mapsto n - s$. Keeping k fixed in this shift would compare different modes.

For example, take $j_q = 1/3$, $b_q = 2/3$, $k = 1$. Then $R^2 M^2 = 2/9$. In the lift $b_q = -1/3$, the label is $k = 0$ and the same mass is obtained. Sending the area to zero while holding that Wilson period leaves $R^2 M^2 = 1/9$ for the chosen mode. Thus a nonintegral Wilson period obstructs six-dimensional enhancement even if the curve shrinks. This is a statement about the charged dispersion and its smooth D2 comparison. The circle Wilson period lies on a curve times a circle, whereas the background holonomy of the original seven-dimensional problem lies on S^3/Γ.

There is a useful way to locate the light Fourier label within one Wilson-period interval. For the Fourier modes of a specified charged parent field and $0 \le b_q \le 1$, only

$k = 0, 1$ compete for the smallest shifted momentum. Their difference is

$$(1 - b_q)^2 - b_q^2 = 1 - 2b_q, \qquad \min_{k\in\mathbb{Z}} R^2 M_{6,k}^2 = j_q^2 + \min\{b_q^2, (1 - b_q)^2\}. \tag{XIII.1.59}$$

The nearest integer is 0 below half a period and 1 above it. At half a period these two Fourier labels have equal mass. This comparison concerns modes of the given parent field; it does not count additional wrapped-brane states. At zero area a massless mode requires an integral Wilson period, because each term in the mass square is nonnegative.

For example, with $j_q = 2/3$, $b_q = 1/5$, the nearest mode has $k = 0$ and

$$R^2 M_{6,0}^2 = \frac{4}{9} + \frac{1}{25} = \frac{109}{225}, \qquad b_q \mapsto \frac{11}{5}, \quad k \mapsto 2, \quad n \mapsto -2. \tag{XIII.1.60}$$

The transformed labels give the same shifted momentum $-1/5$. For $b_q = 4/5$, in contrast, the nearest mode in the original lift is $k = 1$; its shifted momentum is $1/5$ and its mass at the same area is again $\sqrt{109}/(15R)$. Keeping only the mode called $k = 0$ in every lift would miss this equivalence and could misidentify the lowest charged mass.

Finally, the radius alone does not decide which fields can be kept. A six-dimensional gauge description in this IIA frame requires energies below both the KK and string scales:

$$ER \ll 1, \qquad E\ell_s \ll 1, \qquad \ell_s = \left(\frac{\ell_p^3}{R}\right)^{1/2}. \tag{XIII.1.61}$$

For clarity, compare the radius dependence while explicitly recording what is held fixed. Up to the common constant in g_6^2, the relevant scales are

fixed quantity	M_{KK}	M_s	g_6^2
ℓ_s	R^{-1}	ℓ_s^{-1}	$2(2\pi)^3\ell_s^2$
ℓ_p	R^{-1}	$(R/\ell_p^3)^{1/2}$	$2(2\pi)^3\ell_p^3/R$

(XIII.1.62)

The two inequalities in (XIII.1.61) must hold simultaneously. A large KK gap alone does not ensure an energy range below string excitations. Similarly, a small coefficient g_6^2 does not ensure that the zero-mode truncation remains appropriate.

At fixed ℓ_s, shrinking R sends g_s and ℓ_p to zero and the KK gap to infinity, while M_s and g_6^2 stay finite. At zero Wilson shift, tuning $\mathcal{A}_q$ proportional to R keeps the protected W mass finite. This is the scaling with a finite string scale discussed in XI; identifying the decoupled little-string theory requires physical input beyond these scale relations. At fixed ℓ_p, shrinking R also raises the KK gap, but now M_s falls to zero and the second inequality fails at fixed nonzero E. At fixed ℓ_p, increasing R without bound has the opposite obstruction: the KK gap collapses, so the formal decrease of g_6^2 cannot be read as a weak six-dimensional gauge theory at fixed E. When $R^{-1} \ll E \ll \ell_p^{-1}$, the circle modes instead recover the seven-dimensional description. The next chapter changes the geometry rather than just compactifying a spacetime direction: compact divisors of a Calabi–Yau threefold will set the data of a five-dimensional gauge theory.

XIII.1.8 Exercises

For the numerical tasks, use exact integers and fractions, for example `"3/2"`. Use the keys shown below to identify your results. Use `benchmark/tasks.json` to find the question IDs and `benchmark/PROTOCOL.md` for submission.

1. **One sphere.** For A_1, find the two oriented root charges in the unit-period basis as one-entry arrays. Compute the single entry of the unit-period photon kinetic Gram G and M/μ when $\mathcal{A} = (3/2)(2\pi)^2\ell_p^3\mu$ with $\mu > 0$ a mass. Use `roots`, `gram`, and `mass_over_mu`.

2. **Dimensions and a weak limit.** Give the mass dimensions of (A, F, g_7^2). Then give the powers of ℓ_p in $(g_7^2E^3, M_W)$ at fixed $E > 0$ and fixed nonzero physical area. Finally compute $g_7^2/[(2\pi)^4\ell_p^3]$ in the fundamental-trace convention of (XIII.1.44). Use `mass_dimensions`, `lp_exponents`, and `g7_over_unit`.

3. **The same circle mode in two lifts.** Choose $j = 2/5,\ b = 3/4,\ k = 1$. Shift $b \mapsto b-1$ and track the same mode. Give the two D2 flux labels in the order *initial, then shifted*, the shifted Fourier label, R^2M^2, and the latter's value when the area goes to zero at fixed Wilson period. Use `flux_labels`, `shifted_k`, `R2_mass2`, and `R2_collapsed_mass2`.

4. **Which background?** Consider a general ADE singularity with supersymmetrically allowed local data. You are given the metric and the areas but not the C-field background on the link. Which choice does the ordinary enhancement argument use? Explain why the root lattice cannot determine it. Distinguish it from the Wilson period on a compact curve times the external circle. This question does not posit a second frozen A_2 branch.

5. **A different triangle.** Take GH centers at $(0,0,0)u^2, (5,0,0)u^2, (5,12,0)u^2$. Give the marked charge q_{13}, the three dimensionless squares $M_{ij}^2/(2\pi Tu^2)^2$ in order $12, 23, 13$, and $M_{13}/(2\pi Tu^2)$ after aligning the two adjacent differences with the same lengths and preserving the ordering. Use `charges13`, `mass_squares`, and `aligned_mass13`.

For further written practice, use the following questions without changing the numerical submissions above. First, start with arbitrary nonzero triplets $\mathbf{m}_1, \mathbf{m}_2$ and reconstruct the three traceless scalar eigenvalues. Explain which pair of eigenvalues meets when $\mathbf{m}_1 + \mathbf{m}_2 = 0$ while $\mathbf{m}_1 \neq 0$, and identify which positive-root masses remain nonzero. Use the root table to distinguish this collapse from the path in (XIII.1.39).

Second, choose a Wilson period in $(1/2, 1)$ for a declared charged parent mode. Find its nearest Fourier label, translate to the adjacent Wilson lift and give the D2 flux label in each lift. Explain why these changes leave the mass square fixed. State separately what information would be needed to interpret a smooth mass formula as an exact multiplicity statement at a singularity. Both questions are assessed by a reader.

Status and sources

§ 1.1: Photons and the missing charged vectors. The trivial link holonomy is a background choice; the ordinary versus frozen distinction is stated by Tachikawa (2016, § 1, eq. (1.1)) [GEO-E].

§ 1.2: Gauge fields that stay near the singularity. The compact intersection and real Hodge pairing in (XIII.1.1)–(XIII.1.6) use Douglas and Moore (1996, § 2.1) and Hausel et al. (2004, Theorem 1 and § 7.1.1) [MATH]. The product reduction (XIII.1.8) is linearized at zero background four-form field strength [SUGRA]; the explicit inverse and positive quadratic form in (XIII.1.4)–(XIII.1.7) are consequences of the same pairing [MATH]. Absence of localized constant-profile fields does not imply bulk decoupling.

§ 1.3: Electric charges of the wrapped membranes. Equation (XIII.1.10) uses the unit membrane Wess–Zumino coupling [SUGRA]; (XIII.1.11) through (XIII.1.16) give the finite root and charge calculation [MATH]. Hull and Townsend (1995, § 5) identifies the charged seven-dimensional membrane states in the compact K3 setting.

§ 1.4: Mass from calibrated area. The smooth static membrane mass (XIII.1.17) is a leading area calculation [SUGRA]. The cyclic ansatz and periods in (XIII.1.20)–(XIII.1.26) use Douglas and Moore (1996, § 2.1, eqs. (2.1)–(2.2)) in the specified unit-center frame [MATH]. The aligned period equality does not count a threshold state. The path functional, angle formula and oblique example (XIII.1.24)–(XIII.1.25), (XIII.1.27)–(XIII.1.29) are algebraic and integral consequences within the same GH model [MATH].

§ 1.5: The seven-dimensional vector multiplet. The spinor and vector-multiplet count (XIII.1.30)–(XIII.1.32) uses Anderson et al. (2006, eq. (2.1), App. C.1) and the marked ALE periods [SUGRA]. The ordinary enhancement and protected continuation use the ordinary ALE enhancement and the results in Hull and Townsend (1995, §§ 4–5), Berenstein and Corrado (1998, §§ 2–3), and Tachikawa (2016, § 1) [GEO-X]. The signed scalar match (XIII.1.33)–(XIII.1.34) and its inverse-period and partial-collapse consequences (XIII.1.35)–(XIII.1.39) are algebra within that identified gauge theory [MATH].

§ 1.6: The gauge coupling and the Planck scale. Equations (XIII.1.40)–(XIII.1.44) use the leading form action and minimal M2 units, corroborated by Lu (1997, eqs. (1.5), (2.26)–(2.27)) [SUGRA]. The basis transformation (XIII.1.43) and fixed-energy limits, including (XIII.1.47), are dimensional and algebraic consequences [MATH]. Isolation from the bulk is a separate limit question [DEC].

§ 1.7: An external circle and the IIA description. The circle reduction uses Witten (1995, § 2.2) in a common physical frame [SUGRA]; the local brane interpretations also use Townsend (1995) [GEO-E]. The independent RR ratio (XIII.1.50) follows from Polchinski (1995, eqs. (12)–(13)) [SUGRA]. The smooth flux comparison (XIII.1.57) uses the DBI combination in Polchinski et al. (1996, eqs. (2.19)–(2.20)) and the calibrated type IIA calculation in XI; the label and limit arithmetic, including the nearest-label comparison (XIII.1.59)–(XIII.1.60) and radius trajectories (XIII.1.62), is conditional [MATH]. The IIA finite-string-scale interpretation and its low-energy coupling are corroborated by Chang et al. (2014, § 1, eq. (1.1)); full local-sector decoupling is separate [DEC].

References

Anderson, L. B., A. B. Barrett, and A. Lukas (2006). "M theory on the orbifold". In: *Phys. Rev. D* 73, p. 106011. DOI: 10.1103/PhysRevD.73.106011. arXiv: hep-th/0602055.

Berenstein, D. and R. Corrado (1998). *Matrix theory on ALE spaces and wrapped membranes*. arXiv: hep-th/9803048.

Chang, C.-M. et al. (2014). "Little string amplitudes (and the unreasonable effectiveness of 6D SYM)". In: *JHEP* 12, p. 176. DOI: 10.1007/JHEP12(2014)176. arXiv: 1407.7511 [hep-th].

Douglas, M. R. and G. W. Moore (1996). "D-branes, quivers, and ALE instantons". In: arXiv preprint; not published in a journal. arXiv: hep-th/9603167.

Hausel, T., E. Hunsicker, and R. Mazzeo (2004). "Hodge cohomology of gravitational instantons". In: *Duke Math. J.* 122, pp. 485–548. DOI: 10.1215/S0012-7094-04-12233-X. arXiv: math/0207169.

Hull, C. M. and P. K. Townsend (1995). "Enhanced gauge symmetries in superstring theories". In: *Nucl. Phys. B* 451, pp. 525–546. DOI: 10.1016/0550-3213(95)00364-X. arXiv: hep-th/9505073.

Lu, J. X. (1997). *Remarks on M theory coupling constants and M-brane tension quantizations*. arXiv: hep-th/9711014.

Polchinski, J. (1995). "Dirichlet-branes and Ramond–Ramond charges". In: *Phys. Rev. Lett.* 75, pp. 4724–4727. DOI: 10.1103/PhysRevLett.75.4724. arXiv: hep-th/9510017.

Polchinski, J., S. Chaudhuri, and C. V. Johnson (1996). *Notes on D-branes*. arXiv: hep-th/9602052.

Tachikawa, Y. (2016). "Frozen singularities in M and F theory". In: *JHEP* 06, p. 128. DOI: 10.1007/JHEP06(2016)128. arXiv: 1508.06679 [hep-th].

Townsend, P. K. (1995). "The eleven-dimensional supermembrane revisited". In: *Phys. Lett. B* 350, pp. 184–187. DOI: 10.1016/0370-2693(95)00397-4. arXiv: hep-th/9501068.

Witten, E. (1995). "String theory dynamics in various dimensions". In: *Nucl. Phys. B* 443, pp. 85–126. DOI: 10.1016/0550-3213(95)00158-O. arXiv: hep-th/9503124.

Chapter XIII.2

Curves, surfaces, and the 5D prepotential

XIII.2.1 A particle and a string ask for different volumes

An M2-brane wrapped on a compact curve is a particle in the five uncompactified spacetime directions. An M5-brane wrapped on a compact surface leaves a string. Their masses and tensions vary as the internal Kähler class changes. A resolved Calabi–Yau threefold therefore offers more than a diagram of a singularity: its curve and surface volumes are quantities that a 5D observer can in principle measure.

The question of this chapter is how much of a gauge theory those volumes determine. We shall answer it in the smallest example that contains both kinds of object, the total space of the canonical bundle of $F_0 = \mathbb{P}^1 \times \mathbb{P}^1$. Its compact surface $S = F_0$ has two distinguished ruling curves. One will supply the W particle of a pure $SU(2)$ gauge chamber; the surface will supply its primitive magnetic string. The second curve measures a background parameter. We first calculate their intersections on the compact surface, then choose the Kähler coordinates by requiring positive curve areas. This fixes the signs in the cubic prepotential. Differentiating that cubic will let us compare the particle mass, string tension and effective coupling in one frame. Finally we ask which geometric periods these measurements can reconstruct, and which information is lost when only the compact triple intersection is specified.

We work in the local, resolved gauge chamber and use the Cartan generator $H = \mathrm{diag}(1, -1)$ of the selected $SU(2)$ description. Thus $\Phi = aH$ with $a \geq 0$ and a root has value $2a$. The parameter m_0 will be the inverse bare coupling in the prepotential normalization of Intriligator–Morrison–Seiberg. It is a background coordinate, not a second vector multiplet scalar. We use relative units in which the selected M2 curve period equals m_W and the compact M5 area equals the primitive magnetic-string tension. Restoring absolute M2 and M5 action constants is a separate step. Nothing in the following intersection calculation performs the gravitational decoupling limit for us.

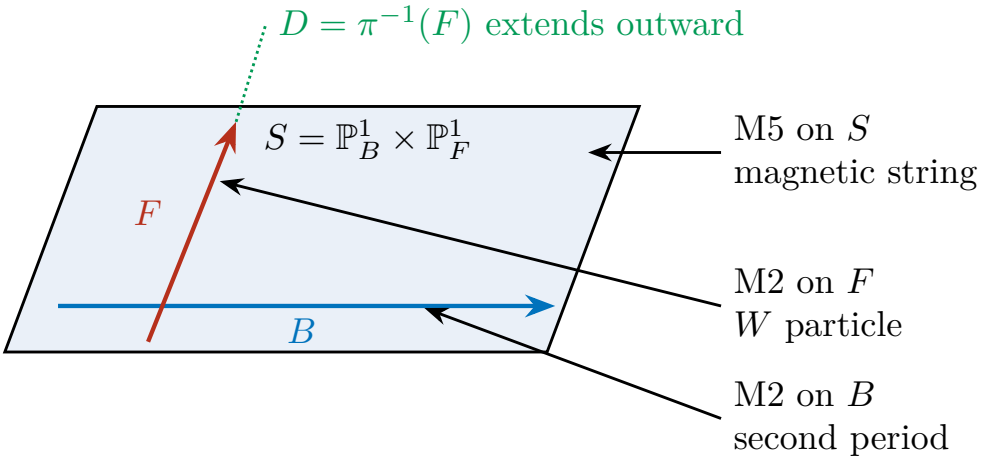


Figure XIII.2.1: The zero section S of $X = \mathrm{Tot}(K_S)$ has ruling curves B and F. An M2 on F supplies the selected W particle and an M5 on the whole compact surface supplies a magnetic string. The bundle projection is $\pi : X \to S$. The noncompact divisor $D = \pi^{-1}(F)$ meets S along F; its coefficient is a background parameter. The drawing records incidences and brane dimensions, not a metric embedding of the total space.

Figure XIII.2.1 shows which cycles the branes wrap and how the background divisor meets the compact surface.

XIII.2.2 What a triple-intersection tensor can measure

Before specializing to one surface, it helps to state the general algebra that makes an intersection calculation useful to a 5D observer. Suppose a smooth local Calabi–Yau threefold contains compact divisors S_i, $i = 1, \dots, r$, and chosen noncompact divisors N_α. A formal divisor class can be expanded in coordinates x^I as

$$\mathcal{A} = \sum_{i=1}^{r} x^i S_i + \sum_{\alpha} x^\alpha N_\alpha, \qquad C_{IJK} = D_I \cdot D_J \cdot D_K. \tag{XIII.2.1}$$

Here D_I runs over the combined list of S_i and N_α, and C_{IJK} is symmetric in all three indices. Compact-divisor coordinates are candidates for dynamical Coulomb directions; the noncompact coefficients are fixed masses or couplings in the local description. The magnetic string associated with S_i responds to a Coulomb variation at fixed background.

In coordinates and orientations for which the physical prepotential is represented by

the cubic of $\mathcal{A}$, the algebraic relations are

$$\begin{aligned}\mathcal{F}_{\text{cubic}} &= \frac{1}{6}C_{IJK}x^I x^J x^K,\\ \partial_i\mathcal{F}_{\text{cubic}} &= \frac{1}{2}C_{iJK}x^J x^K, \qquad \partial_i\partial_j\mathcal{F}_{\text{cubic}} = C_{ijK}x^K, \qquad \partial_i\partial_j\partial_k\mathcal{F}_{\text{cubic}} = C_{ijk}.\end{aligned} \tag{XIII.2.2}$$

The first derivative is quadratic, as an area of a compact complex surface should be. The second is linear, as a 5D inverse gauge coupling should be. The third is an integer intersection number in an integral divisor basis. In the physical dictionary, the first derivative is a relative magnetic-string tension and the second is a vector kinetic matrix, subject to the orientation and normalization of the chosen Coulomb coordinates. These relations are especially useful because a suspected factor or sign error has to survive all three derivatives.

Every triple product with at least one compact insertion can be computed by restricting the other two divisors to that compact surface. For example,

$$S_i N_\alpha N_\beta = \int_{S_i} (N_\alpha|_{S_i})(N_\beta|_{S_i}). \tag{XIII.2.3}$$

By contrast, a product of three noncompact divisors has no intrinsic ordinary degree in a local space. One may choose a relative or compactified prescription, but the resulting background-only polynomial has zero derivative in every dynamical Coulomb direction. This statement assumes the noncompact divisor lifts and the physical coordinates have already been fixed. A change of lift can mix the names assigned to compact and background coefficients, as we calculate in Section XIII.2.8.

For a single compact class and one background coordinate, this structure reduces to a useful diagnostic polynomial,

$$\mathcal{F}(q;m) = \frac{c}{6}q^3 + \frac{\ell}{2}mq^2 + \frac{p}{2}m^2q + U(m). \tag{XIII.2.4}$$

Here c, ℓ, p are compact-supported intersections in the chosen oriented divisor basis, while $U(m)$ depends on the noncompact prescription. Its observable derivatives are

$$T(q;m) = \frac{c}{2}q^2 + \ell mq + \frac{p}{2}m^2, \qquad g(q;m) = cq + \ell m. \tag{XIII.2.5}$$

The local F_0 calculation will give $(c,\ell,p) = (8,2,0)$ in the oriented coordinates $(q,m) = (a, m_0)$. Putting these values into (XIII.2.5) gives the target for that calculation:

$$T(q;m) = \tfrac{8}{2}q^2 + 2mq + \tfrac{0}{2}m^2 = 4q^2 + 2mq, \qquad g(q;m) = 8q + 2m. \tag{XIII.2.6}$$

The $pm^2/2$ term vanishes, but ℓmq survives in T. The background can therefore still change the Hessian. At $q = 1$ and $m = 3$, for example, $T = 4 + 6 = 10$ and $g = 8 + 6 = 14$.

In mass units $[a] = [m_0] = 1$ and $[\mathcal{F}] = 3$. Hence $[\mathcal{F}_{aa}] = 1$ for an inverse 5D gauge coupling and $[\mathcal{F}_a] = 2$ for a string tension. The geometric periods and areas carry powers of length; M2 and M5 tensions convert them into physical units. Our identifications with $2a$ and $\mathcal{F}_a$ use relative units and do not fix those constants.

XIII.2.3 The compact cube from adjunction

Why does a surface know a cubic coupling? A compact divisor in a threefold can meet itself three times. Before assigning a physical meaning to that number, we can calculate it entirely on the surface. Let B and F denote the homology classes of the two projections' fibers on $S = \mathbb{P}^1_B \times \mathbb{P}^1_F$. Their pairing is

$$\begin{array}{c|cc} \cdot & B & F \\ \hline B & 0 & 1 \\ F & 1 & 0 \end{array}. \tag{XIII.2.7}$$

Both self-intersections vanish because two distinct fibers of either projection do not meet; a fiber of one projection meets a fiber of the other once. The product tangent bundle has $c_1(TS) = 2B + 2F$, so

$$K_S = -2B - 2F, \qquad K_S^2 = (-2B - 2F)^2 = 8(B \cdot F) = 8. \tag{XIII.2.8}$$

This is a computation in the compact intersection ring. In particular, it needs no regularization at infinity.

It is helpful to make the operation behind this small table explicit. A curve on a smooth surface is also a divisor there, so its homology class has a Poincaré-dual class in $H^2(S)$. We use B and F for these dual classes when taking products. If $L = \alpha B + \beta F$ is a divisor class and $C = pB + qF$ is a curve class, its degree on that curve is

$$\deg(L|_C) = L \cdot C = \alpha p B^2 + (\alpha q + \beta p) BF + \beta q F^2 = \alpha q + \beta p. \tag{XIII.2.9}$$

The coefficient of B therefore measures a period on F, and the coefficient of F measures a period on B. This exchange is a consequence of the intersection pairing. It matters whenever we read an area from a restricted divisor class.

Now take $X = \mathrm{Tot}(K_S)$ and identify S with its zero section. The normal line bundle of the zero section is K_S. The same statement follows from adjunction:

$$K_S = (K_X + S)|_S = S|_S, \qquad K_X \simeq \mathcal{O}_X. \tag{XIII.2.10}$$

Here $S|_S$ is a divisor class on the surface, while S before the restriction is a divisor of the threefold. Restricting two copies of S to the third one gives

$$S^3 = \int_S (S|_S)^2 = K_S^2 = 8. \tag{XIII.2.11}$$

This use of adjunction is more informative than assigning the cubic coefficient from a known gauge-theory answer: it shows which geometric assumption carries the number.

One can also read adjunction as a statement about line bundles. The divisor S defines $\mathcal{O}_X(S)$, whose restriction to S is its normal bundle. Further restricting to a ruling curve gives

$$\mathcal{O}_X(S)|_S \simeq K_S, \qquad S \cdot F = \deg(K_S|_F) = (-2B - 2F) \cdot F = -2. \tag{XIII.2.12}$$

Thus the same negative normal degree appears when a compact divisor meets a ruling curve. The positive compact cube arises by taking *two* restrictions of that divisor, not by making the normal degree positive:

$$\int_S (-2B-2F)(-2B-2F) = 4\int_S B^2 + 8\int_S BF + 4\int_S F^2 = 8. \tag{XIII.2.13}$$

A negative divisor–curve intersection and a positive triple self-intersection are therefore consistent. They are different operations in the same intersection ring.

The full prepotential also needs a mixed intersection with a noncompact divisor. Let $\pi : X \to S$ be the bundle projection and choose $D = \pi^{-1}(F)$. It is the total space of the canonical line over the curve F, hence is noncompact, and

$$D|_S = F, \qquad S^2D = K_S \cdot F = -2, \qquad SD^2 = F^2 = 0. \tag{XIII.2.14}$$

For the mixed product, restrict the two non-distinguished insertions to the compact surface first:

$$\begin{aligned} S^2D &= \int_S (S|_S)(D|_S) = \int_S (-2B-2F)F = -2, \\ SD^2 &= \int_S (D|_S)^2 = \int_S F^2 = 0. \end{aligned} \tag{XIII.2.15}$$

Equivalently, S^2D is the degree of the normal bundle on $S \cap D = F$. It is not a product of three curve classes on the surface. Restriction turns a triple product in the threefold into a pairing of two divisor classes on the surface.

For practice, let $P = \alpha S + \beta D$ and $Q = \gamma S + \delta D$. The whole compact-supported bilinear calculation is

$$\begin{aligned} SPQ &= \int_S (\alpha K_S + \beta F)(\gamma K_S + \delta F) \\ &= 8\alpha\gamma - 2(\alpha\delta + \beta\gamma). \end{aligned} \tag{XIII.2.16}$$

For $P = S + D$ and $Q = 2S - D$, this gives $SPQ = 16 - 2(-1+2) = 14$. Expanding the threefold product gives $2S^3 + S^2D - SD^2 = 16 - 2 = 14$ as well. The two routes use the same compact pairing and require no choice of D^3. Choosing $\pi^{-1}(B)$ instead would exchange the roles of the rulings. The abstract surface is symmetric under that exchange, but a gauge description must still say which curve is its root.

As a quick test, replace F in (XIII.2.14) by B. The result $S^2\pi^{-1}(B) = -2$ survives, whereas the identity of the curve whose period is held fixed changes. This is why a table of triple intersections without a curve basis cannot yet specify the Coulomb coordinate.

One triple product is deliberately absent from (XIII.2.11)–(XIII.2.14): D^3. Three noncompact divisors do not have an intrinsic ordinary finite intersection degree in this local threefold. A compactification, relative intersection scheme, or equivariant prescription can provide a value, but that value belongs to the chosen prescription. We shall see exactly which field-theory terms are insensitive to it.

XIII.2.4 A positive Kähler class and a signed divisor coordinate

Which curve should have mass $2a$? The answer fixes the sign before we expand any cubic. The compact divisor restricts negatively: $S|_S = K_S = -2B - 2F$. A positive coefficient multiplying S therefore has negative intersection with both ruling curves. In the convention used below, the genuine positive Kähler class on compact curves is

$$\omega = -aS + m_0 D, \qquad \omega|_S = -aK_S + m_0 F = 2aB + (m_0 + 2a)F. \tag{XIII.2.17}$$

Its two ruling periods are

$$t_F := \omega \cdot F = 2a, \qquad t_B := \omega \cdot B = m_0 + 2a. \tag{XIII.2.18}$$

Consequently the positive-area chamber is $a > 0$ and $m_0 + 2a > 0$. The slice $m_0 \geq 0$ has nonnegative inverse bare coupling. A hierarchy $m_0 \gg a$ provides a weakly coupled gauge description at the W scale.

The class F is our selected W curve. Its intersection with the compact divisor gives the A_1 Cartan entry,

$$-S \cdot F = -K_S \cdot F = 2. \tag{XIII.2.19}$$

An M2 on F has mass proportional to $t_F = 2a$. In the stated relative particle unit this is $m_W = 2a$, exactly the root value of $\Phi = aH$. The second curve has period $m_0 + 2a$. Subtracting the W period gives the background coordinate:

$$m_0 = t_B - t_F. \tag{XIII.2.20}$$

This equation defines the geometric lift of the inverse coupling in our chosen divisor basis. It is not an arbitrary identification invented after the prepotential has been expanded.

The periods can be organized by their Coulomb and background coefficients. For any curve class C, define the intersection coefficients

$$q_C = -S \cdot C, \qquad b_C = D \cdot C. \tag{XIII.2.21}$$

We call q_C its *Coulomb-period coefficient* and b_C its *background-period coefficient*. Their role follows directly from the chosen Kähler class:

$$t_C = \omega \cdot C = -a(S \cdot C) + m_0(D \cdot C) = q_C a + b_C m_0. \tag{XIII.2.22}$$

At fixed m_0, the period slope is therefore $\partial_a t_C = q_C$. For the selected root curve F, the coefficient $q_F = 2$ agrees with the physical electric charge in our stated Cartan frame, and $t_F = 2a$ gives its relative M2 particle mass. Interpreting q_C as an electric charge for a general wrapped class would additionally require its gauge-field reduction and M2 coupling dictionary. Here we compute the period coefficients for general C and keep the physical charge comparison to the selected root.

For the two ruling curves the four required intersections are

C	$S \cdot C$	$D \cdot C$	q_C	b_C	t_C
F	-2	0	2	0	$2a$
B	-2	1	2	1	$m_0 + 2a$

. (XIII.2.23)

The Coulomb-period coefficients of B and F coincide, but the period of B has an additional background contribution. This explains why the two curves can have different areas without supplying two independent Coulomb scalars. The period includes both coefficients and the values of the parameters; its slope alone does not determine its value.

We can repeat the calculation for an effective class $C = pB + qF$, with $p, q \geq 0$. Linearity gives

$$q_C = 2(p+q), \qquad b_C = p, \qquad t_C = p(m_0 + 2a) + q(2a). \tag{XIII.2.24}$$

For example, $B + 2F$ has period $m_0 + 6a$ and Coulomb-period coefficient 6. At $(a, m_0) = (1, 3)$ its period is $9 = 5 + 2 \cdot 2$. The same intersection rule thus determines periods for other classes in this surface. It does not assert that every effective class yields a distinct stable one-particle BPS state. Deciding whether a representative is irreducible, and whether the wrapped configuration is a bound state, requires additional information.

The compact surface area provides an independent check on the same map. For the restricted positive Kähler class $\omega|_S = 2aB + (m_0 + 2a)F$,

$$\mathrm{vol}_\omega(S) = \frac{1}{2}\int_S (\omega|_S)^2 = \frac{1}{2}\, 2(2a)(m_0 + 2a) = 2m_0 a + 4a^2. \tag{XIII.2.25}$$

This calculation uses only the compact surface ring. It can be checked before knowing any prepotential. Write $u = t_F$, $v = t_B$, so $\omega|_S = uB + vF$. Then

$$\frac{1}{2}\int_S (uB + vF)^2 = uv, \qquad \mathrm{vol}_\omega(S) = t_F t_B. \tag{XIII.2.26}$$

Both rulings are needed: a surface area is quadratic in curve periods. At fixed m_0, a Coulomb displacement $a \mapsto a + \epsilon$ changes both periods by 2ϵ. The direct geometric area change is consequently

$$\begin{aligned} \Delta\,\mathrm{vol}(S) &= (t_F + 2\epsilon)(t_B + 2\epsilon) - t_F t_B \\ &= 2(t_F + t_B)\epsilon + 4\epsilon^2 = (2m_0 + 8a)\epsilon + 4\epsilon^2. \end{aligned} \tag{XIII.2.27}$$

For $a = 1$, $m_0 = 3$, and $\epsilon = 1/2$, the area grows from $2 \cdot 5 = 10$ to $3 \cdot 6 = 18$. Its initial slope is 14. Later the Hessian of the cubic will reproduce this slope; here it has been found without differentiating that cubic.

The factor $1/2$ comes from the Kähler volume form on a complex surface. At $m_0 = 0$ both ruling periods are $2a$ and the area is $4a^2$. A sign-flipped restriction would make one of the wrapped particle masses negative and could not describe this positive chamber.

It is useful to introduce the *formal signed class*

$$A = -\omega = aS - m_0 D. \tag{XIII.2.28}$$

This is the compact-divisor coordinate in which the algebraic cubic is written with a positive S^3 coefficient. It is not the positive Kähler class. In particular $A \cdot F = -2a$, and a curve volume is $-A \cdot F$. The surface area has no such minus sign because $A^2 = \omega^2$.

Keeping A and ω separate resolves the apparently conflicting sign conventions that arise when one calls both of them J.

There is one compact surface and hence one candidate normalizable Kähler degree of freedom in this local engineering description. The noncompact D labels a background deformation. That distinction is part of the M-theory compactification dictionary: the finite intersection calculation by itself does not construct an L^2 harmonic representative, normalize its kinetic term, or demonstrate that bulk gravity decouples. We will use the dictionary in its toric, crepant-resolvable gauge-phase domain.

XIII.2.5 The cubic, effective metric, and magnetic string

The signed class now does the useful work. Expanding its cube while retaining only terms with at least one compact divisor gives

$$\begin{aligned}\frac{1}{6}A^3 &= \frac{1}{6}\left(a^3S^3 - 3a^2m_0S^2D + 3am_0^2SD^2 - m_0^3D^3\right)\\ &\equiv \frac{1}{6}\left(8a^3 + 6m_0a^2\right) = m_0a^2 + \frac{4}{3}a^3 \quad \text{(mod background-only terms).}\end{aligned} \tag{XIII.2.29}$$

Because $SD^2 = 0$, the only undetermined contribution from D^3 is proportional to m_0^3 and has no a derivative at fixed m_0. The cubic in (XIII.2.29) is therefore well defined as a function of the dynamical scalar up to a background polynomial, once the divisor lift and the curve-period definition (XIII.2.20) are fixed.

The sign is worth checking rather than memorizing. If we wrote $+\omega^3/6$ and differentiated with respect to the positive physical a, the compact-dependent terms would be the negative of (XIII.2.29). The correct derivative in the signed coordinate is

$$\frac{\partial}{\partial a}\frac{1}{6}A^3 = \frac{1}{2}A^2S = \frac{1}{2}\omega^2S = \mathrm{vol}_\omega(S). \tag{XIII.2.30}$$

Thus the same sign choice that gives the positive W mass also gives the positive compact-surface area. No absolute value is applied to the geometric cubic.

The equality can be tested as two independent pieces of arithmetic. The compact tensor expansion gave $\mathcal{F} = m_0a^2 + 4a^3/3$, so at fixed m_0

$$\partial_a\mathcal{F}|_{m_0} = m_0(2a) + \frac{4}{3}(3a^2) = 2m_0a + 4a^2. \tag{XIII.2.31}$$

The surface computation instead squared $\omega|_S$ and integrated its BF coefficient. Agreement tests both the cubic coefficients and the choice of derivative. At $a = 1, m_0 = 3$ both calculations give 10; using $+\omega^3/6$ would give -10 from its derivative, even though the actual area is 10. The test would also detect dropping the $1/2!$ from the surface volume, which would incorrectly give 20.

The words "at fixed m_0" have geometric content. In the signed class they mean

$$\partial_aA|_{m_0} = S, \qquad \partial_aA^3\big|_{m_0} = 3A^2S. \tag{XIII.2.32}$$

One differentiation inserts precisely the primitive compact divisor. If the coefficient of D changed during the differentiation, an additional insertion of D would appear. Such a derivative would compare backgrounds as well as move along the Coulomb branch of one fixed theory. It would not measure the area of S alone.

The field-theory calculation supplies a stringent normalization comparison. In the IMS convention, $\operatorname{Tr} H^2 = 2$. The classical quadratic term is

$$\frac{m_0}{2}\operatorname{Tr}(H^2)a^2 = m_0 a^2. \tag{XIII.2.33}$$

The two roots evaluate to $+2a$ and $-2a$. In the chosen Weyl chamber $a \geq 0$, their one-loop contribution is

$$\frac{1}{12}\big(|2a|^3 + |-2a|^3\big) = \frac{4}{3}a^3. \tag{XIII.2.34}$$

Pure $SU(2)$ has no independent ordinary cubic Casimir term in this comparison. Equations (XIII.2.33) and (XIII.2.34) reproduce (XIII.2.29) term by term. They compare one protected gauge-phase function across two descriptions; they are not two independent demonstrations of a complete QFT equivalence.

The first and second derivatives are the quantities most directly used in the 5D effective theory:

$$T^{(\mathrm{rel})}_{\mathrm{mag}} = \mathcal{F}_a = 2m_0 a + 4a^2 = \mathrm{vol}_\omega(S), \tag{XIII.2.35}$$

$$g^{\mathrm{IMS}}_{aa} = \mathcal{F}_{aa} = 2m_0 + 8a. \tag{XIII.2.36}$$

Here $T^{(\mathrm{rel})}_{\mathrm{mag}}$ is the tension of the string obtained from the primitive compact surface in the stipulated magnetic unit. The kinetic term can be written as $-\frac{1}{2}g^{\mathrm{IMS}}_{aa}\partial_\mu a\,\partial^\mu a$ in this scalar normalization. The Hessian also gives the effective Abelian inverse coupling in the same frame. The conversion from geometry to these relative observables has two parts. A physical M2 mass multiplies a curve area by the M2 tension, while a physical wrapped-M5 string tension multiplies a surface volume by the M5 tension:

$$M_C = T_{\mathrm{M2}}\int_C J_{\mathrm{phys}}, \qquad \tau_S = T_{\mathrm{M5}}\frac{1}{2}\int_S J^2_{\mathrm{phys}}. \tag{XIII.2.37}$$

Here J_{phys} carries geometric length units. We have chosen period and magnetic units so that the corresponding *relative* quantities are t_C and $\mathrm{vol}_\omega(S)$ in the IMS comparison. This convention does not set the two dimensionful brane tensions equal. Once the physical period conversion is selected, restoring an absolute string tension also requires the magnetic conversion factor. The equality $T^{(\mathrm{rel})}_{\mathrm{mag}} = \mathcal{F}_a$ uses the relative primitive unit already specified.

Even within relative units, a coordinate rescaling changes a prepotential derivative. Suppose we prefer to use the particle mass itself as a coordinate, $z = 2a$. Keep m_0 fixed. The same function is

$$\widehat{\mathcal{F}}(z; m_0) = \mathcal{F}(z/2; m_0) = \frac{m_0 z^2}{4} + \frac{z^3}{6}. \tag{XIII.2.38}$$

Its first derivative is only half the primitive string tension:

$$\widehat{\mathcal{F}}_z = \frac{1}{2}\mathcal{F}_a, \qquad \partial_z A = \frac{1}{2}S, \qquad T^{(\mathrm{rel})}_{\mathrm{mag}} = 2\widehat{\mathcal{F}}_z = m_0 z + z^2. \tag{XIII.2.39}$$

The factor comes from the divisor inserted by the derivative. The surface wrapped by the primitive string remains S, although the new coordinate derivative inserts $S/2$. Relabeling a scalar does not change which compact surface that string wraps.

The kinetic term transforms at the same time. Since $da = dz/2$,

$$g_{aa}^{\mathrm{IMS}}(da)^2 = g_{zz}(dz)^2, \qquad g_{zz} = \frac{1}{4}g_{aa}^{\mathrm{IMS}} = \widehat{\mathcal{F}}_{zz} = \frac{m_0}{2} + z. \tag{XIII.2.40}$$

For $a = 1, m_0 = 3$, this coefficient is $7/2$ instead of 14; the infinitesimal lengths are equal because $dz = 2da$. In the Lie-algebra expression the same change reads $\Phi = z(H/2)$ and $\mathrm{Tr}(H/2)^2 = 1/2$. Its roots have values $\pm z$, so the IMS expression becomes

$$\frac{m_0}{2}\,\mathrm{Tr}(H/2)^2 z^2 + \frac{1}{12}\big(|z|^3 + |-z|^3\big) = \frac{m_0 z^2}{4} + \frac{z^3}{6} \quad (z \geq 0). \tag{XIII.2.41}$$

This is a change of scalar normalization within the same local gauge calculation. It introduces no new electric lattice or global gauge-group choice. Both the period map and the primitive magnetic unit must be kept when comparing numbers between frames.

The third derivative is $\mathcal{F}_{aaa} = 8$, the compact triple intersection. Its meaning as an Abelian Chern–Simons coefficient depends on the chosen integral electric lattice and convention; 8 does not determine the discrete $SU(2)$ theta choice.

The surface and the Hessian test different aspects of the chamber. The string has positive tension when $a > 0$ and $m_0 + 2a > 0$; the Hessian is positive there because

$$2m_0 + 8a = 2(m_0 + 2a) + 4a > 0. \tag{XIII.2.42}$$

The converse fails at a boundary. At $m_0 = -2a$ with $a > 0$, the B curve and the compact surface have zero area, while the Hessian remains $4a > 0$. A positive scalar metric by itself has missed a tensionless geometric object.

The metric has another direct consequence that can be checked without classifying the endpoint. Along a fixed-m_0 path with $m_0 \geq 0$, the relative scalar distance from $a = 0$ to $a = a_*$ is

$$L(a_*; m_0) = \int_0^{a_*} \sqrt{2m_0 + 8x}\,dx = \frac{(2m_0 + 8a_*)^{3/2} - (2m_0)^{3/2}}{12}. \tag{XIII.2.43}$$

For $m_0 = 0$ this reduces to $L(a_*; 0) = \frac{4\sqrt{2}}{3}a_*^{3/2}$. The end $a_* \to 0$ is at finite distance in this one-scalar metric. The overall normalization of physical distance depends on the kinetic normalization already declared, and finite distance does not by itself identify the endpoint theory. This computation shows a different use of the Hessian: it controls how quickly a Coulomb coordinate is traversed, whereas the string tension measures the area of an entire surface.

XIII.2.6 Changing a background while watching the chamber

Holding a fixed and changing m_0 gives a direct physical test of which parameter is a background. Let $m_0 \mapsto m_0 + \delta$ while remaining in the positive-area chamber. The two

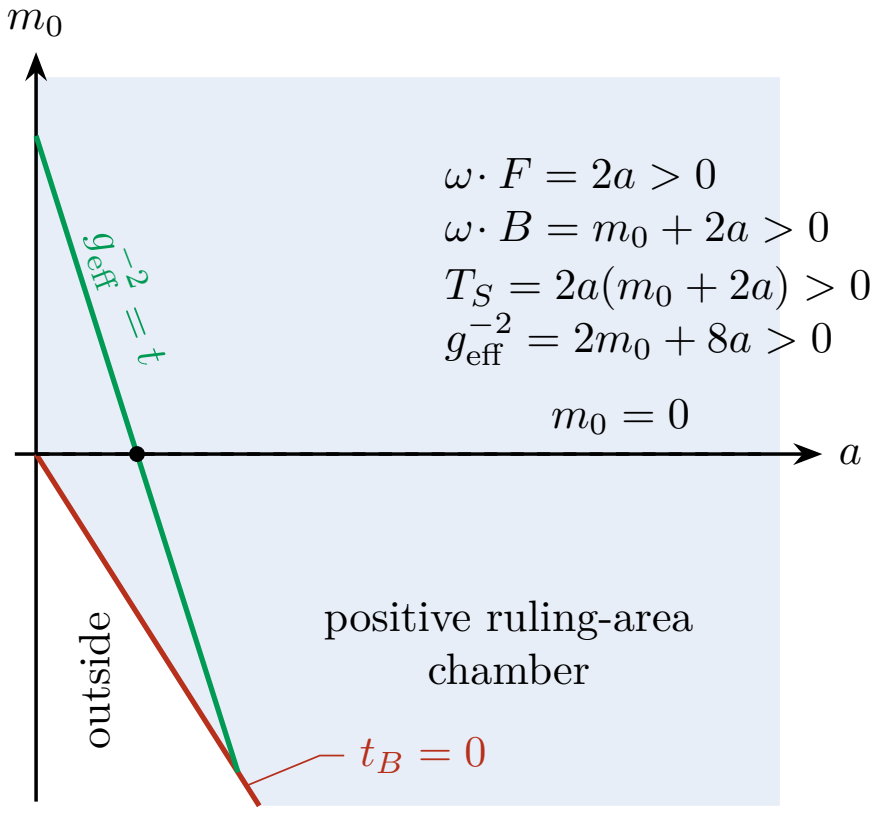


Figure XIII.2.2: The positive local F_0 ruling-area region is to the right of $a = 0$ and above $m_0 = -2a$. Along a fixed effective-Hessian line $2m_0 + 8a = t$, the metric stays positive while the B curve and compact surface can shrink. Here T_S is the relative magnetic-string tension $T_{\text{mag}}^{(\text{rel})}$ and g_{eff}^{-2} is the IMS Hessian g_{aa}^{IMS}. The $m_0 = 0$ slice alone does not establish a UV fixed point.

curve periods become

$$t_F \mapsto t_F, \qquad t_B \mapsto t_B + \delta. \tag{XIII.2.44}$$

The root mass is unchanged. The surface area and effective metric instead respond linearly:

$$\Delta T_{\text{mag}}^{(\text{rel})} = 2a\delta, \qquad \Delta g_{aa}^{\text{IMS}} = 2\delta. \tag{XIII.2.45}$$

For example, at $a = 1$, increasing m_0 from 3 to 4 gives

$$(t_F, t_B, T_{\text{mag}}^{(\text{rel})}, g_{aa}^{\text{IMS}}) : (2, 5, 10, 14) \longmapsto (2, 6, 12, 16). \tag{XIII.2.46}$$

The unchanged first entry is the W mass. The displacement changed the theory's coupling parameter without adding another dynamical Coulomb coordinate.

The distinction between a Coulomb displacement and a background displacement can also be seen without referring to the divisor basis. Use the ruling periods as coordinates on the two-parameter family:

$$u = t_F = 2a, \qquad v = t_B = m_0 + 2a, \qquad a = \frac{u}{2}, \quad m_0 = v - u. \tag{XIII.2.47}$$

The open geometric chamber is the quadrant $u, v > 0$; the nonnegative bare-coupling part has $v \geq u$. A Coulomb motion at fixed m_0 lies on a line $v - u = m_0$, with both periods changing equally. In particular, "keep the second curve fixed" is not the same instruction as "keep the background fixed."

The representative cubic, now in these two periods, is

$$\widetilde{\mathcal{F}}(u, v) = (v - u)\frac{u^2}{4} + \frac{u^3}{6} = \frac{u^2 v}{4} - \frac{u^3}{12}. \tag{XIII.2.48}$$

To extract a primitive tension we need the tangent that keeps $v - u$ fixed. The chain rule gives

$$\partial_a|_{m_0} = 2\partial_u + 2\partial_v, \qquad (2\partial_u + 2\partial_v)\widetilde{\mathcal{F}} = uv = \mathrm{vol}_\omega(S). \tag{XIII.2.49}$$

The area derivative in the same direction is

$$(2\partial_u + 2\partial_v)(uv) = 2(u + v) = 2m_0 + 8a = g_{aa}^{\mathrm{IMS}}. \tag{XIII.2.50}$$

This reproduces the finite geometric area response of (XIII.2.27). No polynomial term depending only on $m_0 = v - u$ can affect these derivatives, since $(\partial_u + \partial_v)(v - u) = 0$.

Now hold v fixed while increasing a. The root period still obeys $u = 2a$, but $m_0 = v - 2a$ changes. Substituting this condition before differentiating gives

$$\begin{aligned} \mathcal{F}(a; v - 2a) &= va^2 - \frac{2}{3}a^3, \\ \left.\frac{d\mathcal{F}}{da}\right|_v &= 2va - 2a^2 = T_{\mathrm{mag}}^{(\mathrm{rel})} - 2a^2. \end{aligned} \tag{XIII.2.51}$$

This derivative is mathematically correct for that path, but is not the primitive string tension. In the original variables it is $\mathcal{F}_a - 2\mathcal{F}_{m_0}$, with $\mathcal{F}_{m_0} = a^2$ for our representative. If an arbitrary background polynomial were retained, the path derivative would also contain its change. A comparison that varies a background is sensitive to the chosen background representative; the fixed-background tension is insensitive to it.

At $a = 1, m_0 = 3$, we have $(u, v) = (2, 5)$ and $T = 10$. Increasing a by $1/2$ at fixed m_0 gives $(3, 6)$ and $T = 18$; at fixed v it instead gives $(3, 5)$, $m_0 = 2$ and $T = 15$. Figure XIII.2.3 shows the different endpoints. The initial derivatives of the representative prepotential along the two paths are respectively 10 and 8. These are different questions asked of the same function, rather than a disagreement between a curve area and a surface area.

There is a sharper test in which the *effective* Hessian is held fixed. Denote its positive value by t and solve (XIII.2.36) for the background:

$$m_0(a) = \frac{t}{2} - 4a, \qquad t_F = 2a, \qquad t_B = \frac{t}{2} - 2a, \qquad T_{\mathrm{mag}}^{(\mathrm{rel})} = ta - 4a^2. \tag{XIII.2.52}$$

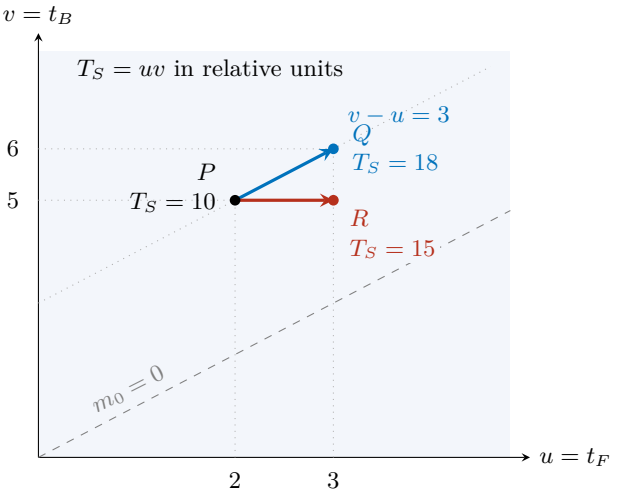


Figure XIII.2.3: Two motions from the same positive-period point $P = (t_F, t_B) = (2, 5)$. The blue path keeps the background $m_0 = t_B - t_F = 3$ fixed and ends at $Q = (3, 6)$. The red path keeps $t_B = 5$ fixed and ends at $R = (3, 5)$, where $m_0 = 2$. Both paths increase a by $1/2$. The product $t_F t_B$ is the compact-surface area at every point, so it becomes 18 at Q and 15 at R, starting from 10 at P. The diagonal grey line is $m_0 = 0$; the illustrated points all have positive bare inverse coupling.

The positive-area interval is $0 < a < t/4$. At its upper end B shrinks and the string becomes tensionless, even though $g_{aa}^{\mathrm{IMS}} = t$ is still strictly positive. For the concrete choice $t = 8$, the point $(a, m_0) = (1, 0)$ has $(t_F, t_B, T_{\mathrm{mag}}) = (2, 2, 4)$; the point $(a, m_0) = (3/2, -2)$ has $(3, 1, 3)$. At $a = 2$ the second curve and the surface reach zero area while the Hessian is still 8. The latter point is a chamber boundary, not an interior smooth gauge vacuum. The intermediate point has positive geometric ruling areas, but its negative m_0 is not a weakly coupled bare gauge description; the continuation tests geometric positivity and the protected polynomial only. Figure XIII.2.2 shows where a fixed-Hessian line leaves the positive ruling-area chamber.

On the simpler path with $m_0 \geq 0$ fixed and $a \to 0^+$, the W mass and magnetic-string tension vanish, whereas the Hessian tends to $2m_0$. At $m_0 = 0$ the polynomial is purely cubic: $T_{\mathrm{mag}}^{(\mathrm{rel})} = 4a^2$ and $g_{aa}^{\mathrm{IMS}} = 8a$. Equivalently, the curves and surface have the limiting behavior

	t_F	t_B	$T_{\mathrm{mag}}^{(\mathrm{rel})}$
$m_0 > 0$ fixed, $a \to 0^+$	$2a$	$m_0 + 2a$	$2m_0 a + O(a^2)$
$m_0 = 0$, $a \to 0^+$	$2a$	$2a$	$4a^2$

. (XIII.2.53)

Only the first ruling shrinks on the first path; both do on the second. These limits identify protected quantities that become small. Whether the singular point defines a particular UV fixed point also depends on the global geometry and physical decoupling data, which have not been extracted from this local cubic.

XIII.2.7 Can the observables reconstruct the two curve periods?

The same relations can be read in reverse. Suppose that, within the selected pure $SU(2)$ chamber, one knows the W mass w, the primitive relative string tension T, and the effective Hessian g. If the local F_0 description is correct, the first ruling period is $t_F = w$ and the area of the product surface is

$$T = t_F t_B = w\, t_B. \tag{XIII.2.54}$$

For $w > 0$ this determines the other period:

$$t_B = \frac{T}{w}, \qquad a = \frac{w}{2}, \qquad m_0 = t_B - t_F = \frac{T}{w} - w. \tag{XIII.2.55}$$

The inverse coupling is therefore inferred from a difference of periods after the W normalization has been fixed. The formula also shows why a zero W mass is a singular point for this reconstruction: one cannot divide by w at the collapsing-curve boundary.

The Hessian is then predicted rather than fitted. From (XIII.2.36) and (XIII.2.18),

$$g = 2m_0 + 8a = 2(t_F + t_B) = 2\left(w + \frac{T}{w}\right). \tag{XIII.2.56}$$

For example, if $w = 2$ and $T = 10$, the geometry requires $t_B = 5$, $m_0 = 3$, and $g = 14$. A measured Hessian of 13 with the same w and T would contradict this *particular* local-F_0 parameter map; changing D^3 could not repair it, because D^3 disappears from all three quantities. The conclusion is about protected gauge-chamber data. It does not claim that three observables identify an entire quantum field theory.

There is also a differential version. At fixed background,

$$\left.\frac{\partial T}{\partial a}\right|_{m_0} = g, \qquad dT = g\, da + w\, dm_0. \tag{XIII.2.57}$$

The first equality is the prepotential relation between a magnetic string and the vector kinetic metric. The second says how a background displacement enters: its coefficient is precisely the W period. It reproduces (XIII.2.45) without treating m_0 as another dynamical scalar.

The same differential tells us precisely where the inverse map fails. The Jacobian of the two observables with respect to the two parameters is

$$\frac{\partial(w, T)}{\partial(a, m_0)} = \begin{pmatrix} 2 & 0 \\ g & w \end{pmatrix}, \qquad \det \frac{\partial(w, T)}{\partial(a, m_0)} = 2w. \tag{XIII.2.58}$$

It is invertible in the open chamber. At the worked point $w = 2$, $T = 10$, its determinant is 4; a small change of either observable can therefore be translated into a unique parameter displacement. Differentiating the inverse formula makes that translation explicit:

$$da = \frac{1}{2}\, dw, \qquad dm_0 = \frac{dT}{w} - \left(1 + \frac{T}{w^2}\right) dw. \tag{XIII.2.59}$$

For instance, changing the tension at fixed nonzero w changes only the background, by dT/w. Close to $w = 0$ this inference becomes sensitive to a small error in the tension. To approach $a = 0$ from inside the positive-area chamber at fixed finite m_0 requires $m_0 \geq 0$. Along any such path $(w, T) \to (0, 0)$, so this limiting pair cannot distinguish backgrounds. The protected polynomial has limiting Hessian $g \to 2m_0$, but the smooth Abelian description fails at the massless-W wall.

As a transfer example, take a nearby allowed pair of observables $w = 3$ and $T = 18$. The reconstruction gives

$$t_B = \frac{18}{3} = 6, \qquad a = \frac{3}{2}, \qquad m_0 = 6 - 3 = 3, \qquad g = 2(3 + 6) = 18. \tag{XIII.2.60}$$

This is precisely the fixed-background endpoint Q of Figure XIII.2.3. With the same $w = 3$ but $T = 15$, we would instead infer $t_B = 5$, $m_0 = 2$, and $g = 16$. The two equal W masses do not fix the theory's coupling parameter. A surface measurement distinguishes the two backgrounds, while the Hessian checks the resulting geometric interpretation.

XIII.2.8 What changes with a divisor basis?

An intersection tensor is useful only with a coordinate map. To see the issue, choose another noncompact divisor lift

$$D' = D + \lambda S. \tag{XIII.2.61}$$

The same signed class is now

$$A = aS - m_0 D = a'S - m_0 D', \qquad a' = a + \lambda m_0. \tag{XIII.2.62}$$

The coefficient a' is generally *not* the physical scalar defined by $m_W = 2a$. Indeed, $D'|_S = F + \lambda K_S$ and

$$m_W = -A \cdot F = 2(a' - \lambda m_0). \tag{XIII.2.63}$$

We can see the same point directly in the transformed intersection tensor. The compact cube stays $S^3 = 8$, but the mixed components become

$$\begin{aligned} S^2 D' &= S^2 D + \lambda S^3 = -2 + 8\lambda, \\ SD'^2 &= SD^2 + 2\lambda S^2 D + \lambda^2 S^3 = -4\lambda + 8\lambda^2. \end{aligned} \tag{XIII.2.64}$$

These changes follow from $D' = D + \lambda S$. If the original basis is integral, $\lambda \in \mathbb{Z}$ gives an integral change of basis. For $\lambda = 1/2$ we work only in the rational span. In that example, $S^2 D' = 2$ while $SD'^2 = 0$. Reading the first number as if a' were still the root-normalized scalar would reverse the apparent sign of the quadratic coupling. The actual root period (XIII.2.63) prevents that mistake.

Choose the representative of (XIII.2.29) with $U(m_0) = 0$ in the original coordinates. Substituting $a = a' - \lambda m_0$ gives

$$\begin{aligned} \mathcal{F} &= m_0(a' - \lambda m_0)^2 + \frac{4}{3}(a' - \lambda m_0)^3 \\ &= \frac{4}{3}a'^3 + (1 - 4\lambda)m_0 a'^2 + (4\lambda^2 - 2\lambda)m_0^2 a' + \left(\lambda^2 - \frac{4}{3}\lambda^3\right) m_0^3. \end{aligned} \tag{XIII.2.65}$$

The mixed coefficients visibly change under a lift change. This is coordinate covariance, not a changed physical mass: one must transform the Coulomb coordinate and the W-period map together.

The induced term proportional to m_0^3 is needed if we compare the *same representative function* in the two coordinates. To see its geometric origin, temporarily assign $D^3 = k$ in one chosen relative prescription. The transformed noncompact cube is then

$$\begin{aligned} D'^3 &= D^3 + 3\lambda S D^2 + 3\lambda^2 S^2 D + \lambda^3 S^3 \\ &= k - 6\lambda^2 + 8\lambda^3. \end{aligned} \tag{XIII.2.66}$$

For $k = 0$, its contribution to $A^3/6$ is $(\lambda^2 - 4\lambda^3/3)m_0^3$, exactly the last term of (XIII.2.65). A choice $D^3 = 0$ in the old prescription does not also give $D'^3 = 0$ after this lift change. One can discard a background-only function after the comparison, but should not mistake that further choice for the coordinate change itself.

Let $G(a', m_0) = \mathcal{F}(a' - \lambda m_0, m_0)$ denote the same representative. At fixed m_0, the old and new compact coordinates have identical increments: $da' = da$. The chain rule therefore yields

$$G_{a'} = \mathcal{F}_a = T^{(\mathrm{rel})}_{\mathrm{mag}}, \qquad G_{a'a'} = \mathcal{F}_{aa} = g^{\mathrm{IMS}}_{aa}, \qquad G_{a'a'a'} = 8. \tag{XIII.2.67}$$

The expressions on the right are evaluated at $a = a' - \lambda m_0$. Explicitly,

$$\begin{aligned} G_{a'} &= 4a'^2 + (2 - 8\lambda)m_0 a' + (4\lambda^2 - 2\lambda)m_0^2, \\ G_{a'a'} &= 8a' + (2 - 8\lambda)m_0. \end{aligned} \tag{XIII.2.68}$$

Substitution of $a' = a + \lambda m_0$ reduces them to $4a^2 + 2m_0 a$ and $8a + 2m_0$. A term linear in a' and quadratic in m_0 can appear in the new cubic even though $SD^2 = 0$ in the old lift. Its derivative is required for the area to stay unchanged.

Background differentiation requires more care, because fixing a' is not fixing the physical root scalar a. The other chain-rule identities are

$$\begin{aligned} G_{m_0} &= \mathcal{F}_{m_0} - \lambda \mathcal{F}_a, \\ G_{a'm_0} &= \mathcal{F}_{am_0} - \lambda \mathcal{F}_{aa}, \\ G_{m_0 m_0} &= \mathcal{F}_{m_0 m_0} - 2\lambda \mathcal{F}_{am_0} + \lambda^2 \mathcal{F}_{aa}. \end{aligned} \tag{XIII.2.69}$$

These are algebraic derivatives on the two-parameter family, not the components of a kinetic matrix for an additional dynamical scalar. They tell us which direction was held fixed. To reproduce the earlier experiment that varied m_0 at fixed a, use

$$\partial_{m_0}|_a = \partial_{m_0}|_{a'} + \lambda\, \partial_{a'}|_{m_0}, \qquad G_{m_0} + \lambda G_{a'} = \mathcal{F}_{m_0}. \tag{XIII.2.70}$$

The corresponding tension response is consequently

$$(\partial_{m_0} + \lambda \partial_{a'})\, G_{a'} = G_{a'm_0} + \lambda G_{a'a'} = 2a. \tag{XIII.2.71}$$

This restores the coefficient of the fixed-a background shift in (XIII.2.45).

For a concrete integral lift, take $\lambda = 1$. The point $(a, m_0) = (1, 3)$ has new coordinate $a' = 4$, and

$$G(a', m_0) = \frac{4}{3}a'^3 - 3m_0a'^2 + 2m_0^2a' - \frac{1}{3}m_0^3. \tag{XIII.2.72}$$

At $(a', m_0) = (4, 3)$ this gives $G = 13/3$, $G_{a'} = 10$, and $G_{a'a'} = 14$, agreeing with the original frame. But its background derivative at fixed a' is $G_{m_0} = -9$, whereas at fixed a it is

$$G_{m_0} + G_{a'} = -9 + 10 = 1 = \mathcal{F}_{m_0}. \tag{XIII.2.73}$$

The difference has a simple geometric explanation: increasing m_0 while holding $a' = 4$ decreases $a = a' - m_0$, so the W mass decreases. The old fixed-a experiment instead keeps that mass constant and moves a' along with m_0. The changed mixed coefficients describe these different coordinate directions on one and the same family.

There is a narrower ambiguity even with the lift fixed. Assigning a prescription-dependent value $D^3 = k$ adds $-km_0^3/6$ to (XIII.2.29). At fixed m_0 it changes no derivative with respect to a. In contrast, changing the lift as in (XIII.2.61) can put background parameters into the coefficient of S. One must not describe every noncompact ambiguity as a background-only constant before saying which physical coordinates are being held fixed.

Finally, the compact cube does not identify a UV theory. The Hirzebruch surface F_1 also has $K^2 = 8$: with a section E of $E^2 = -1$ and a fiber f with $f^2 = 0$, $E \cdot f = 1$ and $K_{F_1} = -2E - 3f$, so $K_{F_1}^2 = 8$. Yet F_1 has a (-1)-curve while the two generators of the F_0 Mori cone have square zero. The anticanonical degrees make the difference quantitative:

$$-K_{F_0} \cdot B = -K_{F_0} \cdot F = 2, \qquad -K_{F_1} \cdot E = 1, \quad -K_{F_1} \cdot f = 2. \tag{XIII.2.74}$$

Thus even when both compact surfaces have cube 8, their primitive curve areas on the $m_0 = 0$ compact ray need not have the same ratios. The curve chambers and possible contractions therefore carry information invisible to the one number S^3. It is still less reasonable to extract a global gauge group, discrete theta angle, or complete BPS spectrum from that number. Such questions need further geometric or physical input.

XIII.2.9 Exercises

For Exercises 1–5, give exact polynomial answers. Use `a` for the Coulomb coordinate, `m` for m_0, and `d` for a parameter change or the basis-shift coefficient as specified. Write fractions in exact form, such as `4/3`. Use `benchmark/tasks.json` to find the question IDs and `benchmark/PROTOCOL.md` for submission. Include the derivation, with a complete written explanation for Exercise 6.

1. **Intersections to cubic (E1).** Using (XIII.2.7) and $D|_S = F$, calculate S^3, S^2D, and the compact-dependent prepotential. Submit `cube`, `mixed`, and `prepotential`.

2. **Coupling displacement (E2).** Differentiate (XIII.2.29) to obtain its Hessian and primitive relative string tension. Then hold a fixed and replace m_0 by $m_0 + d$;

find the changes of both quantities. Submit `hessian`, `tension`, `delta_hessian`, and `delta_tension`.

3. **The sign of the Kähler class (E3).** Start from the positive class $\omega = -aS + m_0 D$. Compute its periods on F and B. Give the compact-dependent polynomial obtained from the correct signed prescription $A^3/6 = -\omega^3/6$, and the wrong-sign compact-dependent polynomial from $+\omega^3/6$. Submit `omega_f`, `omega_b`, `physical_from_omega`, and `raw_omega_cubic`. Explain verbally why only one sign has the positive surface-area derivative.

4. **Noncompact cubic (E4).** For illustration only, choose a relative prescription $D^3 = 1$. Expand $A^3/6$ and separate its compact-dependent part from the background-only part. Submit `compact_dependent` and `background_only`. Recalculate $\partial_a \mathcal{F}$ and say which part survives.

5. **Change the divisor lift (E5).** Take $D' = D + dS$ and call the coefficient of S in the new signed expansion a'; enter that coefficient as `a` in this exercise. Express the old physical scalar in terms of the new coefficient. Start with the representative of (XIII.2.29) with $U(m_0) = 0$ and substitute $a = a' - dm_0$. Retain every generated term, including the background-only term in (XIII.2.65). Give the resulting prepotential and the W mass as functions of `a`, `m`, `d`. Submit `physical_a`, `prepotential_new`, and `w_mass_new`. State why setting $m_W = 2a'$ would be a coordinate error.

6. **Equal cubes (written E6).** Compute $K_{F_1}^2$ from its section and fiber pairing. Identify one geometric feature distinguishing F_1 from F_0 that the equal cubes omit. Explain why this omission prevents the cube from identifying the UV completion or discrete gauge data.

The following additional problems are written practice. They do not change the five graded submissions above.

7. **A period and its coefficients.** For $C = 2B + F$, compute q_C, b_C, and t_C. At fixed m_0, compare $\partial_a t_C$ with the Coulomb-period coefficient. Explain which extra question would have to be answered before calling this class a new stable BPS particle.

8. **Choose the derivative before evaluating it.** At $(a, m_0) = (1, 3)$, compute the initial area response to increasing a while holding m_0 fixed, and while holding t_B fixed. Then use $\widetilde{\mathcal{F}}(u, v)$ to compute the corresponding two first derivatives of the representative prepotential. Explain why the prepotential derivatives and the area derivatives have different units.

9. **An integral lift.** Set $\lambda = 1$ and use (XIII.2.72). At $(a', m_0) = (4, 3)$, calculate the tension response to m_0 first at fixed a', then at fixed a. Account for their difference using the chain rule. Re-express the same primitive tension in the coordinate $z = 2a$ and explain why $\widehat{\mathcal{F}}_z$ alone is insufficient.

Take-home message of this chapter

On local F_0, the compact surface and its two ruling curves give three linked observables: $m_W = 2a$, $T^{(\mathrm{rel})}_{\mathrm{mag}} = 2m_0 a + 4a^2$, and $g^{\mathrm{IMS}}_{aa} = 2m_0 + 8a$. Adjunction fixes the compact cube, but the physical polynomial also needs a signed Kähler-coordinate map and a fixed noncompact divisor lift. The protected gauge-phase data do not by themselves determine the singular UV theory.

Status and sources

Section XIII.2.1: wrapped branes. The M2-particle and M5-string interpretation and the distinction between dynamical compact modes and noncompact backgrounds use the M-theory dictionary [GEO-X] of Jefferson et al. (2018, PDF pp. 12–14, eqs. (2.6)–(2.15)) in the stated local gauge phase. Decoupling gravity and other coupled sectors remains a separate condition [DEC].

Section XIII.2.2: intersection derivatives. Equation (XIII.2.2) follows from the symmetric cubic [MATH]. Its tension and kinetic interpretations use JKKV (2.9)–(2.12) [GEO-X] in the chosen orientation.

Section XIII.2.3: compact intersections. The degree rule, ruling pairing, adjunction and the explicit restriction calculations give (XIII.2.11) and (XIII.2.14) [MATH]. An ordinary local degree for D^3 is not part of that calculation.

Section XIII.2.4: periods and sign. The periods and area in (XIII.2.18) and (XIII.2.25) are computed from $\omega|_S$ [MATH]. The period-coefficient table and effective-class periods follow by linearity of the same intersections. For general classes these are coefficient calculations, with no additional electric-charge dictionary or BPS-state inventory asserted. The root-fiber charge uses JKKV (2.15); its sign discussion at Jefferson et al. (2018, PDF p. 16, eq. (3.1) and following paragraph) motivates distinguishing A from ω [GEO-X]. For the area we use the 1/2! in JKKV (2.10), which the later signed-volume shorthand omits.

Section XIII.2.5: IMS comparison. The cubic expansion, scalar distance, root-coordinate rescaling, and independent area/derivative comparison are calculations in the chosen coordinates [MATH]. The factors in the absolute-versus-relative brane formulas recall the same wrapped-brane dictionary; their numerical action constants are not determined here. The trace form and root-minus-weight formula come from Intriligator et al. (1997, PDF pp. 10–11, eq. (2.22) and chamber discussion); (XIII.2.33)–(XIII.2.34) give our $SU(2)$ substitution. We use IMS's cubic root power; the inspected JKKV (2.2) prints 2. The interpretation of (XIII.2.35)–(XIII.2.36) uses JKKV (2.9)–(2.12) in the stated relative magnetic unit [GEO-X]. The two cubics compare one protected function in a common gauge phase; they do not establish a complete equivalence or absolute M5 tension.

Section XIII.2.6: paths and limits. Equations (XIII.2.45), (XIII.2.52) and (XIII.2.53) and the period-plane tangent calculation follow from the period and derivative formulas [MATH]. In particular, fixed t_B and fixed m_0 are different paths on the same two-parameter family. The collapse rates do not settle the decoupling or UV question

[DEC].

Section XIII.2.7: inverse map. Equation (XIII.2.55) and the Jacobian (XIII.2.58) are algebra in the same period and tension frame [MATH]; they do not introduce a new brane dictionary.

Section XIII.2.8: lift and equal cubes. Equations (XIII.2.64) and (XIII.2.65) follow by changing the lift and coordinates, including the full fixed-background chain rule and the induced noncompact cube, [MATH]. For the Hirzebruch canonical square and rank-one context of (XIII.2.74), see Jefferson et al. (2018, PDF pp. 32–33, especially eq. (4.5)). The local calculation does not determine a UV SCFT, complete BPS spectrum, global gauge choice or discrete theta angle.

References

Intriligator, K. A., D. R. Morrison, and N. Seiberg (1997). "Five-dimensional supersymmetric gauge theories and degenerations of Calabi-Yau spaces". In: *Nucl. Phys. B* 497, pp. 56–100. DOI: 10.1016/S0550-3213(97)00279-4. arXiv: hep-th/9702198.

Jefferson, P. et al. (2018). "On Geometric Classification of 5d SCFTs". In: *JHEP* 04, p. 103. DOI: 10.1007/JHEP04(2018)103. arXiv: 1801.04036 [hep-th].

Chapter XIII.3

Matter and masses from blown-up surfaces

XIII.3.1 Adding matter without adding a gauge scalar

A moving rational curve supplies the W boson in the rank-one construction of the previous chapters. Can the same compact surface supply a charged hypermultiplet while keeping just one Coulomb scalar? We will blow up a point on a ruled surface. The generic fiber keeps moving, but the fiber through the chosen point acquires two isolated components. Their areas determine a new mass parameter. Their signed charges explain why the components describe the two weights of one fundamental hypermultiplet.

We use the surface intersection and wrapped-brane conventions of Chapters 1 and 2. We work with ordinary M-theory without background flux. Take the local limit in which the regulated internal volume grows relative to the gravitational coupling while the compact periods are held finite in field-theory units. The 5D Planck scale then diverges. We take the compact gauge mode to be localized and normalizable and the asymptotic mass and coupling parameters to be fixed backgrounds. We also assume that unwanted modes decouple from the protected sector under study. An infinite internal volume alone does not imply that all bulk or Kaluza–Klein modes become heavy.

XIII.3.2 A ruled surface with one split fiber

How does a point blowup isolate part of a fiber while preserving the ruling? Start with the product $\mathbb{P}^1_B \times \mathbb{P}^1_F$ and project onto the first factor. The section class is B and the fiber class is F. Choose a point p on the product and blow it up. Write

$$S = \mathrm{Bl}_p(\mathbb{P}^1_B \times \mathbb{P}^1_F), \qquad X = \mathrm{Tot}(K_S), \tag{XIII.3.1}$$

where S sits in X as the zero section. We use the same letters B, F for the total transforms. A generic representative of either class avoids p. The curves through p need

a different description.

Choose coordinates (x, y) centered at p, with the projection locally given by x. The two charts of the surface blowup have maps

$$(x, y) = (u, uv), \qquad (x, y) = (tw, w), \qquad w = uv, \quad t = v^{-1} \tag{XIII.3.2}$$

on their common domain. The exceptional curve E is $u = 0$ in the first chart and $w = 0$ in the second. In the second chart the fiber $x = 0$ has equation $tw = 0$. Its proper transform R is $t = 0$, so R and E meet transversely, each with multiplicity one. The proper transform L of the section $y = 0$ meets E in the other tangent direction. Figure XIII.3.1 shows which components survive as separate curves.

$$R = F - E, \qquad L = B - E, \qquad F = E + R. \tag{XIII.3.3}$$

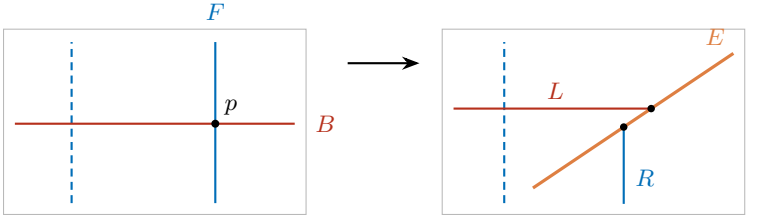


Figure XIII.3.1: The ruling before and after blowing up p. On the right the fiber through p is replaced by $E \cup R$. The proper transforms L and R meet E at distinct points. The dashed fiber still moves.

The product supplies $B \cdot F = 1$ and $B^2 = F^2 = 0$. Total transforms have zero pairing with E, whose normal line in the surface is $\mathcal{O}(-1)$, as one sees from $w = vu$ in the blowup charts. The intersection matrices in the two useful bases are therefore

$$(C_i \cdot C_j)_{(B,F,E)} = \begin{pmatrix} 0 & 1 & 0 \\ 1 & 0 & 0 \\ 0 & 0 & -1 \end{pmatrix}, \qquad (C_i \cdot C_j)_{(E,R,L)} = \begin{pmatrix} -1 & 1 & 1 \\ 1 & -1 & 0 \\ 1 & 0 & -1 \end{pmatrix}. \tag{XIII.3.4}$$

In particular, the two components of the special fiber each have self-intersection -1. Their sum has square $-1 + 2 - 1 = 0$, as a moving fiber should.

The distinction between a total transform and a proper transform is already visible in the equation $x = tw$. Pulling back the divisor $x = 0$ retains both factors. Removing the exceptional factor $w = 0$ leaves the proper transform $t = 0$. Thus the area of a generic fiber is retained by its total class, while the area assigned to the proper transform subtracts the exceptional area. The intersection calculation keeps track of that subtraction. For example,

$$E \cdot R = E \cdot (F - E) = 1, \qquad R^2 = (F - E)^2 = -1, \qquad R \cdot L = (F - E) \cdot (B - E) = 0. \tag{XIII.3.5}$$

The last zero has a geometric meaning. Before the blowup, the selected section and fiber met at p. After the blowup their distinct tangent directions meet distinct points of the exceptional line. Their old intersection has been replaced by two incidences with E.

The product has canonical class $-2B-2F$. In the first blowup chart the pullback of its local canonical form is

$$dx \wedge dy = u\, du \wedge dv. \tag{XIII.3.6}$$

The factor u gives the exceptional term $+E$ in the new canonical class. Using the pairing above gives

$$\begin{aligned} K_S &= -2B-2F+E, & K_S^2 &= 8-1=7, \\ K_S\cdot F &= -2, & K_S\cdot E = K_S\cdot R &= K_S\cdot L = -1. \end{aligned} \tag{XIII.3.7}$$

The blowup changes the compact cubic through K_S^2. It leaves the pairing with a generic fiber unchanged.

Adjunction distinguishes the genus of a curve from whether that curve can move. For a smooth curve C in the surface, its arithmetic genus is

$$p_a(C) = 1+\tfrac{1}{2}(C^2+K_S\cdot C), \qquad p_a(E)=p_a(R)=p_a(L)=p_a(F)=0. \tag{XIII.3.8}$$

All four curves are rational, but only the fiber belongs to the ruling. For E, R, L the normal line in S has degree -1, with no sections; for F it has degree zero and one section. The latter moves the fiber along the base. The blowup therefore changes the deformation problem for the special fiber components while leaving the generic family available to carry the gauge root.

We will need all compact curve inequalities to locate a wall. To obtain them, choose p at the torus fixed point where the two chosen curves meet. The fan starts with the four coordinate rays. Inserting the sum of the first two rays at the blowup gives

$$\big(v_L, v_E, v_R, v_B, v_F\big) = \big((1,0),(1,1),(0,1),(-1,0),(0,-1)\big) \tag{XIII.3.9}$$

in cyclic order. Removing the disjoint rays v_L, v_R undoes two point blowups. The three remaining rays give the fan of $\mathbb{P}^2$. In the resulting plane basis, L and R are the exceptional classes, E is the proper transform of the line joining the blown-up points, and H is the pullback of a line.

$$H = B+F-E, \qquad E = H-L-R, \qquad (C_i\cdot C_j)_{(H,L,R)} = \operatorname{diag}(1,-1,-1). \tag{XIII.3.10}$$

Thus S is dP_2. The subscript counts the plane blowups, while its del Pezzo degree is seven.

A plane curve of degree d can have multiplicity at most d at either point. For multiplicities b_1, b_2, its proper transform has class

$$dH - b_1L - b_2R = dE + (d-b_1)L + (d-b_2)R. \tag{XIII.3.11}$$

Together with L, R this covers the irreducible curves of S. The classes E, R, L are represented by curves and are linearly independent, so their positive span is exactly the cone of effective numerical curve classes. For instance, a line through just the first

point has class $H - L = E + R = F$. This gives the same fiber class without treating both components as independent movable fibers.

The cone description can be used without drawing a new curve each time. Write a numerical effective class as $C = uE + vR + wL$, with $u, v, w \geq 0$. Bilinearity gives

$$\begin{aligned} C^2 &= -u^2 - v^2 - w^2 + 2uv + 2uw, \\ -K_S \cdot C &= u + v + w, \qquad C \cdot E = -u + v + w. \end{aligned} \tag{XIII.3.12}$$

The anticanonical degree is strictly positive for any nonzero effective class. This will both ensure that a compact curve stays in the zero section and determine its electric charge. The self-intersection and incidence information are also needed: electric charge alone does not determine the kind of particle supplied by a curve.

Compare $C = F = E + R$ with $C = 2E$. Both have anticanonical degree two, but their intersections with E are different:

$$F \cdot E = 0, \qquad (2E) \cdot E = -2, \qquad F^2 = 0, \qquad (2E)^2 = -4. \tag{XIII.3.13}$$

Distinct irreducible effective curves on a smooth surface have nonnegative intersection. Any effective divisor in class $2E$ must therefore contain E; after subtracting it the remaining class is E again. This is a fixed multiple of the isolated exceptional curve. It cannot replace the moving fiber in the gauge construction. This test uses geometry beyond the charge pairing and will be useful when interpreting the charge table.

Lifting the five rays in (XIII.3.9) to height one and joining them to $(0, 0, 1)$ gives the smooth crepant fan of X. The interior ray is the compact divisor S. Compact curves cannot move out of the zero section. A compact curve projecting nontrivially to S would give a section of the pullback of K_S on its normalization. This line bundle has negative degree by (XIII.3.7) and (XIII.3.11). The section must vanish. A curve projecting to one point cannot be compact in an affine line fiber. We can therefore test compact curve positivity using the three rays of S.

XIII.3.3 Coulomb charge and real mass

Which combination of curve areas measures the mass at fixed Coulomb scalar? The blowup gives one additional independent curve area but no additional compact divisor. To separate the new mass from the Coulomb scalar, we first specify the backgrounds. Let $\pi : X \to S$ be the bundle projection and let D_0, D_m be the noncompact divisor classes

$$D_0 = \pi^{-1}(F), \qquad D_m = \pi^{-1}(E) - \tfrac{1}{2} D_0. \tag{XIII.3.14}$$

The half in the second definition is allowed because this is a real background direction. It does not make D_m a primitive integral divisor. We will see why subtracting this half is useful when we compare the bare coupling.

The normal bundle of the zero section is K_S, so $S|_S = K_S$. In the period units of Chapter 2, write the positive class and the gauge scalar as

$$\omega = -aS + m_0 D_0 + m D_m, \qquad \Phi = a H_g, \qquad H_g = \operatorname{diag}(1, -1), \qquad a > 0. \tag{XIII.3.15}$$

Here m_0 denotes the inverse bare coupling parameter in the fundamental-trace convention and m is the signed real mass. For a curve with an assigned orientation, its central charge in this frame is a signed period. Define the three charges by its coefficients.

$$\begin{aligned} Z_C &= \omega \cdot C = q_C a + I_C m_0 + f_C m, \\ q_C &= -K_S \cdot C, \qquad I_C = F \cdot C, \qquad f_C = (E - F/2) \cdot C. \end{aligned} \tag{XIII.3.16}$$

An effective curve with its complex orientation has $V_C = Z_C > 0$ in the open chamber. Reversing the orientation reverses the charges and Z_C. If the corresponding BPS particle exists, its mass is $|Z_C|$, in either orientation. Table XIII.3.1 evaluates the pairings.

Table XIII.3.1: Oriented curve charges in the chosen mass and coupling frame.

C	C^2	q_C	I_C	f_C	Z_C
F	0	2	0	0	$2a$
B	0	2	1	$-1/2$	$2a + m_0 - m/2$
E	-1	1	0	-1	$a - m$
R	-1	1	0	1	$a + m$
L	-1	1	1	$1/2$	$a + m_0 + m/2$
H	1	3	1	$1/2$	$3a + m_0 + m/2$

The moving fiber gives the W boson of the ordinary rank-one gauge patch. Its electric charge 2 agrees with the positive root evaluated on H_g. The two isolated curves have the same positive electric charge in their effective orientations. To read a representation, however, compare the two weights at the same flavor charge $+1$. They have oriented classes and signed charges

$$C_+ = R, \quad C_- = -E, \qquad C_+ - C_- = F, \qquad Z_+ = m + a, \quad Z_- = m - a. \tag{XIII.3.17}$$

Their electric charges are $+1, -1$, separated by the root charge 2. At $|m| < a$ the lower weight has negative Z_-, and the effective curve E represents its conjugate orientation. This explains why one cannot read the two weights by simply taking both positive areas as signed charges.

There are two different operations in this reading of the weights. At fixed curve orientation, varying m changes a signed period. At fixed geometry, reversing the orientation changes all charges at once. For the two flavor-$+1$ weights one finds

$$Z_+ + Z_- = 2m, \qquad Z_+ - Z_- = 2a, \qquad |Z_+| + |Z_-| = 2a \quad (|m| < a). \tag{XIII.3.18}$$

Thus the signed sum measures the mass background, while the sum of the positive particle masses in this chamber equals the W mass. The equality of positive masses follows from the split-fiber relation. It gives no information about interactions or the existence of an additional bound state. The representation is read using the fixed flavor charge, and the effective orientations are used to test the Kähler cone.

The physical matter rule for an ordinary split fiber of this type pairs its two isolated components into one full fundamental hypermultiplet. Equivalently the two half hypermultiplets make one full flavor. The intersection calculation supplies the weights and background charges used in this identification. It cannot by itself establish particle stability. We can compare with the weak gauge description at $m_0 \gg a > 0$ and $|m| < a$, at energies below the nonzero W and quark masses.

Conversely, the three effective periods give the gauge coordinates. The sum of the two fiber components fixes the W mass and their difference fixes the splitting.

$$a = \frac{V_E + V_R}{2}, \qquad m = \frac{V_R - V_E}{2}, \qquad m_0 = V_L - a - \frac{m}{2}. \tag{XIII.3.19}$$

Because $F \cdot E = F \cdot R = 0$, the quark periods are insensitive to m_0. The third period is needed to specify the coupling frame. The conditions for the original compact cone are

$$a > |m|, \qquad a + m_0 + \frac{m}{2} > 0. \tag{XIII.3.20}$$

For example, the three periods $(V_E, V_R, V_L) = (2, 4, 15/2)$ give $(a, m, m_0) = (3, 1, 4)$. The W mass is 6 and the quark masses are 4 and 2. This example lies in the positive cone. A parametrically weak description requires the separate hierarchy in m_0. A second set of periods makes the sign of the mass easier to see. Suppose a measurement gives $(V_E, V_R, V_L) = (3, 1, 13/2)$. Applying the inverse map rather than assigning a mass by inspection gives

$$a = 2, \qquad m = -1, \qquad m_0 = 5, \qquad (Z_+, Z_-) = (1, -3). \tag{XIII.3.21}$$

The smaller component is now R. The flavor-$+1$ lower weight still uses $-E$, so its mass is three and its signed period is minus three. The root period is four. Decreasing V_R at fixed $V_E + V_R$ would move toward the negative mass wall, with no change in the W mass. By contrast, increasing both component periods equally changes a at fixed m. Infinitesimally these two operations are

	δV_E	δV_R	δV_L
δa at fixed m, m_0	δa	δa	δa
δm at fixed a, m_0	$-\delta m$	δm	$\delta m/2$

(XIII.3.22)

Keeping V_L fixed while changing the split is a different experiment: it varies the named inverse bare coupling. The third period prevents these two background choices from being confused.

XIII.3.4 The massive cubic from curves and weights

Does the surface reproduce the contribution of one full fundamental at nonzero mass? The weight interpretation predicts a particular contribution to the protected prepotential. We can compare it with the cubic from the threefold. The comparison at nonzero m matters because two different choices of coupling coordinate can give the same cubic at $m = 0$.

As in Chapter 2, set $A = -\omega$ for the signed class used in the intersection formula. Products containing S reduce to pairings on the surface. In particular, put $d_m = E - F/2$. Then

$$K_S \cdot d_m = -1 - \tfrac{1}{2}(-2) = 0, \qquad F \cdot d_m = 0, \qquad d_m^2 = -1. \tag{XIII.3.23}$$

Using $S|_S = K_S$ and $D_0|_S = F$, the complete list of needed triple intersections is

$$\begin{aligned} &S^3 = 7, \quad S^2 D_0 = -2, \quad S^2 D_m = 0, \\ &S D_0^2 = 0, \quad S D_0 D_m = 0, \quad S D_m^2 = -1. \end{aligned} \tag{XIII.3.24}$$

All-background cubic terms have no intrinsic degree in this local noncompact calculation. We compare the terms that depend on a at fixed background lifts. The expansion in the original chamber gives

$$\begin{aligned} 6\mathcal{F}_{\mathrm{mid}} &= a^3 S^3 - 3a^2 S^2 (m_0 D_0 + m D_m) + 3a S (m_0 D_0 + m D_m)^2 \\ &= 7a^3 + 6 m_0 a^2 - 3 a m^2. \end{aligned} \tag{XIII.3.25}$$

The vanishing mixed pairing in (XIII.3.23) keeps m from entering the coefficient of a^2 in this chamber.

Each term has a separate geometric origin. The compact self-cube contributes $7a^3$. In the term with two compact insertions, the two signs in $S^2 D_0 = -2$ and in the coefficient $-m_0 D_0$ cancel. The three placements of the background divisor supply $6 m_0 a^2$. The final term uses $S D_m^2 = -1$ and supplies $-3 a m^2$. There are no $a^2 m$ or $a m_0 m$ terms in this frame. An efficient way to reproduce the expansion is to restrict the positive class to the surface first:

$$\omega|_S = 2aB + (2a + m_0 - m/2)F + (-a + m)E. \tag{XIII.3.26}$$

Its square can now be evaluated with only $B \cdot F = 1$ and $E^2 = -1$. This gives a second calculation of the quadratic quantity that the cubic should differentiate to:

$$\tfrac{1}{2}(\omega|_S)^2 = 2a(2a + m_0 - m/2) - \tfrac{1}{2}(a - m)^2 = 2 m_0 a + \tfrac{7}{2} a^2 - \tfrac{1}{2} m^2. \tag{XIII.3.27}$$

The terms linear in am cancel. This cancellation tests the same mass lift that removes $a^2 m$ from the cubic, with a different power of the Coulomb parameter.

We can check the sign of the intersection formula by comparing its first derivative with the surface area. In the same relative magnetic unit as Chapter 2, holding m, m_0 fixed gives

$$\begin{aligned} \partial_a \mathcal{F}_{\mathrm{mid}} &= \tfrac{1}{2}\omega^2 \cdot S = 2 m_0 a + \tfrac{7}{2} a^2 - \tfrac{1}{2} m^2, \\ \partial_a^2 \mathcal{F}_{\mathrm{mid}} &= 2 m_0 + 7a. \end{aligned} \tag{XIII.3.28}$$

The first line is the tension of the primitive magnetic string in these units. The second is the Coulomb-branch metric coefficient. If we had used $+\omega^3/6$ for the gauge prepotential with the same a, the first line would have the opposite sign from the area.

In the gauge description, $\operatorname{Tr} H_g^2 = 2$. The classical quadratic term is $m_0 a^2$, and $SU(2)$ has no continuous classical gauge cubic. Each root contributes positively to the

one-loop cubic and each hypermultiplet weight contributes negatively. Counting both roots and the two weights of one full fundamental gives

$$\begin{aligned}\mathcal{F}_{\text{gauge}} &= m_0 a^2 + \frac{|2a|^3 + |-2a|^3 - |m+a|^3 - |m-a|^3}{12} \\ &= m_0 a^2 + \tfrac{4}{3}a^3 - \tfrac{1}{12}\big(|m+a|^3 + |m-a|^3\big).\end{aligned} \tag{XIII.3.29}$$

This is the protected two-derivative prepotential on the Coulomb branch, with the charged modes integrated out away from their thresholds. In the chamber $a > |m|$, the two signed weights have opposite signs, so

$$(a+m)^3 + (a-m)^3 = 2a^3 + 6am^2. \tag{XIII.3.30}$$

Equations (XIII.3.25) and (XIII.3.29) therefore agree including the $-am^2/2$ term. At $m = 0$ the coefficient of a^3 is $7/6$. Its third derivative is $8 - 1 = 7 = K_S^2$. The one full flavor reduces the root contribution by one in exactly the normalization in which the blowup reduces K^2 by one.

For the changed period input in (XIII.3.21), the two sides can be checked without expanding the absolute values symbolically. The two root masses are both four, while the two hypermultiplet masses are one and three. More explicitly the numerical comparison is

$$\begin{aligned}\mathcal{F}_{\text{gauge}}(2,-1,5) &= 20 + \frac{4^3 + 4^3 - 1^3 - 3^3}{12} = \frac{85}{3}, \\ \mathcal{F}_{\text{mid}}(2,-1,5) &= 20 + \frac{7}{6}\,8 - 1 = \frac{85}{3}, \\ T(2,-1,5) &= \frac{67}{2}, \qquad g_{aa}(2,-1,5) = 24.\end{aligned} \tag{XIII.3.31}$$

Here $T = \partial_a \mathcal{F}$ and $g_{aa} = \partial_a^2 \mathcal{F}$ are evaluated at fixed backgrounds. The calculation compares the full polynomial, its area derivative and its kinetic derivative. The coefficient at $m = 0$ checks the count of weights; the nonzero mass checks how those weights couple to the background.

There is also a useful counting test before substituting numbers. Both roots contribute, so their cubed sum is $16a^3$. A full fundamental has two weights, whose central-chamber sum is $2a^3 + 6am^2$. Consequently

$$\frac{16a^3}{12} - \frac{2a^3 + 6am^2}{12} = \frac{7}{6}a^3 - \frac{1}{2}am^2. \tag{XIII.3.32}$$

Counting the two effective components as two full fundamentals would double the second term before subtraction and give a cubic derivative of six. The surface cube is seven. This comparison is sensitive to the full-flavor multiplicity supplied by the split-fiber rule.

One can instead write the background along $\pi^{-1}(E)$. Holding its named coupling coefficient fixed would change ω by $mD_0/2$, or equivalently send m_0 in (XIII.3.25) to $m_0 + m/2$. The change in the cubic is

$$\Delta\mathcal{F} = \tfrac{1}{2}a^2 m, \qquad \Delta(\partial_a \mathcal{F}) = am. \tag{XIII.3.33}$$

For the sample $(3,1,4)$ the two cubics differ by $9/2$. The quark periods are unchanged but V_L shifts. This explains why matching only the zero-mass coefficient would miss a wrong coupling identification at nonzero mass. The dependence on the coupling frame can be displayed continuously. Let $D_m^{(\lambda)} = \pi^{-1}(E) - \lambda D_0$, where λ is real. If its named coupling is $m_0^{(\lambda)}$, writing the same positive class in the original frame requires

$$m_0 = m_0^{(\lambda)} + (\tfrac{1}{2} - \lambda)m, \qquad D_m^{(\lambda)} = D_m + (\tfrac{1}{2} - \lambda)D_0. \tag{XIII.3.34}$$

The two quark periods remain $a - m$ and $a + m$, because D_0 has zero pairing with both components. The third period and the polynomial written at a fixed named coupling do change:

$$\begin{aligned} V_L &= a + m_0^{(\lambda)} + (1 - \lambda)m, \\ \mathcal{F}^{(\lambda)}(a, m, m_0^{(\lambda)}) &= m_0^{(\lambda)} a^2 + \tfrac{7}{6}a^3 - \tfrac{1}{2}am^2 + (\tfrac{1}{2} - \lambda)ma^2. \end{aligned} \tag{XIII.3.35}$$

Substituting the coordinate transformation restores the original polynomial for the same physical class. At fixed numerical value of the named coupling, however, these are different backgrounds. For $(a, m, m_0) = (2, -1, 5)$, choosing $\lambda = 0$ at that same named value changes $\mathcal{F}$ by -2 and V_L by $-1/2$. The quark masses alone would miss the change. Specifying the full period map is therefore part of specifying the prepotential comparison.

XIII.3.5 Crossing a matter wall

The lower signed weight vanishes at $m = a$ even though the moving fiber still has positive area. Geometrically it is E that reaches zero area. At $m = -a$ it is instead R. To reach a simple wall, keep the other extremal periods strictly positive.

	V_E	V_R	V_L
$m = a$	0	$2a$	$m_0 + 3a/2$
$m = -a$	$2a$	0	$m_0 + a/2$

(XIII.3.36)

In both rows $a > 0$. For example, $(a, m, m_0) = (3, -3, 7/2)$ gives $(6, 0, 5)$ and contracts only R. If we set $m_0 = -3/2$ instead, L vanishes as well, so the single-curve argument below no longer describes the entire contraction. The fixed-m_0 picture in Figure XIII.3.2 separates the matter walls from the boundaries where other compact curves reach zero size.

To follow an actual transverse crossing, fix $a > 0$ and m_0 and write $m = a + \epsilon$ near the upper wall. The continued old periods are

$$V_E = -\epsilon, \qquad V_R = 2a + \epsilon, \qquad V_L = m_0 + \tfrac{3}{2}a + \tfrac{1}{2}\epsilon. \tag{XIII.3.37}$$

If $m_0 + 3a/2 > 0$, a sufficiently small interval around zero keeps the other two periods positive. For $\epsilon < 0$, E has its original effective orientation. For $\epsilon > 0$, a Kähler class in the original resolution would have negative pairing with E. The flop replaces that curve by one whose positive period is ϵ. The W mass remains $2a$ throughout the crossing.

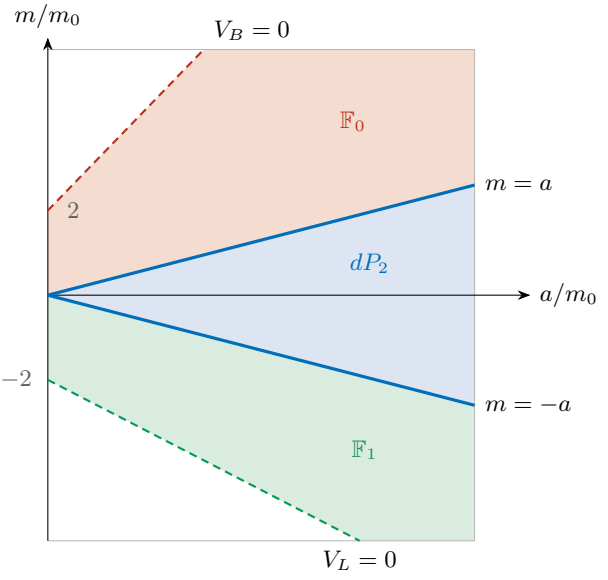


Figure XIII.3.2: Compact curve inequalities at fixed $m_0 > 0$. The central wedge has effective curves E, R, L. Above and below it, the curve that became massless has the opposite effective orientation. The dashed lines mark loss of positivity of the indicated surviving curve. The lower endpoint surface keeps L, while the upper one keeps the section of class B.

For the lower wall, use $m = -a - \epsilon$ at the same fixed a, m_0. Now the corresponding periods are

$$V_R = -\epsilon, \qquad V_E = 2a + \epsilon, \qquad V_L = m_0 + \tfrac{1}{2}a - \tfrac{1}{2}\epsilon. \tag{XIII.3.38}$$

The required open interval exists when $m_0 + a/2 > 0$. These paths describe the two individual mass thresholds using the same distance ϵ from the wall. They also show why a picture of $m = \pm a$ alone is insufficient: the third compact period can end the path before it reaches the desired wall.

Why is the isolated matter wall a flop rather than a contraction of the whole surface? For either $C = E$ or $C = R$, the normal sequence in the threefold is

$$0 \longrightarrow \mathcal{O}_C(-1) \longrightarrow N_{C/X} \longrightarrow \mathcal{O}_C(-1) \longrightarrow 0. \tag{XIII.3.39}$$

The subbundle has degree $C^2 = -1$. The quotient is $K_S|_C$ of degree $K_S \cdot C = -1$. The extension splits because $H^1(\mathbb{P}^1, \mathcal{O}) = 0$. By contrast, the moving fiber has normal degrees $0, -2$. Its zero normal degree in S is consistent with the family of fibers.

For E one can see the local contraction directly in the charts of (XIII.3.2). The same charts apply to R using its plane blowdown. Write z and z' for the canonical line coordinates in the two charts. The base Jacobian satisfies $dw \wedge dt = -v^{-1} du \wedge dv$. A constant sign in the second frame lets us write $z' = vz$. Hence the two charts map to a

single rank-one matrix,

$$\begin{pmatrix} u & z \\ vu & vz \end{pmatrix} = \begin{pmatrix} tw & tz' \\ w & z' \end{pmatrix}. \tag{XIII.3.40}$$

The determinant vanishes. A nonzero matrix determines the line of its columns uniquely, but the zero matrix forgets that line. The forgotten line is the contracted $\mathbb{P}^1$. The second small resolution keeps the line of the rows instead. Call its new isolated curve C'. We can compare its period with the old one on the common blowup.

The same local exchange occurs in the toric diagram. Let $v_O = (0,0)$ be the interior point of (XIII.3.9). The two parallelogram relations

$$v_O + v_E = v_L + v_R, \qquad v_O + v_R = v_E + v_B \tag{XIII.3.41}$$

identify the old and new diagonals for the two flops. These are relations of ray coordinates in the diagram. The fiber relation $F = E + R$ is a relation of curve classes. The distinction matters when using Figure XIII.3.3 to read off which curves lie in the proper transform of the compact surface.

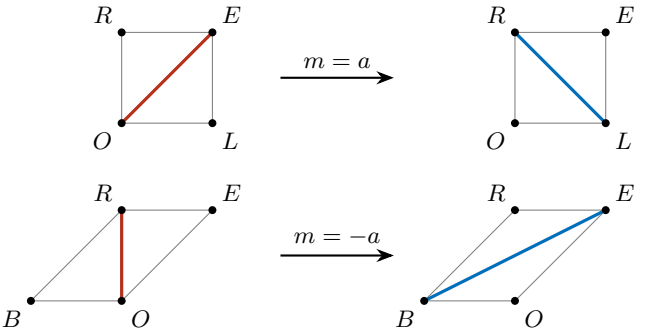


Figure XIII.3.3: Each row shows a parallelogram in the height-one toric diagram before and after a flop. The common diagonal incident to the interior point O is replaced by the other diagonal. The new edge defines a curve that is no longer contained in the compact divisor associated with O.

We can now compute the jump of the compact cubic without reading it from the hypermultiplet formula. Let Y be the common blowup of the two small resolutions, with maps $f : Y \to X$ and $g : Y \to X'$. Its exceptional surface $Q \simeq \mathbb{P}^1 \times \mathbb{P}^1$ has normal bundle $\mathcal{O}(-1,-1)$. Set $t = \omega \cdot C$ in the old orientation and let $d = A \cdot C = -t$. The two divisor pullbacks agree away from Q. On the ruling contracted by g, f^*A has degree d and Q has degree -1, so

$$g^*A' = f^*A + dQ. \tag{XIII.3.42}$$

On the other ruling, contracted by f, the pullback f^*A has degree zero and Q still has degree -1. The image of that ruling under g is the new curve. Hence

$$A' \cdot C' = -d, \qquad \omega' \cdot C' = d = -t. \tag{XIII.3.43}$$

When the continued old period t is negative, the new effective curve has positive period. To evaluate the difference, let u_Q, v_Q be the two ruling divisor classes on Q, with $u_Q^2 = v_Q^2 = 0$ and $u_Q v_Q = 1$ as an intersection number. In the order in which $f^*A|_Q = du_Q$, the restriction of Q itself is $-u_Q - v_Q$. Thus

$$(f^*A)^2 Q = 0, \qquad f^*A\, Q^2 = -d, \qquad Q^3 = 2. \tag{XIII.3.44}$$

For clarity, these numbers follow from multiplying the two ruling classes on the compact exceptional surface. A divisor restricted to Q is integrated there, so only its coefficient of $u_Q v_Q$ contributes. In particular,

$$\begin{aligned} (du_Q)^2 &= 0, \\ (du_Q)(-u_Q - v_Q) &= -d\, u_Q v_Q, \\ (-u_Q - v_Q)^2 &= 2 u_Q v_Q. \end{aligned} \tag{XIII.3.45}$$

The zero in the first line removes the term linear in dQ from the cube difference. The remaining two terms have opposite signs, so keeping the cubic power of Q is essential for its final sign.

Only products supported on Q contribute to the difference. Expanding (XIII.3.42) gives

$$\mathcal{F}_{\text{out}} - \mathcal{F}_{\text{mid}} = \frac{3d^2(-d) + 2d^3}{6} = -\frac{d^3}{6} = \frac{t^3}{6}. \tag{XIII.3.46}$$

As before, background-only terms are fixed consistently when comparing representatives of the gauge prepotential.

The same difference appears in (XIII.3.29). On the far side of a wall, the old signed area $t = a - |m|$ is negative. Its contribution changes from the continued value $-t^3/12$ to $-|t|^3/12 = +t^3/12$. The difference is $t^3/6$, in agreement with (XIII.3.46). At $(a, m, m_0) = (2, 3, 5)$ the difference is $-1/6$. Along either transverse path (XIII.3.37) or (XIII.3.38), the continued vanishing period is $t = -\epsilon$. Thus the outer representative differs from the continued middle representative by

$$\Delta\mathcal{F} = -\frac{\epsilon^3}{6}, \qquad V_{C'} = \epsilon > 0 \quad (\epsilon > 0). \tag{XIII.3.47}$$

This cubic comparison uses the same background-only representative on both sides. In taking Coulomb derivatives below, m and m_0 are held fixed; the transverse-path parameterization serves only to identify which side is effective.

At fixed m, m_0 the continued period satisfies $\partial_a t = 1$. The derivatives of the difference are

$$\partial_a(\Delta\mathcal{F}) = \tfrac{1}{2}t^2, \qquad \partial_a^2(\Delta\mathcal{F}) = t, \qquad \partial_a^3(\Delta\mathcal{F}) = 1. \tag{XIII.3.48}$$

The difference and its first two derivatives vanish on the wall. Thus the cubic derivative rises from 7 to 8 from the middle chamber to either outer chamber. At the wall the light charged component must be kept if one wants an effective action there. The limiting prepotentials agree through the metric. This comparison does not decide which other bound states survive the wall. Chapter 4 develops the broader chamber calculus.

XIII.3.6 Decoupling a heavy flavor

Now ask how to remove the hypermultiplet and keep a finite pure gauge theory. Take $M = |m| > a > 0$ on either outer branch. Both absolute values in (XIII.3.29) are then $M + a$ and $M - a$, in one order or the other. Their contribution is

$$\mathcal{F}_{\text{hyper}} = -\frac{(M+a)^3 + (M-a)^3}{12} = -\frac{M^3}{6} - \frac{Ma^2}{2}. \tag{XIII.3.49}$$

The first term depends only on the mass background. The second renormalizes the inverse coupling. In particular, at fixed m_0 the metric would be

$$\partial_a^2 \mathcal{F}_{\text{out}} = 2m_0 + 8a - M. \tag{XIII.3.50}$$

One cannot take $M \to \infty$ at fixed m_0 and retain a finite positive metric. Instead keep

$$\mu = m_0 - \frac{M}{2}, \qquad m_0 = \mu + \frac{M}{2} \tag{XIII.3.51}$$

with μ fixed and m_0 varying with M. After dropping the background constant $-M^3/6$, the prepotential on the retained gauge branch becomes

$$\mathcal{F}_{\text{pure}} = \mu a^2 + \tfrac{4}{3} a^3. \tag{XIII.3.52}$$

This threshold limit is taken in the already isolated local theory, at fixed a and external energies well below $M - a$. We take $\mu \geq 0$ for the regular branch considered here and $\mu \gg a$ for a weak pure gauge description.

The required coupling shift can be diagnosed before taking the limit. With m_0 fixed the heavy term removes M from the metric. Keeping $m_0 = \mu + M/2$ instead adds exactly the same amount through the classical quadratic term. For $a = 2$ the two trajectories are particularly transparent:

	$m_0 = 8$ fixed		$\mu = 3$ fixed	
M	m_0	g_{aa}	m_0	g_{aa}
10	8	22	8	22
20	8	12	13	22
40	8	-8	23	22

(XIII.3.53)

The fixed-bare trajectory has left the selected positive-metric branch by the last row; continuing its polynomial does not restore a physical gauge patch. The fixed-μ trajectory keeps a finite kinetic coefficient. The two paths start at the same point and then separate because the background coupling is an essential part of the limit. The background term $-M^3/6$ diverges on both paths, but has no Coulomb derivative.

The finite curve periods show why the two signs of the mass can have different geometric endpoints. For $m = +M$, the curve E has flopped. Its flop leaves the proper transform of S as the surface obtained by contracting E in S. The two ruling classes in that surface lift to $B = L + E$ and $F = R + E$. Each lift has zero intersection with E, as required of a pullback from the surface after contraction. Their periods and the new isolated-curve period are

$$m = +M: \qquad V_B = 2a + m_0 - M/2 = 2a + \mu, \quad V_F = 2a, \quad V_{E'} = M - a. \tag{XIII.3.54}$$

The pullback condition can be derived for any survivor D when a (-1) curve C is contracted within the surface. A class pulled back from the new surface must pair to zero with C. Adding a multiple of C gives the unique lift

$$\widetilde{D} = D + (D \cdot C)C, \qquad \widetilde{D} \cdot C = 0, \qquad \widetilde{D} \cdot \widetilde{D}' = D \cdot D' + (D \cdot C)(D' \cdot C). \tag{XIII.3.55}$$

Here the plus sign follows from $C^2 = -1$. Applying this formula with $C = E$ to L, R gives B, F. Their intersection form is

$$\begin{pmatrix} B^2 & B \cdot F \\ F \cdot B & F^2 \end{pmatrix} = \begin{pmatrix} 0 & 1 \\ 1 & 0 \end{pmatrix}. \tag{XIII.3.56}$$

This is a calculation on the compact surface after its contraction. The threefold operation is the flop, which still contains the new isolated curve at any finite M.

Deleting v_E from the surface fan restores the product $\mathbb{F}_0 = \mathbb{P}^1 \times \mathbb{P}^1$. This gives the upper compact cone in Figure XIII.3.2, with $2a + m_0 - m/2 > 0$ in addition to $m > a > 0$.

For $m = -M$, the curve R has flopped. The section L is disjoint from R, and the surviving fiber lifts to $F = E + R$. The remaining section has self-intersection -1 and meets the fiber once. The compact surface is $\mathbb{F}_1$, with

$$m = -M: \qquad V_L = a + m_0 - M/2 = a + \mu, \quad V_F = 2a, \quad V_{R'} = M - a. \tag{XIII.3.57}$$

For the negative branch the same pullback calculation uses $C = R$. The class L is unchanged since $L \cdot R = 0$, whereas E lifts to $E + R = F$. The new surface form is therefore

$$\begin{pmatrix} L^2 & L \cdot F \\ F \cdot L & F^2 \end{pmatrix} = \begin{pmatrix} -1 & 1 \\ 1 & 0 \end{pmatrix}. \tag{XIII.3.58}$$

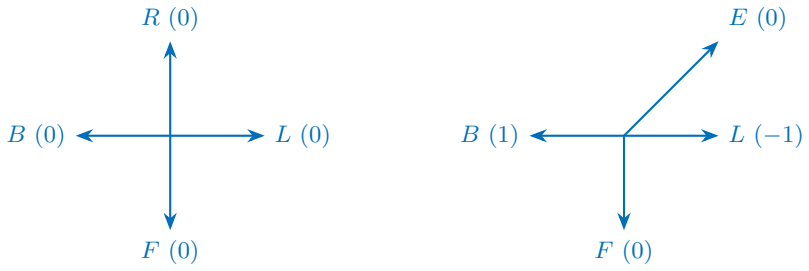
The surviving negative section explains the difference between this endpoint and the product surface. The signs of m have selected different curves to remove from the original compact surface, even though the absolute-value threshold has the same dependence on M.

This time the lower compact cone in Figure XIII.3.2 requires $a + m_0 + m/2 > 0$ in addition to $-m > a > 0$. Both positivity conditions are satisfied along the shifted limit. The flopped curve is still present at finite M. It leaves the finite-mass sector only because $M - a \to \infty$. For example, at $(a, \mu, M) = (2, 3, 10)$ the common fiber period is 4, and the section periods are 7 and 5 on the two sides. The flopped curve has period 8 on either side. Increasing M along this path changes only the last of these periods.

Figure XIII.3.4 gives a direct check of the two compact surface intersection forms. In $\mathbb{F}_1$ the basis L, F has $L^2 = -1$, $L \cdot F = 1$ and $F^2 = 0$. Adjunction on L, F gives $K \cdot L = -1$ and $K \cdot F = -2$, which fix $K = -2L - 3F$. On $\mathbb{F}_0$ the corresponding class is $K = -2B - 2F$. It follows that

$$K^2_{\mathbb{F}_0} = 8, \qquad K^2_{\mathbb{F}_1} = (-2L - 3F)^2 = 4(-1) + 12 = 8. \tag{XIII.3.59}$$

Both have $K \cdot F = -2$ and $F^2 = 0$. The positive restriction on either endpoint is $-aK + \mu F$, whose periods agree with (XIII.3.54) or (XIII.3.57). Using the signed



$\mathbb{F}_0$ after contracting E $\mathbb{F}_1$ after contracting R

Figure XIII.3.4: Surface fans after contracting the indicated curve inside the old compact surface. Removing v_E gives $\mathbb{F}_0$ and removing v_R gives $\mathbb{F}_1$. The numbers at the rays are the self-intersections of the surviving toric boundary curves on those surfaces. The labels refer to the inherited rays.

cube from Chapter 2 now gives $6\mathcal{F} = 8a^3 + 6\mu a^2$ for either endpoint, as in (XIII.3.52). The two compact surfaces differ even though their pure protected polynomials agree. Chapter 5 treats what can distinguish the endpoints beyond these cubic data.

Take-home message of this chapter

A blowup splits one gauge fiber into two isolated curves. At fixed flavor charge their signed periods give the two weights of a single fundamental hypermultiplet. The compact cubic checks their contribution at nonzero mass. Crossing either isolated mass wall changes the effective curve orientation, and taking that mass large requires holding $m_0 - |m|/2$ fixed.

XIII.3.7 Exercises

E1. Charges in the plane basis. Use the basis (H, L, R) and its diagonal intersection form. Compute the three charges of H and the signed central charges of R, $-E$ and L in the same coupling frame as the chapter. Use the answer keys `qH`, `IH`, `fH`, `ZR`, `ZminusE` and `ZL`.

E2. An isolated contraction. At $(a, m, m_0) = (3, -3, 7/2)$ identify the extremal curve that vanishes and compute the remaining periods V_E, V_L. Find both degrees of the normal bundle of the vanishing curve and the compact surface left after the flop. Use the keys `curve`, `normal1`, `normal2`, `VE`, `VL` and `surface`. Enter the curve as `E`, `R` or `F`, and the surface as `F0` or `F1`. Explain in words why the normal bundle splits in this example.

E3. A finite threshold limit. For $M > a > 0$ compute the combination of m_0, M held fixed, the background term to be removed, the resulting pure prepotential in a, μ, and the outer-branch metric before shifting m_0. Use the keys `shift`, `subtraction`, `pure` and `fixedBareMetric`. State which curve becomes heavy on each branch.

E4. Derivatives at the positive mass wall. Fix $m > 0$ and m_0 with $m_0 + 3m/2 > 0$. Work close to $a = m$, keeping the other compact curve periods positive as in the isolated-wall calculation. Write the contribution of the one full hyper for $a > m$ and for $0 < a < m$ in the two adjacent chambers. Compute the outer-minus-middle differences at $a = m$ for its second and third derivatives in a. Use `inside`, `outside`, `jump_a2` and `jump_a3`. Keep the background term in the outer polynomial for this comparison.

E5. A weight and a particle. The relation $F = E + R$ makes the corresponding positive periods additive in the original chamber, although a generic fiber has a moving irreducible representative. Explain why the equality of periods does not determine whether a bound state persists. Why is $-E$ used for the weight of flavor charge $+1$ although E is effective? The class $2E$ has gauge charge 2. Use its intersection with E to explain why this does not make it a second moving W curve.

For E1 through E4, submit one JSON object for each exercise. Use strings for exact integers, fractions such as `"3/2"`, and polynomials in `a`, `m`, `m0`, `M` and `mu` as requested. The written parts of E2 and E3 and the whole of E5 are for discussion with a reader.

Written transfer practice. These questions supplement E1–E5 and require written reasoning. Start from positive periods $(V_E, V_R, V_L) = (5, 1, 9)$. Reconstruct (a, m, m_0) and determine which component contracts first if m is decreased at fixed a, m_0. Check the other two periods at that wall. Explain how your answer would change if V_L rather than m_0 were held fixed during the variation. Next replace D_m by $D_m^{(1/4)}$. Find the coupling coordinate that keeps the same positive class, and compare it with keeping the old numerical coupling value. Identify a compact period that distinguishes those choices. Finally take $a = 1$, $\mu = 2$ and $M = 6$, then increase M on both shifted heavy branches. Compute the finite fiber and section periods and the growing flopped-curve period; explain why the limiting cubic alone cannot tell the two surfaces apart.

Status and sources

§3.1. The local limit. The isolated local sector, fixed backgrounds and normalizable gauge mode are premises ([DEC]). See Jefferson et al. (2018, published version, §2.2, Eqs. (2.7)–(2.8) and preceding text).

§3.2. The blowup. The split fiber, compact curve cone and crepant fan are calculations for this object ([MATH]). For the blowup formulas and $\mathrm{Bl}_1 \mathbb{F}_0 = dP_2$, see Jefferson et al. (2018, §4.1, Eq. (4.3), and App. A.1, Eqs. (A.4)–(A.5)). The periods use the positive cone, with the opposite sign for the formal class in the cubic. Equations (XIII.3.8)–(XIII.3.13) develop adjunction and effective-class consequences of the same surface pairing.

§3.3. Charges and one full flavor. The pairings and inverse map in (XIII.3.16) and (XIII.3.19) use the fixed background lift ([MATH]). The W and one-full-fundamental interpretations use the ordinary toric gauge phase and the split fiber rule ([GEO-X]). See Intriligator et al. (1997, arXiv v1, §8 and §8.1, PDF p. 29 before Eq. (8.10)) and Jefferson et al. (2018, Eq. (2.15) and Fig. 16). The web comparison in Aharony et al. (1998, arXiv v2, §III.D, Eqs. (59)–(61)) has $\phi = 2a$, $q = 2n_e$, $Q_f = f$ and the same instanton charge I. Its two color-brane lengths match the B, L periods in this flavor orientation. The changed-period example and general background-frame transformation in (XIII.3.21) and (XIII.3.34)–(XIII.3.35) are algebraic consequences of the signed cubic and its change of variables, with no integral-lattice interpretation.

§3.4. The cubic. The signed intersections and root/weight substitution ([MATH]) use Intriligator et al. (1997, arXiv v1, Eqs. (2.22), (4.1), (8.3)–(8.4)). The identification with protected prepotential and relative magnetic tension ([GEO-X]) uses Jefferson et al. (2018, Eqs. (2.9)–(2.12) and §3.2 n. 4). The cubic root power is taken from the former Eq. (2.22), and the surface volume includes the factor 1/2 of the latter Eq. (2.10). With $\phi = 2a$ and $1/g_0^2 = m_0$ in the same relative magnetic unit, Aharony et al. (1998, Eqs. (60)–(61)) gives twice (XIII.3.29) and the same tension upon taking its ϕ derivative.

§3.5. The walls. The two conifold neighborhoods and jump in (XIII.3.46) are local calculations ([MATH]). The isolated matter threshold uses the gauge interpretation ([GEO-X]). See Jefferson et al. (2018, §3.5.1) and Aharony et al. (1998, §III.D.1) for the distinction between the charged threshold and the question of other bound states.

§3.6. The limits. The coupling shift, finite periods and surface cubes ([MATH]) follow from (XIII.3.49)–(XIII.3.59). See Intriligator et al. (1997, §2.3 after Eq. (2.22)) for the field-theory threshold and Jefferson et al. (2018, §4.1, Eq. (4.5)) for the ruled-surface intersections. The retained pure gauge polynomial is protected phase data ([GEO-X]). It does not establish a UV identification, the global form, discrete theta or a full particle spectrum. The trajectory comparison and orthogonal pullbacks in (XIII.3.53)–(XIII.3.58) expand the same threshold and surface-intersection calculations.

References

Aharony, O., A. Hanany, and B. Kol (1998). "Webs of (p,q) five-branes, five-dimensional field theories and grid diagrams". In: *JHEP* 01, p. 002. DOI: 10.1088/1126-6708/1998/01/002. arXiv: hep-th/9710116.

Intriligator, K. A., D. R. Morrison, and N. Seiberg (1997). "Five-dimensional supersymmetric gauge theories and degenerations of Calabi-Yau spaces". In: *Nucl. Phys. B* 497, pp. 56–100. DOI: 10.1016/S0550-3213(97)00279-4. arXiv: hep-th/9702198.

Jefferson, P. et al. (2018). “On Geometric Classification of 5d SCFTs”. In: *JHEP* 04, p. 103. DOI: 10.1007/JHEP04(2018)103. arXiv: 1801.04036 [hep-th].

Chapter XIII.4

Flops, thresholds, and gauge-theory chambers

XIII.4.1 A charged particle reaches zero mass

For the particle from an M2-brane on an isolated curve, its area sets the mass. If the area goes to zero, the geometry must change before the same signed period can become negative. What changes in the five-dimensional action, and how do we tell whether there is a smooth chamber on the other side? The mass of the particle will involve an absolute value. Its contribution to the action also depends on the sign inside that absolute value.

We use the blown-up ruled surface of Chapter 3 and the relative period and tension units of Chapter 2. The reader needs the intersection form of a point blowup and the toric description of curves by edges, which we recall as we use them. We will follow the changing curve in the fan, compute the intersection jump on a common blowup, and compare it to the charged hypermultiplet contribution. The same geometry will then give an example of a boundary at which an entire surface collapses.

We work in ordinary flux-free M-theory with one normalizable vector from the compact divisor. The regulated transverse volume in gravitational units is taken to infinity with the displayed periods fixed. We assume that unwanted bulk modes decouple or lie outside the chosen energy window. The backgrounds are held fixed when we differentiate with respect to the dynamical scalar.

XIII.4.2 The curve at the wall

Which curve can go through zero area while the other compact curves remain finite? Start with $S = \mathrm{Bl}_{p}(\mathbb{F}_0)$, the degree-seven del Pezzo surface, where p is the torus fixed point at the intersection of a section and a fiber. Use the pullback classes B, F and

exceptional curve E. Then

$$B^2 = F^2 = B \cdot E = F \cdot E = 0, \quad B \cdot F = 1, \quad E^2 = -1, \qquad K_S = -2B - 2F + E. \tag{XIII.4.1}$$

The proper transforms of the fiber and section through p are $R = F - E$ and $L = B - E$. The threefold is initially the local canonical bundle of S, so $S|_S = K_S$ by adjunction. Fix the background divisors $D_0 = D_F$ and $D_m = D_E - D_F/2$, where D_v is the toric divisor of ray v. In the initial fan $D_F|_S = F$ and $D_E|_S = E$. Throughout a flop we identify the divisors by strict transform. Define

$$\omega = -aS + m_0 D_0 + m D_m, \qquad A = -\omega, \qquad Z(C) = \omega \cdot C. \tag{XIII.4.2}$$

An effective curve has positive Z inside its chamber. For an oriented wrapped particle the coefficient of a is the charge $-S \cdot C$ and the physical BPS mass is $|Z(C)|$ in these units. The half in D_m is a real change of background coordinates.

For example, $K_S \cdot R = -1$, $F \cdot R = 0$ and $(E - F/2) \cdot R = 1$. The same three pairings for E, L give

$$\begin{aligned} &Z(E) = a - m = e, \quad Z(R) = a + m = r, \quad Z(L) = a + m_0 + m/2 = \ell, \\ &Z(F) = e + r = 2a, \quad Z(B) = e + \ell, \qquad\qquad h = e + r + \ell. \end{aligned} \tag{XIII.4.3}$$

The periods e, r, ℓ are independent. Indeed $a = (e + r)/2$, $m = (r - e)/2$, and $m_0 = \ell - (e + 3r)/4$. In the ordinary gauge patch $\Phi = a\,\mathrm{diag}(1, -1)$ with $a > 0$. The ruling F has the W charge, and $R, -E$ give the two signed weights of common flavor charge $+1$. There m_0 is the bare inverse squared coupling in our units. Away from the gauge patch it is still the same background coordinate.

It is useful to reconstruct the Kähler class on S from these three periods. Restricting (XIII.4.2) gives

$$\begin{aligned} \omega|_S &= 2aB + (2a + m_0 - m/2)F + (-a + m)E \\ &= (e + r)B + (e + \ell)F - eE. \end{aligned} \tag{XIII.4.4}$$

The negative coefficient of E is consistent with its positive area: $E^2 = -1$, so $\omega \cdot E = e$. A coefficient in a divisor basis is not itself the area of that basis curve. Pairing the same class with $F - E$ and $B - E$ returns r and ℓ. Squaring it gives

$$\frac{1}{2}(\omega|_S)^2 = (e + r)(e + \ell) - \frac{e^2}{2} = r\ell + e(r + \ell) + \frac{e^2}{2}. \tag{XIII.4.5}$$

This calculation already explains why the surface need not collapse when e vanishes: its limiting volume is $r\ell$. The wall removes one exceptional curve while retaining a surface of finite area in both independent ruling directions. Each of a, m_0, m and each curve period has mass dimension one in these units. The surface volume therefore has dimension two, as required for a string tension.

To see what replaces E, use the height-one rays

$$\begin{aligned} &O = (0, 0), \quad L = (1, 0), \qquad E = (1, 1), \\ &R = (0, 1), \quad B = (-1, 0), \quad F = (0, -1). \\ &(\omega_O, \omega_L, \omega_E, \omega_R, \omega_B, \omega_F) = (-a, 0, m, 0, 0, m_0 - m/2). \end{aligned} \tag{XIII.4.6}$$

The coordinates shown are the first two coordinates of each ray. The star of O consists of triangles OLE, OER, ORB, OBF, OFL; the edges Ov give the surface curves. In particular OE names the edge of the curve E, while D_E names the divisor meeting S along that curve.

Consider an internal edge uv with neighboring triangles uvx and uvy. Each opposite divisor meets the edge curve C_{uv} once. Intersecting a principal toric divisor with the curve then forces the relation below, since its degree must vanish for every lattice character. Transversality of D_u, D_v gives the splitting of the normal bundle. Here the vertices in the relation stand for their height-one lifts.

$$\begin{aligned} x + y + b_u u + b_v v &= 0, \\ (D_x, D_y, D_u, D_v) \cdot C_{uv} &= (1, 1, b_u, b_v), \\ Z(C_{uv}) = \omega_x + \omega_y + b_u\omega_u + b_v\omega_v, &\quad N_{C_{uv}/X} = \mathcal{O}(b_u) \oplus \mathcal{O}(b_v). \end{aligned} \tag{XIII.4.7}$$

For a concrete use of the rule, write the unknown relation for OE as $L+R+b_O O+b_E E = 0$. The two spatial coordinates and the height-one coordinate give three equations, with one redundant spatial equation:

$$1 + b_E = 0, \qquad 1 + b_E = 0, \qquad 2 + b_O + b_E = 0. \tag{XIII.4.8}$$

Thus $b_O = b_E = -1$. Applying the divisor coefficients of (XIII.4.6) to this relation yields $0 + 0 - (-a) - m = a - m$. The same short procedure gives quite different normal degrees for the ruling edge OF. Its opposite rays are B, L:

$$B + L - 2O + 0F = 0, \qquad (D_B, D_L, D_O, D_F) \cdot C_{OF} = (1, 1, -2, 0), \qquad Z(C_{OF}) = 2a. \tag{XIII.4.9}$$

The zero normal degree permits motion of the fiber. In the present fan this edge does not lie in a convex quadrilateral with a second smooth diagonal: B, O, L are collinear. The lattice relation therefore distinguishes the isolated exceptional curve from a ruling before we assign a field-theory interpretation to either. The height-one equation also enforces $b_u + b_v = -2$, the vanishing of the first Chern class of the threefold on the curve.

The curve OE has $L + R - O - E = 0$, so $Z = e$ and both normal degrees are -1. There are no infinitesimal deformations of this curve. As e goes to zero with $r, \ell > 0$, the lifted triangles OLE and OER lie on the same lower plane. Their union is the unit square $OLER$ in Figure XIII.4.1.

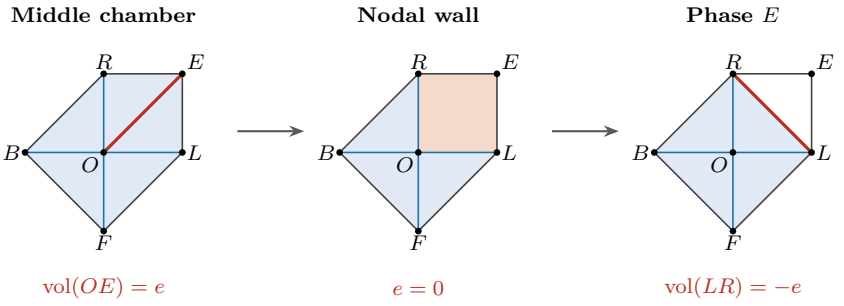


Figure XIII.4.1: The three lower subdivisions near $e = 0$. The blue region consists of cells incident to O on either smooth side. In the square at the wall, neither diagonal is retained. The new compact curve LR lies outside the compact surface except at one point.

We can identify the singularity from the square itself. A dual lattice point (x, y, z) for its cone satisfies

$$z \geq \max(0, -x) + \max(0, -y). \tag{XIII.4.10}$$

Choose one of $(1, 0, 0), (-1, 0, 1)$ to build x, and one of $(0, 1, 0), (0, -1, 1)$ to build y. Any remaining z is a sum of $(0, 0, 1)$, which is the sum of either opposite pair. This proves generation and gives the primitive binomial relation. The affine patch is the node $uv = st$, with the four variables belonging to these semigroup generators. Its two smooth subdivisions keep the same four rays, so contracting the diagonal removes a curve and no divisor. This is a small contraction, and exchanging its resolution is a flop.

After the exchange, LR is the internal edge between LER and OLR. Its relation $O + E - L - R = 0$ reverses the sign. The old adjacent edges OL and OR have new opposite rays, giving

Edge in phase E	Relation	Period
LR	$O + E - L - R = 0$	$-e$
OL	$F + R - 2O = 0$	$\ell + e$
OR	$B + L - 2O = 0$	$r + e$

(XIII.4.11)

The edges OB, OF have the same periods as OL, OR, respectively. The four rays around O now form the square fan of $\mathbb{F}_0$. Thus the other periods stay positive for sufficiently small negative e. It is LR that has area $-e$. Continuing e below zero does not assign a negative area to the old holomorphic curve. With the divisors identified, we can now compare their intersections.

XIII.4.3 How triple intersections change

Why does a change along a single curve affect a cubic of divisors? Let $f\colon Y \to X$ and $g\colon Y \to X'$ be the maps from the common blowup of the two resolutions. Over the old

$(-1,-1)$ curve, the exceptional divisor is $Q = \mathbb{P}^1 \times \mathbb{P}^1$, with $\mathcal{O}_Y(Q)|_Q = \mathcal{O}(-1,-1)$. The first factor is the old base and the second the fiber of f. The map g contracts the first factor, as in Figure XIII.4.2. For a matched divisor pair D, D', write $d = D \cdot C$. Pullbacks agree away from Q, so their difference is a multiple of Q. Restricting to each ruling determines the multiple.

$$\begin{aligned} f^*D|_Q &= (d,0), \\ g^*D' = f^*D + dQ, &\quad g^*D'|_Q = (0,-d). \end{aligned} \tag{XIII.4.12}$$

The first entry of $g^*D'|_Q$ must be zero because g contracts that ruling. The second entry says that the new curve has degree $-d$ against the matched divisor. This explains the reversal of the numerical curve class without choosing an area sign by hand.

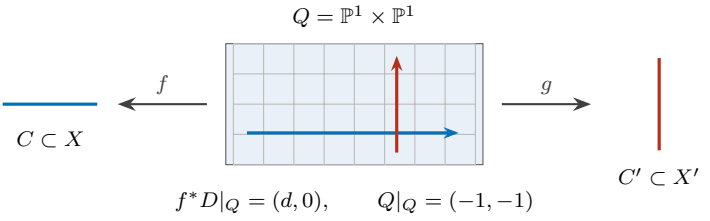


Figure XIII.4.2: The two contractions of Q in the common blowup. The horizontal ruling maps isomorphically to C under f and is contracted by g. The vertical ruling maps to C' under g. Restricting f^*D and Q to these rulings fixes the sign of the correction dQ.

Let H_1, H_2 be the degree-one pullbacks on Q. Since $H_i^2 = 0$ and $H_1 H_2 = 1$, the terms in the difference are

$$\begin{aligned} (f^*D)^2 Q &= (dH_1)^2 = 0, \\ f^*D\, Q^2 &= dH_1(-H_1 - H_2) = -d, \\ Q^3 &= (-H_1 - H_2)^2 = 2. \end{aligned} \tag{XIII.4.13}$$

Cubing (XIII.4.12) and using the projection formula gives $D'^3 - D^3 = 3d^2(-d) + 2d^3 = -d^3$. Taking the coefficient of a product of three independent divisor parameters gives

$$\Delta(D_i D_j D_k) = -(D_i \cdot C)(D_j \cdot C)(D_k \cdot C), \qquad \Delta = \text{new} - \text{old}. \tag{XIII.4.14}$$

To see the normalization in the polarization, put $D = x_1 D_1 + x_2 D_2 + x_3 D_3$. The coefficient of $x_1 x_2 x_3$ in D^3 is $6 D_1 D_2 D_3$; the same coefficient in $-d^3$ is $-6 d_1 d_2 d_3$. The factors of six cancel. Repeated indices follow by identifying two or three divisors after the polynomial identity has been established. For example,

$$\Delta(S^2 D_m) = -(S{\cdot}C)^2 (D_m{\cdot}C), \qquad \Delta(S D_0 D_m) = -(S{\cdot}C)(D_0{\cdot}C)(D_m{\cdot}C). \tag{XIII.4.15}$$

These mixed products are needed when the mass depends on backgrounds. Keeping only S^3 would determine one Coulomb cubic coefficient but would lose the terms that make the two actions agree at the wall.

All terms in this difference are supported on Q. In the noncompact threefold an intersection with a compact divisor is intrinsic. A difference of cubics can be compared using the common blowup even though an absolute triple product of three noncompact divisors is not fixed by the local geometry.

Use $A = -\omega$ in the protected prepotential of the local vector. The derivatives with respect to a are taken at fixed m_0, m.

$$\mathcal{F} = \frac{A^3}{6}, \qquad T = \partial_a \mathcal{F} = \frac{\omega^2 S}{2}, \qquad g = \partial_a T, \qquad \kappa = \partial_a g. \tag{XIII.4.16}$$

Here T is the wrapped M5 string tension in the relative magnetic unit, g the gauge kinetic coefficient, and κ the Coulomb Chern–Simons coefficient in the chosen normalization. The class A has degree $-t$ on the old curve, where $t = \omega \cdot C$. The jump in the cubic representative matched by the blowup is therefore

$$\Delta\mathcal{F} = \frac{t^3}{6} \qquad (t > 0 \text{ old},\ t < 0 \text{ new}). \tag{XIII.4.17}$$

Using the positive class ω in the cubic would reverse the sign in this equation.

For OE the old degrees in the basis (S, D_0, D_m) are $(-1, 0, -1)$. Write the compact-supported entries in the order $S^3, S^2D_0, S^2D_m, SD_0^2, SD_0D_m, SD_m^2$. The jump and the two tensors are

$$\begin{aligned} \Delta I &= (1, 0, 1, 0, 0, 1), \\ I_{\text{mid}} &= (7, -2, 0, 0, 0, -1), \\ I_E &= (8, -2, 1, 0, 0, 0). \end{aligned} \tag{XIII.4.18}$$

One can check the last row directly. In the old surface pairing (XIII.4.1), $K_S^2 = 8-1 = 7$, $K_S \cdot (E - F/2) = 0$ and $(E - F/2)^2 = -1$. In the new fan D_E misses S' and D_F cuts a ruling. On $\mathbb{F}_0$, with the two rulings B', F' and $B'F' = 1$,

$$S'|_{S'} = -2B' - 2F', \qquad D_0|_{S'} = F', \qquad D_m|_{S'} = -F'/2. \tag{XIII.4.19}$$

Thus $S'^3 = 8$, $S'^2 D_m = 1$, and all three entries quadratic in the background divisors vanish. This checks the change of the mixed cubic coefficient as well as the pure Coulomb coefficient.

There is a second sign to fix when using the tensor. The tensor is written on (S, D_0, D_m), whereas the cubic class is $A = aS - m_0 D_0 - mD_m$. If its six compact-supported entries are $I_{300}, I_{210}, I_{201}, I_{120}, I_{111}, I_{102}$ in the stated order, its part containing a is

$$\begin{aligned} 6\mathcal{F}_{\text{comp}} = I_{300}a^3 - 3I_{210}a^2 m_0 - 3I_{201}a^2 m \\ + 3I_{120}am_0^2 + 6I_{111}am_0 m + 3I_{102}am^2. \end{aligned} \tag{XIII.4.20}$$

The minus signs accompany one background factor and two Coulomb factors. Two background factors restore a plus sign. This is also a useful way to distinguish the geometric divisor degrees from the coefficients of a signed particle mass.

Expanding A^3 in the two tensors gives the respective polynomials containing a,

$$\mathcal{F}_{\text{mid}} = m_0 a^2 + \frac{7a^3}{6} - \frac{am^2}{2}, \qquad \mathcal{F}_{E,\,\text{comp}} = (m_0 - m/2)a^2 + \frac{4a^3}{3}. \tag{XIII.4.21}$$

The matched new polynomial is $\mathcal{F}_E = \mathcal{F}_{\rm mid} + e^3/6 = \mathcal{F}_{E,\,\rm comp} - m^3/6$. For example, subtracting the two compact polynomials alone gives

$$\mathcal{F}_{E,\rm comp} - \mathcal{F}_{\rm mid} = \frac{e^3+m^3}{6}, \qquad (\mathcal{F}_{E,\rm comp} - \mathcal{F}_{\rm mid})\big|_{a=m} = \frac{m^3}{6}. \tag{XIII.4.22}$$

The common blowup instead fixes a difference that vanishes at the wall, $e^3/6$. The subtraction of $m^3/6$ aligns the two representatives. A background polynomial may be freely chosen when specifying a single local action; comparing its value with a second action requires the choices to be matched.

At fixed backgrounds the constant is irrelevant to T, g, κ. It must be retained when comparing the values of the two prepotential representatives at the wall. We next recover the whole difference from the mass that changes sign.

XIII.4.4 The hypermultiplet threshold

Which part of the effective action detects the sign of a mass? In the ordinary weak gauge patch, a massive Abelian hypermultiplet of signed mass Z contributes $-|Z|^3/12$ to the Coulomb prepotential. The sign matters to the fermion loop even though the particle mass is $|Z|$. For the one full fundamental in this example, the terms in the usual gauge calculation are

$$\mathcal{F}_{\rm gauge} = m_0 a^2 + \frac{2|2a|^3}{12} - \frac{|a+m|^3 + |m-a|^3}{12}. \tag{XIII.4.23}$$

The two roots contribute equally. The two terms with a minus sign come from the weights $R, -E$, with signed masses $r, -e$. In the middle gauge chamber $a > 0$, $r, e > 0$, so

$$(a+m)^3 + (a-m)^3 = 2a^3 + 6am^2. \tag{XIII.4.24}$$

The resulting a^3 and am^2 coefficients in (XIII.4.23) give $\mathcal{F}_{\rm mid}$ in (XIII.4.21).

At $m > 0$, decrease a through $a = m$ with the other generating compact curve periods remaining strictly positive, $r, \ell > 0$. The root terms and the r term keep their signs. For the weight $Z = m - a$, the old contribution is $+Z^3/12$ and the new one is $-Z^3/12$. In the old effective curve orientation $t = e = -Z$ this is

$$\Delta\mathcal{F}_{\rm hyper} = -\frac{Z^3}{6} = \frac{t^3}{6}. \tag{XIII.4.25}$$

Reversing the chosen charge orientation writes the same one-weight term in a different way. It does not supply a second light hypermultiplet. The other signed weight is finite across the wall; its continued value is a coupling parameter in this calculation, not a stability test for a curve representing it in the new fan.

More generally, when the only additional light mode is the hyper from a primitive isolated curve, write t as an affine function of the coordinates $\phi = (a, m_0, m)$ and let

$q_i = \partial_i t$. The comparison of the two cubic representatives gives

$$\begin{aligned} \partial_i \Delta\mathcal{F} &= \frac{1}{2} q_i t^2, \\ \partial_i \partial_j \Delta\mathcal{F} &= q_i q_j t, \\ \partial_i \partial_j \partial_k \Delta\mathcal{F} &= q_i q_j q_k. \end{aligned} \tag{XIII.4.26}$$

At $t = 0$, the prepotential and its first two derivatives agree. The third derivative changes by a constant. In particular the E crossing has $q_a = 1$ in the old effective orientation, so $\Delta\kappa = 1$. In the flavor $+1$ orientation $q_a = -1$, but the jump is $-Z^3/6$, giving the same $\Delta\kappa$. This is a change of the Abelian Chern–Simons coefficient; it does not determine a discrete non-Abelian theta parameter.

For a worked crossing take $(m_0, m) = (5, 3)$ and lower a from 4 to 2. Initially $(e, r, \ell) = (1, 7, 21/2)$. At $a = 3$ the old periods are $(0, 6, 19/2)$. From the matched cubics,

$$\begin{aligned} T_{\mathrm{mid}} &= 2m_0 a + \tfrac{7}{2}a^2 - \tfrac{1}{2}m^2, \qquad g_{\mathrm{mid}} = 2m_0 + 7a, \\ T_E &= 2(m_0 - m/2)a + 4a^2, \qquad g_E = 2(m_0 - m/2) + 8a. \end{aligned} \tag{XIII.4.27}$$

Both sides give $T = 57$ and $g = 31$ at the wall. At $a = 2$, the old signed periods are $(-1, 5, 17/2)$, so the new positive periods are $(1, 15/2, 4)$. The two ruling areas of $S' = \mathbb{F}_0$ now give $T_E = (15/2) \cdot 4 = 30$, and the cubic gives $g_E = 23$. The change from the continued old polynomial at this point is $\Delta\mathcal{F} = -1/6$. Figure XIII.4.3 shows the common value of g and its change of slope from 7 to 8 when crossing from right to left.

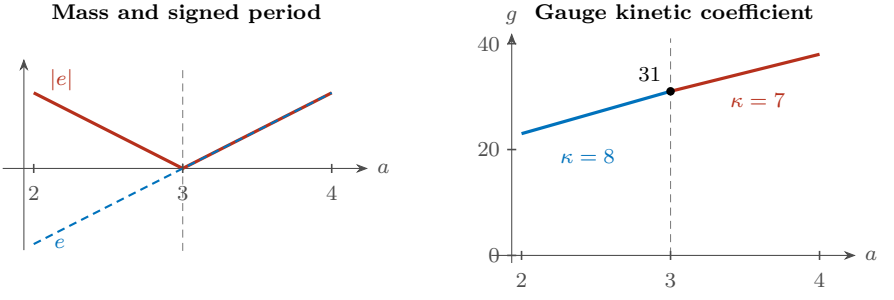


Figure XIII.4.3: The E crossing at $(m_0, m) = (5, 3)$. On the left, the old signed period $e = a - 3$ and the physical mass $|e|$ separate after the flop. On the right, the gauge kinetic coefficient is continuous while its derivative κ changes; the vertical scale starts at $g = 0$. Follow the trajectory from larger to smaller a.

Changing the sign of the flavor mass tests whether the orientation rule has been understood. Take $(m_0, m) = (6, -2)$ and lower a across 2. Now $r = a - 2$ vanishes, whereas $e = a + 2$ and $\ell = a + 5$ stay positive. The old OR relation reverses under the R move, and the matched polynomial becomes

$$\begin{aligned} \mathcal{F}_R &= \mathcal{F}_{\mathrm{mid}} + \frac{r^3}{6} = \frac{4}{3}a^3 + (m_0 + m/2)a^2 + \frac{m^3}{6}, \\ T_R &= 4a^2 + 2(m_0 + m/2)a, \qquad g_R = 8a + 2m_0 + m. \end{aligned} \tag{XIII.4.28}$$

At the wall both representatives give $T = 36$ and $g = 26$. At $a = 1$ the three generating periods in phase R are

$$(-r, \ell, e + r) = (1, 6, 2), \qquad T_R = 14, \qquad g_R = 18, \qquad \mathcal{F}_R - \mathcal{F}_{\text{mid}} = -\frac{1}{6}. \tag{XIII.4.29}$$

The new effective curve has area $-r$, and the other effective curves supply the remaining two positive entries. The equality of the numerical cubic correction with the earlier E example comes from choosing the same continued signed period -1; the background dependence and the replaced edge are different. Here the flavor-$+1$ signed mass r itself changes from positive to negative, so its old and new loop terms are $-r^3/12$ and $+r^3/12$. No extra orientation minus sign is needed.

The same mass gradient controls all matched derivatives. For the three old isolated curves these gradients are

$$q_E = (1, 0, -1), \qquad q_R = (1, 0, 1), \qquad q_L = (1, 1, 1/2), \qquad q_i = \partial_{(a,m_0,m)} t_i. \tag{XIII.4.30}$$

Their first entries are all one, so each of the three oriented simple moves raises the Coulomb cubic coefficient by one. Their mixed jumps differ. In particular q_L contains the inverse-coupling background coordinate; its threshold cannot be obtained by selecting the other weight of the same perturbative fundamental. These real coordinate gradients are sufficient for the polynomial comparison; they do not specify a primitive integral flavor lattice.

This arithmetic illustrates the period and coupling match. A parametrically weak version of the positive-mass crossing uses m_0 large compared with $a, |m|$ and the wall $a = m > 0$. At nonzero t the action without the hypermultiplet applies at probe energies below $|t|$ and the other integrated-out scales. Near the wall, one can instead keep the light hyper and work below the other masses, with the other sectors isolated as above. Exactly at $t = 0$ the window below $|t|$ closes. Continuity of the limiting couplings does not justify removing a massless field. To see which other walls permit the same geometric operation, we must now track the rest of the curve cone.

XIII.4.5 Five Kähler chambers

How do we find every allowed adjacent fan and its positive curve periods? Use phase names mid, E, L, R, LR according to which old edges have been flopped. The signed periods e, r, ℓ still refer to the same coordinates, not to the areas of the same effective curves in every fan. At the OL and OR edges the central relations are

$$E + F - O - L = 0, \qquad E + B - O - R = 0. \tag{XIII.4.31}$$

Thus each has normal degrees $(-1, -1)$ and respective periods ℓ and r. For the L move, OLE, OFL are replaced by LEF, OEF. The new edge EF between them has relation $O + L - E - F = 0$ and area $-\ell$. The old OR relation is unchanged. The OE edge now lies between OEF, OER, so its relation is $F + R - 2O = 0$. It measures $e + \ell$ rather than e. Finally OF now has $E + B + F - 3O = 0$, with period h. This one calculation accounts for the entire L row below.

The edges in the L fan make a useful example of how to turn a triangulation into an actual cone, rather than simply a drawing. Its five internal edges give

Edge	Opposite-ray relation	Period
EF	$O+L-E-F=0$	$-\ell$
OR	$E+B-O-R=0$	r
OE	$F+R-2O=0$	$e+\ell$
OB	$R+F-2O=0$	$e+\ell$
OF	$E+B+F-3O=0$	h

(XIII.4.32)

The first edge is outside S because neither endpoint is O. Nevertheless its curve is compact: it is shared by two triangles in the threefold fan. Its positivity is therefore part of relative ampleness. The last row needs no new inequality, since $h=r+(e+\ell)$. The cone is cut out by three independent strict conditions, $-\ell>0$, $r>0$, $e+\ell>0$.

After the second, disjoint R move the edge OR is replaced by BE. The compact star has become a triangle, and the new full list is

EF	$O+L-E-F=0$	$-\ell$
BE	$O+R-B-E=0$	$-r$
OE	$B+F+E-3O=0$	h
OB	$E+F+B-3O=0$	h
OF	$E+B+F-3O=0$	h

(XIII.4.33)

The three edges through O have the same numerical curve class on the plane. The two exterior curves remain independent, with areas $-\ell$ and $-r$. The collapse of the plane can therefore leave two other compact curves at finite area.

For a check that the list is complete, the boundary $LERBF$ has normalized area five by summing consecutive determinants. It has five primitive sides, so Pick's formula leaves just one interior lattice point, O. A smooth subdivision with these rays has five unit triangles. The triples with absolute determinant one are

$$OLE,\ OLR,\ OLF,\ OER,\ OEB,\ OEF,\ ORB,\ OBF,\\ LER,\ LEF,\ ERB.$$

(XIII.4.34)

Every candidate subdivision chooses five of these with disjoint interiors and uses all six points. Area equality then fills the polygon, and the primitive edges fit without further subdivision. One can carry out the enumeration starting at the boundary edges LE, ER. If LER is present, the remaining diamond $LRBF$ has both diagonals through O and must be triangulated by its star. Otherwise LE is incident to OLE or LEF, and ER to OER or ERB. In each case the remaining triangles are forced by the exposed edges and the requirement of no overlap. For example, LEF and OER force OEF against EF, ORB against OR, and OBF closes the remaining face. This gives the five sets in Table XIII.4.1.

Phase	Triangles	Strict Mori periods	Other periods
mid	OLE, OER, ORB, OBF, OFL	e, r, ℓ	$e+\ell, e+r$
E	LER, OLR, ORB, OBF, OFL	$-e, \ell+e, r+e$	$\ell+e, r+e$
L	LEF, OEF, OER, ORB, OBF	$-\ell, r, e+\ell$	$e+\ell, h$
R	ERB, OEB, OLE, OBF, OFL	$-r, \ell, e+r$	$e+r, h$
LR	LEF, ERB, OEF, OEB, OBF	$-\ell, -r, h$	h, h

Table XIII.4.1: The compact curve periods in every smooth fan of the prescribed six rays. The strict Mori periods generate the curve inequalities. The last column includes the other internal edges with multiplicity.

For the convex full-dimensional support here, the complete toric wall curves generate the relative Mori cone. They are the internal edges, including edges away from O. To read the ample cone directly, lift each vertex to height ω_v. Let λ_{uvx} be the affine function through the three lifted vertices. Apply it to the relation (XIII.4.7). Since $x + y + b_u u + b_v v = 0$ in height-one coordinates, we get

$$\omega_y - \lambda_{uvx}(y) = \omega_y + \omega_x + b_u\omega_u + b_v\omega_v = Z(C_{uv}). \tag{XIII.4.35}$$

Strict positivity bends the lower surface along the edge. Convexity follows by restricting the piecewise affine surface to a line crossing the edges, where each successive slope increases. Thus these are exactly the strict support inequalities for the lower triangulations. For example, positive periods on S alone in the L phase would miss the constraint $-\ell > 0$ on the exterior curve EF. The h entry in that row is redundant since $h = (e+\ell) + r$. One can construct points in a chamber instead of guessing them. In phase L prescribe positive numbers

$$u = -\ell, \qquad v = r, \qquad w = e + \ell. \tag{XIII.4.36}$$

Then $\ell = -u$, $r = v$, $e = w + u$, and the inverse period map gives

$$a = \frac{u+v+w}{2}, \qquad m = \frac{v-u-w}{2}, \qquad m_0 = -\frac{5u+3v+w}{4}. \tag{XIII.4.37}$$

Every positive triple supplies a strict supporting lift for this fan. For instance $(u, v, w) = (1/2, 1, 5/2)$ yields $(a, m_0, m) = (2, -2, -1)$. The negative value of m_0 does not violate any of these inequalities; its interpretation as a weak bare gauge coupling applies only in the ordinary gauge patch. Conversely, testing only the periods on S would accept $(a, m_0, m) = (3, -2, -1)$ in phase L: its surface periods are $r = 2$, $e + \ell = 9/2$, but its exterior area is $-\ell = -1/2$. The surface is positive while the chosen threefold fan is not Kähler.

The strict inequalities in each row have solutions; sample points in order (a, m_0, m) are

$$(4, 5, 3), \quad (2, 5, 3), \quad (2, -2, -1), \quad (2, 5, -3), \quad (9/10, -2, -1) \tag{XIII.4.38}$$

in the order of the table. This calculation shows that each listed smooth fan really occurs as a Kähler chamber.

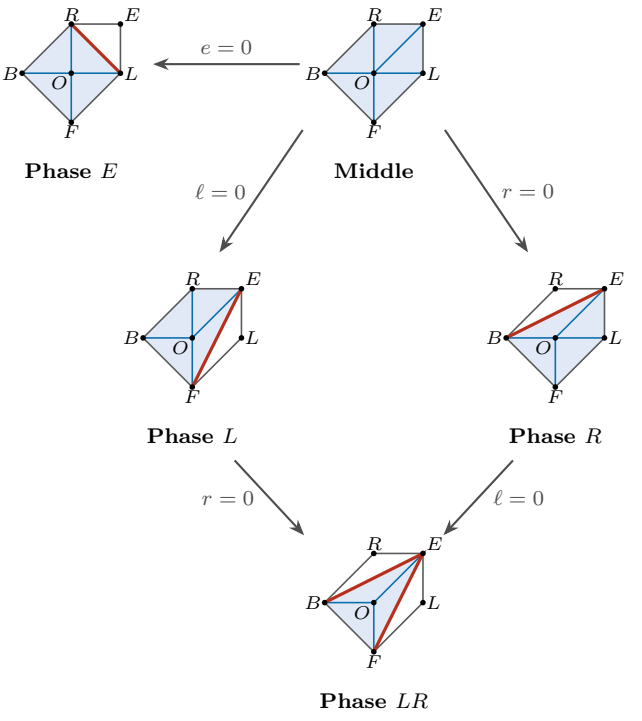


Figure XIII.4.4: The five smooth subdivisions and their flop adjacencies. The blue triangles meet O, the ray of the compact surface. Red edges correspond to compact curves that are not contained in that surface. The labels on the arrows give the old periods that vanish on moving away from the middle phase.

Figure XIII.4.4 shows why the L and R moves commute. In the central surface, $(B-E)(F-E) = 1-1 = 0$ and the curves are distinct, hence disjoint. The two operations replace disjoint pairs of open triangles. The unchanged old relation for the other edge gives the same degree row and period after the first move. At $\ell = r = 0$ and $e > 0$, the two coplanar pairs form cells $OLEF$ and $OERB$ with disjoint interiors. The two nodes are distinct. In contrast, $E \cdot L = E \cdot R = 1$ and the E move changes their period rows. Its simultaneous degeneration with one of those curves cannot use the disjoint-curve argument.

The intersection calculation also works directly in the new stars. If v runs through the cyclic surface fan, let C_v be its toric curve, and let v_-, v_+ be its neighbors. With counterclockwise cyclic order the pairing is

$$C_v^2 = -\det(v_-, v_+), \quad C_v C_{v_+} = 1, \quad K_S = -\sum_v C_v. \tag{XIII.4.39}$$

Other distinct nonneighboring curves are disjoint. Restrict D_v to C_v when Ov is present

and to zero otherwise. This formula gives, in L, the cyclic squares $(0,-1,0,1)$ for E,R,B,F. Write $b=C_R$, $f=C_E$ so $b^2=-1$, $bf=1$, $f^2=0$. The opposite fiber is $C_B=f$ and $C_F=b+f$, as follows from the two character relations for the rays. This is the surface $\mathbb{F}_1$. In particular,

$$K_S=-2b-3f,\qquad D_0|_S=b+f,\qquad D_m|_S=\frac{f-b}{2}. \tag{XIII.4.40}$$

The surface fan also shows how these restrictions were found. The character $(1,0)$ pairs with the cyclic rays E,R,B,F to give $C_E-C_B=0$, while $(0,1)$ gives $C_E+C_R-C_F=0$. Thus $C_B=f$ and $C_F=b+f$. In the determinant formula, $\det(E,B)=1$ gives $C_R^2=-1$, whereas $\det(F,R)=0$ gives $C_E^2=0$. The divisor D_L misses S after the flop, but the strict transforms of D_E,D_F still cut C_E,C_F. Consequently their restrictions need to be recomputed on the new fan, even though the divisor names are unchanged.

The two independent surface periods can be inverted without using the prepotential. If $\omega|_S=\alpha b+\gamma f$, then

$$\omega\cdot f=\alpha=e+\ell,\qquad \omega\cdot b=-\alpha+\gamma=r,\qquad \gamma=r+e+\ell. \tag{XIII.4.41}$$

This distinguishes the coefficient of f from the period of b, which is essential because $b^2=-1$. Squaring gives $\frac{1}{2}(-\alpha^2+2\alpha\gamma)$, the expression for T_L below. It is a direct surface-volume computation that can be compared with the derivative of a threefold cubic.

For example, the mixed products involving the noncompact lifts are computed on the compact surface:

$$\begin{aligned} K_S\cdot(b+f)&=(-2b-3f)\cdot(b+f)=-3,\\ (b+f)\cdot(f-b)/2&=1/2,\qquad (f-b)^2/4=-3/4. \end{aligned} \tag{XIII.4.42}$$

The periods of b,f are $r,e+\ell$, respectively. Consequently

$$\begin{aligned} \omega|_S&=(e+\ell)b+(r+e+\ell)f,\\ T_L&=(e+\ell)r+\tfrac{1}{2}(e+\ell)^2,\\ g_L&=2r+3(e+\ell). \end{aligned} \tag{XIII.4.43}$$

The positive fiber and section periods make both T_L and g_L positive even when the original ℓ is negative.

In R, the squares for L,E,B,F are $(-1,0,1,0)$. Here $C_L=b$, $C_E=C_F=f$, $C_B=b+f$, so $D_0|_S=f$ and $D_m|_S=f/2$. In LR the star of O has three rays, and C_E,C_B,C_F are lines of class H in $\mathbb{P}^2$. Thus $K_S=-3H$, $D_0|_S=H$, $D_m|_S=H/2$. These restrictions give the tensors and volumes in Table XIII.4.2.

Phase and surface	Compact-supported tensor I	T
mid, dP_2	$(7,-2,0,0,0,-1)$	$(e+\ell)(e+r)-e^2/2$
E, $\mathbb{F}_0$	$(8,-2,1,0,0,0)$	$(e+\ell)(e+r)$
L, $\mathbb{F}_1$	$(8,-3,-1/2,1,1/2,-3/4)$	$(e+\ell)r+(e+\ell)^2/2$
R, $\mathbb{F}_1$	$(8,-2,-1,0,0,0)$	$(e+r)\ell+(e+r)^2/2$
LR, $\mathbb{P}^2$	$(9,-3,-3/2,1,1/2,1/4)$	$h^2/2$

Table XIII.4.2: The intersection tensor, in the order of (XIII.4.18), and the relative tension in each chamber.

The central expression expands to $r\ell + e(r+\ell) + e^2/2$. Together with the positive periods in the other rows this makes every T positive on its strict cone. Differentiating at fixed backgrounds gives

$$\begin{aligned} g_{\text{mid}} &= 2\ell + 2r + 3e, \quad & g_E &= 2(e+\ell) + 2(e+r), \\ g_L &= 2r + 3(e+\ell), \quad & g_R &= 2\ell + 3(e+r), & g_{LR} &= 3h. \end{aligned} \tag{XIII.4.44}$$

All are positive on their strict cones. The common blowup calculation gives another route to the cubics. The shifts from the middle representative are

$$(0,\ e^3,\ \ell^3,\ r^3,\ \ell^3 + r^3)/6 \tag{XIII.4.45}$$

in table order. For completeness, reconstruct the polynomials for the two less familiar lifts. Set $\beta = m_0 + m/2$, so $\ell = a + \beta$. Expanding the L and LR tensors gives

$$\begin{aligned} \mathcal{F}_{L,\text{comp}} &= \frac{4}{3}a^3 + \left(\frac{3}{2}m_0 + \frac{1}{4}m\right)a^2 + \left(\frac{1}{2}m_0^2 + \frac{1}{2}m_0 m - \frac{3}{8}m^2\right)a, \\ \mathcal{F}_{LR,\text{comp}} &= \frac{3}{2}a^3 + \frac{3}{2}\beta a^2 + \frac{1}{2}\beta^2 a = \frac{h^3 - \beta^3}{18}. \end{aligned} \tag{XIII.4.46}$$

The linear term in a in the first polynomial is forced by the mixed background intersections. In the plane phase, the same result follows immediately from $A|_S = -(3a+\beta)H = -hH$ and $T = h^2/2$, followed by integration at fixed β. Matching all five representatives fixes their relative background constants:

$$\begin{aligned} \mathcal{F}_L &= \mathcal{F}_{L,\text{comp}} + \frac{\beta^3}{6}, \\ \mathcal{F}_R &= \mathcal{F}_{R,\text{comp}} + \frac{m^3}{6}, \\ \mathcal{F}_{LR} &= \mathcal{F}_{LR,\text{comp}} + \frac{\beta^3 + m^3}{6}. \end{aligned} \tag{XIII.4.47}$$

For example, the L correction has divisor degrees $(-1,1,1/2)$ on (S, D_0, D_m). Its tensor jump is

$$\Delta I_L = (1,-1,-1/2,1,1/2,1/4), \qquad \Delta\mathcal{F}_L = \frac{(a + m_0 + m/2)^3}{6}. \tag{XIII.4.48}$$

The mixed signs and half factors agree term by term with (XIII.4.46). This check uses more information than agreement of $\partial_a^3 \mathcal{F}$ alone.

The double shift can be computed in either order because the other degree row stays fixed. Removing the a-independent terms recovers exactly the polynomials from the compact tensors. We can now follow a trajectory by solving the period inequalities at every step, and compare the resulting domain to the weaker conditions from T and g.

XIII.4.6 Flop or end of a chamber?

Does every zero period permit another diagonal exchange? We will lower a first along a path with two flops and then compare two ways in which a compact surface, rather than an isolated curve, can collapse. Use the fixed-background slice $(m_0, m) = (-2, -1)$. In this slice the old signed functions are

$$e = a + 1, \quad r = a - 1, \quad \ell = a - \frac{5}{2}, \quad h = 3a - \frac{5}{2}. \tag{XIII.4.49}$$

Starting at $a = 4$, the first old period to vanish is ℓ. It is the area of the isolated OL curve. Its dependence on m_0 distinguishes it from either perturbative quark weight. Here the parameter m_0 is outside the weak gauge domain. If the primitive wrapped hyper is the only additional light mode, the local signed threshold still matches the $\ell^3/6$ jump. The existence of the simple flop follows from the geometry and does not require this assumption about the other modes.

In the L phase $-\ell = 5/2 - a$ becomes positive, and the other two strict periods are $r = a - 1$ and $e + \ell = 2a - 3/2$. Hence r vanishes first, at $a = 1$. After the R move, the two exterior periods $-\ell, -r$ are positive and the plane line has period h. The strict intervals on the path are

Phase	mid	L	LR
Interval	$(5/2, 4]$	$(1, 5/2)$	$(5/6, 1)$

(XIII.4.50)

with the wall points included in the closure. For $0 \le a < 5/6$, mid and R fail because $\ell < 0$, E because $e > 0$, and L because $r < 0$. The period $h < 0$ excludes LR. This is a boundary of the union of the five toric cones on the chosen slice.

The order of these transitions has a simple dependence on the backgrounds. Keep the same fan and choose

$$m = -M, \qquad m_0 = -\lambda + M/2, \qquad M < \lambda < 3M, \qquad M > 0. \tag{XIII.4.51}$$

The same local geometry now has a controllable ordering of its walls. The four signed functions become

$$e = a + M, \qquad r = a - M, \qquad \ell = a - \lambda, \qquad h = 3a - \lambda. \tag{XIII.4.52}$$

The first wall is $a = \lambda$. In phase L the remaining strict periods are $a - M$ and $2a + M - \lambda$. At $a = M$ the second of these is $3M - \lambda > 0$, so the next move is indeed R. In phase

LR, the plane period reaches zero at $a = \lambda/3 < M$. Thus the descending open intervals are

$$\text{mid} : a > \lambda, \qquad L : M < a < \lambda, \qquad LR : \lambda/3 < a < M. \tag{XIII.4.53}$$

The upper bound $\lambda < 3M$ does real work: it leaves the other surface period positive at the second flop and separates that flop from the plane collapse. At the final boundary the exterior areas are

$$(-\ell, -r)\big|_{a=\lambda/3} = \left(\frac{2\lambda}{3},\ M - \frac{\lambda}{3}\right) > 0. \tag{XIII.4.54}$$

Taking $M = 2$, $\lambda = 7/2$ changes the backgrounds to $(m_0, m) = (-5/2, -2)$. Starting at $a = 4$, the three transitions occur at $7/2$, 2 and $7/6$. A reader can find them by testing only three positive generators in each visited cone, rather than by extrapolating a single cubic or solving every signed mass at once. The original path is the member $M = 1$, $\lambda = 5/2$.

Return to the original backgrounds $(m_0, m) = (-2, -1)$. At $a = 2$, the formally continued middle prepotential gives

$$T_{\text{mid}} = -8 + 14 - \tfrac{1}{2} = \tfrac{11}{2}, \qquad g_{\text{mid}} = -4 + 14 = 10, \qquad \ell = -\tfrac{1}{2}. \tag{XIII.4.55}$$

Neither positive quantity signals the negative curve period. The correct L periods are $(1/2, 1, 5/2)$ and give $T_L = 45/8$, $g_L = 19/2$. At the first wall $T = 91/8$ and at the second $T = 1/8$. The compact surface thus has positive volume at both simple flops. The exterior EF period is still $3/2$ at the second wall. Figure XIII.4.5 shows the order in which the curves vanish as a decreases.

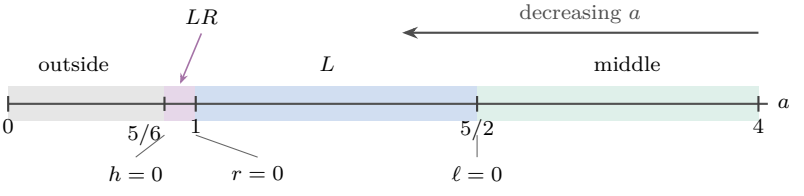


Figure XIII.4.5: Decrease a at fixed $(m_0, m) = (-2, -1)$. The first two marked points are isolated flops. At $h = 0$ the plane collapses, and the shaded interval below $5/6$ belongs to none of the five toric cones.

At $a = 5/6$ the three periods on the compact plane coincide and vanish, while the other periods survive:

$$h = 0, \qquad (-\ell, -r) = (5/3, 1/6), \qquad T = \tfrac{1}{2}h^2 \longrightarrow 0, \quad g = 3h \longrightarrow 0. \tag{XIII.4.56}$$

In the lower subdivision, the three triangles through O merge into the single cell EBF. In the projected triangle $O = (E + B + F)/3$. The lift is coplanar precisely when

$$\omega_O = \tfrac{1}{3}(\omega_E + \omega_B + \omega_F) = -\tfrac{5}{6}. \tag{XIII.4.57}$$

Here O is strictly interior to the triangle and the two other vertices lie strictly above its supporting plane. Removing its star maps S to the point of the cone over EBF. This is the collapse of the whole plane, whose line class measures every curve area on it. The exterior triangles LEF and ERB remain.

For comparison, use phase E at $(m_0, m) = (5, 3)$ and decrease a toward zero. Here the collapsing class has period $r + e = 2a$. The ruling curves of this class sweep $S' = \mathbb{F}_0$. The limit is

$$\begin{aligned}(r+e, \ell+e, -e) &= (2a, 2a+7/2, 3-a),\\ T &= (2a)(2a+7/2) \longrightarrow 0,\\ g &= 8a+7 \longrightarrow 7.\end{aligned} \tag{XIII.4.58}$$

The coarsened cells incident to O are BFL and BLR, with O on the edge BL. To see the coarsening, at $a = 0$ the four lifted vertices B, L, R, O lie on the plane $z = 0$, and B, F, L, O lie on $z = -7y/2$. These planes are both lower supports, and share the edge BL. Contracting the ruling maps S' to the orbit closure of the two-ray cone over BL, a curve. Figure XIII.4.6 distinguishes the two images.

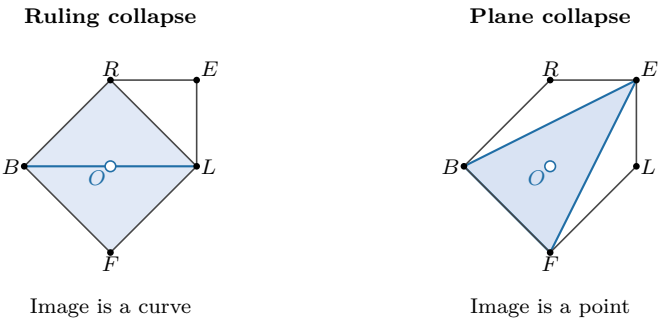


Figure XIII.4.6: The two limiting lower subdivisions. At the ruling collapse the ray O becomes redundant along BL, so the compact divisor maps to a curve. At the plane collapse O becomes redundant inside EBF, so the divisor maps to a point. A hollow marker shows the position of the removed ray.

The way the tension vanishes makes the geometric distinction quantitative. In the plane example of (XIII.4.51), put $a = \lambda/3 + \delta$ with $\delta > 0$. At fixed backgrounds,

$$h = 3\delta, \qquad T_{LR} = \frac{9}{2}\delta^2, \qquad g_{LR} = 9\delta. \tag{XIII.4.59}$$

All curve areas within the plane shrink together, so its volume has a quadratic zero. For the E phase let $\mu = m_0 - m/2 > 0$ and $m > 0$. For sufficiently small positive a, its periods are $m - a$, $2a + \mu$, $2a$, and

$$T_E = (2a)(2a+\mu) = 2\mu a + 4a^2, \qquad g_E = 2\mu + 8a. \tag{XIII.4.60}$$

One ruling remains of finite size μ while the other shrinks. The volume therefore has a linear zero and its first derivative has a nonzero limit. These are derivatives at

fixed m_0, m; holding two period combinations fixed instead would describe a different trajectory and would not compute the same gauge coefficient.

The square of a ruling fiber in S' is zero, and its canonical degree is -2. Its normal bundle in the threefold fits into

$$0 \longrightarrow \mathcal{O} \longrightarrow N_{\mathrm{fiber}/X} \longrightarrow \mathcal{O}(-2) \longrightarrow 0. \tag{XIII.4.61}$$

The extension splits since $H^1(\mathbb{P}^1, \mathcal{O}(2)) = 0$. In particular the fiber moves, in contrast to the isolated $\mathcal{O}(-1) \oplus \mathcal{O}(-1)$ curve. With the ordinary gauge interpretation, the $2a$ period is the mass of the W-boson becoming massless at the $SU(2)$ enhancement. The relative M5 string tension vanishes in both divisorial examples. The tension alone does not determine the light string spectrum.

There is one useful simultaneous limit for which the simple-curve calculation remains separated geometrically. Take a positive number α and set

$$(a, m_0, m) = (\alpha, -\alpha/2, -\alpha), \qquad (e, r, \ell) = (2\alpha, 0, 0). \tag{XIII.4.62}$$

The two quadrilaterals $OLEF$ and $OERB$ have disjoint interiors, so the singularities they describe are distinct. Since (a, m_0, m) and (e, r, ℓ) are invertible coordinates, one can vary r and ℓ independently at fixed positive e near this point. The four nearby chambers are

	$r > 0$	$r < 0$
$\ell > 0$	mid	R
$\ell < 0$	L	LR

$(|r|, |\ell| \ll e).$ (XIII.4.63)

All the other generating periods stay positive in this neighborhood. Moving around the two walls in either order changes the matched cubic by the same sum,

$$\frac{\ell^3}{6} + \frac{r^3}{6} = \frac{r^3}{6} + \frac{\ell^3}{6}. \tag{XIII.4.64}$$

The substantive reason is that each curve and its divisor degrees survive the other operation; the equality of two polynomial sums records that geometric fact. At $\alpha = 2$ the coarsened cells are $OLEF, OERB, OBF$. The last triangle remains unchanged. A simultaneous E and L collapse instead involves curves meeting at a point and changes the remaining period rows, as the first flop calculation showed. The separated-node reasoning cannot be transferred to that locus.

The geometric criterion is which cells coalesce and whether the compact divisor is still a ray of the subdivision. The action below a single-particle threshold accounts for an isolated flop. It cannot by itself describe a contraction of a family of curves or a surface. The five cones here concern smooth toric subdivisions of one affine cone. Their adjacency and matching protected couplings do not decide the identity of complete ultraviolet theories in other frames.

Take-home message of this chapter

Keep the divisors fixed by strict transform and keep the old effective orientation when computing a jump. Across an isolated flop, the new positive area is $-t$ and the matched cubic changes by $t^3/6$. The first two derivatives agree at $t = 0$, while the third detects the charged threshold. To determine where that description applies, test every generating compact curve and inspect what contracts.

XIII.4.7 Exercises

Use exact arithmetic in (a, m_0, m), and compare polynomials in the common wall representative. Use `benchmark/tasks.json` to find the question IDs and `benchmark/PROTOCOL.md` for submission. Explain each geometric conclusion in words.

1. **The L edge.** In the middle phase take $e, r > 0$ and decrease ℓ through zero. Compute the jump in the six entries in (XIII.4.18) and the full new-minus-old polynomial including its term independent of a. Identify the two replaced triangles and explain why neither perturbative quark weight vanishes on this wall in general.

2. **The other quark weight.** Hold $m < 0$ and m_0 fixed and decrease a through $a = -m$ with the other old periods positive. Find $\Delta\mathcal{F}$, ΔT, Δg, and $\Delta\kappa$. Evaluate the first three differences at the wall. Explain why their continuity does not allow the light hypermultiplet to be integrated out there.

3. **The dimension of the contraction.** At $(a, m_0, m) = (3, 5, 3)$, $(0, 5, 3)$, and $(5/6, -2, -1)$, classify the boundary as an isolated flop, a surface-to-curve contraction, or a surface-to-point contraction. Give the limiting T, g at each. Identify the vanishing curves and explain why the second boundary is invisible to a test of positive g alone.

4. **A path with different backgrounds.** Hold $(m_0, m) = (0, -2)$ and decrease a from 4 to 0. Give the phase and endpoints of every open interval, including any interval outside the toric domain. Does the whole path stay in the closure of the five cones? Identify the two interior walls and the final boundary. Explain which information is missing if one checks the quark weights alone.

5. **Two nodes.** At $(a, m_0, m) = (1, -1/2, -1)$ identify the two vanishing periods in the middle chamber and the two resulting quadrilateral cells. Explain why the cubic shifts commute and why the same reasoning does not apply at a simultaneous collapse of E and a curve meeting it. This is a written explanation.

6. **Construct a chamber input.** In phase L, choose $(u, v, w) = (2, 3, 1)$ in (XIII.4.36). Recover (a, m_0, m), verify all five internal-edge periods directly from their relations, and compute T_L in two ways. Then vary u while keeping v, w fixed. Explain why this derivative is not $\partial_a T$ at fixed backgrounds. This is separate written transfer practice.

7. **Order and degeneration of a path.** Use the backgrounds (XIII.4.51). Explain the roles of both bounds $M < \lambda < 3M$ in the three open intervals. Approach $\lambda = 3M$ from below and identify which positive period at the second flop also tends to zero. Explain why the isolated two-step argument must then be reconsidered. Compare with the two-node locus (XIII.4.62), using the actual curve intersections. This is written transfer practice; no stronger physical interpretation of the merged boundary is assumed.

Status and sources

§XIII.4.1. [DEC] assumes normalizability and separation from unwanted bulk modes in addition to the transverse-volume limit. The signed class and relative magnetic unit use the relative period convention of Chapter 2.

§XIII.4.2. [MATH] is the pairing and period map (XIII.4.1)–(XIII.4.3). The explicit restriction and wall solves (XIII.4.4)–(XIII.4.9) are algebraic consequences of the stated resolutions and curve pairings in the same frame.

[MATH] uses Cox et al. (2011), Prop. 6.4.4, (6.4.6)–(6.4.7), printed pp. 302–303 in the inspected September 2010 text. [MATH] is the square semigroup and reversed degrees (XIII.4.10)–(XIII.4.11).

§XIII.4.3. [MATH] is the compactly supported difference (XIII.4.12)–(XIII.4.14). The polarization, tensor expansion and matched background check (XIII.4.15), (XIII.4.20), (XIII.4.22) expand the compactly supported flop comparison while retaining the allowed noncompact polynomial ambiguity.

[GEO-X] uses the protected dictionary (XIII.4.16) in the ordinary flux-free local sector, from Jefferson et al. (2018), arXiv:1801.04036v3, §2.2 (2.9)–(2.12), PDF p. 13. We use A for the signed cubic and take the half factor from (2.10), not the shorthand near (3.1).

§XIII.4.4. [MATH] is the branch and derivative comparison (XIII.4.25)–(XIII.4.26). [GEO-X] uses the ordinary matter and gauge patch of Intriligator et al. (1997), hep-th/9702198v2, §8.1 near (8.10), (8.14)–(8.17), PDF pp. 29–31, and §2.3 (2.22), PDF pp. 10–11. Use the cubic root term in IMS (2.22), rather than the exponent printed in 1801.04036v3 (2.2). [GEO-E] assumes a single additional wrapped hyper, including when invoked at L. See Witten (1996), hep-th/9603150v1, §2.2 (2.1)–(2.7), PDF pp. 6–9, and Jefferson et al. (2018), v3 §3.5.1, PDF pp. 21–22. The opposite-mass example and coordinate gradients (XIII.4.28)–(XIII.4.30) are consequences of the branch and derivative comparison under the stated ordinary gauge and matter hypotheses.

[MATH] is the numerical E comparison (XIII.4.27), separate from a weak hierarchy.

§XIII.4.5. [MATH] also uses Cox et al. (2011), Theorems 6.3.12 and 6.3.20, printed pp. 291 and 294 in the indexed September 2010 text, with convex full support and complete wall curves. [MATH] enumerates the smooth fans (XIII.4.34)–(XIII.4.38). [MATH] computes the compact pairings (XIII.4.39)–(XIII.4.44). The edge tables, inverse cone coordinates, surface inverse map and expanded cubics (XIII.4.32), (XIII.4.33), (XIII.4.36)–(XIII.4.37), (XIII.4.41), and (XIII.4.46)–(XIII.4.48) develop the area and cubic comparisons for the same prescribed rays.

[MATH] derives the disjoint-flop sum (XIII.4.45).

§XIII.4.6. [MATH] gives the path and counterexample (XIII.4.50)–(XIII.4.55). [MATH] is the coarsening calculation (XIII.4.56)–(XIII.4.58). The parameter variations (XIII.4.51)–(XIII.4.54), tension scalings (XIII.4.59)–(XIII.4.60), and separated-node family (XIII.4.62)–(XIII.4.64) are consequences of the chamber and wall calculations. The conditions on M, λ, α, μ are part of those examples.

[GEO-X] uses the ordinary gauge interpretation and relative M5 tension. See Witten (1996), v1 §2.4(a),(b), PDF pp. 12–15, and Jefferson et al. (2018), v3 (2.10). The ultraviolet equivalences proposed in the latter source's §3.1 do not follow from the local calculation.

§XIII.4.7. E1–E4 check submitted exact answers in the same frame. The explanations, E5 and added transfer exercises are assessed in writing. The expanded calculations use the same local and fixed-background assumptions.

References

Cox, D. A., J. B. Little, and H. K. Schenck (2011). *Toric Varieties*. Vol. 124. Graduate Studies in Mathematics. American Mathematical Society. DOI: 10.1090/gsm/124.

Intriligator, K. A., D. R. Morrison, and N. Seiberg (1997). "Five-dimensional supersymmetric gauge theories and degenerations of Calabi-Yau spaces". In: *Nucl. Phys. B* 497, pp. 56–100. DOI: 10.1016/S0550-3213(97)00279-4. arXiv: hep-th/9702198.

Jefferson, P. et al. (2018). "On Geometric Classification of 5d SCFTs". In: *JHEP* 04, p. 103. DOI: 10.1007/JHEP04(2018)103. arXiv: 1801.04036 [hep-th].

Witten, E. (1996). "Phase Transitions in M Theory and F Theory". In: *Nucl. Phys. B* 471, pp. 195–216. DOI: 10.1016/0550-3213(96)00212-X. arXiv: hep-th/9603150.

Chapter XIII.5

Rank-one SCFT limits and their counterexamples

XIII.5.1 What shrinks at strong coupling?

An M5-brane wrapping a compact surface gives a magnetic string in five dimensions. If its tension tends to zero, has the surface shrunk to a point? A ruled surface gives a reason to hesitate. Its fibers may shrink while its base stays finite. A wrapped M2-brane distinguishes these limits: it measures the period of one curve at a time. We will use that difference to find three contraction limits and to diagnose a proposed limit that fails even though its formal scalar metric is positive.

We use the wrapped-brane dictionary and signed intersection prepotential from Chapter XIII.2. The new geometric operation is to build a contraction by coarsening a toric fan. We recall the relevant fan construction when we use it. First we compute periods, tensions and the scalar metric inside a smooth chamber. Then we construct a map at its boundary and ask which cycles the map actually contracts. Finally we compare the resulting local models with named five-dimensional fixed points. The map is a statement about the threefold. The last step uses a physical identification of the sector supported there.

We assume the ordinary flux-free local limit. The normalizable compact mode and the selected wrapped configurations are retained, and gravity and any unwanted bulk modes decouple from the local protected sector. Noncompactness by itself does not establish these assumptions. The abelian Coulomb action describes the smooth chamber; we follow its protected quantities to the boundary without using that action to describe the new massless particles or tensionless strings there.

XIII.5.2 The three tests along a contraction path

How do a particle period, a string tension and the metric test different things? Let $X = \mathrm{Tot}(K_S)$ for a smooth compact surface S and identify S with its zero section. The

vertical tangent bundle is $\pi^* K_S$, where $\pi : X \to S$ is the bundle projection. Taking determinants of the tangent sequence gives

$$K_X \simeq \pi^*(K_S \otimes K_S^{-1}) \simeq \mathcal{O}_X, \qquad N_{S/X} \simeq K_S. \tag{XIII.5.1}$$

The second equality holds because displacements normal to the zero section are displacements in the fiber. Restricting the divisor to itself therefore gives

$$S|_S = K_S, \qquad S^3 = \int_S K_S^2. \tag{XIII.5.2}$$

Multiplication of every fiber coordinate by a number in $[0, 1]$ retracts X to S. Thus $[S]$ generates $H_4(X, \mathbb{Z})$ for the connected surfaces considered here. This is the primitive wrapped surface in our string-tension calculation.

Write the positive Kähler class and the class used in the intersection polynomial as

$$\omega = -aS + mD, \qquad A = -\omega = aS - mD, \qquad J_S = \omega|_S = -aK_S + md, \qquad d = D|_S. \tag{XIII.5.3}$$

Here $a > 0$ is the compact Coulomb coordinate. The noncompact divisor D fixes the lift of the background m; omit it for the plane. The sign in ω makes the periods positive when $-K_S$ is positive on the compact curves and $m = 0$. The sign in A gives the cubic in the magnetic convention in which the primitive tension is the fixed-m derivative with respect to a. We keep both signs through the calculation.

An effective curve is represented by a holomorphic curve with its holomorphic orientation. The mass of a calibrated wrapped M2, when the wrapped state exists, is its positive period in the relative units used here. Its signed compact pairing is the coefficient of a:

$$p_C = \int_C \omega = -a\, S \cdot C + m\, D \cdot C, \qquad M_C = p_C, \qquad q_a(C) = \partial_a p_C|_m = -S \cdot C. \tag{XIII.5.4}$$

The mass formula applies in a Kähler chamber. A negative value of p_C for an effective curve means the proposed class fails the Kähler test. Replacing it by $|p_C|$ would lose that information. Positive periods on the generators of a cone of effective curves imply positivity on their nonzero effective sums. This use of the cone does not count stable bound states.

For the M5 on S the relative tension is the Kähler volume $\frac{1}{2}\int_S J_S^2$. The Coulomb metric is the second derivative of the prepotential with respect to the dynamical coordinate. To see how these two quantities arise from the same polynomial, set $\kappa = K_S^2$, $\nu = K_S \cdot d$, and $\mu = d^2$. Every term containing S in A^3 reduces to an intersection on S:

$$\begin{aligned} 6\mathcal{F} &= a^3 S^3 - 3a^2 m S^2 D + 3a m^2 S D^2 \qquad \text{modulo background-only terms} \\ &= \kappa a^3 - 3\nu m a^2 + 3\mu m^2 a. \end{aligned} \tag{XIII.5.5}$$

No finite intersection degree for D^3 is needed. Terms depending only on m disappear from both Coulomb derivatives; terms containing a depend on the specified lift.

Differentiating before specializing any trajectory gives

$$T = \partial_a \mathcal{F}\big|_m = \tfrac{1}{2}(\kappa a^2 - 2\nu m a + \mu m^2) = \tfrac{1}{2}\int_S (-aK_S + md)^2, \tag{XIII.5.6}$$

$$g_{aa} = \partial_a^2 \mathcal{F}\big|_m = \kappa a - \nu m. \tag{XIII.5.7}$$

The factors are fixed by the cubic and the surface volume. If $[a] = [m]$ is mass, the cubic has mass dimension three, the tension dimension two and the kinetic coefficient dimension one. Varying m selects another fixed-background slice. It does not supply a second kinetic coordinate.

There is a practical distinction between using the polynomial on a slice and evaluating it on a path through backgrounds. For a family $m = m(a)$, the chain rule gives

$$\frac{\mathrm{d}^2}{\mathrm{d}a^2}\mathcal{F}(a, m(a)) = \mathcal{F}_{aa} + 2m'\mathcal{F}_{am} + (m')^2\mathcal{F}_{mm} + m''\mathcal{F}_m. \tag{XIII.5.8}$$

Only the first term is the coefficient of the compact kinetic term at the selected background. The other terms measure how the family moves between theories with different couplings. This matters even if the trajectory is a straight ray. For the ruled polynomial that we will derive below, $\mathcal{F} = ma^2 + 4a^3/3$, a ray $m = \lambda a$ gives

$$\mathcal{F}_{aa}|_{m=\lambda a} = (8 + 2\lambda)a, \qquad \frac{\mathrm{d}^2}{\mathrm{d}a^2}\mathcal{F}(a, \lambda a) = (8 + 6\lambda)a. \tag{XIII.5.9}$$

The discrepancy is not a choice of normalization for the same metric. Indeed, add an allowed background-only term cm^3, where c is constant. It leaves every compact period, tension and fixed-background metric unchanged, but

$$\partial_a^2(cm^3) = 0, \qquad \frac{\mathrm{d}^2}{\mathrm{d}a^2}(c\lambda^3 a^3) = 6c\lambda^3 a. \tag{XIII.5.10}$$

A metric assigned to the varying-background family by total differentiation would therefore depend on a polynomial that was irrelevant to the compact action. We will use tilted rays to test period signs, always taking compact derivatives before making the substitution. For a first example, take an actual positive compact ray $m = 0$ with $\kappa > 0$. Then $g_{aa} = \kappa a$ while $T = \kappa a^2/2$. The radial distance to its boundary, in this metric normalization, is

$$L(0, a_*) = \int_0^{a_*} \sqrt{\kappa a}\,\mathrm{d}a = \frac{2}{3}\sqrt{\kappa}\, a_*^{3/2}. \tag{XIII.5.11}$$

Thus the metric vanishes at the end of a finite-distance trajectory; its sign and the length describe the interior effective theory approaching the boundary. Neither is a test of the positivity of each curve period. The tension is also a different measurement: it integrates over the surface, so it can vanish when fibers shrink over a finite base. We will compute precisely this limit in the ruled examples. First we take a surface with only one curve generator and ask what additional geometric step turns its vanishing period into a point contraction.

XIII.5.3 The local projective plane and the E0 limit

Can a single surface collapse at finite distance without a weak gauge chamber? On $S = \mathbb{P}^2$ the generator ℓ of curve classes is a projective line. We use the same symbol for its divisor class on S. Two lines meet in one point, and adjunction on a line gives

$$\ell^2 = 1, \qquad K_S \cdot \ell + \ell^2 = 2g(\ell) - 2 = -2, \qquad K_S = -3\ell. \tag{XIII.5.12}$$

Consequently the positive class restricts to $3a\ell$. Every nonzero effective curve has degree $d_\ell > 0$, so its period is d_ℓ times the line period. There are no compact curves outside the zero section. Indeed, a curve with nonconstant projection would give, on its normalization, a nonzero section of a negative-degree pullback of K_S. A curve with constant projection would lie in an affine line, which has no compact curve. The same argument will apply to the ruled surfaces with $-K_S$ ample.

On the ray $a > 0$ the line and surface yield

$$S^3 = 9, \qquad t := p_\ell = 3a, \qquad \mathcal{F}(a) = \frac{9a^3}{6} = \frac{3}{2}a^3, \tag{XIII.5.13}$$

$$T = \frac{1}{2}(3a\ell)^2 = \frac{9}{2}a^2, \qquad g_{aa} = 9a. \tag{XIII.5.14}$$

The ray is Kähler on the surface because a positive multiple of the line class is Kähler. To realize it in the total space, one can compactify the bundle in $\mathbb{P}(\mathcal{O} \oplus K_S)$. Add a sufficiently small positive relative Fubini–Study class to the pullback of the surface Kähler class. The relative hyperplane bundle is trivial on the total-space chart, so the result restricts to the desired class on X. The same realization works for the surface Kähler classes used below.

The line mass vanishes linearly and the string tension quadratically. The distance from a_* is $2a_*^{3/2}$ by (XIII.5.11). A useful way to compare coordinates is to use the line period itself. The kinetic term transforms with two Jacobian factors, whereas the primitive string still wraps S:

$$\mathcal{F}(t) = \frac{t^3}{18}, \qquad g_{tt} = g_{aa}\Big(\frac{\mathrm{d}a}{\mathrm{d}t}\Big)^2 = \frac{t}{3}, \qquad T = \frac{t^2}{2} = 3\partial_t \mathcal{F}. \tag{XIII.5.15}$$

Indeed, $\partial_a = 3\partial_t$. The line scalar does not divide the primitive magnetic surface by three. The factor is also visible directly by substituting $J_S = t\ell$ in the wrapped area. This is a change of scalar coordinate, not a new choice of charge lattice.

Now we need a map. A toric diagram at height one is a slice through rays in the lattice $\mathbb{Z}^3$. Coning over each triangle gives a maximal cone in a fan. For the local plane take the exterior rays v_i and the interior ray r:

$$v_1 = (1, 0, 1), \quad v_2 = (0, 1, 1), \quad v_3 = (-1, -1, 1), \qquad r = (0, 0, 1). \tag{XIII.5.16}$$

The triangles rv_iv_{i+1}, with cyclic indices, give the three cones of the local resolution. In the quotient by r, their exterior rays are the plane surface fan. Each consecutive pair in that fan has determinant 1, so each cone of the threefold is smooth. The height-one condition makes the canonical class of the threefold trivial. In a chart for (r, v_i, v_{i+1}),

take the three monomial coordinates dual to the three rays. The two dual to the exterior rays vanish to order zero along r and serve as surface coordinates. The coordinate dual to r vanishes to order one there. In the overlap with the next chart the fiber coordinates satisfy

$$z_{i+1} = \chi^{w_i} z_i, \qquad \langle w_i, r \rangle = 0, \tag{XIII.5.17}$$

where χ^{w_i} is a monomial in the surface coordinates. The transition is linear in the fiber, and the zero section is the divisor at r. By adjunction its normal bundle is K_S.

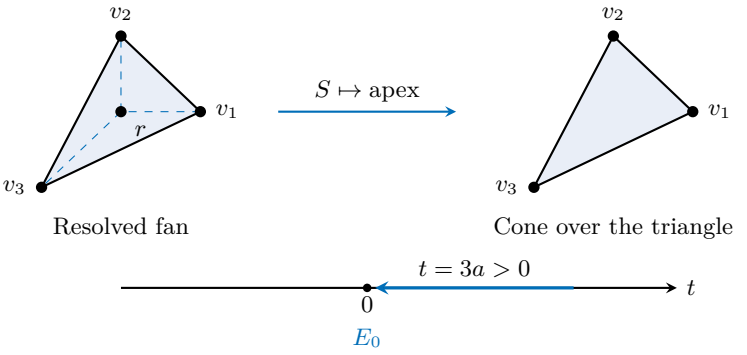


Figure XIII.5.1: The local plane contraction. In the left height-one diagram, the interior point r represents S and the three triangles give the smooth cones. On the right, a single cone uses the same exterior rays. The map deletes the ray through r and sends the entire divisor to the cone apex. The line period t tends to zero along the positive ray; the physical label of the resulting local sector is E_0.

The fan on the left of Figure XIII.5.1 refines the fan of the single affine cone $\sigma = \mathrm{Cone}(v_1, v_2, v_3)$ on the right. A subdivision with the same support gives a proper birational toric map to the affine variety U_σ. All proper faces are unchanged. The open toric orbits outside S are therefore unmodified, while the interior ray maps to the full cone, hence its divisor maps to the apex. In this example one can identify the target explicitly. The matrix with the v_i as columns has determinant 3 and

$$\det \begin{pmatrix} 1 & 0 & -1 \\ 0 & 1 & -1 \\ 1 & 1 & 1 \end{pmatrix} = 3, \qquad r = \tfrac{1}{3}(v_1 + v_2 + v_3). \tag{XIII.5.18}$$

In the lattice generated by the v_i the cone is the affine coordinate octant. The full lattice enlarges it by the generator with all three fractional coordinates $1/3$, so $U_\sigma = \mathbb{C}^3/\mathbb{Z}_3$ with simultaneous scalar multiplication. A nonidentity element fixes only the origin. The same target follows from the section ring:

$$\bigoplus_{j \geq 0} H^0(\mathbb{P}^2, \mathcal{O}(3j)) \simeq \mathbb{C}[x, y, z]^{\mathbb{Z}_3}, \tag{XIII.5.19}$$

since a monomial is invariant exactly when its total degree is divisible by three. This identifies a singularity, in addition to identifying the vanishing periods.

The section ring also makes the contraction visible in local coordinates. Present the total space as the quotient of $(x, y, z) \neq (0, 0, 0)$ together with a fiber coordinate η by

$$(x, y, z, \eta) \sim (\lambda x, \lambda y, \lambda z, \lambda^{-3}\eta), \qquad \lambda \in \mathbb{C}^*. \tag{XIII.5.20}$$

The ten products $\eta x^i y^j z^k$ with $i + j + k = 3$ are invariant under this equivalence and define the map to the affine section cone. To examine it on $x \neq 0$, set $h = y/x$, $k = z/x$ and $w = \eta x^3$. In this chart its coordinates, ordered by degree in h, k, are

$$(w, wh, wk, wh^2, whk, wk^2, wh^3, wh^2k, whk^2, wk^3). \tag{XIII.5.21}$$

When $w = 0$ all ten vanish, independently of h, k; the zero section maps to the apex. When $w \neq 0$, the first three recover the source coordinates:

$$w = \eta x^3, \qquad h = \frac{wh}{w}, \qquad k = \frac{wk}{w}. \tag{XIII.5.22}$$

On the other two surface charts the same recovery uses ηy^3 or ηz^3. At every point outside the zero section one of these is nonzero. Thus the coordinates explain directly why the contraction loses an entire $\mathbb{P}^2$ at the apex and loses no points away from it. The fan refinement establishes properness; these local expressions describe what that proper map does.

The line period also gives a short transfer calculation. A smooth plane conic has class 2ℓ. At the same value of a it has

$$p_{2\ell} = 2p_\ell = 6a, \qquad (2\ell)^2 = 4, \qquad \frac{p_{2\ell}}{p_\ell} = 2. \tag{XIII.5.23}$$

Both periods vanish on the same ray because the cone has one generator; the conic does not introduce an independent tuning. This calculation compares calibrated areas for the specified classes. It does not count single-particle states of degree two or decide their stability against two line classes. It also supplies another test of the proposed ruling: neither the line nor a higher effective multiple has the zero square needed for disjoint fibers.

In the local decoupling limit with no additional discrete background, the plane contraction is the standard construction of the E_0 fixed point. The identification uses the particular singularity and its physical comparison with the brane construction. To see why the conventional pure $SU(2)$ ruling mechanism is absent, observe that any nonzero effective curve $d_\ell \ell$ has square $d_\ell^2 > 0$. Fibers of a ruling have square zero, since two different fibers are disjoint. Here there is no such class and no independent base period to hold finite as the line shrinks. The next surfaces have both a base and a fiber; a tensionless string alone will no longer specify the limit.

XIII.5.4 Two ruled surfaces with the same prepotential

When does shrinking a surface mean shrinking it to a point rather than collapsing its fibers? On F_n choose the section E of self-intersection $-n$ and a fiber f of the projection

to $\mathbb{P}^1$. For $F_0 = \mathbb{P}^1 \times \mathbb{P}^1$ either factor can be the fiber. The intersection pairing is

$$E^2 = -n, \qquad E \cdot f = 1, \qquad f^2 = 0. \tag{XIII.5.24}$$

The section and fiber generate the effective curve cone. In fact f and $E + nf$ are nef, meaning that they have nonnegative degree on every effective curve. The first comes from the ruling base. The second has a representative given by the section disjoint from E, or a ruling from the other factor for F_0. Its intersection with any other irreducible curve is nonnegative, and its own square is $n \geq 0$. If $C = xE + yf$, pairing with these two nef classes gives x and y, respectively. Both generators themselves are effective, so no further inequalities are needed on S.

Adjunction on the two rational curves determines K_S from the pairing. Write $K_S = uE + vf$. Then

$$K_S \cdot f = u = -2, \qquad K_S \cdot E = -nu + v = n - 2, \qquad K_S = -2E - (n+2)f, \tag{XIII.5.25}$$

$$K_S^2 = 4(-n) + 4(n+2) = 8. \tag{XIII.5.26}$$

Changing n changes the section square and its canonical degree, but the two changes cancel in K_S^2. For $n = 0, 1$, $-K_S$ has positive degree on both extremal curves and positive square, hence it is ample. The negative-degree argument of the plane section excludes compact curves outside the zero section in these two models.

The noncompact lift is $D = \pi^{-1}(f)$, so $D|_S = f$. Using this same lift in both models gives the tensor and the restricted Kähler class

$$(S^3, S^2D, SD^2) = (K_S^2, K_S \cdot f, f^2) = (8, -2, 0), \tag{XIII.5.27}$$

$$J_S = 2aE + \big((n+2)a + m\big)f. \tag{XIII.5.28}$$

Pairing with E and f gives

$$(p_E, p_f) = \big(m + (2-n)a,\ 2a\big). \tag{XIII.5.29}$$

Both periods must be positive. In these examples this makes J_S Kähler: it is positive on the effective generators and its square is positive, as the volume calculation below shows. Equivalently, it is in the interior of the real ample cone. We can then realize the class in the total space as in the plane case. The background m shifts the section period and leaves the fiber period unchanged.

It is useful to invert this dictionary before taking limits. Suppose the two measured positive periods are p_E and p_f. Solving (XIII.5.29) gives

$$a = \frac{p_f}{2}, \qquad m = p_E - \frac{2-n}{2}p_f, \qquad a > 0, \quad m > -(2-n)a. \tag{XIII.5.30}$$

The last inequalities describe the chamber in parameter space. A constant value of m is a straight line in the positive period quadrant, with slope

$$\left.\frac{\mathrm{d}p_E}{\mathrm{d}p_f}\right|_m = \frac{2-n}{2}. \tag{XIII.5.31}$$

For F_0 the slope is one, while for F_1 it is one half. Thus the same instruction "hold the background fixed" follows different lines in the two measured period planes. The compact coordinate is half the fiber period in each; the background is a different linear combination of the two periods. This is why one must specify which quantities are held equal when comparing the surfaces.

The cubic, tension and metric reduce to

$$\mathcal{F} = \frac{1}{6}(8a^3 + 6ma^2) = ma^2 + \frac{4}{3}a^3, \tag{XIII.5.32}$$

$$T = 2ma + 4a^2, \qquad g_{aa} = 2m + 8a. \tag{XIII.5.33}$$

There is a direct way to see what the tension measures. Reconstruct $J_S = p_f E + (p_E + np_f)f$ from the two periods. Then

$$\tfrac{1}{2}J_S^2 = \tfrac{1}{2}\big(-np_f^2 + 2p_f(p_E + np_f)\big) = p_f p_E + \tfrac{n}{2}p_f^2. \tag{XIII.5.34}$$

For F_0 it is just the product of the two ruling periods. For F_1 the extra $p_f^2/2$ compensates for the smaller section period at the same a, m. In particular, equality of the two tensions does not imply equality of the periods.

Conversely, equal periods in the chosen generators need not give equal areas on two different surfaces. Substituting (XIII.5.30) into the metric gives

$$T = p_f p_E + \frac{n}{2}p_f^2, \qquad g_{aa} = 2p_E + (n+2)p_f. \tag{XIII.5.35}$$

As a changed-input example choose a positive scale u and ask for $(p_E, p_f) = (5u, 2u)$ in each model. Then

	a	m	T	g_{aa}
F_0	u	$3u$	$10u^2$	$14u$
F_1	u	$4u$	$12u^2$	$16u$

(XIII.5.36)

The difference in T is $2u^2 = p_f^2/2$, precisely the self-intersection correction in the area formula. The backgrounds differ because the canonical degree of E differs. By comparison, at equal input $a = u, m = 3u$ the cubics and their compact derivatives agree, but the section periods are $5u$ and $4u$. These two comparisons separate the geometric intersection pairing from the continuous polynomial written in a fixed parameter frame.

At fixed $m > 0$ the leading term is $2ma$ as $a \to 0^+$. Both T and the fiber period vanish, but

$$(p_E, p_f) \longrightarrow (m, 0), \qquad g_{aa} \longrightarrow 2m \qquad (m > 0 \text{ fixed}). \tag{XIII.5.37}$$

Over a patch of the base, the canonical bundle restricts along each fiber as $\mathcal{O}_{\mathbb{P}^1}(-2)$ because $K_S \cdot f = -2$. The corresponding contraction is the transverse A_1 cone. To see this, write its section ring using homogeneous coordinates x, y on the fiber:

$$\bigoplus_{j \geq 0} H^0(\mathbb{P}^1, \mathcal{O}(2j)) = \mathbb{C}[x^2, xy, y^2] \simeq \mathbb{C}[U, V, W]/(UW - V^2). \tag{XIII.5.38}$$

The base survives and the singularity is fibered over it. When $m \gg a > 0$, the light wrapped fiber gives the W in the pure $SU(2)$ chamber, while the wrapped section is

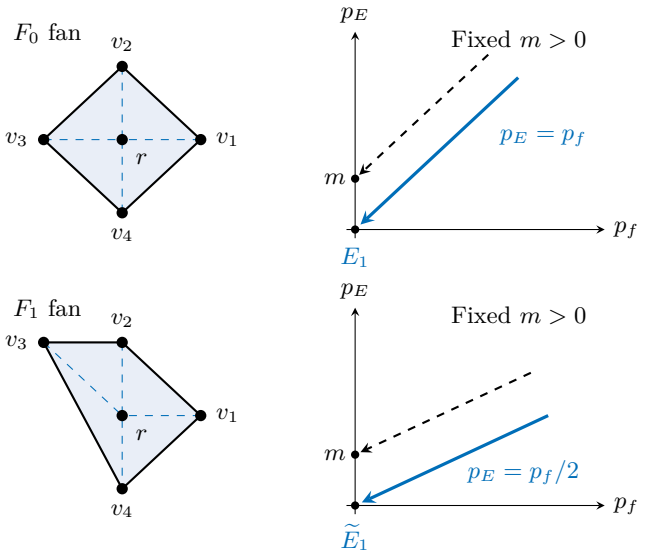


Figure XIII.5.2: The ruled contractions in the toric and period descriptions. At left the dashed segments are the subdivision at r. Erasing them and r gives the affine cone over the solid boundary. At right the solid arrow follows $m = 0$ and the dashed arrow follows a fixed positive m. Both decrease a; only the solid arrow reaches the origin. The two local sectors at the origins are identified separately as E_1 and $\widetilde{E}_1$.

heavy. Here m sets the inverse gauge coupling scale in the relative units of the next section. The small-a limit at fixed m is the restoration of the gauge symmetry of this deformed theory.

The hierarchy can be read without assigning a state to every effective curve. For the two selected generator periods,

$$\frac{p_E}{p_f} = \frac{m}{2a} + \frac{2-n}{2}, \qquad \frac{T}{p_f} = m + 2a, \qquad \lim_{a\to 0^+} \frac{T}{p_f} = m. \tag{XIII.5.39}$$

The finite last ratio is the remaining base scale measured by the surface volume per shrinking fiber. Along this path T vanishes to first order in a, whereas at $m = 0$ it vanishes to second order. The vanishing order is useful only after identifying which path was taken: the same surface admits both behaviors.

At a fixed positive background the compact metric also makes the approach finite. Its distance from a_* to the fiber wall is

$$L_m(0, a_*) = \int_0^{a_*} \sqrt{2m + 8a}\, \mathrm{d}a = \frac{(2m + 8a_*)^{3/2} - (2m)^{3/2}}{12}. \tag{XIII.5.40}$$

For $a_* \ll m$ it is $\sqrt{2m}\, a_*$ to leading order. Taking $m \to 0$ in this expression recovers $(2/3)\sqrt{8}\, a_*^{3/2}$. Both boundaries are at finite distance on their respective fixed-background slices; the distance alone does not distinguish a finite base from a point contraction.

At zero background the two paths instead obey

$$F_0:\ p_E = p_f = 2a, \qquad F_1:\ p_E = p_f/2 = a, \qquad (p_E, p_f) \longrightarrow (0,0). \tag{XIII.5.41}$$

Here $T = 4a^2$, $g_{aa} = 8a$ and the metric distance to the origin is $(2/3)\sqrt{8}\, a_*^{3/2}$. The origin in period space differs from the endpoint at $p_E = m$ of the fixed positive-background path. To see that it represents a point contraction, use the same height-one construction as for the plane.

The ordered surface rays, before lifting to height one, are

$$u_1 = (1,0), \qquad u_2 = (0,1), \qquad u_3 = (-1,n), \qquad u_4 = (0,-1). \tag{XIII.5.42}$$

Take $v_i = (u_i, 1)$, and keep $r = (0,0,1)$ for the star. Each consecutive determinant $\det(u_i, u_{i+1})$ equals 1. To see whether the boundary is strictly convex, orient each edge in the indicated order and take the determinant with each nonincident vertex. For the edge u_1u_2, the test against u_3 gives

$$\det(u_2 - u_1, u_3 - u_1) = \det \begin{pmatrix} -1 & -2 \\ 1 & n \end{pmatrix} = 2 - n. \tag{XIII.5.43}$$

For all four edges the two determinants, taken in cyclic order of the remaining vertices, are

$$(2-n, 2), \quad (2, 2-n), \quad (2+n, 2), \quad (2, 2+n). \tag{XIII.5.44}$$

They are strictly positive for $n = 0, 1$. The origin is inside since every consecutive determinant about it is positive. The star at r is therefore a subdivision of a single convex cone with unchanged proper faces. Removing r gives the proper birational map collapsing exactly S to the apex. The proper faces are smooth, being faces of the smooth star cones. The affine target has four extremal rays in rank three, so it is singular at its apex.

Figure XIII.5.2 puts the two operations side by side. The upper and lower subdivisions both yield a point contraction, but the slopes of the zero-background paths differ because E has different canonical degree. We next compare these different section charges with the same perturbative gauge polynomial.

XIII.5.5 What distinguishes the two pure gauge theories?

Why do equal compact cubes and equal pure polynomials miss a discrete theta choice? First reproduce the cubic from the weak gauge chamber. Use the Cartan generator $H = \operatorname{diag}(1, -1)$ so the adjoint eigenvalue differences are $\pm 2a$. The inverse bare coupling parameter m multiplies $\operatorname{Tr} H^2/2$ and the two vector roots contribute their absolute cubes. On the positive ray the pure gauge formula gives

$$\mathcal{F}_{\text{gauge}} = \frac{1}{2} m \operatorname{Tr}(H^2) a^2 + \frac{1}{12}\big(|2a|^3 + |-2a|^3\big) = ma^2 + \frac{4}{3}a^3. \tag{XIII.5.45}$$

The factor of two from the roots and the trace of H^2 fix the relative coefficients. The equality with (XIII.5.32) includes the term with m; at $m = 0$ alone we would test only the compact cube. The perturbative charged vector content and the quadratic coupling agree in both pure chambers.

Now measure the charges of the selected wrapped particles. The fiber has no background charge, while the section has one unit. With $I(C) = \partial_m p_C = D \cdot C$ we find

$$(q_a(f), I(f)) = (2, 0), \qquad (q_a(E), I(E)) = (2 - n, 1). \tag{XIII.5.46}$$

These are relative pairings with the chosen compact coordinate and fixed divisor lift. For F_1 the section is the exceptional curve of the blowup of the plane at one point. The pencil of lines through the point gives the ruling after blowup. If ℓ is the pullback of a line, then $f = \ell - E$, with $f^2 = 0$ and $E \cdot f = 1$. The odd self-intersection of this section contrasts with the even intersection form of the product:

$$(xE + yf)^2 = -nx^2 + 2xy. \tag{XIII.5.47}$$

For F_1 the choice $x = 1, y = 0$ gives -1; for F_0 every integral pair gives an even square. This is a geometric distinction independent of the common intersection polynomial.

The separate brane comparison uses a scalar ϕ for which the W has electric charge $n_e = 1$. The central charge of the selected states is

$$Z = n_e\phi + I/g_0^2, \qquad \phi = 2a, \quad m = 1/g_0^2, \quad q_a = 2n_e. \tag{XIII.5.48}$$

The fiber agrees with the W in both models. For the selected unit instanton the brane construction gives $n_e = 1$ or $n_e = 1/2$ for the two respective chambers. In the units of (XIII.5.48) the comparisons are

	Z_W	Z_{inst}
F_0	$\phi = 2a$	$\phi + 1/g_0^2 = 2a + m$
F_1	$\phi = 2a$	$\phi/2 + 1/g_0^2 = a + m.$

(XIII.5.49)

The instanton entries match the sections in (XIII.5.29). The different electric charge is visible at nonzero a even though the instanton background coefficient is the same. This comparison uses particular protected states, rather than identifying the entire instanton spectrum from a period.

One can use these mass formulas in reverse. Suppose the selected W has period $w > 0$ and the selected unit-instanton state has period $b > 0$ in either chamber. The common compact coordinate and the required backgrounds are

$$a = \frac{w}{2}, \qquad m_{F_0} = b - w, \qquad m_{F_1} = b - \frac{w}{2}. \tag{XIII.5.50}$$

For example, $b = 3w$ gives positive backgrounds $2w$ and $5w/2$, respectively. The local area and metric at these equal measured periods follow by inserting $p_f = w, p_E = b$ in (XIII.5.35):

$$(T_{F_0}, T_{F_1}) = (3w^2, \tfrac{7}{2}w^2), \qquad (g_{aa,F_0}, g_{aa,F_1}) = (8w, 9w). \tag{XIII.5.51}$$

This is a comparison of two backgrounds, one in each model. It does not contradict equality of their formulas at equal a, m. Measuring a common W period and a common selected instanton period is a different experiment from choosing a common inverse bare coupling. The theta distinction still requires its independent physical identification below.

In five dimensions the pure $SU(2)$ gauge theory has a discrete theta choice because $\pi_4(SU(2)) = \mathbb{Z}_2$. Let $\epsilon = 0, 1$ index the two classes of this group. The two characters give weights

$$\chi_\theta(\epsilon) = e^{i\theta\epsilon}, \qquad \chi_\theta(1)^2 = 1, \qquad \theta = 0, \pi. \tag{XIII.5.52}$$

This sign multiplies the nontrivial class without changing the perturbative vector-root sum in (XIII.5.45). The independent comparison with the brane configurations assigns the chamber of F_0 to $\theta = 0$ and that of F_1 to $\theta = \pi$. Their point limits are the E_1 and $\widetilde{E}_1$ theories, respectively, in the isolated local sector without additional discrete backgrounds. Their continuous flavor Lie algebras are different, as collected in Table XIII.5.1.

Table XIII.5.1: The two ruled chambers and their sourced fixed-point identifications. Charges in the two middle columns are in the common compact coordinate a. Flavor refers to the continuous Lie algebra at the point limit.

Surface	S^3	$q_a(f)$	$q_a(E)$	θ	Endpoint	Flavor
F_0	8	2	2	0	E_1	$\mathfrak{su}(2)$
F_1	8	2	1	π	$\widetilde{E}_1$	$\mathfrak{u}(1)$

On F_0 at $m = 0$, exchange of the two rulings exchanges their equal periods. This is a geometric correlate of the E_1 comparison. Demonstrating flavor enhancement requires the physical current sector. Neither the exchange nor the parity in (XIII.5.47) derives the theta assignments, and the comparison here leaves the global flavor form and line operators open. We have seen two valid geometries with equal cubics and distinct physics. The same cubic can even occur on a proposed path that fails to define a Kähler class.

XIII.5.6 Positive metric, forbidden period

How can the formal derivatives be positive when a proposed route is invalid? Keep F_1 and move from $m = 0$ into negative backgrounds. At fixed $a > 0$ the Kähler wall is at $m = -a$, where the section period vanishes. The condition $g_{aa} > 0$ instead continues down to $m > -4a$, and the formal positive surface area continues down to $m > -2a$. These inequalities give different walls:

$$p_E > 0 \Longleftrightarrow m > -a, \qquad T > 0 \Longleftrightarrow m > -2a, \qquad g_{aa} > 0 \Longleftrightarrow m > -4a. \tag{XIII.5.53}$$

The last two conditions use the formal continuation of the same polynomial. Choose a point between the first two walls at every $a > 0$. Differentiating first at fixed m and

then evaluating on $m = -3a/2$ gives

$$(p_E, p_f) = (-a/2, 2a), \qquad (T, g_{aa}) = (a^2, 5a). \tag{XIII.5.54}$$

All four quantities tend to zero with a, but the section period approaches zero from the forbidden side. Its holomorphic orientation has not changed. The proposed ray is inadmissible in this resolution. This argument concerns the original effective cone; a neighboring flop chamber would have to be analyzed with its own effective curves.

A fixed negative background gives another way to encounter the same wall, without varying a coupling during the motion. Set $m = -M$ with $M > 0$ on F_1. Starting at $a > M$ and decreasing a, the first vanishing period is

$$p_E = a - M, \qquad p_f = 2a, \qquad a_{\text{wall}} = M. \tag{XIII.5.55}$$

At that wall the remaining measurements are

$$(p_f, T, g_{aa})\big|_{a=M, m=-M} = (2M, 2M^2, 6M). \tag{XIII.5.56}$$

The surface retains positive area and the fiber retains positive period when the section collapses. Continuing the same resolved-chamber formulas towards $a = 0$ would cross this wall first. Thus the expression for a positive Hessian near a proposed endpoint is insufficient even for deciding whether that endpoint is reachable inside the specified chamber. No physical phase beyond the wall is needed to locate the failure.

The changed surface F_0 illustrates why the area is a separate measurement. With the same fixed $m = -M$, the section wall occurs at $a = M/2$, where

$$(p_E, p_f, T, g_{aa}) = (0, M, 0, 2M). \tag{XIII.5.57}$$

The surviving ruling has finite period even though the surface area now vanishes. The product surface is symmetric between its two rulings; this is the reversed choice of which ruling is shrinking. This statement concerns the surface and its periods and adds no identification of a new phase.

The same failure can occur at zero background if the surface changes. For F_0 through F_3 the intersection form gives the same cubic and the same formal values $T = 4a^2$ and $g_{aa} = 8a$ at $m = 0$. The section period on that ray changes sign:

$$\frac{p_E}{a}\Big|_{m=0} = 2 - n. \tag{XIII.5.58}$$

The fiber period stays $2a$. Table XIII.5.2 shows which part of the test separates the geometries.

More generally, put $m = \lambda a$ only after computing the derivatives. At each positive a the three inequalities become

$$\begin{aligned} p_E = a(\lambda + 2 - n) > 0 &\iff \lambda > n - 2, \\ T = 2(\lambda + 2)a^2 > 0 &\iff \lambda > -2. \end{aligned} \tag{XIII.5.59}$$

$$p_f = 2a > 0, \qquad g_{aa} = 2(\lambda + 4)a > 0 \iff \lambda > -4. \tag{XIII.5.60}$$

The area and metric conditions are independent of n, but the effective section condition changes with n. On F_1, the interval $-2 < \lambda < -1$ has positive formal area and metric while the section period is negative. On F_3, positivity on the surface instead requires $\lambda > 1$. A common numerical endpoint $(p_E, p_f) = (0, 0)$ for these rays records none of this information about their interiors.

Table XIII.5.2: The compact ray at $a > 0$ and $m = 0$. The metric and area columns are formal expressions where the periods do not define a Kähler class.

Surface	p_E/a	T/a^2	g_{aa}/a	Section period
F_0	2	4	8	Positive
F_1	1	4	8	Positive
F_2	0	4	8	On the boundary
F_3	-1	4	8	Outside the chamber

The equality case has its own geometry. On F_2 the point $u_2 = (0, 1)$ is the midpoint of u_1u_3 in the toric diagram. Removing it would change the subdivision of a proper face of the cone. On the bundle side,

$$K_{F_2}|_E \simeq \mathcal{O}_{\mathbb{P}^1}, \qquad \pi^{-1}(E) \simeq \mathbb{P}^1 \times \mathbb{C}. \tag{XIII.5.61}$$

Here the canonical degree is zero by (XIII.5.25). The curves $\mathbb{P}^1 \times \{z\}$ form a family indexed by a noncompact parameter, all in the class of the zero-section curve E. The period test with equality therefore allows an entire family of zero periods. It is different from approaching a strict isolated contraction through the positive interior. No new physical phase identification for F_2 follows from this equality.

The period and fan controls are measuring the same canonical degree at this stage. Adjunction and the determinant test combine as

$$-K_{F_n} \cdot E = 2 - n = \det(u_2 - u_1, u_3 - u_1). \tag{XIII.5.62}$$

For $n = 0, 1$, strict positivity keeps u_2 as a genuine corner and makes the canonical line negative on E. For $n = 2$, degree zero accompanies a straight boundary edge and permits the translated compact curves in (XIII.5.61). For $n = 3$, the degree changes sign and u_2 ceases to be a corner. This equality is a calculation for these specified fans; it explains their three different behaviors without providing a criterion for arbitrary compact surfaces.

For F_3 the negative p_E can be made positive by tilting the path. This is a useful second test because the first failure is now absent on S. On the family $m = 2a$,

$$(p_E, p_f) = (a, 2a), \qquad (T, g_{aa}) = (8a^2, 12a). \tag{XIII.5.63}$$

The positive periods now approach zero from the allowed side on the surface. The metric in (XIII.5.63) is $\partial_a^2 \mathcal{F}\big|_m$ evaluated at $m = 2a$. By contrast, substituting before differentiating gives

$$\frac{\mathrm{d}^2}{\mathrm{d}a^2} \mathcal{F}(a, 2a) = \frac{\mathrm{d}^2}{\mathrm{d}a^2} \left(\frac{10}{3} a^3 \right) = 20a. \tag{XIII.5.64}$$

This derivative varies the inverse coupling at the same time as the compact coordinate. It is not the kinetic coefficient. The question is whether the tilted path yields the same type of isolated contraction as the strict examples.

A change of path does not change the fan. In F_3 the point u_2 lies strictly inside the triangle of the three other exterior points:

$$u_2 = \tfrac{2}{5}u_1 + \tfrac{2}{5}u_3 + \tfrac{1}{5}u_4. \tag{XIII.5.65}$$

Thus a single cone over that triangle cannot keep u_2 as an exterior ray. Deleting just r cannot have the same effect as in F_0 or F_1. A curve outside S gives a direct obstruction, even without requiring a toric map. In this case the canonical degree of the section is $+1$, so

$$K_{F_3}|_E \simeq \mathcal{O}_{\mathbb{P}^1}(1), \qquad \Gamma_s = \{(x, s(x)) : x \in E\} \subset X \tag{XIII.5.66}$$

for any nonzero holomorphic section s of the restricted bundle. Its graph Γ_s is a compact copy of E. It meets S at the unique zero of s and lies outside S elsewhere. Every regular function on this complete curve is constant. Hence any morphism from X to an affine variety maps Γ_s to a single point. If the map sends S to a point, the intersection forces Γ_s to map to the same point. The map cannot be an isomorphism away from S and have exceptional locus exactly S. This excludes the proposed contraction into an affine target in the specified smooth model. It does not exclude other exceptional sets, embeddings or phases.

One can see the graph obstruction in coordinates on E. Take homogeneous coordinates $[s : t]$ and the section s of $\mathcal{O}_{\mathbb{P}^1}(1)$. Its graph has exactly one intersection with the zero section, at $[0 : 1]$:

$$\Gamma_s \cap S = \{[0 : 1]\}, \qquad \Gamma_s \simeq \mathbb{P}^1, \qquad H^0(\Gamma_s, \mathcal{O}) = \mathbb{C}. \tag{XIII.5.67}$$

For an affine target $Y = \operatorname{Spec} R$, a morphism restricted to Γ_s pulls every $r \in R$ back to a constant. Its image is therefore one point. Since the intersection point already lies in S, that point is the image of S. The obstruction persists for every tilt that makes the surface periods positive: changing a Kähler class does not remove Γ_s from this total space. In particular, $\lambda > 1$ in (XIII.5.59) repairs the sign on F_3 but leaves this argument unchanged. In F_2 a nonzero constant section of the trivial line over E produces a translated curve disjoint from S; this is the related reason that one must track the proper faces and the extra compact curves, rather than infer an isolated exceptional set from the zero-section area alone.

The three named endpoints consequently use three pieces of information. The positive interior path makes the wrapped periods physical. The fan map specifies the exceptional locus and the singular target. The separate M-theory and brane comparison, with the local decoupling premise, assigns E_0, E_1 or $\widetilde{E}_1$ to that particular isolated local sector. The F_2 and F_3 controls keep these steps distinct: a saturated period fails the strict-interior test, while a repaired positive surface ray still need not supply the required contraction map. With several compact surfaces, the next chapter will have to follow curves shared by two surfaces as well as the volumes of each surface.

Take-home message of this chapter

A curve period, a surface volume and a scalar metric answer different questions. For F_0 and F_1, shrinking the fibers at fixed positive background makes the magnetic string tension vanish while the base survives. The zero-background rays lead instead to point contractions. The common cubic neither identifies the two fixed points nor replaces the effective curve test.

XIII.5.7 Exercises

1. **Degree and its limits.** On the blowup of the plane at k distinct points, write ℓ for the pullback of the line and E_i for the exceptional curves. The canonical class is $K = -3\ell + \sum_i E_i$ with $\ell \cdot E_i = 0$ and $E_i \cdot E_j = -\delta_{ij}$. Compute K^2 at $k = 1, 2, 3$ and on the unblown product surface F_0. Submit `bl1`, `bl2`, `bl3`, `f0` to `degrees`. Explain why each blowup changes the square by one and why the square does not determine ampleness or a field theory.

2. **A coordinate and a wrapped surface.** In local $\mathbb{P}^2$, express the cubic with zero additive terms, the metric component, the primitive tension and the factor relating that tension to $\partial_t \mathcal{F}$ in the line-period coordinate t. Submit `cubic`, `metric`, `tension`, and `derivative_multiplier` to `line`. Use only t as a variable. Explain why changing coordinates does not divide the wrapped four-cycle.

3. **Three paths in one period plane.** For F_1, compute the limits at fixed $m > 0$ as $a \to 0^+$ and submit `fixed_section_limit`, `fixed_fiber_limit`. Give the periods at $m = 0$ as `zero_section`, `zero_fiber`. On $m = -3a/2$ compute the section period and fixed-background Hessian, `bad_section` and `bad_metric`. Submit all six to `paths`, using a, m as appropriate. Explain which curves collapse in the first two limits, and why the third path fails.

4. **Data beyond the pure cubic.** Compute the compact charges of the fiber and section for F_0 and F_1, using `fiber_f0`, `section_f0`, `fiber_f1`, `section_f1`. Give the sourced theta angles in units of π as `theta_over_pi_f0`, `theta_over_pi_f1`, and the continuous flavor Lie algebras as `flavor_f0`, `flavor_f1`. Submit to `discrete`; use the tokens `su2` and `u1` for the Lie algebras. Explain why the parity of the intersection form is a distinction between the models but is not the source of the theta assignment.

5. **A positive path without the proposed map.** In F_3, submit the periods, formal tension and metric on the compact ray as `zero_section`, `zero_fiber`, `zero_tension`, `zero_metric`. Then give the section period and the metric evaluated at $m = 2a$ as `varying_section`, `varying_metric`. Use a as the only variable. Submit to `counterexample`. Explain the two different failures: a wrong sign on the first ray and the compact curve outside S on the second. What physical premise would still be needed for a fixed-point identification if a geometric contraction had been exhibited?

Written transfer practice. The following questions use the same geometric method and do not change the numerical submissions above.

1. Set $(p_E, p_f) = (7u, 4u)$ with $u > 0$ on F_0 and F_1. Recover the background in each model and compute the two surface areas. Then keep a, m equal instead: which measured period must change? Explain why the two comparisons answer different questions.

2. For a proposed F_1 ray $m = \lambda a$, classify λ by positivity of the section, area and metric. Choose one value that has positive metric and negative area, and another that has positive area but a negative section period. Do not replace any period by its absolute value. Are either of these rays a continuation inside the original Kähler chamber?

3. In the plane chart $x \neq 0$, use (XIII.5.21) to recover the source coordinates away from the zero section. Repeat on $y \neq 0$. Explain why neither coordinate recovery works at the apex and why this is exactly where a surface has been contracted.

4. Add cm^3 to the ruled prepotential and follow $m = 2a$. Compute the change of the total second derivative and compare it with the change of the fixed-background Hessian. Explain which one is a kinetic coefficient and why the distinction is necessary in the tilted F_3 control.

Use `benchmark/tasks.json` to find the question IDs and `benchmark/PROTOCOL.md` for submission. For these fields, use exactly the listed keys, with no duplicates and at most 2048 characters for the answer object. For numeric values use integers of magnitude at most 10^6 or exact polynomial strings of at most 120 characters. Use explicit `*` and `**`, rational division by nonzero constants, and only the variables listed for the task. Integer literals have magnitude at most 10^6; constant bases of powers have the same bound. Exponents must be integer literals from 0 to 3. The expression tree is limited to 42 nodes, and its degree bound, computed before cancellation, is 6 for tasks with variables. Use short reduced expressions to stay within these limits. Equivalent exact expressions within the grammar are accepted. Written explanations are assessed separately by a reader.

Status and sources

§5.1–5.2: Local premise and signed frame. The rigid isolated sector and fixed background for differentiation are a premise ([DEC]). The bundle, primitive surface and restriction calculation (XIII.5.1)–(XIII.5.2) are ([MATH]). The relative wrapped-brane and kinetic dictionary ([GEO-X]) uses Jefferson et al. (2018, arXiv v3, §2.2, Eqs. (2.9)–(2.12)). In the shrinkability discussion of that source the signed class J corresponds to A here. We retain the $1/2$ in its Eq. (2.10) for the surface volume. The distance integral (XIII.5.11) is part of ([MATH]).

The chain-rule and background-polynomial comparisons (XIII.5.8)–(XIII.5.10) are algebraic consequences of the same fixed-background frame; they add no kinetic direction.

§5.3: The plane. The line lattice and absence of a ruling are ([MATH]). The signed cubic and line coordinate (XIII.5.13)–(XIII.5.15) are ([MATH]). The fan and quotient computation (XIII.5.16)–(XIII.5.19) establish the plane case of ([MATH]).

The local map (XIII.5.20)–(XIII.5.22) realizes that same contraction in section-ring coordinates; the conic calculation (XIII.5.23) reuses the line lattice and curve pairing without specifying a spectrum. The physical E_0 identification ([GEO-X]) is the particular local plane endpoint in Morrison and Seiberg (1997, arXiv v2, §§3.2–3.3) and Aharony et al. (1998, arXiv v3, §IV.B, Fig. 25).

§5.4: Ruled surfaces. Curve generators, canonical classes and fixed lift in (XIII.5.24)–(XIII.5.29) are ([MATH]); see also Jefferson et al. (2018, arXiv v3, §4.1, Eqs. (4.3), (4.5)). The period and area limits are ([MATH]), and the explicit subdivisions in (XIII.5.42)–(XIII.5.44) give the two ruled cases of ([MATH]).

The inverse period map, equal-period examples, scale ratios and fixed-positive-background distance (XIII.5.30)–(XIII.5.40) are consequences of the line lattice and signed period formulas in the same lift; the distance is evaluated on a fixed-background slice. The protected area and weak pure gauge interpretation use ([GEO-X]); see Morrison and Seiberg (1997, arXiv v2, §3.3, Figs. 2–3) and Aharony et al. (1998, arXiv v3, §III.G). The comparison with the neighboring chamber uses the same relative period units. The F_1 period pair follows from the displayed restriction and its separate mass comparison.

§5.5: Common cubic and distinct identifications. The compact charges and parity ([MATH]) and the matches in (XIII.5.45) and (XIII.5.48) ([MATH]) use Intriligator et al. (1997, arXiv v2, Eq. (2.22)) for the cubic root sum and Aharony et al. (1998, arXiv v3, §III.A, Eq. (47), §§III.F–G) for the selected particles. For the independent discrete theta and endpoint matches ([GEO-E]) see Morrison and Seiberg (1997, arXiv v2, §§2, 3.3) and Aharony et al. (1998, arXiv v3, §II.E, Fig. 10 and §§III.F–H); the historical E_1 current enhancement uses Seiberg (1996, arXiv v2, §4, Eq. (4.5) and following discussion). The identification requires the endpoint interpretation in addition to the relative wrapped-brane dictionary.

The inverse selected-mass calculation (XIII.5.50)–(XIII.5.51) reuses the compact charges, parity and the two mass-patch comparisons and introduces no additional protected state.

§5.6–5.7: Obstructions and degrees. The sign tests and compact-graph obstruction are ([MATH]), with the map obstruction scoped to exceptional locus exactly S in an affine target.

The fixed-negative-background walls, general tilted-ray inequalities, canonical-degree comparison and coordinate graph explanation are algebraic consequences of the period formulas and compact-graph obstruction; no endpoint is attached to the controls. For the distinction between strict contraction and the broader proposed shrinkability criterion, see Jefferson et al. (2018, arXiv v3, §§3.2–3.3, 4.1). The point-blowup exercise uses the canonical class and the orthogonal exceptional pairing ([MATH]).

References

Aharony, O., A. Hanany, and B. Kol (1998). "Webs of (p, q) five-branes, five-dimensional field theories and grid diagrams". In: *JHEP* 01, p. 002. DOI: 10.1088/1126-6708/1998/01/002. arXiv: hep-th/9710116.

Intriligator, K. A., D. R. Morrison, and N. Seiberg (1997). "Five-dimensional supersymmetric gauge theories and degenerations of Calabi–Yau spaces". In: *Nucl. Phys. B* 497, pp. 56–100. arXiv: hep-th/9702198.

Jefferson, P. et al. (2018). "On geometric classification of 5d SCFTs". In: *JHEP* 04, p. 103. DOI: 10.1007/JHEP04(2018)103. arXiv: 1801.04036 [hep-th].

Morrison, D. R. and N. Seiberg (1997). "Extremal transitions and five-dimensional supersymmetric field theories". In: *Nucl. Phys. B* 483, pp. 229–247. DOI: 10.1016/S0550-3213(96)00592-5. arXiv: hep-th/9609070.

Seiberg, N. (1996). "Five-dimensional SUSY field theories, nontrivial fixed points and string dynamics". In: *Phys. Lett. B* 388, pp. 753–760. DOI: 10.1016/S0370-2693(96)01215-4. arXiv: hep-th/9608111.

Chapter XIII.6

Several compact surfaces and the canonical-singularity program

XIII.6.1 Two surfaces and a shared curve

In the one-surface construction, an M2-brane wrapped on a curve gives a particle and an M5-brane wrapped on the compact surface gives a magnetic string. Their masses and tensions measure two different things: the area of a curve and the volume of a surface. What changes when there are two compact surfaces? Each supplies a Coulomb direction, but a curve shared by them can carry charge under both. Its area can vanish while the two surface volumes stay positive. Following this curve through zero area will show how two different resolutions describe adjacent regions of the same local geometry.

We work in the local five-dimensional M-theory construction, with gravity decoupled as a premise and the background periods held fixed when differentiating the prepotential. We use units in which an M2-brane mass is its Kähler period. Our example is the toric geometry $Y^{3,0}$. It has a pure gauge chamber of algebra $\mathfrak{su}(3)$ and Chern–Simons level zero; $SU(3)_0$ will denote that gauge description. The global group and line operators would require a choice of boundary data. We will derive the chamber from an explicit fan, and then use a separate hypersurface example to see what compact surfaces can miss.

The prerequisites are the wrapped M2/M5 interpretation and the signed intersection convention of the preceding chapters, together with elementary toric fans. The new operation is restriction to an intersecting pair of surfaces. It turns a threefold intersection into a calculation on a ruled surface. We will use it to compute the mixed couplings, reconstruct their gauge interpretation and decide which degeneration is actually reached. The same polygon will stay with us throughout the calculation, so each change of the cubic can be traced to a change of an effective curve.

XIII.6.2 The fan and its compact curves

How can we tell which curves have to stay positive? Start with a convex lattice polygon in a height-one plane. For a point $P = (u, v)$ in the polygon, write $v_P = (u, v, 1)$ for the corresponding three-dimensional ray. Our points are

P	D_1	D_2	D_3	D_4	E_1	E_2
u	0	1	0	-1	0	0
v	3	0	0	3	1	2

(XIII.6.1)

and the boundary cycle is D_3, D_2, D_1, D_4. We use the same symbols for the rays and their toric divisors, with v_P marking a lattice vector when necessary. The polygon has area 3 and four primitive sides, so Pick's formula gives two interior points. A divisor over an interior point is compact: the fan obtained by taking the star of that ray and quotienting by it covers the whole quotient plane.

The triangulation on the left of Figure XIII.6.1 joins each successive axial segment in D_3, E_1, E_2, D_1 to each of D_2, D_4. Taking the cone over every triangle specifies the fan. Each triangle has normalized area one: its axial side has length one and the third vertex is one lattice unit off the axis. The associated three-dimensional determinants have magnitude one, so the threefold is smooth. The height-one condition gives a crepant resolution, that is, the canonical divisor pulls back without an exceptional term.

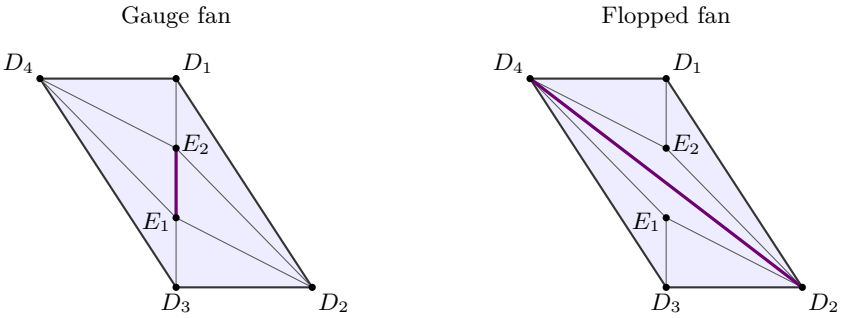


Figure XIII.6.1: Two triangulations of the same polygon. The left fan has the wall E_1E_2; the right fan replaces it by D_2D_4. Interior edges represent compact invariant curves. The boundary and all six rays are shared.

Smoothness does not yet show that the triangulation is the one defined by a Kähler chamber. To check projectivity over the affine cone, lift the four boundary points to height zero and both interior points to height -1. A triangle is a lower face if its affine plane agrees with its three heights and is strictly below the other three heights. For the bottom, middle and top triangles, the planes are

	bottom	middle	top
D_2 side	$-v$	$u - 1$	$3u + v - 3$
D_4 side	$-3u - v$	$-u - 1$	$v - 3$.

(XIII.6.2)

For example, the middle plane on the D_2 side gives -1 at both E_i and 0 at D_2. It gives -2 at D_4 and -1 at each end of the axis, all below their heights of zero. The other five planes pass the same test by substitution in (XIII.6.1). This strict lower hull gives a projective toric subdivision. The subdivision leaves the boundary faces of the cone unchanged, so the resolution is an isomorphism away from the cone vertex.

An interior edge UV belongs to two triangles, with opposite vertices R, S. Its invariant curve has divisor degrees given by the coefficients of the wall relation

$$v_R + v_S + Av_U + Bv_V = 0. \tag{XIII.6.3}$$

The coefficient of an opposite vertex is one because the two smooth coordinate charts meet the curve transversely at its two fixed points. The edge coefficients follow by pairing the curve with the principal divisors of the three lattice characters. In the order $(D_1, D_2, D_3, D_4, E_1, E_2)$, three independent relations are

$$f_1 = (1, 0, 0, 0, 1, -2), \quad f_2 = (0, 0, 1, 0, -2, 1), \quad C = (0, 1, 0, 1, -1, -1). \tag{XIII.6.4}$$

For instance, the opposite vertices of E_1E_2 are D_2, D_4; their ray sum is $v_{E_1} + v_{E_2}$. This gives the last row of (XIII.6.4). Using the same wall rule for all seven edges gives

edge	curve class
D_1E_2	$f_1 + C$
$D_2E_2,\ D_4E_2$	f_1
E_1E_2	C
$D_2E_1,\ D_4E_1$	f_2
D_3E_1	$f_2 + C$

(XIII.6.5)

It is useful to repeat the calculation for a wall on just one of the surfaces. The edge D_2E_2 has opposite vertices E_1, D_1. The height components of the rays require the sum of coefficients to vanish, while their u components force the coefficient of D_2 to be zero. The remaining v equation gives

$$v_{E_1} + v_{D_1} - 2v_{E_2} = 0. \tag{XIII.6.6}$$

The corresponding curve degrees are

$$D_1 \cdot f_1 = 1, \qquad E_1 \cdot f_1 = 1, \qquad E_2 \cdot f_1 = -2, \qquad D_2 \cdot f_1 = 0. \tag{XIII.6.7}$$

The vanishing D_2 degree is compatible with the curve lying in D_2. It is the degree of $\mathcal{O}_X(D_2)|_{f_1} = N_{D_2/X}|_{f_1}$, the normal line of the divisor restricted to the curve. The other normal direction, N_{f_1/D_2}, has degree $E_2 \cdot f_1 = -2$ because $f_1 = D_2 \cap E_2$. Neither number counts points of a transverse intersection with a divisor containing the curve. For the edge D_1E_2 the relation instead reads

$$v_{D_2} + v_{D_4} + v_{D_1} - 3v_{E_2} = 0. \tag{XIII.6.8}$$

Subtract the f_1 row from this row and the result is the C row. This establishes the class $f_1 + C$ in the table without deciding from its position in the drawing whether it should be called a section.

The minor in columns D_1, D_3, D_4 is a unit, so the three relations give a primitive integral basis of the relation lattice. For this projective toric map the relative cone of effective curves is generated by the compact invariant curves. Thus the three inequalities on f_1, f_2, C are both necessary and sufficient for strict positivity in this chamber. Testing only the fiber classes would miss the common curve.

The characters in the u, v and height directions also give the linear equivalences

$$D_4 \sim D_2, \qquad E_1 \sim D_1 - D_2 - 2D_3, \qquad E_2 \sim -2D_1 - D_2 + D_3. \tag{XIII.6.9}$$

For example, the v character gives $3D_1 + 3D_4 + E_1 + 2E_2 \sim 0$; the height character gives the sum of all six divisors. Solving these together with $D_2 - D_4 \sim 0$ yields (XIII.6.9). The wall calculation identifies the compact curves by charge. The stars of E_1 and E_2 now tell us what the same curves look like inside the compact surfaces.

XIII.6.3 The common section and the intersection tensor

What fixes the mixed intersections of the two compact divisors? Let $S_1 = E_2$, $S_2 = E_1$, and choose $D = D_4$ for the noncompact divisor. The quotient by the ray v_P sends (u, v, w) to $(u, v) - wP$. At $P = E_2$ the neighboring rays in cyclic order are D_2, D_1, D_4, E_1; at $P = E_1$ use D_4, D_3, D_2, E_2. Their images are

	first flank	outer axial	second flank	inner axial
E_2	$(1, -2)$	$(0, 1)$	$(-1, 1)$	$(0, -1)$
E_1	$(-1, 2)$	$(0, -1)$	$(1, -1)$	$(0, 1)$.

(XIII.6.10)

In a smooth surface fan, a curve with ray r has square $-b$ if its neighboring rays sum to br. Both rows therefore give squares $(0, 1, 0, -1)$. The axial curves are sections and the flanks are fibers of the ruling. In particular, both surfaces are $\mathbb{F}_1$, with a common negative section C; a square -2 section would give a different surface and different mixed intersections.

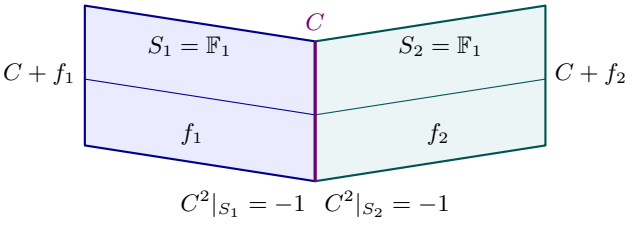


Figure XIII.6.2: The two rulings meet along their negative sections. Each surface contributes one normal direction of degree -1 along C. The noncompact divisor D restricts to a fiber on each surface.

On S_i write C and f_i for the negative section and fiber. Adjacent toric boundary curves meet once and opposite ones do not meet. The positive section is $C + f_i$, as

is also seen in (XIII.6.5). The canonical class is minus the sum of the four boundary curves. Thus

$$C^2 = -1, \qquad Cf_i = 1, \qquad f_i^2 = 0, \qquad K_i = -2C - 3f_i. \tag{XIII.6.11}$$

Adjunction in the Calabi–Yau threefold gives $S_i|_{S_i} = K_i$. The other compact divisor restricts to the common section and D restricts to the flank fiber. Along the transverse intersection, the two normal directions split:

$$N_{C/X} = N_{C/S_1} \oplus N_{C/S_2} = \mathcal{O}_{\mathbb{P}^1}(-1) \oplus \mathcal{O}_{\mathbb{P}^1}(-1). \tag{XIII.6.12}$$

Their degree sum is -2, as required by $\det N_{C/X} = K_C$. In this example the fan constructs the embedding; checking the degree sum alone would not construct an embedding from abstract surface data.

For a triple product with a compact factor, restrict the other two divisors to that surface and take their intersection there. For example, $S_1^2 S_2 = K_1 C = 2 - 3 = -1$ and $S_1 S_2 D = C f_1 = 1$. The full table for the compact-dependent cubic in S_1, S_2, D is

	S_i^3	$S_i^2 S_j$ $(i \neq j)$	$S_i^2 D$	$S_1 S_2 D$	$S_i D^2$
degree	8	-1	-2	1	0

(XIII.6.13)

since $K_i^2 = 4(-1) + 12 = 8$ and $K_i f_i = -2$. There is no ordinary compact intersection degree for D^3 in this local model. Any background-only cubic may be separated off when computing Coulomb derivatives. The mixed entries in (XIII.6.13) already show why two independent copies of a rank-one calculation would give the wrong answer.

For clarity, the mixed degree can also be obtained using the other surface. Restriction to S_1 uses its canonical class; restriction to S_2 uses two copies of its common section. The two operations agree,

$$S_1^2 S_2 = (S_1|_{S_1})(S_2|_{S_1}) = K_1 C = -1, \qquad S_1^2 S_2 = (S_1|_{S_2})^2 = C^2 = -1. \tag{XIII.6.14}$$

This is where the embedding of the shared curve enters the cubic. The condition on its normal degree relates two surface calculations that would otherwise have been independent. Similarly,

$$S_i^2 D = K_i f_i = -2, \qquad S_i D^2 = f_i^2 = 0, \qquad S_1 S_2 D = C f_i = 1. \tag{XIII.6.15}$$

The final entry is nonzero even though the fiber square is zero. The mixed threefold product involves the section and a fiber on the same surface. Replacing it by a fiber square would erase a coupling between the two Coulomb directions.

The divisor degrees also display the charge coupling of the common curve. In the divisor basis (S_1, S_2) its two degrees are $(-1, -1)$, whereas the degrees of f_1 are $(-2, 1)$. The minus signs in $\omega = hD - pS_1 - qS_2$, with background coefficient h and Coulomb coordinates p, q, turn these into the coefficients of the periods in the next section. Thus a curve can couple to both Coulomb variables even when it lies entirely in one surface. Its charge information is an intersection calculation, not a count of how many surfaces it meets in the toric drawing.

XIII.6.4 The signed cubic and the gauge chamber

Which gauge theory reproduces those mixed terms? In the convention used here, the Kähler class and the formal divisor for the cubic are

$$\omega = hD - pS_1 - qS_2, \qquad A = -\omega. \tag{XIII.6.16}$$

The variable h is a background mass parameter, identified with the bare inverse gauge coupling in the perturbative regime. The variables p, q are simple-coroot coefficients of the Coulomb scalar. To relate the periods to the lower hull, use the coefficients of ω as the lifting heights H_P. In the ray order of (XIII.6.1) they are

$$(H_{D_1}, H_{D_2}, H_{D_3}, H_{D_4}, H_{E_1}, H_{E_2}) = (0, 0, 0, h, -q, -p). \tag{XIII.6.17}$$

Adding an affine function to all heights leaves the lower subdivision unchanged. For the wall relation (XIII.6.3), write the two edge coefficients as a_U, a_V and let ℓ be the plane through the lifted points at U, V, R. The difference $H_S - \ell(S) = H_R + H_S + a_U H_U + a_V H_V$ is the dot product of the wall row with the height vector. It is also the period of that wall curve, since the row records its divisor degrees. In particular the rows in (XIII.6.4) give

$$\begin{aligned} x &= \omega f_1 = 2p - q, \qquad y = \omega f_2 = 2q - p, \\ z &= \omega C = H_{D_2} + H_{D_4} - H_{E_1} - H_{E_2} = h + p + q = h + x + y. \end{aligned} \tag{XIII.6.18}$$

In the toric source these are ξ_3, ξ_2, ξ_7, and its divisor coefficients (μ_4, ν_1, ν_2) are $(h, -q, -p)$. This sign and order matter: the Kähler coefficients are not the Coulomb coordinates on which we differentiate.

The inverse change of variables is particularly useful for choosing a point in the geometric chamber. Solving the first two equations gives

$$\begin{pmatrix} x \\ y \end{pmatrix} = \begin{pmatrix} 2 & -1 \\ -1 & 2 \end{pmatrix} \begin{pmatrix} p \\ q \end{pmatrix}, \qquad \begin{pmatrix} p \\ q \end{pmatrix} = \frac{1}{3} \begin{pmatrix} 2 & 1 \\ 1 & 2 \end{pmatrix} \begin{pmatrix} x \\ y \end{pmatrix}, \qquad h = z - x - y. \tag{XIII.6.19}$$

Positive root masses do not require arbitrary positive p, q. They require $q < 2p$ and $p < 2q$. The further condition $z > 0$ comes from the common curve and is independent of these root inequalities when h is allowed to vary.

For example, choose the periods rather than the divisor coefficients,

$$(x, y, z) = (2, 3, 4), \qquad (p, q, h) = (7/3, 8/3, -1). \tag{XIII.6.20}$$

Every row of (XIII.6.5) then has positive period. For the middle face on the D_2 side the plane is $3u + v/3 - 3$. It lies below the lifts at D_1, D_3, D_4 by $2, 3, 4$ respectively. These are precisely the relevant convexity gaps. This is a valid point of the original geometric chamber despite the negative value of h. A weakly coupled gauge interpretation uses the additional hierarchy on h stated below; geometric positivity itself does not impose that hierarchy.

In this convention the physical compact-dependent prepotential is $A^3/6$. Expanding the cube with the tensor (XIII.6.13) gives

$$\begin{aligned} 6\mathcal{F}_a &= 8(p^3+q^3) - 3(p^2q+pq^2) + 6h(p^2+q^2) - 6hpq, \\ \mathcal{F}_a &= h(p^2+q^2-pq) + \frac{4}{3}(p^3+q^3) - \frac{1}{2}(p^2q+pq^2). \end{aligned} \tag{XIII.6.21}$$

The terms with two identical factors have multiplicity three; the term with three distinct factors has multiplicity six. For example, the latter is $6(pS_1)(qS_2)(-hD)$, of degree $-6hpq$. Using $+\omega^3/6$ in this convention would change the sign of all the terms that carry Coulomb derivatives.

For a separate gauge calculation, put

$$\Phi = \operatorname{diag}(p, q-p, -q). \tag{XIII.6.22}$$

The three positive roots evaluate to $x, y, x+y$. The pure five-dimensional gauge formula, in fundamental trace normalization, is the quadratic classical term, the classical Chern–Simons term at level k, and the contribution of the massive roots. On $x, y > 0$ it reads

$$\begin{aligned} \mathcal{F}_{\mathrm{g}} &= \frac{h}{2}\operatorname{Tr}\Phi^2 + \frac{k}{6}\operatorname{Tr}\Phi^3 + \frac{x^3+y^3+(x+y)^3}{6}, \\ \operatorname{Tr}\Phi^2 &= 2(p^2+q^2-pq), \qquad \operatorname{Tr}\Phi^3 = 3pq(p-q). \end{aligned} \tag{XIII.6.23}$$

The factor $1/6$ in the root term comes from pairing each root with its negative in the absolute-value sum. Substituting (XIII.6.18) gives (XIII.6.21) at $k = 0$. The signed change at level k is $kpq(p-q)/2$. For $(p, q, h) = (3, 2, 4)$, the three periods are $(4, 1, 9)$, the zero-level prepotential is $179/3$, and level $+1$ adds 3. The symmetric point $p = q$ could not distinguish the two level signs.

The equality of the root and intersection cubics can be followed without expanding all six absolute values. First combine the two simple roots,

$$x^3 + y^3 + (x+y)^3 = 2(x^3+y^3) + 3xy(x+y). \tag{XIII.6.24}$$

Substituting $x = 2p - q$ and $y = 2q - p$ then gives

$$x^3 + y^3 + (x+y)^3 = 8(p^3+q^3) - 3(p^2q+pq^2). \tag{XIII.6.25}$$

Division by six reproduces the compact cubic entries 8 and -1. The trace-square term supplies the entries with one background factor. This comparison separates the two jobs in the matching. The root spectrum fixes the Coulomb cubic in the chosen Weyl chamber, while h sets the classical kinetic term. No choice of a background-only constant can repair an incorrect mixed term, since such a term survives Coulomb differentiation.

The gauge identification has a geometric diagnostic as well. In the circle reduction of this phase the source's piecewise linear fiber area, as a function of the real base coordinate r, can be written

$$\chi(r) = \begin{cases} -3r - 2x + z, & r < -x, \\ -r + z, & -x < r < 0, \\ r + z, & 0 < r < y, \\ 3r - 2y + z, & y < r. \end{cases} \tag{XIII.6.26}$$

The three slope jumps of $+2$ are the three gauge D6-branes of the reduction, with no additional flavor kink. In this reduction the effective level is $k_{\text{eff}} = -(s_L + s_R)/2$, where s_L, s_R are the left and right asymptotic slopes. Here $s_L = -3$ and $s_R = 3$, giving level zero. The separations of the kinks give the two simple-root masses, and their sum is the third positive-root mass. The three heights are

$$\big(\chi(-x), \chi(0), \chi(y)\big) = (x + z, z, y + z). \tag{XIII.6.27}$$

In this reduction they are the instanton masses, in order along the base. Geometrically they are the periods of $f_1 + C, C, f_2 + C$. A weak-coupling corner is $h > 0$ with x, y small compared with h. To find the rest of the chamber, we need to check the periods themselves and the derivatives of the cubic at fixed h.

XIII.6.5 Curve positivity and the point contraction

Can the gauge kinetic matrix tell us whether we are still in the same resolution? First compute the magnetic tensions geometrically. If a surface has fiber period u and section period z, the class with these periods is

$$\omega|_{S_i} = uC + (z + u)f_i, \qquad \frac{1}{2}\int_{S_i} \omega^2 = u\left(z + \frac{u}{2}\right). \tag{XIII.6.28}$$

Indeed, intersecting the class with C gives $-u + z + u = z$. Squaring with (XIII.6.11) gives $-u^2 + 2u(z + u)$ before division by two. Taking $u = x, y$ for the two surfaces yields the relative M5 tensions. The same result comes from varying $A^3/6$ with respect to p, q at fixed h, since variation inserts S_1, S_2 and $A^2 = \omega^2$. In particular,

$$\partial_q \mathcal{F}_a = 4q^2 + h(2q - p) - pq - \frac{p^2}{2} = y\left(z + \frac{y}{2}\right). \tag{XIII.6.29}$$

For $(p, q, h) = (3, 2, 4)$ this gives $19/2$; the last term in the middle expression contributes $-9/2$.

Differentiating once more in the same Coulomb coordinates gives

$$H = \frac{\partial^2 \mathcal{F}_a}{\partial(p, q)^2} = \begin{pmatrix} 3x & 0 \\ 0 & 3y \end{pmatrix} + z\begin{pmatrix} 2 & -1 \\ -1 & 2 \end{pmatrix}. \tag{XIII.6.30}$$

The second matrix has eigenvalues one and three. Hence the kinetic matrix is positive definite throughout $x, y, z > 0$.

One can see the two independent positivity conditions directly from its principal minors,

$$H_{pp} = 3x + 2z, \qquad \det H = (3x + 2z)(3y + 2z) - z^2 = 9xy + 6z(x + y) + 3z^2. \tag{XIII.6.31}$$

Both are positive in the original cone. At the changed-input point (XIII.6.20), the tension and metric calculations give

$$(T_1, T_2) = (10, 33/2), \qquad H = \begin{pmatrix} 14 & -4 \\ -4 & 17 \end{pmatrix}, \qquad \det H = 222. \tag{XIII.6.32}$$

The off-diagonal element is the response of one string tension to the other Coulomb variable. Its value is $-z$, so the coupling is measured by the area of the shared section.

Root periods are often easier to visualize than coroot coefficients, but changing coordinates changes the entries of the metric. At fixed h let $J = \partial(p,q)/\partial(x,y)$ be the inverse Cartan matrix in (XIII.6.19). Since this change is linear, the metric in the root coordinates is

$$G = J^{\mathsf{T}} H J = \frac{1}{3}\begin{pmatrix} 4x+y+2z & 2x+2y+z \\ 2x+2y+z & x+4y+2z \end{pmatrix}, \qquad z = h+x+y. \tag{XIII.6.33}$$

The two matrices give the same line element. Their numerical eigenvalues need not agree because J is not orthogonal. Positive definiteness is preserved by the invertible coordinate change. Holding z fixed while differentiating the prepotential written in x, y would instead vary h and would no longer compute this fixed-background metric. The matrix H in (XIII.6.30) uses the coroot coordinates (p, q). If we first let the three eigenvalues λ_i of Φ vary independently in the gauge expression, their unmixed second derivatives, evaluated on the traceless slice, are instead

$$\left(\partial^2_{\lambda_i}\mathcal{F}_{\mathrm{g}}\right)_{i=1}^{3} = \big(h+2x+y,\ h+x+y,\ h+x+2y\big) = \big(h+3p,\ z,\ h+3q\big) \qquad (k=0). \tag{XIII.6.34}$$

For example, each root term $(\lambda_i - \lambda_j)^3/6$ contributes the positive separation once to each of its two diagonal derivatives. These three numbers are useful in the circle reduction, but do not replace the two-dimensional Hessian in (XIII.6.30).

Try continuing $\mathcal{F}_a$ to the point

$$(x,y,z) = (1,1,-1/4), \qquad \operatorname{spec} H = (9/4, 11/4), \qquad T_1 = T_2 = 1/4. \tag{XIII.6.35}$$

The continued kinetic eigenvalues and tension polynomials are positive. At this point the original fan has no Kähler class with these periods because its effective curve C would have negative area. The two quarter values are formal half-squares. Figure XIII.6.3 marks the same example after rescaling to the slice $h = -1$. At a generic fiber wall, say $x = 0$ with $y, z > 0$, the ruling of S_1 collapses and T_1 vanishes. At $z = 0$ with $x, y > 0$, the shared curve collapses and the two tensions are $x^2/2, y^2/2$. These are distinct degenerations.

The failure of the converse positivity test is a whole open region, rather than an isolated coincidence. Continue the old polynomial on the symmetric locus

$$x = y = r > 0, \qquad z = -cr, \qquad 0 < c < \frac{1}{2}. \tag{XIII.6.36}$$

The eigenvectors $(1,1)$ and $(1,-1)$ diagonalize the continued matrix, and give

$$H(1,1)^{\mathsf{T}} = r(3{-}c)(1,1)^{\mathsf{T}}, \qquad H(1,-1)^{\mathsf{T}} = r(3{-}3c)(1,-1)^{\mathsf{T}}, \qquad T_1 = T_2 = r^2(1/2{-}c). \tag{XIII.6.37}$$

Every displayed value is positive in this interval, while C has negative period everywhere in it. Meanwhile the three new generator periods are $r(1-c), r(1-c), cr$, all positive. The example therefore lies in an open region: these strict inequalities persist under small perturbations, including nonsymmetric choices of x, y. It teaches how to continue

the geometry, rather than how to enlarge the old Kähler cone by using a weaker test. At the same numerical point the string tensions must subsequently be computed from the new surfaces and the new cubic.

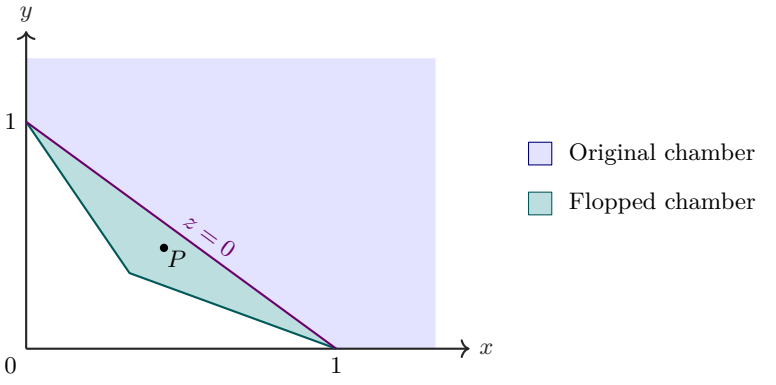


Figure XIII.6.3: A slice at $h = -1$, where $z = x + y - 1$. The original chamber lies above the segment $z = 0$ in the positive quadrant. The small triangle below it is the chamber after the flop, bounded by $x + z = 0$ and $y + z = 0$. The marked point P has $(x, y) = (4/9, 4/9)$, the rescaled example of (XIII.6.35). Boundary lines are excluded from the open chambers.

How can we make both surfaces disappear into a point? Set $h = 0$ and follow the ray

$$(x, y, z) = (t, 2t, 3t), \qquad (p, q) = (4t/3, 5t/3), \qquad t > 0. \tag{XIII.6.38}$$

All curve areas scale with t. The tensions are $7t^2/2$ and $8t^2$. Substituting the ray into (XIII.6.30) gives

$$H = t \begin{pmatrix} 9 & -3 \\ -3 & 12 \end{pmatrix}, \qquad ds^2 = (dp, dq) H (dp, dq)^{\mathsf{T}} = 36t\, dt^2. \tag{XIII.6.39}$$

The length along the ray to $t = 0$ is $4t^{3/2}$ in these relative units. Along the ray the only nonzero heights in (XIII.6.17) are $H_{E_1} = -5t/3$ and $H_{E_2} = -4t/3$. At the endpoint both vanish and the lower hull becomes one cell, the original polygon. This coarsening gives the projective contraction to the affine cone vertex. Vanishing volumes alone would not establish it.

The finite distance is not special to the ratio $1 : 2$. At $h = 0$ take any fixed positive numbers a, b and set

$$x = at, \quad y = bt, \quad z = (a + b)t, \quad (p, q) = \frac{t}{3}(2a + b, a + 2b), \qquad t > 0. \tag{XIII.6.40}$$

The common section and both fibers now vanish with the same scale. The two surface volumes and the radial metric are

$$T_1 = a(3a/2 + b)t^2, \qquad T_2 = b(a + 3b/2)t^2, \qquad ds^2 = K(a, b)t\, dt^2, \tag{XIII.6.41}$$

where direct substitution in (XIII.6.30) gives

$$K(a,b) = (a+b)(2a^2+ab+2b^2) > 0, \qquad L(0,t) = \frac{2}{3}\sqrt{K(a,b)}\,t^{3/2}. \tag{XIII.6.42}$$

For $a = 1, b = 2$ these expressions give $K = 36$ and the preceding length. Equivalently, homogeneity gives $\mathcal{F}_a = K(a,b)t^3/6$ on the ray, so its second radial derivative is Kt. Every such ray has the same limiting height subdivision, the single original polygon. The algebra permits different rates of approach inside the cone while the toric morphism identifies the endpoint.

For comparison, take (x, y) to zero at fixed $h > 0$. Then p, q vanish and $H_{D_4} = h$ is the only nonzero height. The lower hull has planes 0 and $-hu$ on the right and left of the whole axial diagonal D_3D_1, respectively. The ruling fibers collapse and both tensions vanish, but C still has period h. This limit keeps a curve of finite area rather than contracting the entire locus to a point. Neither the finite distance nor the point contraction alone identifies a UV field theory.

XIII.6.6 Crossing the flop wall

What geometry takes over when the area of C changes sign? The relation $v_{D_2} + v_{D_4} = v_{E_1} + v_{E_2}$ gives a quadrilateral with two possible diagonals. Its diagonals share a midpoint in the polygon. By (XIII.6.18), $z/2$ is the difference of the heights of the lifted diagonals over that midpoint. At $z = 0$ the four lifted points are coplanar, and the two triangles meeting along E_1E_2 form one cell. At $z < 0$ the diagonal D_2D_4 is lower, and we exchange the two middle triangles for $D_2D_4E_1$ and $D_2D_4E_2$. These triangles are also unimodular. The four outer triangles stay unchanged. For instance, at $(p, q, h) = (1, 1, -9/4)$ the planes of the two new middle triangles are

$$\ell_1 = \frac{3}{4}u - \frac{1}{4}v - \frac{3}{4}, \qquad \ell_2 = \frac{3}{2}u + \frac{1}{4}v - \frac{3}{2}. \tag{XIII.6.43}$$

The first lies $1/4$ below the height of E_2, the second $1/4$ below the height of E_1. Both planes lie strictly below the heights at D_3, D_1. For example, the second gives $-3/4$ at D_1, whose height is zero. The outer triangles remain lower faces, with support planes

$$-v, \qquad -\frac{3}{4}u - v, \qquad 3u + v - 3, \qquad \frac{9}{4}u + v - 3 \tag{XIII.6.44}$$

for the bottom right, bottom left, top right and top left. Together these planes give a strict lower-hull witness.

The wall rule (XIII.6.3) makes that chamber test precise. The new edge D_2D_4 has class $-C$; its opposite vertices are now E_1, E_2. For D_2E_2, for example, the new opposite vertices are D_1, D_4, and the relation is $v_{D_1} + v_{D_4} + v_{D_2} - 3v_{E_2} = 0$. For all edges the result is

edge	curve class after the flop
$D_1E_2,\ D_2E_2,\ D_4E_2$	$f_1 + C$
$D_3E_1,\ D_2E_1,\ D_4E_1$	$f_2 + C$
D_2D_4	$-C$.

(XIII.6.45)

The three strict inequalities are now

$$x + z > 0, \qquad y + z > 0, \qquad -z > 0. \tag{XIII.6.46}$$

For the example (XIII.6.35), the new periods are $(3/4, 3/4, 1/4)$, all positive. The first two are actual line areas on the flopped surfaces. In the $h = -1$ slice the three inequalities give the triangle $2x + y > 1$, $x + 2y > 1$, $x + y < 1$ shown in Figure XIII.6.3. The two newly drawn segments from $(1/3, 1/3)$ to $(1, 0)$ and $(0, 1)$ come from the first two inequalities. These constraints, together with $x + y < 1$, describe a smaller region than $z < 0$ alone.

The new surface stars give another way to read the changed curve classes. Each star has only three neighbors. For E_2 they are D_2, D_1, D_4, whose quotient rays in (XIII.6.10) sum to zero. For E_1 they are D_4, D_3, D_2, with the same zero sum. In each case two neighbors form an integral basis and the third is their negative sum. This is the fan of $\mathbb{P}^2$. There is no cone containing both interior rays, so the two compact divisors are disjoint. The curve of class $-C$ joins them, meeting each once. On either surface the restriction of D is a line L_i, with $L_i^2 = 1$ and $K_i' = -3L_i$. Thus

$$(S_i')^3 = 9, \qquad (S_i')^2 D = -3, \qquad S_i' D^2 = 1, \qquad S_1' S_2' = 0. \tag{XIII.6.47}$$

Expand the signed cube and omit the term in h^3 to obtain

$$\mathcal{F}_b = \frac{3}{2}(p^3 + q^3) + \frac{3h}{2}(p^2 + q^2) + \frac{h^2}{2}(p + q). \tag{XIII.6.48}$$

For instance the $h^2 p/2$ term comes from $(S_1')D^2 = 1$; it varies with the Coulomb modulus and must be retained. At fixed h, the two derivatives are

$$\partial_p \mathcal{F}_b = \frac{1}{2}(x + z)^2, \qquad \partial_q \mathcal{F}_b = \frac{1}{2}(y + z)^2. \tag{XIII.6.49}$$

They are just the two $\mathbb{P}^2$ half-squares, since the line areas are $x + z$ and $y + z$.

The new kinetic matrix is correspondingly simple,

$$H_b = \begin{pmatrix} 9p + 3h & 0 \\ 0 & 9q + 3h \end{pmatrix} = \begin{pmatrix} 3(x + z) & 0 \\ 0 & 3(y + z) \end{pmatrix}. \tag{XIII.6.50}$$

The vanishing mixed entry reflects the disjoint compact divisors in this resolution. For the point (XIII.6.35), its two entries are $9/4$, and the new tensions are both $9/32$. These differ from the formal old values $1/4$. The distinction is physical within the relative wrapped-brane dictionary: the compact surface has changed, so its volume is now the square of a line class on $\mathbb{P}^2$. The connecting curve has positive area $1/4$, but it is not a curve lying inside either projective plane. The same curve period that locates the wall measures the change in the cubic:

$$\mathcal{F}_b - \mathcal{F}_a = \frac{(h + p + q)^3 - h^3}{6} = \frac{z^3 - h^3}{6}. \tag{XIII.6.51}$$

At fixed h, shift the representative $\mathcal{F}_b$ by $h^3/6$. The difference then vanishes to third order at the wall: the value, gradient and Hessian agree there, while the third derivative transverse to the wall jumps.

In fact the derivative matching can be displayed before choosing a path. Define the aligned representative $\widehat{\mathcal{F}}_b = \mathcal{F}_b + h^3/6$. With $\nabla = (\partial_p, \partial_q)$ at fixed h, the jump is

$$\widehat{\mathcal{F}}_b - \mathcal{F}_a = \frac{z^3}{6}, \qquad \nabla(\widehat{\mathcal{F}}_b - \mathcal{F}_a) = \frac{z^2}{2}\begin{pmatrix}1\\1\end{pmatrix}, \qquad H_b - H = z\begin{pmatrix}1 & 1\\1 & 1\end{pmatrix}. \quad \text{(XIII.6.52)}$$

The rank-one matrix records the single period whose sign changes. There is no discontinuity in the metric on the common wall; its first derivative normal to that wall changes. The term $h^3/6$ does not alter any of these Coulomb derivatives. In contrast, removing $h^2(p+q)/2$ would change both string tensions by $-h^2/2$, so it cannot be absorbed in the background ambiguity.

For an asymmetric crossing hold $h = -3$ and choose

$$p = 4/3 + \varepsilon, \qquad q = 5/3 + \varepsilon, \qquad (x, y, z) = (1 + \varepsilon, 2 + \varepsilon, 2\varepsilon). \quad \text{(XIII.6.53)}$$

For small positive ε the old fan is Kähler. For $-1/3 < \varepsilon < 0$ the new periods are $1 + 3\varepsilon, 2 + 3\varepsilon, -2\varepsilon$, all positive, so the flopped fan takes over. At the wall both cubics give

$$(T_1, T_2) = (1/2, 2), \qquad H_a = H_b = \operatorname{diag}(3, 6), \qquad (\widehat{\mathcal{F}}_b - \mathcal{F}_a)|_{\text{path}} = \frac{4}{3}\varepsilon^3. \quad \text{(XIII.6.54)}$$

The derivative of order three of the last difference is 8. This example keeps both surfaces of finite volume at the wall while only the connecting section disappears. It explains why the local change is a flop and why the simultaneous point contraction discussed earlier is a different limit. The flopped resolution is a chamber of the same affine geometry and has no perturbative gauge description in this construction. The fan provides both chambers without asking the original gauge polynomial to describe the new one.

*XIII.6.7 What a canonical singularity can add

(Optional.) Does counting compact divisors determine all the sectors of a singular geometry? A family of hypersurfaces gives a test in which the divisor count stays fixed while the resolved space changes. Recall that for a normal $\mathbb{Q}$-Gorenstein variety the discrepancy of an exceptional prime divisor is its coefficient in the difference between the canonical divisor of a resolution and the pullback of the original canonical divisor:

$$K_{\widetilde{X}} - \pi^* K_X = \sum_E a_E E. \quad \text{(XIII.6.55)}$$

Canonical means all exceptional discrepancies are nonnegative; terminal means they are positive. A crepant map has zero canonical difference. The absence of exceptional divisors for one map does not settle terminality or rule out a small crepant resolution: the conifold admits such a resolution, with an exceptional curve and no exceptional divisor. The definitions test exceptional divisors over the space, not just the divisors visible in a chosen model.

Consider the isolated hypersurface singularity at the origin

$$X_m : \quad u_1^3 + u_2^3 + u_3^3 + u_4^m = 0, \qquad m = 3, 4, 5. \quad \text{(XIII.6.56)}$$

Blow up the origin in the ambient $\mathbb{C}^4$. Its canonical divisor changes by $3E$ and the total transform of X_m contains $3E$ because the lowest degree in its equation is three. Adjunction on the strict transform therefore cancels the two contributions:

$$(K_{\widetilde{\mathbb{C}}^4} + \widetilde{X}_m)\Big|_{\widetilde{X}_m} = \pi^*(K_{\mathbb{C}^4} + X_m)|_{\widetilde{X}_m}\,. \tag{XIII.6.57}$$

The map is crepant, but the equation of the exceptional divisor only sees the degree-three part. For $m = 3$ that part cuts out a smooth cubic in $\mathbb{P}^3$. For $m = 4, 5$ it cuts out the same irreducible projective cone over a smooth plane cubic.

To distinguish $m = 4$ from $m = 5$, use the blowup chart $u_4 = s$, $u_i = sv_i$ for $i = 1, 2, 3$. Cancel s^3 to find the strict-transform equation

$$g_m = v_1^3 + v_2^3 + v_3^3 + s^{m-3} = 0. \tag{XIII.6.58}$$

For $m = 3$ the derivatives in the v_i can all vanish only at $v_i = 0$, where the equation is $1 = 0$.

The exceptional divisor and the strict transform answer different smoothness questions. In the $m = 4, 5$ cases, setting $s = 0$ gives the same equation $v_1^3 + v_2^3 + v_3^3 = 0$. Its derivatives all vanish at the cone vertex. The total-space equation also depends on the ambient coordinate s, whose derivative enters its Jacobian:

$$\partial_s g_m = (m-3)s^{m-4}, \qquad \partial_{v_i} g_m = 3v_i^2 \qquad (m = 4, 5). \tag{XIII.6.59}$$

For $m = 4$, s can even be eliminated explicitly,

$$s = -(v_1^3 + v_2^3 + v_3^3). \tag{XIII.6.60}$$

The three v_i are therefore smooth local coordinates on the threefold. Its exceptional surface is a singular level set inside that smooth coordinate neighborhood. For $m = 5$, the equation is instead $s^2 = -(v_1^3 + v_2^3 + v_3^3)$; its first derivatives all vanish at the origin. Knowing the same exceptional surface has therefore not determined the local geometry transverse to it. For $m = 5$ the singular ideal on this chart is

$$(g_5, \partial_{v_1} g_5, \partial_{v_2} g_5, \partial_{v_3} g_5, \partial_s g_5) = (v_1^2, v_2^2, v_3^2, s). \tag{XIII.6.61}$$

It is supported at one point. On a chart based on any of the first three coordinates the equation has a unit cubic term. At $s = 0$, vanishing of the chart derivatives would force the remaining cubic coordinates to zero and leave that term uncanceled. Off the exceptional divisor the blowup is an isomorphism and (XIII.6.56) is smooth. Hence this one chart detects every residual singular point.

m	Exceptional cubic	Strict transform
3	Smooth cubic surface	Smooth
4	Cone over a smooth plane cubic	Smooth
5	Same cone as for $m = 4$	One residual point

Closset and collaborators identify the residual $m = 5$ point as the terminal example $E_6^{(-1)}$. In their magnetic quiver analysis of this example they associate four free twisted

hypermultiplets with the point. They distinguish these from a separate contribution from three-cycles and examine discrete gauging in the electric description. The chart calculation locates the residual point. The sector assignment comes from their quiver analysis. Coulomb rank counts vector multiplets, so neutral free hypermultiplets leave it unchanged.

The rank-two example established a contraction by an explicit morphism and followed its gauge chamber through a flop. In the broader canonical-singularity program, positivity of effective curve areas, compatibility of surface gluings, existence of a contraction and identification of the singularity's physical sectors are separate questions. The hypersurface calculation shows why the last of them can require information beyond the compact divisor list.

Take-home message of this chapter

In the pure $SU(3)_0$ chamber the two $\mathbb{F}_1$ surfaces share a negative section. Its intersection degrees fix the mixed cubic terms, and its area supplies a chamber inequality that the kinetic matrix cannot replace. Flopping this curve replaces the surfaces by two disjoint projective planes and changes the cubic at third order. A crepant contraction organizes the Coulomb geometry; residual singularities and boundary data can carry information outside that calculation.

XIII.6.8 Exercises

1. For the E_1E_2 edge, use the four lifted rays to compute the two normal degrees in the order (S_1, S_2), and then use restriction on S_1 to compute $S_1^2S_2$ and S_1S_2D. Submit the four integers as `n1`, `n2`, `mixed`, `withD` to E1. Explain why the sign of the shared curve square matters.

2. At $(p, q, h) = (5/4, 1, -11/4)$, compute the three periods of the new generators, in order $f_1 + C$, $f_2 + C$, $-C$. Decide which chamber contains the point. Also compute the difference of the two cubic representatives at this point, with both background-only terms removed as in the chapter. Submit `line1`, `line2`, `bridge`, `delta` to E2.

3. Continue the old polynomial to $p = q = 2$, $h = -9/2$. Compute the smaller kinetic eigenvalue, the tension on S_1, and the period of C. Then set $p = q = 0$ at a separate fixed value $h = 2$ and compute the period of the same class there. Submit `eigen`, `tension`, `oldCurve`, `limitCurve` to E3. Explain why neither the first pair of positive values nor the vanishing tensions in the limit imply a contraction to a point.

4. Derive the fixed-h mixed derivative of $\mathcal{F}_a$ and the change of the gauge polynomial when k increases from zero to one. Compute the latter also at $p = 3, q = 2$. Submit `mixed`, `levelShift`, `sample` to E4. Keep the signs in the specified trace and coroot conventions.

5. Written exercise. For $m = 4, 5$ compare the exceptional cubic with the residual singular ideal. Why can two crepant blowups each add one compact divisor and

still give different smoothness results? Which step, beyond the chart calculation, is needed to attach a free sector?

6. Written transfer exercise. At fixed h, derive (XIII.6.33) by changing coordinates in the line element. Explain why differentiating at fixed z changes the background. Evaluate the metric and both tensions at $(x, y, z) = (2, 3, 4)$ and check positivity without numerical eigenvalues.

7. Written transfer exercise. Follow (XIII.6.53) to $\varepsilon = 1/10$ and $\varepsilon = -1/10$. List the effective generator periods in the appropriate resolution, compute both string tensions and compare the two Hessians. Derive their agreement at the wall and their change to first order in ε.

8. Written transfer exercise. On the $h = 0$ ray with $(a, b) = (2, 3)$, compute the two surface volumes, radial line element and distance to the origin. Explain which toric coarsening supplies the point contraction and what remains finite if the fibers instead shrink at a fixed positive h.

For E1 through E4 submit the indicated keys in a JSON object. Use strings for integers, fractions such as `"3/2"`, and polynomials in p, q, h for E4. Discuss the written explanations and E5–E8 with a reader.

Status and sources

§6.1: Local premise. Gravity is decoupled and h is a background ([DEC]); wrapped-brane masses and tensions use relative units ([GEO-X]). See Jefferson et al. (2018, §2.2, Eqs. (2.9)–(2.12)).

§6.2–6.3: Fan and restrictions. The fan, Mori rows, gluing and tensor ([MATH]) use $(P, Q) = (3, 0)$ in Closset and Del Zotto (2019, Eqs. (6.1)–(6.2)) and Saxena (2020, §3.3, Eqs. (3.35)–(3.39), Fig. 9 caption). The expanded wall-relation examples and two-surface restrictions are algebraic consequences of these same fans. The figures reconstruct the fans from these data. For gluing, see Jefferson et al. (2018, §3.4, Eqs. (3.2)–(3.3)).

§6.4: Cubic and gauge phase. The signed cubic match ([MATH]) uses Intriligator et al. (1997, arXiv v2, Eq. (2.22)) and Saxena (2020, Eqs. (3.40)–(3.42)). The gauge and particle dictionary ([GEO-X]) uses Saxena (2020, Eqs. (3.41)–(3.45), App. A).

§6.5: Tensions and contraction. The fixed-background calculation ([MATH]) gives (XIII.6.29) by differentiating Saxena's Eq. (3.42), in agreement with Eq. (3.48) via Eq. (3.45). The second tension in Saxena (2020, Eq. (3.47)) omits $-p^2/2$. The inverse-coordinate metric, determinant, continued symmetric family and positive-ray extension are algebraic consequences of the same fixed-h cubic; they add no UV identification. For the broader program, see Jefferson et al. (2018, §3.2).

§6.6: Flop. The flopped fan gives the Mori rows and cubic ([MATH]). The new metric, rank-one derivative jump and asymmetric crossing path are calculated from those same two cubics. For the phase interpretation see Saxena (2020, §3.3 and §5).

§6.7: Residual geometry and sectors. The blowup and chart ([MATH]) use Closset, Giacomelli, et al. (2021, arXiv v4, Eqs. (4.3)–(4.4), Tables 2–3). The smooth $m = 4$ control ([MATH]) follows by differentiating (XIII.6.58). The $m = 5$ sector assignment ([GEO-E]) is that source's case-specific quiver analysis, §1.1 and Eqs. (4.10)–(4.11).

References

Closset, C. and M. Del Zotto (2019). "On 5d SCFTs and their BPS quivers. Part I". In: arXiv: 1912.13502 [hep-th].

Closset, C., S. Giacomelli, et al. (2021). "5d and 4d SCFTs: canonical singularities, trinions and S-dualities". In: *JHEP* 05, p. 274. DOI: 10.1007/JHEP05(2021)274. arXiv: 2012.12827 [hep-th].

Intriligator, K. A., D. R. Morrison, and N. Seiberg (1997). "Five-dimensional supersymmetric gauge theories and degenerations of Calabi–Yau spaces". In: *Nucl. Phys. B* 497, pp. 56–100. arXiv: hep-th/9702198.

Jefferson, P. et al. (2018). "On geometric classification of 5d SCFTs". In: *JHEP* 04, p. 103. DOI: 10.1007/JHEP04(2018)103. arXiv: 1801.04036 [hep-th].

Saxena, V. (2020). "Rank-two 5d SCFTs from M-theory at isolated toric singularities: a systematic study". In: *JHEP* 04, p. 198. DOI: 10.1007/JHEP04(2020)198. arXiv: 1911.09574 [hep-th].

Chapter XIII.7

Flavor data from the noncompact geometry

XIII.7.1 One modulus and six masses

A wrapped M2-brane measures the area of a curve. That area can depend on the Coulomb scalar, which fluctuates in a five-dimensional vector multiplet, and on masses, which are values of background vector multiplet scalars. How do we separate these two contributions when all we are given is the threefold and its curve periods?

We will answer this question for the canonical bundle of the plane blown up at six points. There is one compact surface. Moving its Coulomb scalar changes some curve periods but leaves an entire rank-six lattice of periods unchanged. To give those six periods a physical meaning, we choose a ruling that leads to a weak $SU(2)$ description with five fundamental hypermultiplets. This choice lets us read off the five quark masses and the deformation that sets the inverse coupling.

The same calculation produces an E_6 root diagram. A root is initially a signed class, so its period can vanish even when there is no curve to wrap. We will compare two actual contractions to locate the missing geometric step. The weak gauge description then gives a separate question about currents: which ones can appear only at the conformal point? The example with five blowups shows how the same method changes the answer.

We use the M2 calibration and local signed prepotential from Chapters 1–2, the split fibers of Chapter 3, and the distinction between a contraction and its physical identification from Chapter 5. From Volume IV we need the intersection form of an ordinary plane blowup, adjunction and the Hodge index theorem. We recall the needed charge conventions before evaluating periods.

XIII.7.2 Compact support and boundary periods

Which Kähler variation can we make without changing the boundary data? Let S_n be the blowup of $\mathbb{P}^2$ at n distinct ordinary points, with $n = 5$ or 6. We take the points in general position until the separate comparison in §XIII.7.5. The line pullback is H, and E_i is the exceptional curve over the ith point. We identify curve and divisor classes on the surface by Poincaré duality. The intersection form and the canonical and anticanonical classes are

$$\begin{aligned} H^2 = 1, \qquad H \cdot E_i = 0, \qquad E_i \cdot E_j = -\delta_{ij}, \\ K = -3H + \sum_{i=1}^{n} E_i, \qquad h = -K, \qquad K^2 = 9 - n. \end{aligned} \tag{XIII.7.1}$$

Thus dP_6 means six blowups and has degree three. The subscript counts blowups; the degree is the self-intersection of h.

Let $X = \mathrm{Tot}(K_{S_n})$ and $\pi : X \to S_n$ be the bundle projection. Write S for the compact zero section as a divisor in X. The tangent vectors along a fiber are sections of $\pi^* K_{S_n}$. Taking the determinant of the cotangent sequence, and restricting the normal line of the zero section, give

$$K_X \simeq \pi^*(K_{S_n} \otimes K_{S_n}^{-1}) \simeq \mathcal{O}_X, \qquad \mathcal{O}_X(S)|_S \simeq N_{S/X} \simeq K_{S_n}. \tag{XIII.7.2}$$

In divisor notation the second equality says $[S]|_S = K$. It fixes the sign of the compact change of Kähler class.

The homotopy $(p, v) \mapsto (p, tv)$, with t going from 1 to 0, retracts the total space to the zero section. Consequently ordinary integral degree-two cohomology remembers the whole surface lattice:

$$H^2(X, \mathbb{Z}) \simeq H^2(S, \mathbb{Z}) = P := \mathbb{Z}H \oplus \bigoplus_{i=1}^{n} \mathbb{Z}E_i. \tag{XIII.7.3}$$

To remember compact support as well, use the Thom class u of the oriented real two-plane bundle underlying K_{S_n}. In degree two the Thom isomorphism is $H_c^2(X, \mathbb{Z}) = H^0(S, \mathbb{Z})u$. Forgetting support and pulling back to the zero section gives the Euler class of the normal line, namely its first Chern class:

$$H_c^2(X, \mathbb{Z}) = \mathbb{Z}u \longrightarrow P, \qquad u \longmapsto K, \qquad \dim_{\mathbb{R}}\bigl(P_{\mathbb{R}}/\mathbb{R}K\bigr) = n. \tag{XIII.7.4}$$

A real variation of periods modulo the compact direction therefore has six coordinates on dP_6, and five on dP_5.

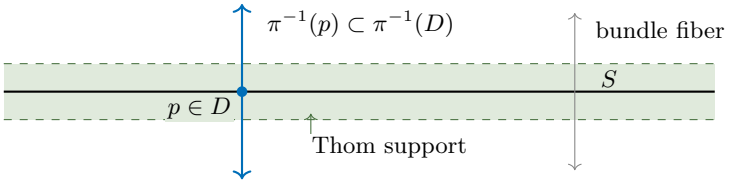


Figure XIII.7.1: A bundle cross section over the surface S. The solid horizontal segment denotes the zero section in the slice. The blue vertical line at $p \in D$ depicts one full fiber of $\pi^{-1}(D)$, the noncompact lift of a curve D on S. The shaded neighborhood marks the possible support of a Thom representative near S; its width is schematic and gives no metric or kinetic information.

Let J be the Kähler form, $T_{M2} = 1/[(2\pi)^2 \ell_p^3]$ the M2 tension in terms of the eleven-dimensional Planck length ℓ_p, and $\omega = T_{M2} J$. For a concrete lift, take a surface divisor D and pull it back. Every point of D has a full complex line above it in Fig. XIII.7.1. This is a noncompact representative, and its class restricts to D on the zero section. The quotient in (XIII.7.4) tests the *class*, not just a drawn representative: for example $\pi^* K$ can also be represented by a compactly supported form in ordinary cohomology. Adding a multiple of $[S]$ to a lift leaves its quotient class fixed. Choose a real surface cohomology class $j \in P_{\mathbb{R}}$ representing the chosen background lift. Since $\pi^* K = [S]$, in the split $\omega = -a[S] + \pi^* j$ a shift $j \mapsto j + \lambda K$ is compensated by $a \mapsto a + \lambda$ at fixed ω.

It helps to check the compensation directly on a curve. Write $V_C = a\, h \cdot C + j \cdot C$. The two changes of lift give

$$(a + \lambda)h + (j + \lambda K) = ah + j, \qquad \Delta V_C = \lambda(h + K) \cdot C = 0. \tag{XIII.7.5}$$

This is a change of coordinates for a fixed period class. A change of a with j held fixed instead changes V_{E_1} by the same amount. To specify a physical deformation we must therefore say which background lifts are held fixed. The ruling below supplies such a choice. The quotient by K is independent of that choice, while the individual coordinates on it require a marking.

In the ordinary flux-free local M-theory limit we retain the one compact-divisor vector and fix the boundary vector multiplets. This prescription gives a as a dynamical scalar and the n quotient directions as real background masses. The Thom argument counts available cohomology classes; the existence of the retained local sector and its decoupling from unwanted bulk fields are physical input. Compact support alone does not calculate a kinetic norm for a harmonic form.

For a compact calibrated holomorphic curve C the M2 mass is the positive period V_C. We use the same symbol V_C for the signed linear functional on any integral class:

$$V_C = \omega \cdot C, \qquad \delta\omega = -\delta a [S] \quad \Longrightarrow \quad \delta V_C = q(C)\, \delta a, \qquad q(C) = h \cdot C. \tag{XIII.7.6}$$

The tension has units of inverse length cubed and $\int_C J$ has units of area, so V_C and a have units of mass. On the exceptional curve E_1, the sign in (XIII.7.2) gives

$$K \cdot E_1 = -1, \qquad q(E_1) = 1, \qquad \delta V_{E_1} = \delta a. \tag{XIII.7.7}$$

We can now look for integral combinations whose periods are insensitive to this change. Their periods depend only on the fixed quotient data.

XIII.7.3 The lattice orthogonal to the canonical class

Which combinations of curve periods measure only the boundary data? A signed class has the form $C = dH - \sum_i b_i E_i$ with $d, b_i \in \mathbb{Z}$. Its period is unchanged under the compact variation exactly when C belongs to $L = K^{\perp} \subset P$. Within this lattice a root is a class of square -2. The two tests, from (XIII.7.1), are

$$3d = \sum_i b_i, \qquad d^2 - \sum_i b_i^2 = -2. \tag{XIII.7.8}$$

The first equation specifies L without a norm restriction. We first find a basis of this entire integral kernel, so that a list of plausible roots cannot miss a finite-index extension.

Consider the zero-degree differences and one degree-one class

$$\alpha_i = E_i - E_{i+1} \quad (1 \le i < n), \qquad \beta = H - E_1 - E_2 - E_3. \tag{XIII.7.9}$$

Each satisfies both tests. For any $C \in L$, subtract $d\beta$ and set $b'_i = b_i - d\,\mathbf{1}_{i\le 3}$, where $\mathbf{1}_{i\le 3}$ is 1 for $i \le 3$ and 0 otherwise. Then $\sum_i b'_i = 0$. The coefficient of E_i in a chain sum of the α_j is the difference of successive chain coefficients. Integrating these differences gives

$$C - d\beta = -\sum_{i=1}^{n} b'_i E_i = \sum_{j=1}^{n-1} c_j \alpha_j, \qquad c_j = -\sum_{i=1}^{j} b'_i. \tag{XIII.7.10}$$

The final exceptional coefficient works because the sum of the b'_i vanishes. The expansion is unique: the degree determines the coefficient of β, and the exceptional coefficients then determine each c_j. This proves that the marking is an integral basis, before any determinant calculation.

For a useful test, apply the integral expansion to the degree-two class $Q = 2H - \sum_{i=1}^{6} E_i$. Subtracting 2β gives $b' = (-1,-1,-1,1,1,1)$, so the partial sums in (XIII.7.10) give

$$Q = \alpha_1 + 2\alpha_2 + 3\alpha_3 + 2\alpha_4 + \alpha_5 + 2\beta. \tag{XIII.7.11}$$

The exceptional coefficients telescope. For example the E_3 coefficient is $-2+3-2 = -1$, where the final term comes from 2β. This example will be important twice. It is the root that a line-only enumeration misses, and in the gauge marking it supplies the last weight of the positive-grade spinor. The expansion uses signed classes and makes no incidence assumption about six points lying on a conic.

The form on P has one positive direction, and $K^2 > 0$, so L is negative definite. Its negative is the form in which roots have length squared two. For instance, $\beta \cdot \alpha_j$ is 1 if $j = 3$ and 0 otherwise: the coefficients of E_j and E_{j+1} in β agree except at $j = 3$. The

matrix of the negative form on dP_6 is

$$-\big(C_r \cdot C_s\big)_{C_r, C_s \in (\alpha_1, \ldots, \alpha_5, \beta)} = \begin{pmatrix} 2 & -1 & 0 & 0 & 0 & 0 \\ -1 & 2 & -1 & 0 & 0 & 0 \\ 0 & -1 & 2 & -1 & 0 & -1 \\ 0 & 0 & -1 & 2 & -1 & 0 \\ 0 & 0 & 0 & -1 & 2 & 0 \\ 0 & 0 & -1 & 0 & 0 & 2 \end{pmatrix}. \tag{XIII.7.12}$$

Draw one edge for each off-diagonal entry -1. The result is the E_6 diagram. On dP_5 we delete α_5, since there is no E_6 exceptional curve there, and keep β. The diagram is then D_5, with one arm shortened.

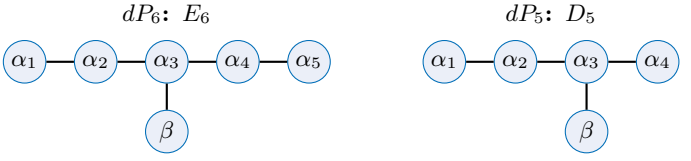


Figure XIII.7.2: The lattice markings for six and five blowups. Vertices are the classes in (XIII.7.9). An edge means intersection $+1$ on the surface, or -1 in the positive Cartan form. In both diagrams β meets only α_3. The right arm ends at α_4 for five blowups. These vertices label signed classes.

The graph also gives the determinant. To eliminate an arm of length one, divide out its diagonal entry 2 and subtract $1/2$ from the central diagonal. An arm of length two has determinant 3 and inverse entry $2/3$ at the vertex joined to the center. Eliminating the three arms thus gives

$$\begin{aligned} \det(E_6) &= 3 \cdot 3 \cdot 2 \left(2 - \tfrac{2}{3} - \tfrac{2}{3} - \tfrac{1}{2}\right) = 3, \\ \det(D_5) &= 3 \cdot 2 \cdot 2 \left(2 - \tfrac{2}{3} - \tfrac{1}{2} - \tfrac{1}{2}\right) = 4. \end{aligned} \tag{XIII.7.13}$$

Here each determinant is that of the corresponding Cartan matrix. We will use the first determinant again to measure the difference between integral roots and integral functionals on them.

To count every root without assuming the diagram classification, bound the degree using both tests in (XIII.7.8). The Cauchy–Schwarz inequality gives

$$9d^2 = \Big(\sum_i b_i\Big)^2 \le n \sum_i b_i^2 = n(d^2 + 2) \quad \Longrightarrow \quad (9 - n)d^2 \le 2n. \tag{XIII.7.14}$$

For $n = 6$ only $d = 0, \pm 1, \pm 2$ are possible. At degree zero the square condition requires two entries of magnitude one, and the sum condition gives opposite signs. At positive degree 1 or 2, $d^2 + 2 = 3d$. Thus $\sum_i b_i(b_i - 1) = 0$, and each term is a nonnegative

integer. The allowed classes are therefore

d	Classes at that degree on dP_6	Count
0	$E_i - E_j, \quad i \neq j$	30
1	$H - E_i - E_j - E_k, \quad i < j < k$	20
2	$2H - \sum_{i=1}^{6} E_i$	1

(XIII.7.15)

At negative degree take the negatives of the positive-degree classes. The total is $30 + 2 \cdot 20 + 2 \cdot 1 = 72$. Searching only lines and exceptional differences would miss the degree-two pair. At $n = 5$, (XIII.7.14) instead gives $|d| \leq 1$. The same counting now gives $5 \cdot 4 + 2\binom{5}{3} = 40$.

A reflection gives a useful local operation on this list. For a root α, the coefficient along α in the orthogonal projection of C is $(C \cdot \alpha)/(-2)$. Reversing that projection yields

$$s_\alpha(C) = C + (C \cdot \alpha)\alpha, \qquad s_{\alpha_3}(\beta) = \beta + \alpha_3 = H - E_1 - E_2 - E_4. \tag{XIII.7.16}$$

The sign in this formula can be checked without choosing a matrix representation. Put $t = C \cdot \alpha$ and use $\alpha^2 = -2$. Then

$$\begin{aligned} (C + t\alpha)^2 &= C^2 + 2t^2 - 2t^2 = C^2, \\ (C + t\alpha) \cdot \alpha &= -t, \qquad s_\alpha^2(C) = C. \end{aligned} \tag{XIII.7.17}$$

For $\alpha = E_i - E_{i+1}$ the operation exchanges the two exceptional classes, leaving H fixed. It is a change of the lattice marking that permutes the corresponding period labels. This gives a direct way to recognize the chain of reflections before using the full diagram.

The reflection preserves the intersection form and fixes K because $K \cdot \alpha = 0$. This is a Weyl operation on signed classes. It need not take an effective curve on a given marked surface to another effective curve on that surface. To evaluate the signed root periods as explicit combinations of physical parameters, we now choose a weak gauge description.

XIII.7.4 A weak gauge frame for the six masses

How do we identify the five quark masses and the inverse coupling among the six fixed coordinates? Start with the pencil of lines through p_1. Blowing up p_1 resolves the common intersection of the pencil, and $B = E_1$ is a section of the resulting ruling. The generic fiber has class $F = H - E_1$. For each $i \geq 2$, the line through p_1 and p_i acquires two components after blowing up p_i: the new exceptional curve E_i and the strict transform $R_i = F - E_i$. Their pairings are

$$F^2 = 0, \quad B \cdot F = 1, \qquad F = E_i + R_i, \quad E_i^2 = R_i^2 = -1, \quad E_i \cdot R_i = 1. \tag{XIII.7.18}$$

There are $n - 1$ distinct pairs because no three points including p_1 are collinear. The classes $(F, B, E_2, \ldots, E_n)$ form an integral basis: $H = F + B$ and $E_1 = B$ undo the change of marking.

Choose the background lifts π^*F and $\pi^*(E_i - F/2)$, with coefficients m_0 and m_i. The half-fiber shift treats the two components symmetrically. The combination on the surface and the complete period class are

$$j = m_0 F + \sum_{i=2}^{n} m_i (E_i - F/2), \qquad \omega = -a[S] + \pi^* j, \qquad \omega|_S = ah + j. \quad \text{(XIII.7.19)}$$

The lifts are real coordinates and may use rational classes. They need not give integral charges on all curves.

Evaluate (XIII.7.19) on $C = dH - \sum_i b_i E_i$. Besides the electric charge q, call the pairing with F the instanton grade I, and the pairings with $E_i - F/2$ the flavor coordinates f_i:

$$\begin{gathered} q = 3d - \sum_i b_i, \qquad I = F \cdot C = d - b_1, \qquad f_i = b_i - \tfrac{1}{2} I \quad (i \geq 2), \\ V_C = qa + I m_0 + \sum_{i=2}^{n} f_i m_i. \end{gathered} \quad \text{(XIII.7.20)}$$

In the ordinary split-fiber gauge description the W weights are ± 2 in the coroot $H_g = \operatorname{diag}(1, -1)$. Indeed $q(F) = 2$ and $I(F) = f_i(F) = 0$. The two fundamental weights with the same flavor charge are represented by R_i and $-E_i$. They give

C	q	I	f_j	V_C
R_i	1	0	δ_{ij}	$a + m_i$
$-E_i$	-1	0	δ_{ij}	$-a + m_i$

(XIII.7.21)

The actual components are R_i and E_i. The orientation reversal in the second signed weight keeps the same flavor charge; its absolute central charge equals the E_i period in the positive chamber. The ordinary matter rule assigns one full fundamental to each separate split fiber. It gives five fundamentals for dP_6 and four for dP_5.

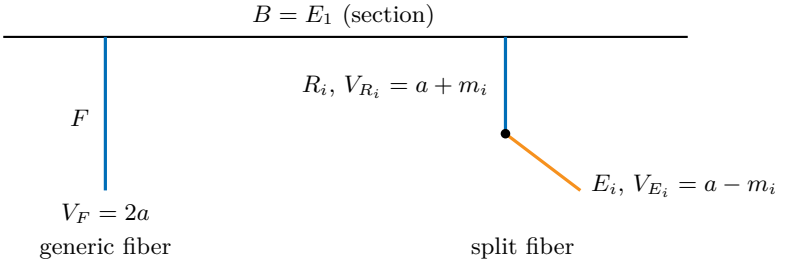


Figure XIII.7.3: A generic fiber of the ruling through p_1 and the split fiber through p_i on the blown-up surface. The section B meets the generic fiber and the strict-transform component R_i. The two positive component periods add to $V_F = 2a$. Their difference, with R_i taken first, is $2m_i$.

The period of B has $q = I = 1$ and $f_i = -1/2$. Together with the two components in Fig. XIII.7.3, this gives a way to solve for the parameters:

$$\begin{aligned} V_F &= 2a, \qquad V_{E_i} = a - m_i, \qquad V_{R_i} = a + m_i, \\ V_B &= a + m_0 - \tfrac{1}{2}\sum_{i=2}^{n} m_i, \\ a &= \tfrac{1}{2}V_F, \qquad m_i = a - V_{E_i}, \\ m_0 &= V_B - a + \tfrac{1}{2}\sum_{i=2}^{n} m_i. \end{aligned} \tag{XIII.7.22}$$

In the order $V_F, V_{E_2}, \dots, V_{E_n}, V_B$ and variables $a, m_2, \dots, m_n, m_0$, the period matrix is lower triangular, with diagonal $2, -1, \dots, -1, 1$. Its absolute determinant is two. This is an invertible real coordinate change; a is half a fiber period. At weak coupling m_0 is positive and large compared with the fiber and quark periods. The condition $a > |m_i|$ only makes each pair positive. We must still test all effective curve generators when we use the smooth Kähler chamber.

Pairing with L kills precisely $\mathbb{R}K$ on $P_{\mathbb{R}}$, since L has codimension one and the form is nondegenerate. It follows that $P_{\mathbb{R}}/\mathbb{R}K \simeq L_{\mathbb{R}}^{*}$ by evaluation. In the six-root marking of (XIII.7.9) the signed periods are

$$\begin{aligned} V_{\alpha_1} &= m_0 + m_2 - \tfrac{1}{2}\sum_{i=2}^{6} m_i, \\ V_{\alpha_i} &= m_{i+1} - m_i \quad (2 \le i \le 5), \qquad V_{\beta} = m_2 + m_3. \end{aligned} \tag{XIII.7.23}$$

In particular the last five expressions determine the five quark masses: the four differences fix them up to a common shift, and the sum fixes that shift. Then the first expression fixes m_0. The same six parameters are thus accessible from the root periods alone, with no measurement of a.

We can make the inverse from root periods explicit. Let $z_j = V_{\alpha_j}$ for $j = 1, \dots, 5$, and let $z_\beta = V_\beta$. Starting with m_2, the four differences are integrated successively. Define

$$\begin{aligned} D_2 &= 0, \qquad D_i = \sum_{j=2}^{i-1} z_j \quad (3 \le i \le 6), \\ m_2 &= \tfrac{1}{2}(z_\beta - z_2), \qquad m_i = m_2 + D_i, \\ m_0 &= z_1 - m_2 + \tfrac{1}{2}\sum_{i=2}^{6} m_i. \end{aligned} \tag{XIII.7.24}$$

The factor of two in m_2 comes from the sum $m_2 + m_3$, after the difference $m_3 - m_2$ is known. It has no bearing on the number of real background coordinates. The root measurements determine all six backgrounds but contain no information about a. A fiber measurement then recovers a. Thus the same set of periods provides a practical separation between the compact motion and a change of boundary data.

For example, increase a by δ at fixed masses. Each exceptional period and each split-component period increases by δ, the fiber increases by 2δ, and V_B increases by δ. Nevertheless,

$$\Delta V_C = q(C)\delta, \qquad \Delta z_1 = \cdots = \Delta z_5 = \Delta z_\beta = 0. \tag{XIII.7.25}$$

The cancellations in the root periods implement the quotient by the compact direction. A variation of one quark mass gives a different pattern, which we can follow while testing the entire effective cone.

Take $a = 4$, $m_0 = 7$ and $(m_2, \dots, m_6) = (1, -2, 1/2, 0, 3/2)$ in a common mass unit. Equation (XIII.7.22) gives

$$\begin{aligned} V_F = 8, \qquad V_B = 21/2, \qquad (V_{E_2}, \dots, V_{E_6}) = (3, 6, 7/2, 4, 5/2), \\ V_\beta = -1, \qquad V_H = V_F + V_B = 37/2. \end{aligned} \tag{XIII.7.26}$$

This example is a period check rather than a weak-coupling hierarchy. The effective cone of smooth dP_6 is generated by its 27 lines: six exceptional curves, fifteen pair lines $H - E_i - E_j$, and six conics through five of the points. For the pair lines the smallest period uses E_1 and E_3. For a conic the smallest period omits the exceptional curve of smallest period, E_6. The three minima are

$$\begin{aligned} \min V_{E_i} &= 5/2, \\ \min V_{H-E_i-E_j} &= 37/2 - 21/2 - 6 = 2, \\ \min V_{2H-\sum_{i\neq j} E_i} &= 37 - 59/2 + 5/2 = 10. \end{aligned} \tag{XIII.7.27}$$

Every generator is positive, although the signed root period V_β is negative. A signed root period is not a Kähler inequality.

To see a zero root period move through the interior of the Kähler cone, change only one background. Set, in a common mass unit,

$$a = 2, \qquad m_0 = 3, \qquad m_2 = t, \qquad m_3 = m_4 = m_5 = m_6 = 0. \tag{XIII.7.28}$$

Here t is a real mass coordinate. The elementary periods are $V_H = 9 - t/2$, $V_{E_1} = 5 - t/2$, $V_{E_2} = 2 - t$ and $V_{E_i} = 2$ for $i \geq 3$. To check the full cone, partition the 27 generators by whether their plane representatives pass through p_1 and p_2. With $Q_j = 2H - \sum_{i\neq j} E_i$, their periods are

Generators	Multiplicity	V_C
$E_1\ ;\ E_2\ ;\ E_i\ (i \geq 3)$	$1 + 1 + 4$	$5 - t/2\ ;\ 2 - t\ ;\ 2$
$H - E_1 - E_2$	1	$2 + t$
$H - E_1 - E_i\ (i \geq 3)$	4	2
$H - E_2 - E_i\ (i \geq 3)$	4	$5 + t/2$
$H - E_i - E_j\ (3 \leq i < j \leq 6)$	6	$5 - t/2$
$Q_1\ ;\ Q_2\ ;\ Q_j\ (j \geq 3)$	$1 + 1 + 4$	$8\ ;\ 5 - t/2\ ;\ 5 + t/2$

(XIII.7.29)

Every row is obtained by subtracting exceptional periods from V_H or $2V_H$. For instance Q_1 contains all five of $E_2, \dots, E_6$ and has period $2(9 - t/2) - [(2 - t) + 4 \cdot 2] = 8$. This cancellation is useful for checking the signs in the background lift.

All entries are positive for $-2 < t < 2$. At the two endpoints the first vanishing generators are different,

$$V_{H-E_1-E_2}\big|_{t=-2} = 0, \qquad V_{E_2}\big|_{t=2} = 0, \qquad V_\beta = t. \tag{XIII.7.30}$$

The root period changes sign at $t = 0$, well before either actual curve wall is reached. The blowup points have stayed in general position throughout, so no root has become effective. This example shows why a root hyperplane is useful for organizing background masses but cannot replace an effective-cone test. It also gives two different failures of the positive chamber when the same input mass is moved in opposite directions.

The prepotential checks which parameter really multiplies the gauge kinetic term. In the signed convention of Chapter 2 we form $A = -\omega$. Only terms with at least one compact factor have an intrinsic degree here. The needed pairings are $h \cdot F = 2$, $h \cdot (E_i - F/2) = 0$ and $(E_i - F/2) \cdot (E_j - F/2) = -\delta_{ij}$. Hence

$$h \cdot j = 2m_0, \qquad j^2 = -\sum_{i=2}^{n} m_i^2. \tag{XIII.7.31}$$

Using $[S]|_S = K$ in each triple intersection gives the compact terms in $A^3/6$:

$$\begin{aligned} \mathcal{F}(a; m) &= \tfrac{1}{6}\big(a^3K^2 - 3a^2K \cdot j + 3aj^2\big) \\ &= \tfrac{9-n}{6}a^3 + m_0a^2 - \tfrac{a}{2}\sum_{i=2}^{n} m_i^2. \end{aligned} \tag{XIII.7.32}$$

The omitted term depends only on the backgrounds. The polynomial has units of mass cubed, and its a derivatives are taken at fixed backgrounds.

For the $SU(2)$ one-loop comparison, $\mathrm{Tr}_{\mathbf{2}}\, H_g^2 = 2$ gives the tree term m_0a^2. There is a pair of roots ± 2 and a pair of weights ± 1 for each fundamental. In the chamber $a > |m_i|$ with all actual curve generators positive, the corresponding root and weight sums give

$$\begin{aligned} \mathcal{F}_{\text{gauge}} &= m_0a^2 + \tfrac{1}{12}\left[2(2a)^3 - \sum_{i=2}^{n}\big(|a + m_i|^3 + |a - m_i|^3\big)\right], \\ (a + m_i)^3 + (a - m_i)^3 &= 2a^3 + 6am_i^2. \end{aligned} \tag{XIII.7.33}$$

Since $16 - 2(n-1) = 2(9-n)$, the two cubics agree including the mass terms. The coefficient of a^2 is m_0, whereas the section period differs from m_0 by $a - \sum_i m_i/2$.

The dependence on a background becomes particularly transparent when we differentiate at fixed m_0, m_i. The first derivative and the gauge Hessian are

$$\begin{aligned} \mathcal{F}_a &= \tfrac{9-n}{2}a^2 + 2m_0a - \tfrac{1}{2}\sum_i m_i^2, \\ \mathcal{F}_{aa} &= (9-n)a + 2m_0, \qquad \mathcal{F}_{aaa} = 9 - n. \end{aligned} \tag{XIII.7.34}$$

The first expression has mass-squared units and the Hessian has mass units, as required for a five-dimensional inverse coupling in this normalization. On the central branch a

quark mass changes the term linear in a but drops out of the Hessian. Moving m_0 by δm_0 instead shifts the Hessian by $2\delta m_0$. This is the operational distinction between the quark masses and the coupling deformation in the chosen frame.

For the family (XIII.7.28) these quantities become

$$\mathcal{F} = 16 - t^2, \qquad \mathcal{F}_a = 18 - \tfrac{1}{2}t^2, \qquad \mathcal{F}_{aa} = 12. \tag{XIII.7.35}$$

The derivatives here are evaluated after taking them at fixed backgrounds, then setting $a = 2$. The section period is $5 - t/2$ and varies with t, while the Hessian is constant. The difference directly rules out identifying the section period with the inverse coupling. A derivative along a path that also varies masses would answer a different question.

A useful check is to take one mass beyond the central branch on the gauge side. For $M = |m_i| > a \geq 0$ the contribution of that hypermultiplet is

$$-\tfrac{1}{12}\big[(M+a)^3 + (M-a)^3\big] = -\tfrac{1}{6}M^3 - \tfrac{1}{2}Ma^2. \tag{XIII.7.36}$$

Keeping $m_0 - M/2$ fixed and dropping the constant in a leaves the gauge polynomial with one fewer flavor, whose central cubic is the one with one fewer blowup in (XIII.7.32). This is a threshold check of the parameter map. It does not construct a geometric path across a Kähler wall. We next ask when a wall defined by a root period is a wall of the actual geometry.

XIII.7.5 A zero root period and a shrinking curve

When does a zero root period describe an actual contraction? On the smooth del Pezzo surface the anticanonical class h is ample. This means, in particular, that it intersects every nonzero effective curve positively. At zero background the period class is ah. For $a > 0$,

$$V_C = 0 \quad (C \in L), \qquad V_D = a\,h \cdot D > 0 \quad (D \text{ a nonzero effective curve on } S). \tag{XIII.7.37}$$

These statements are compatible because L contains no nonzero effective classes on this surface. Nor can an effective compact root hide outside the zero section. A compact irreducible curve in X either projects to a curve on S, with positive h-degree, or lies in a fiber $\mathbb{C}$, which contains no compact curves. In the first case the projection from the curve's normalization pulls K_S back to a line of negative degree. A map to the total space over that projection supplies a section of this line. A line of negative degree on a complete curve has no nonzero section, so the map takes values in the zero section.

We can make one root effective by changing the positions of the blowup points. Take the six projective points, written as homogeneous triples,

$$P_{\text{col}} = \big((1,0,0),(0,1,0),(1,1,0),(0,0,1),(1,2,1),(3,5,1)\big). \tag{XIII.7.38}$$

For comparison, let P_{gen} replace only p_3 by $(1,1,2)$. Use a 3×3 determinant with the point coordinates as rows to test collinearity. For instance the determinant for 123 is

the third coordinate of p_3, so it changes from 0 to 2. For reproducibility, grouping the other triples by smallest index and taking them in lexicographic order gives

Smallest index	P_{col}	P_{gen}
1	$(0,1,1,1,1,1,1,-2,-5,-3)$	$(2,1,1,1,1,-3,-9,-2,-5,-3)$
2	$(-1,-1,-1,1,3,2)$	$(-1,1,5,1,3,2)$
3	$(-1,-2,-1)$	$(-1,-2,-3)$
4	(-1)	(-1)

(XIII.7.39)

The conic test is a determinant as well. The values of $(x^2, y^2, z^2, xy, xz, yz)$ at the six points are the rows. The rows for p_1, p_2, p_4 fix the first three coefficients to zero in any candidate conic. In the original row order the full determinants are

$$\det M_{\mathrm{col}} = -\begin{vmatrix} 1 & 0 & 0 \\ 2 & 1 & 2 \\ 15 & 3 & 5 \end{vmatrix} = 1, \qquad \det M_{\mathrm{gen}} = -\begin{vmatrix} 1 & 2 & 2 \\ 2 & 1 & 2 \\ 15 & 3 & 5 \end{vmatrix} = -21. \tag{XIII.7.40}$$

Neither marking has a conic through all six points. The only line through three points is $z = 0$ in P_{col}.

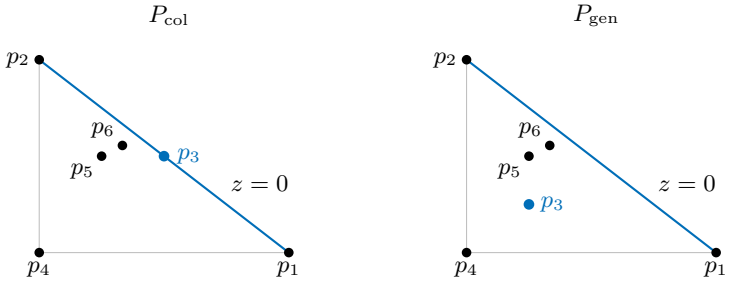


Figure XIII.7.4: The two point configurations in the affine chart $x + y + z \neq 0$, plotted at $(x/(x+y+z), y/(x+y+z))$. The solid line is the segment of $z = 0$ between p_1 and p_2. It contains p_3 on the left. Only p_3 moves in the right panel. The determinant tests also check the other triples and the possible conic.

The classification (XIII.7.15) turns these incidences into an effectivity test. The pullback H is nef, meaning that it has nonnegative intersection with every effective curve. It excludes negative degree. A degree-zero effective divisor is a nonnegative sum of exceptional curves, so a difference $E_i - E_j$ cannot be effective. At positive degree the pushforward to the plane is a line or a conic. If its strict transform has multiplicity r_i at the ith blowup and we add $c_i E_i$ with $c_i \geq 0$, the resulting class has $b_i = r_i - c_i$. Therefore $b_i = 1$ requires the plane curve to pass through p_i. Conversely the unique line in Fig. XIII.7.4 has the right multiplicities and a smooth rational strict transform R. It gives

$$R = H - E_1 - E_2 - E_3, \qquad R^2 = 1 - 3 = -2, \qquad K \cdot R = -3 + 3 = 0. \tag{XIII.7.41}$$

This is the only effective root in the collinear case, and there are none for P_{gen}. The collinear marking coalesces two special fibers of the pencil through p_1. The earlier distinct-fiber matter calculation used the general-position ruling.

To contract R alone on the surface, we need a class that is positive on the other curves. Let (ij) denote the line through p_i, p_j. The unions

$$(14) \cup (25) \cup (36), \qquad (15) \cup (26) \cup (34) \tag{XIII.7.42}$$

are cubics through all six points. They have no common plane component. Each passes through each point with multiplicity one by the triple test, so their strict transforms have class h and no common exceptional component. An irreducible curve cannot be contained in both divisors. Its intersection with at least one of them is nonnegative. This proves that h is nef. Since $h^2 = 3 > 0$, it is also big. For an irreducible curve D with $h \cdot D = 0$, the Hodge index theorem gives $D^2 < 0$, and adjunction gives

$$2p_a(D) - 2 = D^2 + K \cdot D = D^2. \tag{XIII.7.43}$$

The arithmetic genus $p_a(D)$ is nonnegative. Thus $D^2 = -2$, and the incidence calculation identifies $D = R$. The weak del Pezzo contraction theorem over $\mathbb{C}$ now applies: the anticanonical morphism contracts the h-trivial configuration crepantly to a Du Val point. A single exceptional (-2)-curve is the A_1 case.

There is a Kähler approach to this surface contraction. Put $D_* = 7H - \sum_i E_i$. Then $D_*^2 = 43$ and $D_* \cdot E_i = 1$. A strict transform of an irreducible degree-d plane curve has each multiplicity at most d. Its intersection with D_* is therefore at least $7d - 6d = d > 0$. The surface ampleness criterion makes D_* ample, and $ah + \epsilon D_*$ is ample for $a, \epsilon > 0$. On this ray,

$$\begin{aligned} V_R &= \epsilon D_* \cdot R = (7-3)\epsilon, \\ \mathrm{Vol}(S) &\longrightarrow \frac{3a^2}{2T_{M2}^2} > 0 \quad (\epsilon \to 0^+,\ a > 0). \end{aligned} \tag{XIII.7.44}$$

The volume uses $J|_S = (ah + \epsilon D_*)/T_{M2}$ and the Kähler formula $\int_S J^2/2$. The collapsing root is a curve in a surface that remains finite.

The separation of scales on this ray can also be read before taking the limit. The pairings are $h \cdot D_* = 15$ and $D_*^2 = 43$, so the exact surface volume is

$$\mathrm{Vol}(S) = \frac{1}{T_{M2}^2}\left(\frac{3}{2}a^2 + 15a\epsilon + \frac{43}{2}\epsilon^2\right), \qquad V_R = 4\epsilon. \tag{XIII.7.45}$$

At fixed $a > 0$ the M2 on R becomes light while the M5 wrapping S retains a finite tension proportional to its volume. If we instead set the backgrounds to zero on the smooth cubic and reduce a, every fixed effective curve period is linear in a, whereas the surface volume is quadratic in a. These two operations remove different exceptional sets. The volume expansion makes that distinction visible without assigning any extra current to an individual root.

What is the transverse geometry in the threefold? The restriction of K_S to $R \simeq \mathbb{P}^1$ has degree zero and is trivial, so $\pi^{-1}(R) \simeq \mathbb{P}^1 \times \mathbb{C}$. To determine the contracted germ

we need the surface map $\rho : S \to \overline{S}$, not just this bundle restriction. Crepancy gives $K_S = \rho^* K_{\overline{S}}$. Near the A_1 point the dualizing line is locally trivial. Taking total spaces there is taking the surface resolution times a line:

$$\widetilde{A_1} \times \mathbb{C} \longrightarrow A_1 \times \mathbb{C}, \qquad \mathbb{P}^1 \times \mathbb{C} \longrightarrow \{0\} \times \mathbb{C}. \tag{XIII.7.46}$$

In the ordinary local prescription a transverse ADE fiber can support a background algebra when its base is noncompact. In the local limit that sends the base volume to infinity, a vector constant along it has divergent kinetic coefficient and is held fixed. This is the geometric mechanism for a background symmetry, conditional on that limit. The one A_1 family supplies no count of the full fixed-point currents.

Return to smooth dP_6 and set all backgrounds to zero. This time we send a to zero, rather than varying complex structure to make one root effective. The anticanonical embedding of a smooth degree-three del Pezzo gives a smooth cubic in $\mathbb{P}^3$ with $K_S = \mathcal{O}_S(-1)$. A point of $\mathcal{O}_S(-1)$ is a pair $([u], x)$ where $x \in \mathbb{C}^4$ lies on the line represented by $[u] \in S$. Forgetting $[u]$ gives the map to the affine cone. For $x \neq 0$ the inverse is $x \mapsto ([x], x)$; for $x = 0$ the full zero section maps to the vertex. In the Fermat example the cone and its gradient are

$$G(x) = \sum_{i=1}^{4} x_i^3 = 0, \qquad \nabla G = 3(x_1^2, x_2^2, x_3^2, x_4^2). \tag{XIII.7.47}$$

The gradient vanishes only at the vertex. The smooth-ray periods give, for example, $V_{E_1} = a$ and $\mathrm{Vol}(S) = 3a^2/(2T_{M2}^2)$. The M2 mass on this line and the M5 tension from wrapping the surface both tend to zero. The geometric scales vanish, but the calibrated wrapped-brane calculation does not quantize the resulting apex.

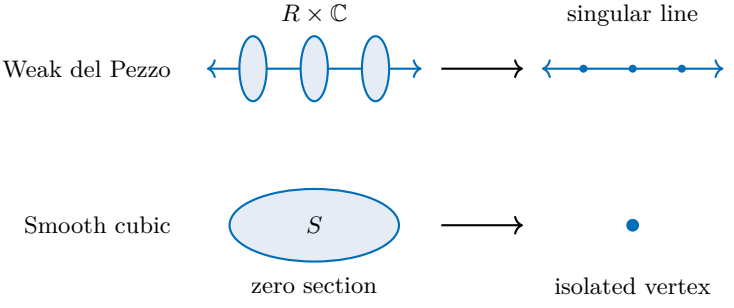


Figure XIII.7.5: Two different exceptional sets and their images. In the weak del Pezzo case, each $\mathbb{P}^1$ over the noncompact complex line contracts to one point on that line. In the smooth cubic case, the compact zero section S maps to one vertex, and the map is an isomorphism away from S. The panels depict the maps and their exceptional sets, rather than metric shapes.

Figure XIII.7.5 distinguishes a background ADE mechanism over a line from the isolated apex of the rank-one model. In the smooth case all root periods were already zero before reaching the apex. We therefore turn to the weak gauge description to ask what new operators can supply the additional currents.

XIII.7.6 The currents missing at weak coupling

Which currents would distinguish the fixed point from the weak gauge presentation? At zero quark masses and $m_0 > 0$, five full fundamentals give ten half-hypermultiplets of the pseudoreal doublet. Their rotations give $\mathfrak{so}(10)$. The instanton current is proportional to $*\,\mathrm{Tr}(\mathsf{F}\wedge\mathsf{F})$, with F the gauge curvature. The Bianchi identity gives its conservation. We normalize its $\mathfrak{u}(1)_I$ charge k to one on a unit instanton; m_0 is the associated background scalar. Four full fundamentals give $\mathfrak{so}(8)\oplus\mathfrak{u}(1)_I$ by the same argument. Generic quark masses break the nonabelian part further. At $a = m_0 = m_i = 0$, the ordinary local del Pezzo identification gives the rank-one E_6 theory for $n = 6$ and E_5 for $n = 5$. We first grade the lattice and then compare with a protected current calculation to see what the larger algebras require.

A root has $q = 0$. Use $I = F\cdot C$ and $f = (f_2,\ldots,f_n)$ from (XIII.7.20), and let e_i be the unit vector in the ith flavor direction. The $I = 0$ roots give

$$\begin{aligned} E_i - E_j &\longmapsto e_j - e_i \qquad (i,j\geq 2,\ i\neq j),\\ \pm(H - E_1 - E_i - E_j) &\longmapsto \pm(e_i + e_j) \quad (2\leq i<j\leq n). \end{aligned} \tag{XIII.7.48}$$

The complete neutral root set is thus the D_{n-1} set $\pm e_i \pm e_j$. For $n = 6$ the first row has $5\cdot 4$ roots and the second has $2\binom{5}{2}$, giving 40 in all. These are the roots of the weak $\mathfrak{so}(10)$ part.

At grade $+1$, each flavor coordinate is $b_i - 1/2$. The types in (XIII.7.15) that have this grade can be read directly from $d - b_1$:

Root on dP_6	Number of plus signs in $2f$	Multiplicity
$E_1 - E_i$	1	5
$H - E_i - E_j - E_k \quad (i,j,k\geq 2)$	3	$\binom{5}{3} = 10$
$2H - \sum_i E_i$	5	1

(XIII.7.49)

For instance $E_1 - E_2$ has $b_1 = -1$, $b_2 = 1$ and gives $f = (1,-1,-1,-1,-1)/2$. The three rows exhaust all five-entry sign vectors with an odd number of plus signs. They are the weights of one chiral spinor of $\mathfrak{so}(10)$. Grade -1 has the opposite vectors, of even plus parity since five signs are flipped. It gives the conjugate spinor. No other grades occur in the root inventory.

An adjoint representation also has zero weights from its Cartan generators. All six are at grade zero. Five complete the $\mathfrak{so}(10)$ adjoint and one is the neutral topological generator. Hence the Lie-algebra branching is

$$\mathbf{78} = \mathbf{45}_0 \oplus \mathbf{1}_0 \oplus \mathbf{16}_{+1} \oplus \overline{\mathbf{16}}_{-1}. \tag{XIII.7.50}$$

With five blowups the same neutral formulas give $4\cdot 3 + 2\binom{4}{2} = 24$ roots. There is no degree-two root. The first two types in (XIII.7.49) give $4 + \binom{4}{3} = 8$ weights at grade $+1$. Flipping four signs preserves plus parity, so the conjugate spinor is of the same type. With five Cartan generators the branching for $\mathfrak{e}_5 = \mathfrak{so}(10)$ is

$$\mathbf{45} = \mathbf{28}_0 \oplus \mathbf{1}_0 \oplus \mathbf{8}_{s,+1} \oplus \mathbf{8}_{s,-1}. \tag{XIII.7.51}$$

Here s labels the selected $\mathfrak{so}(8)$ spinor, up to triality. Table XIII.7.1 keeps the root counts separate from the Cartan multiplicities.

Surface	$I=-1$	$I=0$	$I=+1$	Cartan at 0	Adj. dimension
dP_6	16	40	16	6	78
dP_5	8	24	8	5	45

Table XIII.7.1: The three columns headed by I count roots. To obtain the adjoint weight multiplicity at grade zero, add the Cartan column to the neutral root count. The charged columns need no such addition.

Why should the gauge description contain the two missing sectors? A local instanton operator fixes the gauge bundle on a small linking S^4 to have nonzero instanton number. In the unit instanton background, the gaugino zero modes give the multiplet containing the candidate current vector. The fundamental matter supplies $2N_f$ real fermionic zero modes Γ^A, with $N_f = n-1$. Their quantization is a Clifford algebra. Pair the real modes into N_f complex creation operators $c_i^\dagger$ and annihilation operators c_i, with number operators $N_i = c_i^\dagger c_i$. In flavor axes chosen by these pairs,

$$\{\Gamma^A, \Gamma^B\} = \delta^{AB}, \qquad \{c_i, c_j^\dagger\} = \delta_{ij}, \qquad f_i = N_i - \tfrac{1}{2} \quad (N_i = 0, 1). \tag{XIII.7.52}$$

This gives the full spinor before the gauge projection. The residual gauge center acts by minus one on each Γ^A because the fermions are in the gauge doublet. It therefore acts on the spinor states by occupation parity, up to the overall phase of the vacuum. The gauge projection, with the chosen chirality convention, keeps one parity:

$$(-1)^{\sum_i N_i} = \text{fixed sign}, \qquad \dim \mathcal{H}_{\text{projected}} = 2^{N_f - 1}. \tag{XIII.7.53}$$

This is the physical origin of a chiral spinor in a charged sector. The conjugate sector has opposite instanton charge. For $N_f = 5$ the parity choice can be labeled so that the positive grade matches the odd-plus weights above. The zero-mode analysis identifies candidate vectors; it does not prove conservation from an area integral or count a soliton spectrum at a general Coulomb point.

The protected comparison tests the currents at the conformal origin. Choose a Poincaré supercharge Q and its radial conjugate $Q^\dagger$. Their anticommutator is $\Delta = \{Q, Q^\dagger\} = E - 2j_1 - 3R_{\text{sym}}$, where E is the scaling dimension, j_1, j_2 are the rotation Cartans and R_{sym} is the R-symmetry Cartan. With flavor Cartans H_i, flavor fugacities z_i and instanton fugacity u, the index on $S^4 \times S^1$ is

$$\mathcal{I} = \operatorname{Tr}_{\mathcal{H}(S^4)} \left[(-1)^{\mathsf{F}} e^{-\beta_0 \Delta} x^{2(j_1 + R_{\text{sym}})} y^{2j_2} u^k \prod_i z_i^{H_i} \right]. \tag{XIII.7.54}$$

Here F in $(-1)^{\mathsf{F}}$ denotes fermion number and β_0 is the regulator parameter. The commuting fugacities agree on paired states, so the signed trace cancels pairs with $\Delta > 0$. The z_i keep flavor weights visible; they are chemical potentials in the trace, not the real mass deformations of the flat-space model.

In a conserved flavor current multiplet the scalar primary, called the moment map, is an R-symmetry triplet of dimension three. Its highest R-weight component has

$$(E, j_1, j_2, R_{\rm sym}) = (3, 0, 0, 1) \quad \Longrightarrow \quad \Delta = 0, \qquad x^{2(j_1+R_{\rm sym})} = x^2.$$

For moment maps in a weak flavor representation $\mathbf{r}$ of instanton charge k, these bosonic states contribute $+x^2 u^k \chi_{\mathbf{r}}(z)$, with $\chi_{\mathbf{r}}$ the flavor character. The trace probes the conserved vector through this scalar in the same multiplet. To test for the charged multiplets we use the normalized localization results for the two theories:

$$\begin{aligned} N_f = 5: &\quad [x^2]\mathcal{I} = \chi_{\mathbf{45}} + 1 + u\chi_{\mathbf{16}} + u^{-1}\chi_{\overline{\mathbf{16}}} = \chi^{E_6}_{\mathbf{78}}, \\ N_f = 4: &\quad [x^2]\mathcal{I} = \chi_{\mathbf{28}} + 1 + (u + u^{-1})\chi_{\mathbf{8}_s} = \chi^{E_5}_{\mathbf{45}}. \end{aligned} \tag{XIII.7.55}$$

In this comparison the sign of k is chosen to agree with the sign of the root grade on the adjoint branching. For $N_f = 5$ the neutral part alone gives 46 at $z_i = 1$, whereas the instanton and anti-instanton sectors supply 16 each. Their separate fugacity powers test more than the total 78. This is the protected evidence for the additional currents, beyond the lattice pattern and the existence of the cone. The comparison is made at order x^2 at the fixed point, and does not identify the curve lattice with the full spectrum of operator charges.

A character keeps more information than its value at unit fugacities. We can exhibit this without calculating another index coefficient. Set the first flavor fugacity to y^2 and the other four to one. A weight $f_2 = \pm 1/2$ then contributes $y^{\pm 1}$, while a vector weight $\pm e_2$ contributes $y^{\pm 2}$. In the neutral D_5 root set, the roots using the first axis give $8(y^2 + y^{-2})$; the other four axes give 24 roots. Adding the five Cartan weights gives

$$\chi_{\mathbf{45}} = 29 + 8(y^2 + y^{-2}), \qquad \chi_{\mathbf{16}} = \chi_{\overline{\mathbf{16}}} = 8(y + y^{-1}). \tag{XIII.7.56}$$

The equality of the two spinor expressions holds after this specialization. For either chirality, fixing the first sign leaves eight choices of the other four with the required parity. Resolving all five fugacities distinguishes the two chiralities again.

Substitution in the order-x^2 coefficient yields

$$[x^2]\mathcal{I}\big|_{z_2 = y^2,\ z_{i>2} = 1} = 30 + 8(y^2 + y^{-2}) + 8(u + u^{-1})(y + y^{-1}). \tag{XIII.7.57}$$

At $y = u = 1$ it is 78. At $y = u = 2$ it is 114. The latter number is a character evaluation, not a new count of currents. Its value changes because different weights carry different fugacity powers. Replacing every flavor character by its dimension would instead give $46 + 16(u + u^{-1})$, which loses this test of flavor weights. In this way the refined comparison checks both the instanton grades and the spinor weight pattern already obtained from the surface lattice.

XIII.7.7 What the root lattice leaves undetermined

Does the root calculation distinguish the possible global forms of the flavor symmetry? It does give a useful integral quotient. Let $L^* = \mathrm{Hom}(L, \mathbb{Z})$ be the integral dual. Use the

positive pairing $-C \cdot D$ on L to compare roots with dual vectors. Since the coefficients of K have greatest common divisor one, K is primitive. Also L is primitive: it is the kernel of $K\cdot$ on P. The map to the dual is

$$P \longrightarrow L^*, \qquad C \longmapsto \big(D \mapsto -C \cdot D\big). \tag{XIII.7.58}$$

The kernel is $P \cap \mathbb{Q}K = \mathbb{Z}K$. Because L is primitive, P/L is free, so an integral functional on L extends to one on P. The pairing on P is unimodular by (XIII.7.1); every extended functional is pairing with an element of P. Thus the map is onto. The quotient and the index for dP_6 are

$$P/\mathbb{Z}K \simeq L^*, \qquad [L^* : L] = |\det(E_6)| = 3. \tag{XIII.7.59}$$

The index uses the Cartan matrix of the map from L to L^* in integral bases. The quotient L^*/L records which integral functionals do not come from a root-lattice vector.

The orthogonal projection of a curve class onto $L \otimes \mathbb{Q}$ represents its flavor functional. For dP_6 and the exceptional line E_1 it gives

$$w(C) = C - \frac{h \cdot C}{3} h, \qquad w(E_1) = E_1 - \frac{h}{3}, \qquad q(E_1) = 1. \tag{XIII.7.60}$$

The projection pairs integrally with L because h pairs to zero. It is not integral as a vector of P: for instance its E_2 coefficient is $1/3$. Multiplying by three gives

$$3w(E_1) = 3E_1 - h = -3H + 4E_1 + \sum_{i=2}^{6} E_i \in L. \tag{XIII.7.61}$$

The displayed integral class pairs to zero with K since the sum of its exceptional coefficients is nine. The weight thus has order three modulo L.

There is a useful relation between the compact charge and this quotient, entirely within the lattice calculation. For any integral class C, let $q = h \cdot C$. Since $h \cdot E_1 = 1$, the class $C - qE_1$ is integral and lies in L. Linearity of the orthogonal projection therefore gives

$$w(C) - q\, w(E_1) = C - qE_1 \in L, \qquad [w(C)] = q\,[w(E_1)] \text{ in } L^*/L. \tag{XIII.7.62}$$

For example an exceptional line, a pair line and a five-point conic all have h-degree one and hence the same nonzero quotient class. The fiber has charge two and its projection has twice that class. A charge-zero integral class already belongs to L, so its projection has trivial class.

This also explains how fractional coefficients arise in (XIII.7.60). The rational decomposition separates the electric direction from its orthogonal flavor part,

$$C = w(C) + \frac{q}{3} h, \qquad h \cdot w(C) = 0. \tag{XIII.7.63}$$

Neither summand has to be integral, although their sum is an integral curve class. Equation (XIII.7.62) is the integrality constraint coupling these two parts in this marking. It is not yet a statement about which flavor representations occur among

genuine local operators. That question requires the physical selection of operators as well as the lattice of possible functionals.

The important distinction is the electric charge in (XIII.7.60). The M2 on E_1 carries gauge charge one. Its projected flavor weight does not demonstrate a gauge-invariant local operator with that center character. Conversely, the adjoint currents alone cannot distinguish a simply connected group from its adjoint form, since the center acts trivially on the adjoint. Table XIII.7.2 identifies the extra inputs that would distinguish the possibilities.

Object	What we computed	Further input for a group claim
Root lattice and currents	Cartan form and the adjoint branching	Center action on genuine local operator representations
Projected M2 weight	A nontrivial class of order three, with electric charge one	Compatible actions of gauge and flavor centers and the gauge-invariant operator spectrum
Defects and backgrounds	No computation of their allowed charges	Admissible lines or rays and the background bundles on which the theory can be defined

Table XIII.7.2: The integral quotient is a calculation on the marked surface. The tests in the third column concern different physical objects. In particular the quotient does not determine a higher-form symmetry.

The planned treatment of symmetries and anomalies addresses the global symmetry problem, which requires a separate center analysis. A proposed magnetic quiver, of the kind studied in X, poses a different comparison. Its balanced nodes may suggest a current algebra, but a match of Higgs and Coulomb branches requires the full quiver and an independent protected test of the two branches at the same deformation locus. Exercise 5 asks for such a test.

Take-home message of this chapter

The periods orthogonal to K measure fixed backgrounds. A root of this lattice is a signed class: its period can vanish in the smooth chamber with no effective root curve. The protected instanton sectors at the isolated rank-one fixed point supply the current comparison. The adjoint and the lattice quotient leave the faithful global group undetermined by these calculations.

XIII.7.8 Exercises

1. **Change the marking to five blowups.** On dP_5, take the four successive differences $E_i - E_{i+1}$ followed by $H - E_1 - E_2 - E_3$. Compute the positive Cartan matrix, its determinant and the number of roots with both orientations. Submit the ordered matrix as `cartan`, the determinant as `det`, and the root count as `count` to `e1`. Derive the degree bound and explain which root type is lost.

2. **Extract masses from periods.** On dP_6, in a common mass unit let

$$(V_F, V_B, V_{E_2}, V_{E_3}, V_{E_4}, V_{E_5}, V_{E_6}) = (10, 21/2, 3, 6, 9/2, 13/2, 4).$$

Submit $(a, m_0, m_2, m_3, m_4, m_5, m_6)$ as `parameters` and the signed periods on $(\alpha_1, \ldots, \alpha_5, \beta)$ as `root_periods` to `e2`. Calculate the two lists separately, using the input curve periods for one calculation of the signed root periods.

3. **Check actual curves in three markings.** Use P_{gen} and P_{col} from §XIII.7.5, and a third marking with six points $(1 : t : t^2)$ for $t = 0, 1, \ldots, 5$. For each, find all effective roots. Submit `generic`, `collinear` and `conic` to `e3`. Each is a list of vectors $(d, b_1, \ldots, b_6)$ representing $dH - \sum_i b_i E_i$. Use only the effective orientation and list each root once. Explain why the quadratic parametrization puts the six points on a conic with no collinear triple.

4. **Count the adjoint by grade.** For dP_6 and dP_5 use $I = (H - E_1) \cdot C$. Submit `e6` and `d5` to `e4`, each an ordered list of adjoint weight multiplicities at $(-1, 0, +1)$. Include Cartan weights. In a separate answer name the manifest algebras at vanishing quark masses and positive m_0, the algebras at the fixed points, and the sectors whose contribution distinguishes them.

5. **Design a test of a magnetic-quiver proposal.** A proposed three-dimensional magnetic quiver has an E_6-shaped balanced subgraph. What would you specify and compare before identifying its Coulomb branch with the five-dimensional fixed point's Higgs branch? Say which quiver and deformation data you would fix before comparing the branch dimensions. If those dimensions agreed, propose a protected test that can still detect a difference in the flavor representations of the two branches. Explain what extra data the faithfully acting flavor group requires. Distinguish gauge-invariant local operators, gauge-charged wrapped states and line or ray data. This is a written exercise.

Two further written problems test transfer of the method. They have no numerical submission contract.

6. **Follow a background through the smooth chamber.** For (XIII.7.28), derive every row of (XIII.7.29) from the elementary periods. Find the six simple-root periods and reconstruct the input masses with (XIII.7.24). Explain why the root β is not effective at $t = 0$, and identify the actual curve that first violates positivity beyond each endpoint. Then increase a to 3 at fixed backgrounds. Determine the new interval in t allowed by all 27 generators and explain which measured periods are unchanged.

7. **Compare a charge and a flavor functional.** Compute $w(F)$ and its order modulo L on dP_6. Verify (XIII.7.62) for F and for $H - E_2 - E_3$. Use the six simple-root pairings to test that the projections are integral functionals even though their surface coefficients are fractional. Explain why these calculations do not settle the global form of the flavor group.

Use `benchmark/tasks.json` to find the question IDs and `benchmark/PROTOCOL.md` for submission. For the first four exercises, use exactly the specified fields, with no duplicate keys and at most 10,000 characters for the answer object. An entry is a JSON integer or a quoted exact integer or fraction of fewer than 100 characters. A fraction may have a sign before its numerator and must have a positive denominator with no leading zero. No decimal approximations are accepted. A reader assesses the exact values and the written derivations and explanations.

Status and sources

§7.1–7.2: Compact support and masses. ([MATH]) is the bundle, retraction and Thom restriction in (XIII.7.2)–(XIII.7.4). The fixed-boundary interpretation ([GEO-E]) uses the relative period convention of Chapter 2 and Closset et al. (2021, arXiv v4, Eq. (1.3), Table 3). The M2 calibration ([GEO-E]) uses the calibrated M2 units and Morrison and Seiberg (1997, arXiv v2, §3.2, discussion following Eq. (3.7)). These physical assignments assume the ordinary decoupled local sector and realized calibrated curves.

§7.3: The root lattice. ([MATH]) follow from (XIII.7.10)–(XIII.7.16). For the root norm, pairing and Weyl action see Douglas et al. (1997, arXiv v2, §2.1, Eqs. (2.1)–(2.3)). The integral expansion establishes saturation independently of the determinants; the degree bound gives the complete inventory.

§7.4: Ruling, signed weights and cubic. The pencil and the actual line classes use Douglas et al. (1997, arXiv v2, §2.1) ([MATH]). ([MATH]) is the signed period calculation (XIII.7.19)–(XIII.7.23). The fundamental pair rule ([GEO-E]) uses Intriligator et al. (1997, arXiv v2, §8.1, around Eqs. (8.6)–(8.10)) and Douglas et al. (1997, arXiv v2, §3), in the specified weak gauge chamber. The protected cubic interpretation ([GEO-E]) matches Intriligator et al. (1997, arXiv v2, Eqs. (2.22), (8.4)) at fixed background in the calibrated relative units. The threshold calculation does not furnish a flop.

In Morrison and Seiberg (1997, arXiv v2, Eqs. (3.1)–(3.4), (3.7)), $\Gamma_i = R_i$, $\Gamma_i' = E_i$ and $H_i|_S = F/2 - R_i = E_i - F/2$. Since $H_0|_S = F/4$, the evaluated positive periods give $\phi = a$, $t_0 = 4m_0$. The coupling on the common central branch is $t(\phi) = 4m_0 + 2(9-n)a = 2\mathcal{F}_{aa}$. We translate the evaluated periods and coupling, without substituting the source's intermediate signed divisor expression for our Kähler class. In the notation of Douglas et al. (1997, arXiv v2, §2.1), the full fiber period is $2a$ and the component difference in our order is $2m_i$.

§7.5: Effectivity and two contractions. ([MATH]) distinguish the ample ray, the explicit collinear marking and its weak anticanonical model. For the characteristic-zero contraction and crepancy see Dolgachev (2025, Thm. 8.3.2(ii)–(iii), Prop. 8.1.10) and Gao (2025, arXiv v3, §§2.4–2.5). The threefold product in (XIII.7.46) uses the pullback of the dualizing line. The local background mechanism ([GEO-E]) uses Bhardwaj (2020, arXiv v2, §1, printed p. 3) and the ordinary transverse ADE dictionary under fixed local boundary conditions. The isolated cubic contraction ([MATH]) uses the smooth anticanonical embedding, summarized in Vakil (n.d., pp. 1–2); the Fermat model is listed in Closset et al. (2021, arXiv v4, §4.1, Table 3).

§7.6: Grading and physical currents. ([MATH]) is the graded branching in (XIII.7.48)–(XIII.7.51). The fixed-point identification ([GEO-X]) uses Morrison and Seiberg (1997, arXiv v2, §3.2), Seiberg (1996, arXiv v2, §3, Eqs. (3.5)–(3.8), §§4–5), and Closset et al. (2021, arXiv v4, Table 3) for the Fermat example. The moment-map multiplet and the zero-mode argument use Tachikawa (2015, arXiv v3, Eqs. (2.1), (2.3), (3.2), (3.4)). ([BPS:1/8|idx]) compares the single refined order-x^2 coefficient in (XIII.7.55) using Kim et al. (2012, arXiv v2, Eqs. (3.1)–(3.2),

§4.2, Eqs. (4.20)–(4.23)). This is the normalized $S^4 \times S^1$ trace in the source scheme at the conformal origin, with the selected supercharge and its conjugate. There is no Coulomb-branch particle wall crossing in the comparison and no claim about other orders or contact terms.

§7.7–7.8: Integral quotient and further tests. ([MATH]) follows from (XIII.7.58)–(XIII.7.61). A separate case-specific global-form computation is given in Apruzzi et al. (2022, arXiv v3, §3.9.1, Eqs. (3.68)–(3.69)). Neither that computation nor a magnetic-quiver identification follows from the lattice quotient or the current character.

The additional algebraic consequences of the same model are the lift compensation in (XIII.7.5), the integral conic expansion and reflection check in (XIII.7.11) and (XIII.7.17), the inverse and changed-input period calculations in (XIII.7.24)– (XIII.7.30), the fixed-background cubic derivatives in (XIII.7.34), and the ray volume in (XIII.7.45) ([MATH]). Equation (XIII.7.57) is a specialization of the sourced order-x^2 character, with no claim at other index orders. Equations (XIII.7.62)– (XIII.7.63) are integral consequences of the displayed symmetry calculation ([MATH]); their interpretation does not determine a faithful global group.

References

Apruzzi, F. et al. (2022). "The global form of flavor symmetries and 2-group symmetries in 5d SCFTs". In: *SciPost Phys.* 13, p. 024. arXiv: 2105.08724 [hep-th].

Bhardwaj, L. (2020). "Flavor symmetry of 5d SCFTs, Part 1: General setup". In: arXiv: 2010.13230 [hep-th].

Closset, C. et al. (2021). "5d and 4d SCFTs: Canonical singularities, trinions and S-dualities". In: *JHEP* 05, p. 274. arXiv: 2012.12827 [hep-th].

Dolgachev, I. V. (2025). "Classical algebraic geometry, Part II". August 10 draft.

Douglas, M. R., S. Katz, and C. Vafa (1997). "Small instantons, del Pezzo surfaces and type I' theory". In: *Nucl. Phys. B* 497, pp. 155–172. arXiv: hep-th/9609071.

Gao, R. (2025). "Quasi-étale covers of Du Val del Pezzo surfaces and Zariski dense exceptional sets in Manin's conjecture". In: arXiv: 2406.16240 [math.AG].

Intriligator, K. A., D. R. Morrison, and N. Seiberg (1997). "Five-dimensional supersymmetric gauge theories and degenerations of Calabi–Yau spaces". In: *Nucl. Phys. B* 497, pp. 56–100. arXiv: hep-th/9702198.

Kim, H.-C., S.-S. Kim, and K. Lee (2012). "5-dim superconformal index with enhanced E_n global symmetry". In: *JHEP* 10, p. 142. arXiv: 1206.6781 [hep-th].

Morrison, D. R. and N. Seiberg (1997). "Extremal transitions and five-dimensional supersymmetric field theories". In: *Nucl. Phys. B* 483, pp. 229–247. DOI: 10.1016/S0550-3213(96)00592-5. arXiv: hep-th/9609070.

Seiberg, N. (1996). "Five-dimensional SUSY field theories, nontrivial fixed points and string dynamics". In: *Phys. Lett. B* 388, pp. 753–760. DOI: 10.1016/S0370-2693(96)01215-4. arXiv: hep-th/9608111.

Tachikawa, Y. (2015). "Instanton operators and symmetry enhancement in 5d supersymmetric gauge theories". In: *PTEP* 2015, 043B06. arXiv: 1501.01031 [hep-th].

Vakil, R. (n.d.). "Complex algebraic surfaces, Class 15". Lecture notes.

Chapter XIII.8

Wrapped particles, partition functions, and the IIA circle limit

XIII.8.1 What changes when the circle shrinks?

A wrapped M2-brane measures a curve area as a particle mass in five dimensions. Put the external theory on a circle and let the particle go around it. Its mass now determines an exponential weight. What should we hold fixed as the circle shrinks if we want to retain a four-dimensional instanton contribution? A particle of fixed mass has a weight that tends to one. The instanton weight must instead tend to zero at just the rate needed to compensate the poles in the localization formula.

We will calculate that rate and the resulting coefficient in local F_0, the canonical bundle over $\mathbb{P}^1 \times \mathbb{P}^1$. The two one-box placements in the vertex sum correspond to the two gauge fixed points. Comparing them determines the instanton fugacity at finite circumference. Its limit gives the first Seiberg–Witten prepotential coefficient in the electric frame of Chapter XI.7.

We use the wrapped-brane masses and curve frame of Chapter XIII.2, the vertex gluing and protected trace of Chapters V.7–V.8, and the weak electric periods of Chapters XI.6–XI.7. We keep one base degree and sum all fiber degrees, since the fiber fugacity approaches one as the circle shrinks.

XIII.8.2 Wrapped particles and circle parameters

What exponent appears when a five-dimensional particle goes around the circle? Let R be the radius of the product circle, and let the M2 wrap a smooth calibrated curve C of area A_C. Its tension T_{M2} converts area to mass. Write β for circumference and θ_C

for the dimensionless three-form phase of a single positive winding.

$$\beta = 2\pi R, \qquad M_C = T_{\mathrm{M2}} A_C, \qquad S_{E,C}(n) = n\beta M_C - in\theta_C \quad (n = 1, 2, \ldots). \tag{XIII.8.1}$$

The area is independent of the circle coordinate. The Euclidean membrane volume is therefore the area times the length $n\beta$. The phase also scales with n, because the same oriented worldvolume is covered n times. The corresponding weight is

$$Q_C = e^{-\beta M_C + i\theta_C}, \qquad e^{-S_{E,C}(n)} = Q_C^n. \tag{XIII.8.2}$$

Choose this circle as the M-theory reduction circle and use common M-theory and IIA mass units. Let ℓ_p and ℓ_s be the eleven-dimensional Planck and string lengths, g_s the physical IIA string coupling, and $\alpha' = \ell_s^2$. The circle dictionary gives

$$R = g_s \ell_s, \qquad \ell_p^3 = R\ell_s^2, \qquad \beta T_{\mathrm{M2}} = \frac{2\pi R}{(2\pi)^2 \ell_p^3} = \frac{1}{2\pi\alpha'}. \tag{XIII.8.3}$$

A Euclidean membrane on $C \times S^1$ has the circle in its worldvolume. Reduction along it leaves a fundamental-string worldsheet on C. The three-form phase with one leg on the circle becomes the NS two-form phase on that worldsheet. With J the Kähler form and B_{NS} the two-form, the flat coordinate is

$$\theta_C = \frac{1}{2\pi\alpha'} \int_C B_{\mathrm{NS}} \pmod{2\pi}, \qquad t_C = \frac{1}{4\pi^2\alpha'} \int_C (B_{\mathrm{NS}} + iJ), \qquad Q_C = e^{2\pi i t_C}. \tag{XIII.8.4}$$

The equalities here use $A_C = \int_C J$ in the matching metric units. They identify a flat exponential, which need not be the algebraic coordinate of a mirror curve.

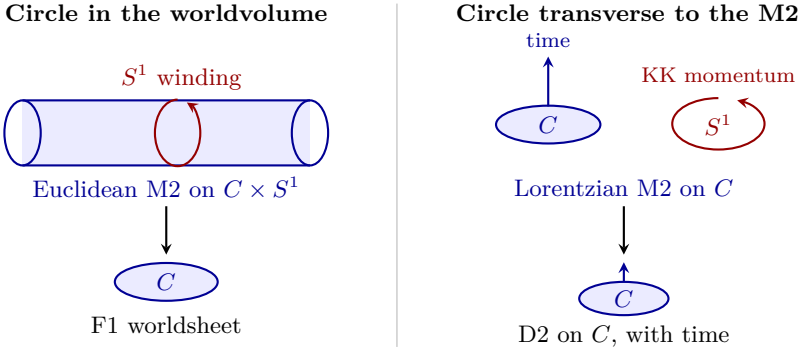


Figure XIII.8.1: Two choices of circle relative to the membrane. On the left, the positive Euclidean winding follows the external circle inside the worldvolume $C \times S^1$; reducing that circle gives a fundamental-string worldsheet on C. On the right, the external circle is transverse to an M2 on C with a Lorentzian time direction; reduction leaves the time direction and gives a D2 on C. Momentum along the transverse circle becomes D0 charge.

Figure XIII.8.1 distinguishes two uses of the wrapped membrane. A Lorentzian M2 particle obtained by wrapping C has an unwrapped time direction. With a circle transverse to the membrane it reduces to a D2 particle on C. The particle's Fourier momentum before reduction is quantized in units of $1/R$. IIA reads the corresponding integer as D0 charge. The integer n in (XIII.8.2) instead counts wraps of an Euclidean history. It multiplies the area term and the phase in that history.

Now let B, F be the base and fiber classes of the two rulings of F_0. In the electric chamber of Chapter XIII.2 write $a_5 > 0$ for the Coulomb scalar and $m_0 \geq 0$ for the background period. In the signed divisor frame with compact divisor S and background lift D satisfying $D|_S = F$, the period class is $m_0 D - a_5 S$. Restricting S to itself gives the canonical class $K_{F_0} = -2B - 2F$. The intersection numbers give

$$B^2 = F^2 = 0, \qquad B \cdot F = 1, \qquad (m_0 D - a_5 S)|_S = 2a_5 B + (m_0 + 2a_5)F. \quad \text{(XIII.8.5)}$$

The period on B is the coefficient of F in this class, and the period on F is the coefficient of B. Put $w = 2a_5$, the positive W-particle mass, and set the fiber phase to zero on the real reference slice. Then

$$\begin{aligned} M_F &= w, \\ M_B &= m_0 + w, \\ X := Q_f &= e^{-\beta w}, \\ Q_b &= e^{-\beta(m_0+w)+i\theta_b}, \\ \frac{Q_b}{X} &= e^{-\beta m_0 + i\theta_b}. \end{aligned} \qquad \text{(XIII.8.6)}$$

In the pure gauge interpretation, base degree counts instanton degree. The base particle's mass includes the electric period w. Dividing by X isolates the background part of its weight. For example, take a common mass unit μ and choose $a_5 = \mu$, $m_0 = 3\mu$, $\beta\mu = 1$, and $\theta_b = 0$. The base particle then has mass 5μ, but only 3μ remains in the exponent once the fiber weight is divided out:

$$X = e^{-2}, \qquad Q_b = e^{-5}, \qquad Q_b/X = e^{-3}. \quad \text{(XIII.8.7)}$$

A complex continuation can include a fiber Wilson angle in the exponent. The mass statements use the real slice.

To relate circumference to the gauge coupling, take an x^5-independent gauge field with only the four-dimensional field strength turned on. In fundamental-trace normalization write $S_d = \frac{1}{2g_d^2} \int d^d x \ \mathrm{tr}_2 \, F_{\mu\nu} F_{\mu\nu}$. Its classical zero mode obeys

$$S_5^{(0)} = \frac{\beta}{2g_5^2} \int d^4 x \ \mathrm{tr}_2 \, F_{\mu\nu} F_{\mu\nu}, \qquad \frac{1}{g_4^2} = \frac{\beta}{g_5^2}. \quad \text{(XIII.8.8)}$$

For a self-dual or anti-self-dual field the kinetic integrand saturates the topological bound. In differential-form notation $\int \mathrm{tr}_2 \, F \wedge *F = \frac{1}{2} \int d^4 x \ \mathrm{tr}_2 \, F_{\mu\nu} F_{\mu\nu}$. The circle action is thus

$$k = \frac{1}{8\pi^2} \int \mathrm{tr}_2 \, F \wedge F, \qquad S_5^{(0)} = \frac{8\pi^2 \beta |k|}{g_5^2}. \quad \text{(XIII.8.9)}$$

This identifies the instanton unit in the classical action. The equality of two classical kinetic terms does not fix the matching of the geometric m_0 to $8\pi^2/g_5^2$ across thresholds, and g_4 in (XIII.8.8) is not the effective abelian coupling measured by the electric period derivative. With the field strength of mass dimension two in this convention, the action gives $[g_d^2] = \text{mass}^{4-d}$. In particular,

$$[g_5^2] = \text{mass}^{-1}, \qquad [g_4^2] = \text{mass}^{0}, \qquad [\beta] = \text{mass}^{-1}. \tag{XIII.8.10}$$

The four-dimensional pure gauge one-loop coefficient is $b_0 = 4$. Consequently the magnitude of the one-loop instanton factor at matching scale μ is proportional to a fourth power of the ratio of the strong scale to μ. Matching near $\mu \sim 1/\beta$ motivates the following small-circle chart. Its finite scale coefficient P, of dimension mass to the fourth power, is fixed by the electric normalization below.

$$\frac{Q_b}{X} = \beta^4 P, \qquad \beta m_0 = -\log(\beta^4 |P|), \qquad \theta_b = \arg P \pmod{2\pi}. \tag{XIII.8.11}$$

For fixed nonzero P and sufficiently small β, this lies in the positive m_0 chamber. At fixed m_0 the magnitude of Q_b/X tends instead to one. Along the tuned path the instanton weight goes to zero as the Euler factors vanish. The base phase in this chart is already included in P.

It helps to express the tuning in units of the retained scale rather than take the logarithm of a dimensionful circumference. Put $\rho = \beta |P|^{1/4}$. Then the magnitude of the geometric background weight and the required background mass obey

$$|Q_b/X| = \rho^4, \qquad \beta m_0 = -4 \log \rho, \qquad \frac{m_0}{|P|^{1/4}} = -\frac{4 \log \rho}{\rho}. \tag{XIII.8.12}$$

For $0 < \rho < 1$ the mass is positive. As the circle shrinks, it grows faster than $1/\beta$ by a logarithm. The instanton sector survives because its exponential suppression compensates the increasing localization coefficient, rather than because this particle stays light. The electric particle behaves differently. Keeping w fixed makes βw small, and hence X approaches one.

For example, with $|P| = \mu^4$ and $\theta_b = 0$, choose $\beta\mu = 1/2$. The tuned ratio is $1/16$, and $m_0 = 8\mu \log 2$. Halve the circumference while retaining P. The ratio must decrease by another factor of sixteen:

$\beta\mu$	$\lvert Q_b/X \rvert$	m_0/μ
$1/2$	$1/16$	$8 \log 2$
$1/4$	$1/256$	$32 \log 2$

(XIII.8.13)

Keeping the first mass instead at the second circumference would give $e^{-2\log 2} = 1/4$. That follows a different path through parameter space. Thus specifying a small radius alone does not specify the four-dimensional instanton limit. The scale and electric separation held fixed are part of the limiting prescription.

We will compute a protected trace with periodic fermions and a supersymmetry-preserving equivariant prescription for two plane rotations. Periodicity selects a supersymmetric spin structure; the rotation twists must also preserve the supercharge

used in the trace. The weights ϵ_1 and ϵ_2 of the two planes have dimension mass, so it is $\beta\epsilon_i$ that enters a finite-circle weight. The trace is taken in the effective electric chamber and with a fixed vacuum and contact-term convention. To read it as a local gauge observable we assume that gravity and unwanted coupled sectors are sufficiently suppressed. For the external circle, $M_{\mathrm{KK}} = 1/R = 2\pi/\beta$ exceeds any fixed probe energy as β shrinks. That scale separation does not establish local isolation from other sectors of a noncompact compactification.

XIII.8.3 One box in the square vertex

Why do only two terms contribute at base degree one, even though the answer retains infinitely many fiber degrees? In the square web, the two opposite edges carrying Q_b have preferred partitions ν_1, ν_2. Gluing assigns base weight $Q_b^{|\nu_1|+|\nu_2|}$. The other internal edges carry X. Their contributions can be summed as strips while keeping the preferred partitions fixed. Figure XIII.8.2 shows the two allowed placements. The external partitions are empty.

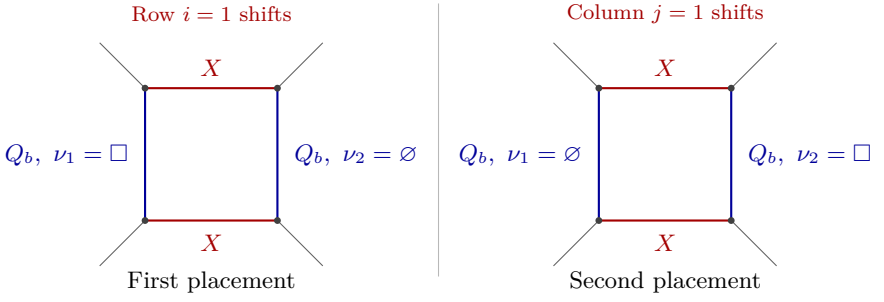


Figure XIII.8.2: The two one-box placements in the local F_0 web. Blue vertical edges carry Q_b and red horizontal edges carry X. The two red edges connect the same preferred partitions in opposite orders. At the top strip a box on ν_1 shifts row $i = 1$; a box on ν_2 shifts column $j = 1$. The bottom strip interchanges the labels and the rotation variables.

Let q, t be the formal rotation variables of the selected vertex product, and use r for their ratio.

$$s = \epsilon_1 + \epsilon_2, \qquad q = e^{-\beta\epsilon_2}, \qquad t = e^{\beta\epsilon_1}, \qquad r = t/q = e^{\beta s}. \tag{XIII.8.14}$$

The opposite signs in q and t are part of this convention; t is a rotation variable, distinct from the flat curve coordinate t_C. We use the final normalized refined vertex product for this local web. The gluing rule is an input. The calculation below evaluates it at two specified pairs of partitions, without deriving the general refined vertex.

At $Q_b = 0$ both preferred partitions are empty. The resulting two strip denominators give the perturbative factor Z_{pert}. With any common constant-map factor omitted, we

have

$$Z_{\mathrm{pert}}(X;q,t)=\prod_{i,j\geq 1}\frac{1}{(1-Xt^{i-1}q^{j})(1-Xq^{i-1}t^{j})}. \tag{XIII.8.15}$$

The positive-base factor is the quotient

$$Z_{\mathrm{inst}}:=\frac{Z_{\mathrm{curve}}}{Z_{\mathrm{pert}}}=1+Q_bC_\beta+O(Q_b^2). \tag{XIII.8.16}$$

If a convention includes a common constant-map factor, the denominator is the whole value of Z_{curve} at $Q_b=0$. The division removes all terms present without base degree; it does not identify the fiber sector as free or Coulomb independent. Expand each $-\log(1-u)$ as $\sum_{n\geq 1}u^n/n$. The two geometric series from the first strip give

$$\sum_{i,j\geq 1}(t^{i-1}q^{j})^n=\left(\sum_{i\geq 1}t^{n(i-1)}\right)\left(\sum_{j\geq 1}q^{nj}\right)=\frac{q^n}{(1-q^n)(1-t^n)}. \tag{XIII.8.17}$$

Add the contribution with q,t interchanged.

$$\log Z_{\mathrm{pert}}=\sum_{n\geq 1}\frac{X^n(q^n+t^n)}{n(1-q^n)(1-t^n)}. \tag{XIII.8.18}$$

For example, the coefficient of X at $q=1/3,t=2/3$ is $9/2$. The $1/n$ and the rotation denominator belong to a connected winding sum. The dependence on X will be needed later to recall how the electric prepotential was normalized. Here we first divide by the vacuum to isolate the base coefficient.

The order of this operation can be seen without manipulating an infinite product. Write the base expansion with coefficient functions of the fiber and rotation variables,

$$Z_{\mathrm{curve}}=Z_0(X;q,t)+Q_bZ_1(X;q,t)+O(Q_b^2). \tag{XIII.8.19}$$

The vacuum is $Z_0=Z_{\mathrm{pert}}$. On the common nonpolar domain,

$$\frac{Z_{\mathrm{curve}}}{Z_0}=1+Q_b\frac{Z_1}{Z_0}+O(Q_b^2),\qquad C_\beta=\frac{Z_1}{Z_0}. \tag{XIII.8.20}$$

Dividing therefore leaves ratios of occupied-strip factors to their empty-strip values. It does not mean setting X to zero. That would remove the fiber dependence that appears in the four-dimensional limit. Nor is subtracting Z_0 from Z_{curve} the same operation. Subtraction leaves the base coefficient Z_1, still multiplied by the entire empty-strip contribution. For a connected quantity the corresponding operation is subtraction of logarithms,

$$\log Z_{\mathrm{inst}}=\log Z_{\mathrm{curve}}-\log Z_0=Q_bC_\beta+O(Q_b^2). \tag{XIII.8.21}$$

This last equality is specific to the linear base term. It explains why the one-box computation already supplies the first connected instanton coefficient, while the fiber vacuum has its own connected winding sum in (XIII.8.18).

For a partition ν, let ν_i be its ith row length and let $\square$ denote a single box. The normalized first strip at cutoff N is

$$R_N(\nu_1,\nu_2;q,t)=\prod_{i,j=1}^{N}\frac{1-Xt^{i-1}q^{j}}{1-Xt^{i-1-(\nu_2)_j}q^{j-(\nu_1)_i}}. \tag{XIII.8.22}$$

The numerator comes from the empty strip. If $\nu_1=\square$ only $i=1$ shifts; if $\nu_2=\square$ only $j=1$ shifts. In each affected line the denominator shifts by one step in the oscillator power, leaving one factor at either end.

$$R_N(\square,\varnothing;q,t)=\prod_{j=1}^{N}\frac{1-Xq^{j}}{1-Xq^{j-1}}=\frac{1-Xq^{N}}{1-X}, \tag{XIII.8.23}$$

$$R_N(\varnothing,\square;q,t)=\prod_{i=1}^{N}\frac{1-Xqt^{i-1}}{1-Xqt^{i-2}}=\frac{1-Xqt^{N-1}}{1-Xq/t}. \tag{XIII.8.24}$$

In $|q|,|t|<1$ the upper boundary factors tend to one. The lower boundaries retain an unshifted fiber factor and a shifted factor, respectively. The second strip is $R_N(\nu_2,\nu_1;t,q)$, so the surviving pair for a box on ν_1 is $(1-X)^{-1}(1-rX)^{-1}$, while a box on ν_2 gives $(1-X)^{-1}(1-X/r)^{-1}$. The rational answers then continue to generic finite-circle weights.

For a box on the first edge, a cutoff of three makes the cancellation particularly visible:

$$\frac{1-Xq}{1-X}\,\frac{1-Xq^{2}}{1-Xq}\,\frac{1-Xq^{3}}{1-Xq^{2}}=\frac{1-Xq^{3}}{1-X}. \tag{XIII.8.25}$$

Only the endpoint factors know that a row was shifted. In the column case the same cancellation begins one step lower in the t power,

$$\frac{1-Xq}{1-Xq/t}\,\frac{1-Xqt}{1-Xq}\,\frac{1-Xqt^{2}}{1-Xqt}=\frac{1-Xqt^{2}}{1-Xq/t}. \tag{XIII.8.26}$$

The lower endpoint is why a shifted root remains in the final answer. Exchanging the two preferred edges in the other strip exchanges which placement carries that root. This is the geometric origin of the two different denominators; it is not an extra multiplicity attached to a single placement. Taking the endpoint limit in a convergent rotation chamber first also avoids interpreting an uncancelled infinite product at the physical real weights, where one rotation variable can exceed one.

There are also one-box hook and framing factors. For each box its arm and leg lengths vanish, so its two hook denominators are $1-q$ and $1-t$. In the selected final product the common one-box power is $\sqrt{qt}$. The squared row norms of the box and its transpose are both one. The relative rotation power is therefore $r^{1/2}$ when the first edge is occupied and $r^{-1/2}$ when the second is occupied. With compatible square roots, the two prefactors are

$$\sqrt{qt}\,r^{1/2}=t,\qquad \sqrt{qt}\,r^{-1/2}=q. \tag{XIII.8.27}$$

With V_i the coefficient from a box on ν_i, this gives

$$V_1 = \frac{t}{(1-q)(1-t)(1-X)(1-rX)}, \tag{XIII.8.28}$$

$$V_2 = \frac{q}{(1-q)(1-t)(1-X)(1-X/r)}. \tag{XIII.8.29}$$

The individual factors appear to have poles at $X = 1$. To see what survives in the sum, put the fractions over a common denominator. The numerator simplifies by

$$t(1-X/r) + q(1-rX) = t + q - X(q+t) = (q+t)(1-X). \tag{XIII.8.30}$$

Thus

$$C_\beta = V_1 + V_2 = \frac{q+t}{(1-q)(1-t)(1-rX)(1-X/r)}. \tag{XIII.8.31}$$

At generic r the pole at $X = 1$ cancels, but the individual terms still require $X \neq 1$. We take X, q, t nonzero and avoid $q, t = 1$ and $rX, X/r = 1$. Complex rotation weights can give exponential-lattice poles as well. This calculation extracts one formal coefficient in Q_b; it needs no convergence assumption on the full base series.

The cancellation at $X = 1$ is useful for understanding the distinction between one fixed point and the sum. Let $K = (1-q)(1-t)$, with q, t held generic and $r \neq 1$. The coefficients of the apparent simple pole are

$$\lim_{X\to 1}(1-X)V_1 = \frac{t}{K(1-r)}, \qquad \lim_{X\to 1}(1-X)V_2 = \frac{q}{K(1-1/r)} = -\frac{t}{K(1-r)}. \tag{XIII.8.32}$$

Each placement is singular, while their sum has the finite rational value

$$C_\beta(1; q, t) = \frac{q+t}{K(1-r)(1-1/r)} \qquad (r \neq 1). \tag{XIII.8.33}$$

This observation does not extend uniformly to $r = 1$. There the two shifted roots also reach $X = 1$, and the double pole in (XIII.8.51) remains. In the physical circle limit both r and X approach one together. We must therefore retain their relative rates, set by s and w, rather than substitute $X = 1$ into the generic finite expression before taking that limit.

A useful sample is inside the chamber of the telescoping products.

$$(q, t, X) = (1/3, 2/3, 1/5), \qquad V_1 = \frac{25}{4}, \qquad V_2 = \frac{25}{12}, \qquad C_\beta = \frac{25}{3}. \tag{XIII.8.34}$$

Both placements matter, and they have different weights. Keeping $q \neq t$ is what will let us detect a rotation factor in the gauge dictionary.

To repeat the calculation with another permitted fiber weight, take

$$(q, t, X) = (1/4, 1/2, 1/6), \qquad r = 2. \tag{XIII.8.35}$$

Now the common plane denominator is $K = 3/8$, while the fiber factors are $1 - X = 5/6$, $1 - rX = 2/3$ and $1 - X/r = 11/12$. Thus

$$V_1 = \frac{1/2}{(3/8)(5/6)(2/3)} = \frac{12}{5}, \tag{XIII.8.36}$$

$$V_2 = \frac{1/4}{(3/8)(5/6)(11/12)} = \frac{48}{55}, \tag{XIII.8.37}$$

$$C_\beta = \frac{36}{11}. \tag{XIII.8.38}$$

The sum is also obtained immediately from the compact expression by using numerator $3/4$ and only the two shifted fiber factors. This sample changes the fiber dependence while retaining the asymmetric rotations. It will let us compare each placement with a different calculation of the gauge fixed points.

XIII.8.4 The two fixed points on the gauge side

Which geometric weight multiplies the one-instanton sum in framed localization? We use the resolved rank-two framed moduli problem and its equivariant fixed-point formula. At instanton charge one, the instanton vector space V is one-dimensional and the framing space W has dimension two. The two fixed points correspond to the choice of occupied framing color. In the trace-free Coulomb slice let

$$a_1 = w/2, \qquad a_2 = -w/2, \qquad d = a_i - a_j \quad (j \neq i), \qquad d = \begin{cases} w & i = 1, \\ -w & i = 2. \end{cases} \tag{XIII.8.39}$$

These a_i are the two framing weights, not the two Seiberg–Witten periods. All tangent weights below are additive before multiplication by β.

To see the tangent representation directly, linearize the Atiyah–Drinfeld–Hitchin–Manin (ADHM) instanton data. The two endomorphisms B_1, B_2 of V carry the plane weights ϵ_1, ϵ_2. The map $I\colon W \to V$ has no extra rotation weight, and the map $J\colon V \to W$ has weight $s = \epsilon_1 + \epsilon_2$ in addition to its color weight. At the fixed point V has weight a_i. A map of a source of weight u to a target of weight v contributes $v - u$. The nonzero component of I is the one from the occupied color. The gauge direction acts on this component; the linearization of $[B_1, B_2] + IJ = 0$ removes the component of J that maps back to that color. The resulting list is in Table XIII.8.1.

Thus the tangent weights are

$$\{\epsilon_1, \epsilon_2, 0, d, s, s - d\} \setminus \{0, s\} = \{\epsilon_1, \epsilon_2, d, s - d\}, \tag{XIII.8.40}$$

where the subtraction is on multisets. The first two directions move the instanton in the two planes. The other two couple its occupied color to the unused one.

The cancellation of directions also has a local coordinate description. Since V has rank one, its complex gauge group rescales I and J in opposite directions. At the fixed point of color i, I_i is nonzero. Use that rescaling to set $I_i = 1$. The complex moment-map equation is

$$[B_1, B_2] + I_i J_i + I_j J_j = 0. \tag{XIII.8.41}$$

Direction	Linear space	Additive weights
B_1, B_2	$\mathrm{End}(V)$ for each plane	ϵ_1, ϵ_2
I	$\mathrm{Hom}(W, V)$	$0, d$
J	$\mathrm{Hom}(V, W)$ with twist	$s, s-d$
Gauge	subtract one direction	0
Moment map	subtract one equation	s

Table XIII.8.1: The linearized framed instanton complex at the one-box fixed point of color i. Here $d = a_i - a_j$ with $j \neq i$ and $s = \epsilon_1 + \epsilon_2$.

For rank-one endomorphisms the commutator vanishes. At the fixed point $I_j = J_i = J_j = 0$, and its linearization is simply $\delta J_i = 0$. The quotient has removed δI_i and the constraint has removed δJ_i. The remaining local coordinates are

$$(\delta B_1, \delta B_2, \delta I_j, \delta J_j), \qquad \mathrm{wt} = (\epsilon_1, \epsilon_2, a_i - a_j, s + a_j - a_i). \tag{XIII.8.42}$$

This gives four complex tangent directions without counting a gauge orbit as a modulus. In particular, assigning both cross directions weight d would miss the rotation carried by J. Their sum is s, as required because IJ transforms with the same plane weight as the moment-map equation. This local calculation establishes the weights used in the sourced fixed-point formula; the localization prescription itself remains an input.

The arm and leg formula for the framed tangent space gives a separate route. For a box at position $(1, 1)$, the arm is its row length minus 1 and the leg in a second diagram is that diagram's first column length minus 1. The self arm and leg are zero, so the self pair is (ϵ_1, ϵ_2). Using the empty diagram's leg -1 gives the two cross weights d and $s - d$, in agreement with (XIII.8.40).

The inverse Euler factor for an additive weight z on the circle is $(1 - e^{\beta z})^{-1}$ in this multiplicative convention. Since $e^{\beta w} = X^{-1}$ and $e^{\beta s} = r$, the two cross weights exponentiate as

occupied color	$e^{\beta d}$	$e^{\beta(s-d)}$
1	X^{-1}	rX
2	X	r/X

(XIII.8.43)

The self directions contribute $e^{\beta\epsilon_1} = t$ and $e^{\beta\epsilon_2} = q^{-1}$. The two complete contributions are

$$A_+ = \frac{1}{(1-q^{-1})(1-t)(1-X^{-1})(1-rX)}, \qquad i = 1, \tag{XIII.8.44}$$

$$A_- = \frac{1}{(1-q^{-1})(1-t)(1-X)(1-r/X)}, \qquad i = 2. \tag{XIII.8.45}$$

In the source formula the native Coulomb variable $Q_{12} = e^{\beta(a_1 - a_2)}$ equals X^{-1} here. The sum is invariant under inversion of that variable. If the printed pair is evaluated at $Q = X$, its first term is A_- and its second is A_+. Exchanging the order preserves the sum but matters when matching a specific placement to its color.

To compare with the vertex, use the three inverse-factor identities

$$1-q^{-1}=-\frac{1-q}{q},\qquad 1-X^{-1}=-\frac{1-X}{X},\qquad 1-r/X=-\frac{r}{X}(1-X/r). \tag{XIII.8.46}$$

Two negative signs cancel in each term. Substitution gives

$$\frac{r}{X}A_+=\frac{rq}{(1-q)(1-t)(1-X)(1-rX)}=V_1, \tag{XIII.8.47}$$

$$\frac{r}{X}A_-=\frac{q}{(1-q)(1-t)(1-X)(1-X/r)}=V_2. \tag{XIII.8.48}$$

If I_{AK} denotes the instanton fugacity multiplying $A_+ + A_-$ in the framed convention, equality of the two one-instanton contributions requires

$$I_{\mathrm{AK}}=r\frac{Q_b}{X},\qquad I_{\mathrm{AK}}(A_+ + A_-)=Q_bC_\beta. \tag{XIII.8.49}$$

On the sample in (XIII.8.34) the raw sum is $5/6$. Multiplication by $1/X$ alone gives $25/6$, half the vertex answer. The rotation factor $r=2$ supplies the missing factor. The comparison thus tests both the background ratio from (XIII.8.6) and the equivariant framing convention. It concerns the two protected observables in their specified vacuum and contact-term conventions.

For the changed input in (XIII.8.35), the raw fractions are $A_+=1/5$ and $A_-=4/55$. Their sum is $3/11$. The conversion factor is $r/X=12$, which produces $36/11$ and agrees with (XIII.8.38). Including the background factor $1/X=6$ but omitting r would give $18/11$. On the unrefined slice these two prescriptions coincide. A comparison at two independent rotation weights is therefore needed to determine this finite-circle normalization. The individual-color matching is stronger than an unlabelled numerical sum because it also tracks which end of the web carries the occupied partition.

Under the Weyl reflection $w\to -w$, the two color contributions exchange. The geometric combination XC_β is also invariant. Indeed,

$$(1-r/X)(1-1/(rX))=X^{-2}(1-X/r)(1-rX),\qquad X^{-1}C_\beta(X^{-1})=XC_\beta(X). \tag{XIII.8.50}$$

We keep Q_b/X fixed in this test, so that Q_bC_β is invariant as a rational expression. At fixed Q_b the geometric coefficient need not be invariant. This is an algebraic reflection test, not a continuation of positive masses through the wall $w=0$.

On the unrefined slice $\epsilon_1=h,\epsilon_2=-h$, one has $q=t=e^{\beta h}$ and $r=1$. Here there is an independent ordinary vertex calculation. For one box the quantum hook gives a squared factor $W_\square^2=(q^{1/2}-q^{-1/2})^{-2}$. The content polynomial is the sum of q^{j-i} over boxes (i,j), hence 1 for $\square$ and 0 for the empty diagram. In the ordinary gluing formula the fiber exponent before squaring the strip is $f_{\nu_1}+f_{\nu_2}+(q-2+q^{-1})f_{\nu_1}f_{\nu_2}$, where f_ν is this content polynomial. At degree one the product of the two content polynomials vanishes. Each pair therefore gives

$$W_\square^2(1-X)^{-2}=\frac{q}{(1-q)^2(1-X)^2},\qquad C_\beta\big|_{q=t}=\frac{2q}{(1-q)^2(1-X)^2}. \tag{XIII.8.51}$$

The factor of two comes from the two possible boxes. This agrees with (XIII.8.31) on the slice where the two shifted roots merge. The ordinary calculation cannot by itself detect a factor of r that is one on that slice.

XIII.8.5 From four finite factors to the SW term

How can a vanishing base weight leave a finite instanton term? Use the matched weak electric chart of Chapter XI.7. Write T_f for the flat logarithmic fiber coordinate, so $X = e^{-T_f}$. In common mass units the IIA length parameter is $\varepsilon = \beta = 2\pi g_s \ell_s$. The IIA chart has $Q_b/X = \beta^4 P$ and $T_f = \beta w + O(\beta^3)$. Expanding the exponential gives

$$1 - X = 1 - e^{-T_f} = T_f + O(T_f^2) = \beta w + O(\beta^2).$$

Denote the weak electric period by a_{SW} and let $L = \Lambda_{\mathrm{SW}}^2$. The matching already fixes

$$w = \sqrt{2}\, a_{\mathrm{SW}}, \qquad a_5 = \frac{w}{2} = \frac{a_{\mathrm{SW}}}{\sqrt{2}}, \qquad P = \frac{L^2}{4}. \tag{XIII.8.52}$$

We use the weak patch $|P/w^4| \ll 1$, away from a vanishing electric period. The scale is complex and already carries the phase. Table XIII.8.2 collects the parameters that will remain fixed or be tuned.

Parameter	Mass power	Role in the limit
$\beta = 2\pi R$	-1	Physical circumference, taken to zero
$w = 2a_5 = \sqrt{2}\, a_{\mathrm{SW}}$	1	Fixed electric separation
ϵ_1, ϵ_2	1	Fixed plane weights in the circle limit
h	1	Weight on the unrefined slice
$P = L^2/4$	4	Fixed complex instanton scale
$g_5^2,\ g_4^2$	$-1,\ 0$	Classical zero mode with $g_4^2 = g_5^2/\beta$

Table XIII.8.2: Parameters in the small-circle comparison. Mass dimensions refer to the physical parameters before their conversion to fugacities.

For the M-theory calculation take the exact representative

$$X = e^{-\beta w}, \qquad Q_b = \beta^4 P X. \tag{XIII.8.53}$$

This has the same leading fiber asymptotics as the IIA chart. The finite-circle corrections below use the exact M-theory choice in (XIII.8.53). At fixed weights the denominator factors have leading terms

$$1 - q = \beta\epsilon_2 + O(\beta^2), \qquad 1 - t = -\beta\epsilon_1 + O(\beta^2), \tag{XIII.8.54}$$

$$1 - rX = \beta(w - s) + O(\beta^2), \qquad 1 - X/r = \beta(w + s) + O(\beta^2). \tag{XIII.8.55}$$

We require $\epsilon_1\epsilon_2(w - s)(w + s) \neq 0$ for this limit. The numerator $q + t$ tends to two. The denominator contributes four inverse powers of the circumference; each corresponds to one tangent direction. With $X \to 1$, (XIII.8.53) gives

$$\lim_{\beta \to 0} Q_b C_\beta = -\frac{2P}{\epsilon_1\epsilon_2(w^2 - s^2)}. \tag{XIII.8.56}$$

A base weight tending to a nonzero constant, as on the fixed-m_0 path, would leave the pole in β. Figure XIII.8.3 summarizes the balance. The limit is taken at one base

degree and with its full fiber dependence. For example, at $q = t$ a finite polynomial in X cannot reproduce the double pole $(1 - X)^{-2}$ that supplies two of the inverse powers as $X \to 1$.

We can measure precisely what a finite fiber cutoff loses. On the unrefined slice define the partial sum $S_N(X) = \sum_{m=0}^{N}(m + 1)X^m$. Multiplying a finite geometric sum by X and differentiating gives

$$\sum_{m=0}^{N} X^{m+1} = \frac{X(1 - X^{N+1})}{1 - X}, \tag{XIII.8.57}$$

$$S_N(X) = \frac{1 - (N + 2)X^{N+1} + (N + 1)X^{N+2}}{(1 - X)^2}. \tag{XIII.8.58}$$

For fixed N, the numerator cancels the apparent denominator at $X = 1$. In fact $S_N(1) = (N + 1)(N + 2)/2$. Consequently, along $X = e^{-\beta w}$ and $Q_b = \beta^4 PX$,

$$\frac{2Q_b}{\beta^2 h^2} S_N(X) = O(\beta^2) \quad \text{at fixed } N, \tag{XIII.8.59}$$

whereas replacing S_N by the full sum $(1 - X)^{-2}$ gives the finite value $2P/(h^2 w^2)$. The coefficientwise limit in base degree is thus not a termwise limit in fiber degree.

The same formula identifies the fiber degrees needed for the limit. Put $u = \beta w > 0$ and let N grow so that $(N + 1)u \to c > 0$. The fraction of the full fiber sum retained then approaches

$$\frac{S_N(e^{-u})}{(1 - e^{-u})^{-2}} \longrightarrow 1 - (1 + c)e^{-c}. \tag{XIII.8.60}$$

To derive it, set $N+1 \simeq c/u$ in the numerator of (XIII.8.58); the two terms proportional to c/u cancel to leave $-(1 + c)e^{-c}$. A cutoff with $c = 1$ retains only $1 - 2/e$ of the limiting coefficient. Recovering the whole answer requires degrees extending beyond this scale. This is an algebraic property of the one-base-degree generating function. It explains why summing the fiber series before shrinking the circle is part of the calculation, even though no sum over higher base degrees is needed.

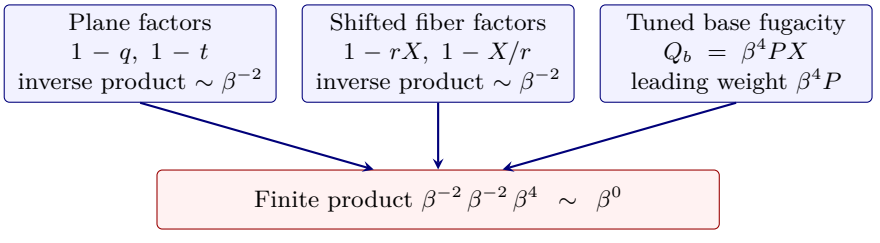


Figure XIII.8.3: Power counting at fixed generic physical weights. The two rotation factors and the two shifted fiber factors supply four inverse powers of β. Tuning the background ratio as $\beta^4 P$ retains their product. With fixed m_0 the base fugacity instead stays of order one and this coefficient diverges.

One can arrive at the same four-dimensional expression by starting from the additive Euler class. For each color the cohomological contribution is the inverse product of the four weights in (XIII.8.40). Summing gives

$$\frac{1}{\epsilon_1\epsilon_2 w(s-w)}+\frac{1}{\epsilon_1\epsilon_2(-w)(s+w)}=\frac{1}{\epsilon_1\epsilon_2 w}\frac{2w}{(s-w)(s+w)}$$
$$=-\frac{2}{\epsilon_1\epsilon_2(w^2-s^2)}. \qquad \text{(XIII.8.61)}$$

In the circle expression the four multiplicative Euler factors approach $-\beta$ times their four additive weights, so the overall sign from these replacements is even. This check also keeps the shift s, which the unrefined value would conceal.

The finite-circle expression contains more information than its limit. Apply $1-e^{-u}=2e^{-u/2}\sinh(u/2)$ to the four factors in (XIII.8.31). The exponentials in their product cancel the numerator's common exponential together with the factor X in Q_b. The result is

$$Q_bC_\beta=\frac{-\beta^4P\cosh(\beta s/2)}{8\sinh(\beta\epsilon_1/2)\sinh(\beta\epsilon_2/2)\sinh(\beta(w-s)/2)\sinh(\beta(w+s)/2)}. \qquad \text{(XIII.8.62)}$$

Each normalized factor $\sinh(\beta z/2)/(\beta z/2)$ starts at $1+\beta^2z^2/24$. The corresponding coefficient from the numerator is $s^2/8$. The relative correction is therefore

$$\frac{s^2}{8}-\frac{\epsilon_1^2+\epsilon_2^2+(w-s)^2+(w+s)^2}{24}=\frac{\epsilon_1\epsilon_2-w^2}{12}. \qquad \text{(XIII.8.63)}$$

This gives the finite expression to second order in the circumference,

$$Q_bC_\beta=\frac{-2P}{\epsilon_1\epsilon_2(w^2-s^2)}\left(1+\frac{\beta^2}{12}(\epsilon_1\epsilon_2-w^2)+O(\beta^4)\right). \qquad \text{(XIII.8.64)}$$

For $(\epsilon_1,\epsilon_2,w)=(1,2,5)$ in a common mass unit, the leading term is $-P/16$ in those units and the relative β^2 coefficient is $-23/12$. The shift $s=3$ reduces the factor w^2-s^2 from the unshifted value 25 to 16. If we instead set $Q_b=\beta^4P$, the whole finite result is multiplied by $X^{-1}=e^{\beta w}$. This leaves the limiting term but adds a linear relative correction βw. Agreement in the limit cannot distinguish the two paths at finite radius.

A second generic choice makes the role of the shifted roots explicit. Take $(\epsilon_1,\epsilon_2,w)=(1,3,6)\mu$ in a common mass unit. The additive weights for the two colors are respectively $(1,3,6,-2)\mu$ and $(1,3,-6,10)\mu$. Their inverse products sum to

$$-\frac{1}{36\mu^4}-\frac{1}{180\mu^4}=-\frac{1}{30\mu^4},\qquad Q_bC_\beta=-\frac{P}{30\mu^4}\left(1-\frac{11}{4}(\beta\mu)^2+O((\beta\mu)^4)\right). \qquad \text{(XIII.8.65)}$$

Here $s=4\mu$, so the root product is $w^2-s^2=20\mu^2$. Dropping that shift would give a different leading coefficient. The sign of the two inverse products is allowed because this is an equivariant index, not a probability. Under a common mass rescaling by κ, the additive coefficient scales as κ^{-4} and the relative quadratic correction as κ^2.

Rescaling P by κ^4 and β by κ^{-1} keeps the finite expression dimensionless. This checks the relation between its Euler factors and the dimension-four strong-scale coefficient.

Now set $\epsilon_1 = h$, $\epsilon_2 = -h$. At finite β the unrefined expression (XIII.8.51) has the expansion

$$\begin{aligned} Q_b C_\beta &= \frac{Q_b}{(1-X)^2}\,\frac{1}{2\sinh^2(\beta h/2)} \\ &= \frac{Q_b}{(1-X)^2}\left(\frac{2}{\beta^2 h^2} - \frac{1}{6} + O(\beta^2 h^2)\right). \end{aligned} \tag{XIII.8.66}$$

Here h is the Laurent variable; β and X are held fixed for the extraction. Since $1 - X \sim \beta w$ on the chart, the two coefficients behave as

$$[h^{-2}]\, Q_b C_\beta \longrightarrow \frac{2P}{w^2}, \qquad [h^0]\, Q_b C_\beta = -\frac{Q_b}{6(1-X)^2} = O(\beta^2). \tag{XIII.8.67}$$

Thus the constant term disappears in four dimensions at this base degree. It was already present in the expansion of the finite-circle winding kernel, so its appearance there does not establish a new primitive genus-one contribution. The same leading extraction can be made from (XIII.8.56). Multiply by $\epsilon_1\epsilon_2$ and send both weights to zero at fixed nonzero ratio and fixed $w \neq 0$. This gives $-2P/w^2$, the sign appropriate before converting from the product of the two weights to the unrefined h^2.

There are two operations in this extraction. First one takes a Laurent coefficient in the rotation weight, with the physical circumference and fiber fugacity fixed. Then one sends the circumference to zero on the tuned path. For the pole coefficient the finite expression is

$$[h^{-2}]\, Q_b C_\beta = \frac{2\beta^2 PX}{(1-X)^2} = \frac{P}{2w^2}\,\frac{(\beta w)^2}{\sinh^2(\beta w/2)}. \tag{XIII.8.68}$$

The last ratio tends to four, yielding $2P/w^2$. For the constant coefficient there is an additional factor of β^2:

$$[h^0]\, Q_b C_\beta = -\frac{\beta^4 PX}{6(1-X)^2} = -\frac{\beta^2 P}{24w^2}\,\frac{(\beta w)^2}{\sinh^2(\beta w/2)}. \tag{XIII.8.69}$$

These expressions exhibit why the two terms have different limits. They also agree with taking the circle limit at fixed nonzero h first in this one-base-degree rational function, which gives $2P/(h^2 w^2)$. The agreement uses the stated path and nonzero w; it supplies no rule for interchanging arbitrary infinite base sums or approaching a vanishing electric period.

To compare to the rigid Seiberg–Witten prepotential $\mathcal{F}_{\mathrm{SW}}$, recall how its normalization was fixed. The phase convention $q = e^{i\lambda}$ turns the unrefined fiber winding term in (XIII.8.18) into a negative sine kernel. Its genus-zero term is $-2\,\mathrm{Li}_3(X)$, where $\mathrm{Li}_3(X) = \sum_{n\geq 1} X^n/n^3$. In the electric chart its rescaled curvature is

$$\beta^{-2}\partial^2_{a_{\mathrm{SW}}}\big[-2\,\mathrm{Li}_3(e^{-\beta\sqrt{2}a_{\mathrm{SW}}})\big] = 4\log(1-X). \tag{XIII.8.70}$$

Its slope in $\log a_{\mathrm{SW}}$ tends to 4, while the weak-period slope of $\partial^2_{a_{\mathrm{SW}}}\mathcal{F}_{\mathrm{SW}}$ is $2i/\pi$. This comparison fixes the multiplier $i/(2\pi)$ for the sine genus-zero coefficient. The continued

h^{-2} coefficient has the opposite sign. At degree one the instanton factor has unit constant term, so taking the logarithm retains precisely the linear term. Applying the previously fixed multiplier to the continued four-dimensional term gives

$$\mathcal{F}_{\mathrm{SW}}^{(1)} = -\frac{i}{2\pi}\,[h^{-2}]\log Z_{\mathrm{inst}}^{(4d)}\big|_{\text{one instanton}} = -\frac{i}{2\pi}\frac{2P}{w^2} = -\frac{iL^2}{8\pi a_{\mathrm{SW}}^2}. \tag{XIII.8.71}$$

In the period convention of Chapter XI.7 this reads

$$\frac{\pi}{i}\mathcal{F}_{\mathrm{SW}}^{(1)} = -\frac{L^2}{8a_{\mathrm{SW}}^2}. \tag{XIII.8.72}$$

This is the independent period result of Chapter XI.7 in the same weak electric frame. Neither the factor in (XIII.8.52) nor the multiplier was fitted to the positive-base coefficient. The agreement uses the common mass normalization, weak scale and isolated protected sector. It compares one instanton order and does not identify the full finite-radius theories.

XIII.8.6 What the index remembers

What can we read about spin from the dependence on X and the rotation weights? Expand the coefficient (XIII.8.31) at fixed base degree in powers of X. A power X^m labels the curve class $B + mF$. Factor out the common plane oscillator factor $\sqrt{qt}/[(1-q)(1-t)]$ and set $y = \sqrt{r}$. Use compatible formal square roots so that $(q+t)/\sqrt{qt} = y + y^{-1}$. The two shifted fiber factors expand as

$$\frac{1}{(1-y^2X)(1-y^{-2}X)} = \sum_{m\geq 0} X^m \sum_{j=0}^{m} y^{2m-4j}. \tag{XIII.8.73}$$

Indeed, j powers from the second geometric series leave $m-j$ from the first, giving the exponent $2(m-j)-2j$. Multiplication by the remaining numerator alternates the two sequences of exponents.

$$(y+y^{-1})\sum_{j=0}^{m} y^{2m-4j} = \sum_{k=0}^{2m+1} y^{2m+1-2k}. \tag{XIII.8.74}$$

This is the character of a spin-$(m+1/2)$ representation when y weights twice the right Cartan eigenvalue. The identity concerns the coefficient after removing the common oscillator factor. Reading it as a protected spin character uses the wrapped-particle trace, with the same chamber and equivariant prescription as before.

At $m = 2$ the normalized coefficient is

$$y^5 + y^3 + y + y^{-1} + y^{-3} + y^{-5}. \tag{XIII.8.75}$$

At $y = 1$ this has value six. To compare with the ordinary sine convention, continue $q = t = e^{i\lambda}$ with $\lambda = -i\beta h$. Then

$$\frac{q}{(1-q)^2} = \frac{1}{(q^{1/2}-q^{-1/2})^2} = -\frac{1}{(2\sin(\lambda/2))^2}, \qquad \frac{1}{(1-X)^2} = \sum_{m\geq 0}(m+1)X^m. \tag{XIII.8.76}$$

The coefficient of the sine kernel for $B + mF$ is therefore $-2(m+1)$, and for $m = 2$ it is -6. This is the same sign that converts the continued Laurent extraction to the sine normalization in (XIII.8.71).

There is a geometric check of this signed value in the local genus-zero curve calculation. The class $B+mF$ has a linear system of bidegree $(1, m)$, up to the order of the two factors. Its defining polynomials are linear in the first pair of homogeneous coordinates and degree m in the second. They have $2(m+1)$ coefficients up to a common scalar. The linear system and its signed Euler value are

$$|B + mF| = \mathbb{P}^{2m+1}, \qquad (-1)^{2m+1}\chi(\mathbb{P}^{2m+1}) = -(2m+2). \tag{XIII.8.77}$$

The last equality uses one cell in each even real dimension from 0 to $4m+2$. The sign is that of the sourced genus-zero local curve interpretation for this system. The algebraic equality and the linear system both reproduce -6 at $m = 2$.

The character formula also teaches transfer between successive fiber degrees. Before multiplication by $y+y^{-1}$, the exponents in (XIII.8.73) are separated by four. Multiplying by y produces $2m+1, 2m-3, \ldots, -2m+1$, while multiplying by y^{-1} produces $2m-1, 2m-5, \ldots, -2m-1$. Interlacing them gives every exponent separated by two, with unit multiplicity. At $m = 1$ and $m = 3$ this yields

$$m = 1: \quad (y + y^{-1})(y^2 + y^{-2}) = y^3 + y + y^{-1} + y^{-3}, \tag{XIII.8.78}$$

$$\begin{aligned} m = 3: \quad & (y + y^{-1})(y^6 + y^2 + y^{-2} + y^{-6}) \\ & = y^7 + y^5 + y^3 + y + y^{-1} + y^{-3} + y^{-5} + y^{-7}. \end{aligned} \tag{XIII.8.79}$$

The dimensions are four and eight, while the signed sine coefficients are -4 and -8. Setting $y = 1$ in the numerator alone would instead give two; the growing multiplicity comes from the fiber denominator. Thus the sum over fiber powers changes protected information at each charge, even though the base degree stays fixed.

The linear-system count explains the same growth directly. With homogeneous coordinates (u_0, u_1) and (v_0, v_1) for the two rulings, a bidegree-$(1, m)$ equation is

$$u_0 \sum_{j=0}^{m} c_j v_0^{m-j} v_1^j + u_1 \sum_{j=0}^{m} d_j v_0^{m-j} v_1^j = 0. \tag{XIII.8.80}$$

There are $m+1$ coefficients of each kind. An overall nonzero rescaling does not change the curve, leaving a projective parameter space of complex dimension $2m+1$. For example, at $m = 1$ the four coefficients produce $\mathbb{P}^3$, with Euler value four and the signed value -4. This compares the complete linear system with the selected protected curve expression. It does not equate the set of its smooth members with an unsigned list of particle states.

Why does a character or a signed Euler value not give an unsigned inventory of particles? In the unrefined trace, after removing the universal short-multiplet factor and at fixed left spin, a right spin j_R contributes the signed dimension $(-1)^{2j_R}(2j_R+1)$. This agrees with the value in (XIII.8.77) for $j_R = m + 1/2$. More generally different inventories can give the same unrefined trace. For two singlets and a doublet the arithmetic is

$$\underbrace{1+1+2}_{\text{reduced dimension}} = 4, \qquad \underbrace{1+1-2}_{\text{unrefined trace}} = 0. \tag{XIII.8.81}$$

This is a test with abstract representations, not a claim that those four states occur in local F_0. It explains why a vanishing index does not force a vanishing sector. The character identity (XIII.8.74) also does not by itself establish the existence or uniqueness of a physical multiplet realizing it.

Finally, which winding terms can enter this index at one base degree? In the connected winding expansion a class with bidegree (b, m) contributes a monomial $(Q_b^b X^m)^n$ at winding n, times the rotation kernel and $1/n$. The bidegree becomes (nb, nm). For positive b and positive integer n,

$$nb = 1 \quad \Longrightarrow \quad (n, b) = (1, 1), \qquad \log Z_{\text{inst}} = Q_b C_\beta + O(Q_b^2). \tag{XIII.8.82}$$

The logarithm leaves the first coefficient unchanged because Z_{inst} has unit constant term. A twice-wound fiber has $b = 0$ and can occur in the vacuum: it is the $n = 2$ term of (XIII.8.18). The winding integer counts repeats of a Euclidean loop. It is distinct from both the number of primitive states and the transverse-circle momentum in Figure XIII.8.1.

The circle in this chapter is sent to zero while a local weak electric scale is retained. Chapter XIII.9 asks when a tower of modes in a five-dimensional construction reveals a six-dimensional origin. One protected coefficient on the shrinking external circle does not answer that question.

XIII.8.7 Exercises

1. Keep a box on the first preferred edge ν_1 of Figure XIII.8.2. Compute its normalized coefficient after dividing by the pure-fiber vacuum. Then compute the factor multiplying Q_b in I_{AK} for the raw framed sum. Submit `box` and `fugacity_ratio` using `q`, `t`, `x`, where $x = X$. Work away from the individual fixed-point poles.

2. Sum the two vertex terms. With physical weights fixed and generic, take $Q_b/X = \beta^p P$ and find the power that gives a finite nonzero limit. Give the limit including P. Submit the integer `power`, the expression `coefficient` in `e1`, `e2`, `w`, `P`, and the list `dimensions` of mass powers of β, ϵ_1, P, g_5^2, g_4^2, in that order. Assume $\epsilon_1\epsilon_2(w^2 - s^2) \neq 0$ and $P \neq 0$.

3. On the unrefined slice, first extract the h^{-2} and h^0 coefficients at fixed finite β, including the factor Q_b. Submit these as `pole_finite` and `constant_finite` using `qb`, `x`, `beta`. Give their limiting values as `pole_4d` and `constant_4d` using `P`, `w`. Finally give (π/i) times the one-instanton prepotential as `sw_rescaled` using `L`, `a`, where $a = a_{\text{SW}}$. Use nonzero w, β and $X \neq 1$ at finite circumference.

4. With the universal short factor removed, take four right singlets, two right doublets and one right triplet, all at the same charge and left spin. Compute the unsigned dimension and the signed trace. Submit the integers `ordinary` and `index`.

5. Explain why two windings of a particle from a positive-base class cannot enter at degree one, while a twice-wound fiber can contribute to the vacuum. Distinguish

this winding label from transverse-circle momentum in the membrane picture. Explain whether a negative or vanishing trace determines the number of states. This is a written exercise.

Use `benchmark/tasks.json` to find the question IDs and `benchmark/PROTOCOL.md` for submission. For Exercises 1–4, use exactly the specified keys, integer values where requested and exact rational expression strings for symbolic answers. Use explicit `*` and `**`, only the stated variables and integer literals, and powers with literal integer exponents of magnitude at most eight. Short equivalent expressions are accepted on the common nonpolar domain. The fifth exercise is assessed by a reader.

For further written practice, choose a nonpolar asymmetric triple (q, t, X) distinct from both examples. Compute the two strip fractions, the two framed fractions and their termwise conversion. Explain which normalization error an unrefined test would miss. Next use (XIII.8.58) to estimate the fiber cutoff needed to retain a prescribed fraction of the circle-limit coefficient. State which variables are held fixed and why a fixed finite cutoff fails. These transfer questions are assessed from the derivation and are separate from the four JSON submissions.

Status and sources

§8.2. Periods and circle dictionary. The signed restriction and periods ([MATH]) use the Chapter XIII.2 frame. The effective electric chamber and the base particle assignment use Aharony et al. (1998, arXiv v3, §II.A and D, Eqs. (14)–(15), (24)–(25)). The classical membrane action ([SUGRA]) assumes the product metric with a calibrated curve; see Gopakumar and Vafa (1998, arXiv v1, Eqs. (3.1)–(3.3)). The two reductions ([GEO-E]) use the ordinary M/IIA lift and the common D2/M2 mass units; see Townsend (1995, arXiv v1, PDF pp. 2, 7). The action matching ([MATH]) is a classical calculation; compare the product-circle setup in Nekrasov (1998, arXiv v3, §2.1). Local isolation ([DEC]) and a supersymmetry-preserving equivariant prescription remain premises. The latter is needed in addition to the periodic spin structure.

§8.3. Vertex coefficient. The ordinary topological vertex input ([WS-T]) is Aganagic et al. (2005, arXiv v3, Eqs. (3.14)–(3.15)). For the separate refined input to the partition-function comparisons use Iqbal, Kozçaz, et al. (2009, arXiv v2, §5.5, normalized product after Eq. (81), Eq. (90) at $m = 0$). The one-box factors in those two final products agree. Their source-native rotation convention is $q = e^{i\epsilon_1^{\mathrm{IKV}}}$, $t = e^{-i\epsilon_2^{\mathrm{IKV}}}$ (§7.6). In (XIII.8.14) these variables are $\epsilon_1^{\mathrm{IKV}} = i\beta\epsilon_2$ and $\epsilon_2^{\mathrm{IKV}} = i\beta\epsilon_1$ up to their exponential periods. The literal framing line in Eq. (80) would give $\sqrt{qt}$ for both one-box terms if inserted before normalization in place of the selected framing. It does not give the t, q factors used here. The calculation selects the two stated final products; it assumes neither a general refinement theorem nor an alternative formula for their gauge fugacity. The empty-strip series, telescopes, and rational sum are ([MATH]).

§8.4. Framed index and ordinary slice. The resolved framed tangent calculation ([MATH]) uses Awata and Kanno (2005, arXiv v3, Eqs. (2.6)–(2.12)), and the linearized complex checks the weights independently. The native $Q_{12} = X^{-1}$ and the printed pair at $Q = X$ exchange the two terms. The finite protected match ([BPS:1/2|idx]) is one coefficient as a meromorphic function of q, t, X, at the fugacity conversion in (XIII.8.49) and with the stated chamber, vacuum and contact terms. No global line lattice or absolute m_0 normalization follows. The

ordinary hook and content check ([MATH]) uses Iqbal and Kashani-Poor (2003, arXiv v4, Eqs. (27), (35)–(39), (47)–(50)).

§8.5. Circle limit and period comparison. The common weak-scale chart ([GEO-E]) uses the complexified Kähler period and the weak period data of XI.6–7 and Iqbal and Kashani-Poor (2003, arXiv v4, Eqs. (1), (66)–(69)). The comparison fixes leading coordinates in common mass units; the absolute microscopic threshold constant is not inferred. ([MATH]) are the four-weight limit, the exact-representative correction and the two unrefined Laurent coefficients. The conversion to $\mathcal{F}_{\mathrm{SW}}$ ([BPS:1/2|holo]) uses the independently fixed slope and signed period coefficient of Chapter XI.7. It holds at first instanton order with the same weak electric periods, scale and local-sector assumptions.

§8.6. Winding and protected information. The interpretation ([BPS:1/2|idx]) uses the wrapped short-particle trace of Gopakumar and Vafa (1998, arXiv v1, Eqs. (3.1)–(3.3)), with the effective chamber, periodic equivariance and vacuum choice as specified above. The signed ordinary check is the remaining part of ([MATH]) in Iqbal and Kashani-Poor (2003, arXiv v4, Eqs. (47)–(50)); the protected interpretation of the spin pattern is sourced in Awata and Kanno (2005, arXiv v3, Eqs. (2.14)–(2.17)). The degree and cancellation identities ([MATH]) and formal character identity ([MATH]) do not reconstruct a spectrum.

Expanded calculations. The dimensionless tuning and changed-radius example are consequences of the common weak-scale chart. The vacuum quotient, endpoint examples, pole cancellation and asymmetric transfer sample develop the refined coefficient calculations. The local ADHM coordinates give a local chart within the same resolved framed complex. The exact fiber-cutoff remainder and joint-cutoff fraction are algebraic consequences of the stated degree and period formulas, at fixed positive real w for the cutoff limit. The second physical-weight example, homogeneity check and exact Laurent coefficients follow from the protected comparison on the specified representative. The interlaced characters and bidegree polynomials follow from the degree and cancellation identities. These calculations are [MATH]; their physical interpretations retain the premises and bounds stated above.

References

Aganagic, M. et al. (2005). "The Topological Vertex". In: *Commun. Math. Phys.* 254, pp. 425–478. DOI: 10.1007/s00220-004-1162-z. arXiv: hep-th/0305132.

Aharony, O., A. Hanany, and B. Kol (1998). "Webs of (p,q) five-branes, five-dimensional field theories and grid diagrams". In: *JHEP* 01, p. 002. DOI: 10.1088/1126-6708/1998/01/002. arXiv: hep-th/9710116.

Awata, H. and H. Kanno (2005). "Instanton Counting, Macdonald Function and the Moduli Space of D-Branes". In: *JHEP* 05, p. 039. DOI: 10.1088/1126-6708/2005/05/039. arXiv: hep-th/0502061.

Gopakumar, R. and C. Vafa (1998). *M-Theory and Topological Strings–II*. DOI: 10.48550/arXiv.hep-th/9812127. arXiv: hep-th/9812127.

Iqbal, A. and A.-K. Kashani-Poor (2003). "Instanton Counting and Chern–Simons Theory". In: *Adv. Theor. Math. Phys.* 7. DOI: 10.4310/ATMP.2003.v7.n3.a4. arXiv: hep-th/0212279.

Iqbal, A., C. Kozçaz, and C. Vafa (2009). "The Refined Topological Vertex". In: *JHEP* 10, p. 069. DOI: 10.1088/1126-6708/2009/10/069. arXiv: hep-th/0701156.

Nekrasov, N. (1998). “Five-Dimensional Gauge Theories and Relativistic Integrable Systems”. In: *Nucl. Phys. B* 531, pp. 323–344. DOI: 10.1016/S0550-3213(98)00436-2. arXiv: hep-th/9609219.

Townsend, P. K. (1995). “The eleven-dimensional supermembrane revisited”. In: *Phys. Lett. B* 350, pp. 184–187. DOI: 10.1016/0370-2693(95)00397-4. arXiv: hep-th/9501068.

Chapter XIII.9

Five-dimensional fixed points and six-dimensional KK origins

XIII.9.1 A circle introduces a scale

A five-dimensional description can hide a length. Compactify a six-dimensional theory on a circle of radius R_6, and one unit of circle momentum costs $1/R_6$ for a neutral massless mode. At energies well below that scale, the circle momentum can be absent from the effective description. Increasing the energy at fixed radius can expose the compactification. A five-dimensional fixed point obtained without a finite circle scale has a different interpretation. How can we tell which construction we have when both geometries contain just one compact surface?

We will build the compact surface from a pencil of plane cubics. The fiber gives a candidate circle scale, and its intersection with the compact divisor tells us whether changing the Coulomb scalar changes that scale. We will then follow an explicit path that makes the scale large without making the curves of a chosen five-dimensional sector heavy. The path passes through a flop; the curve that flops is a section, while the scale we want to remove is a fiber period.

We use the circle kinematics of Volume I and the blowups and adjunction of Volume III. The period sign is the one used in Chapter 2 of this volume: varying the compact scalar a varies the positive Kähler class by $-\delta a[S]$ for a compact surface S. We will use Chapter 4's distinction between a signed period and the mass of a curve effective in a particular chamber, and Chapter 5's distinction between a curve wall and the collapse of a surface to a point.

XIII.9.2 A pencil whose fibers are elliptic

What makes a curve class a candidate to carry circle momentum? We want a genus-one curve that moves in a family and has a period independent of the compact scalar. We start by constructing the family; the genus and the relevant intersections can then be

read from its fiber class.

Over $\mathbb{C}$, use coordinates $[x : y : z]$ on $\mathbb{P}^2$. The affine pencil is

$$P_t = G_0 + tG_1, \qquad G_0 = y^2z - x^2(x+z), \qquad G_1 = x^3 + y^3 + 3z^3. \tag{XIII.9.1}$$

The $t = \infty$ member is the smooth cubic $G_1 = 0$. The finite members have no singular point on $z = 0$. There, the two derivatives in x, y and the remaining derivative in z are

$$3(t-1)x^2, \qquad 3ty^2, \qquad y^2 - x^2. \tag{XIII.9.2}$$

For $t \neq 0, 1$ the first two force $x = y = 0$, which is not a projective point on $z = 0$. At $t = 0$ they force $x = 0$, and at $t = 1$ they force $y = 0$; in either case the third derivative is nonzero at the only candidate.

In the patch $z = 1$ the singularity equations factor:

$$P_x = x\,[3(t-1)x - 2] = 0, \qquad P_y = y\,(2 + 3ty) = 0. \tag{XIII.9.3}$$

Each pair of choices leaves one equation $P_t = 0$. For example, with $x = 0$ and $y = -2/(3t)$, the two terms $y^2 + ty^3$ contribute $4/(27t^2)$. Adding $3t$ gives the second row below. Where a denominator occurs, the corresponding branch exists only for nonzero denominator. Put $x_* = 2/[3(t-1)]$ and $y_* = -2/(3t)$. Then the four evaluations are

(x, y)	$P_t(x, y, 1)$
$(0, 0)$	$3t$
$(0, y_*)$	$(81t^3 + 4)/(27t^2)$
$(x_*, 0)$	$[81t(t-1)^2 - 4]/[27(t-1)^2]$
(x_*, y_*)	$[81t^3(t-1)^2 - 8t + 4]/[27t^2(t-1)^2]$

(XIII.9.4)

The numerators do not vanish at their excluded denominator roots. To see that the singular parameters are distinct, multiply the numerators, dropping the factor of 3 in the first. Call the product D. Polynomial division modulo 11 gives the following degrees, starting with D, D' and continuing with their successive nonzero remainders:

$$(\deg D, \deg D', \deg r_1, \ldots, \deg r_7) = (12, 11, 10, 9, 8, 3, 2, 1, 0). \tag{XIII.9.5}$$

The last remainder is 6 modulo 11. The leading coefficients of D, D' survive the reduction. Thus the gcd over $\mathbb{Q}$ is also constant, and there are twelve simple roots over $\mathbb{C}$. In particular no two rows of (XIII.9.4) give a singularity at the same t.

At each root the affine Hessian is diagonal. Its entries are $-2, +2$ on the respective $x = 0, x = x_*$ branches, and $+2, -2$ on the $y = 0, y = y_*$ branches. The four determinants are therefore

$$\det \mathrm{Hess}_{x,y} P_t = (-4, 4, 4, -4) \quad \text{in the order of (XIII.9.4).} \tag{XIII.9.6}$$

For instance $t = 0$ gives the ordinary node at the origin: the tangent cone is $(y - x)(y + x) = 0$, and $\partial_t P_t(0, 0, 1) = 3$ smooths it as t varies. The other nodes also smooth transversely.

We can see the two branches directly rather than only through the Hessian. At $t = 0$, set $y = rx$ on the complement of $x = 0$ in the affine cubic. Its equation reduces to

$$x^2(r^2 - x - 1) = 0, \qquad x = r^2 - 1, \qquad y = r(r^2 - 1). \tag{XIII.9.7}$$

The two values $r = 1, -1$ map to the same point $(0, 0)$. Their limiting slopes are $+1, -1$, the two distinct tangent lines of the node. Thus the normalization separates two points that were identified on the cubic. This is how a rational normalization can have a nodal image with arithmetic genus one. It also explains why smoothness of a particular fiber is a separate question from the genus computed by adjunction below. In the derivative of $P_t(x(t), y(t), 1)$ on a branch, the terms proportional to P_x, P_y vanish. Simplicity of the root of the substituted equation then gives $\partial_t P_t \neq 0$ at the node. A reducible cubic could not have just one ordinary node: a line and conic must meet with total intersection multiplicity two, giving either two intersection points or a nontransverse singularity. Three lines or a repeated component also fail the single ordinary node test.

A base point is a common zero of G_0, G_1, so it has $\partial_t P_t = 0$ and cannot be any of the nodes just found. If the generators met nontransversely there, some nonzero combination of their differentials would vanish, giving a singular pencil member at that point. They are coprime and hence meet at nine distinct transverse points by Bézout. This transversality has a second use. The two generators give local coordinates at a base point; after the blowup their projective ratio is the direction on the exceptional $\mathbb{P}^1$. That exceptional curve maps once onto the pencil base. It is a section, which means it selects one point on every fiber.

More explicitly, near a base point let $g_0 = G_0$ and $g_1 = G_1$ after trivializing the cubic line bundle. Transversality makes (g_0, g_1) local coordinates. One blowup chart has $g_0 = rg_1$ with exceptional locus $g_1 = 0$. The pencil equation becomes $g_1(r + t) = 0$; after removing its common exceptional factor, the proper transform is

$$r + t = 0, \qquad E_i = \{g_1 = 0\}, \qquad r|_{E_i} = -t. \tag{XIII.9.8}$$

The other chart covers the point at infinity. The pencil map therefore extends over the exceptional curve and has degree one on it. Blowing up has resolved an indeterminate ratio into a regular map, rather than adding an extra fiber component at every parameter. This distinction will matter when the section is flopped out of the compact surface.

Write S_9 for the nine-point blowup and $q : S_9 \to \mathbb{P}^1$ for the resulting map. In the marked basis, H pulls back a line and E_i denotes the ith exceptional curve. Their pairings and the proper transform of a cubic give

$$H^2 = 1, \qquad H \cdot E_i = 0, \qquad E_i \cdot E_j = -\delta_{ij}, \tag{XIII.9.9}$$

$$f = 3H - \sum_{i=1}^{9} E_i = -K_9, \qquad f^2 = 9 - 9 = 0, \qquad K_9 \cdot f = 0, \qquad E_i \cdot f = 1. \tag{XIII.9.10}$$

Here K_i denotes the canonical class of S_i. The equality $f = -K_9$ follows from $K_{\mathbb{P}^2} = -3H$ and the addition of one exceptional class to the canonical class at each blowup. The unit pairing with a section makes f primitive in the integral lattice.

Adjunction, with p_a the arithmetic genus, gives

$$2p_a(f) - 2 = f \cdot (f + K_9) = 0. \tag{XIII.9.11}$$

For a smooth member this is genus one. The nodal member still has arithmetic genus one, with a genus-zero normalization. As Fig. XIII.9.1 shows, the node is a change in shape at one pencil parameter. All members are in the same class f, so their areas still agree. Sending that common area to zero is a separate Kähler operation.

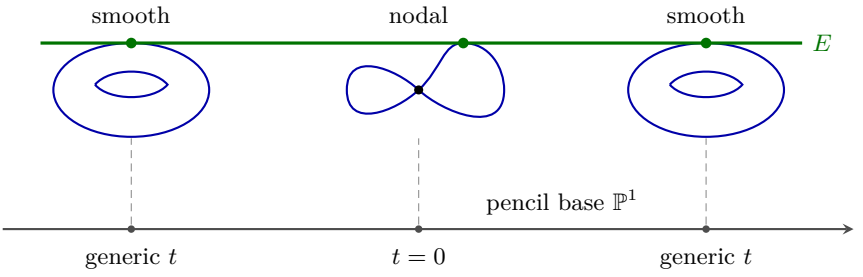


Figure XIII.9.1: Three fibers of $q : S_9 \to \mathbb{P}^1$. The green curve is the marked section E, which meets each fiber once. At $t = 0$ the fiber has one node; it is one of twelve singular members. The drawn fiber shapes are schematic and do not indicate different Kähler areas.

A line through the first point, chosen to avoid the others, supplies a useful comparison. For its proper transform $C = H - E_1$,

$$C^2 = 0, \qquad K_9 \cdot C = -3 + 1 = -2, \qquad p_a(C) = 0. \tag{XIII.9.12}$$

Square zero alone does not distinguish an elliptic fiber from a rational one.

There is also an integral normalization to fix. The multiple $2f$ has the same square and arithmetic genus as f:

$$(2f)^2 = 0, \qquad K_9 \cdot (2f) = 0, \qquad p_a(2f) = 1, \qquad E_i \cdot (2f) = 2. \tag{XIII.9.13}$$

The unit intersection of the actual section with f rules out such a multiple as the primitive fiber class. This matters for the later momentum normalization: assigning one unit to $2f$ would double the wrapped-area scale. The calculation concerns integral classes and periods; it does not assert that every multiple has a new irreducible representative or a distinct single-particle state. Even a numerical class with both the right square and arithmetic genus needs actual effective representatives to give the family we will use. The name dP_9 often denotes this rational elliptic surface. Here $-K_9$ is a fiber class, so it is not ample.

To see which elliptic curve remains after the proposed deformation, choose the last base point p and set $E = E_9$. Blowing down E gives $\pi : S_9 \to S_8$. Set $k = -K_8$. The blowup formula now reads

$$K_9 = \pi^* K_8 + E, \qquad \pi^* k = f + E, \qquad k^2 = (f + E)^2 = 0 + 2 - 1 = 1. \tag{XIII.9.14}$$

For any irreducible curve C in S_8, take its strict transform $\widetilde{C}$ in S_9. If $\widetilde{C}$ maps onto the pencil base, $f \cdot \widetilde{C}$ is its positive map degree and $E \cdot \widetilde{C} \geq 0$. If its image is a point, it must be the whole irreducible fiber, and then $E \cdot \widetilde{C} = 1$. Consequently

$$k \cdot C = (f + E) \cdot \widetilde{C} \begin{cases} > 0, & q(\widetilde{C}) = \mathbb{P}^1, \\ = 1, & q(\widetilde{C}) \text{ is a point.} \end{cases} \tag{XIII.9.15}$$

Together with $k^2 = 1$, this is the Nakai–Moishezon ampleness test for a surface. Thus S_8 is a degree-one del Pezzo surface. The image of a smooth fiber is a smooth genus-one member of class k; it is smooth through p by transversality, and $k \cdot (k + K_8) = 0$. Yet its square is now 1. We next use this change in the intersection lattice to distinguish its physical period from the old fiber period.

XIII.9.3 The period that measures the KK gap

Which period can represent a background circle radius? A candidate must be present in the actual threefold and remain unchanged when we vary its Coulomb scalar. To see the elliptic structure, let $X_9 = \operatorname{Tot} K_{S_9}$ and use $\mathcal{O}_{S_9}(f) = q^* \mathcal{O}_{\mathbb{P}^1}(1)$. Then

$$K_{S_9} = q^* \mathcal{O}_{\mathbb{P}^1}(-1), \qquad B = \operatorname{Tot} \mathcal{O}_{\mathbb{P}^1}(-1), \qquad X_9 = S_9 \times_{\mathbb{P}^1} B. \tag{XIII.9.16}$$

In the fiber product a point of S_9 and a point of B have the same pencil parameter. At fixed $b \in B$ we get the corresponding cubic fiber of S_9, with a point selected by the section E. The compact curve in B is its zero section; its normal bundle is $\mathcal{O}(-1)$, so its self-intersection is -1. The elliptic fiber above a generic point on this curve is smooth. The ordinary M/F construction with this base curve and generic fiber identifies the local parent as the rank-one six-dimensional E-string theory. We use the ordinary untwisted construction with no extra flux, frozen data or local sectors. The single compact base curve represents the one tensor direction. The six-dimensional construction and anomaly analysis are taken up in XIV, and the composite construction in Volume XIII.

In X_9 the surface S_9 is the zero section. Calabi–Yau adjunction says that its divisor class restricted to the surface is its canonical class. Hence

$$[S_9]|_{S_9} = K_9, \qquad S_9 \cdot f = K_9 \cdot f = 0, \qquad S_9 \cdot E = K_9 \cdot E = -1. \tag{XIII.9.17}$$

Write J_{phys} for the positive physical Kähler form, and use the rescaled form ω so a curve period has mass units:

$$T_{\text{M2}} = \frac{1}{(2\pi)^2 \ell_p^3}, \qquad \omega = T_{\text{M2}} J_{\text{phys}}, \qquad t_C = \int_C \omega. \tag{XIII.9.18}$$

Here ℓ_p is the eleven-dimensional Planck length. An existing calibrated M2 wrapped on an effective curve C has mass t_C in the chosen common noncompact units: the tension has units of inverse length cubed and the area has units of length squared. Changing a at fixed background adds $-\delta a[S_9]$ to ω. The two intersections give different responses:

$$\left.\frac{\partial t_f}{\partial a}\right|_{\text{bg}} = 0, \qquad \left.\frac{\partial t_E}{\partial a}\right|_{\text{bg}} = 1. \tag{XIII.9.19}$$

The neutral fiber scale can be held fixed while a section becomes light. On the daughter geometry, by contrast, $[S_8]|_{S_8} = K_8 = -k$. Every irreducible curve in S_8 then has $S_8 \cdot C = -k \cdot C < 0$ by (XIII.9.15), including the genus-one member with charge -1. Its period changes with a.

In the M/F identification the primitive fiber wrapping number maps to spacetime momentum in integer units. In matched noncompact mass units the area scale for one fiber is

$$\mu := t_f = R_6^{-1}, \qquad R_6 > 0. \tag{XIII.9.20}$$

This uses the M/F dictionary in addition to (XIII.9.17). Comparing the wrapped area in an eleven-dimensional metric directly to a radius in another metric would omit the conversion of noncompact mass units.

To see the role of μ, let s be distance around the external spacetime circle of circumference $2\pi R_6$. With untwisted periodic boundary conditions a Fourier wave must obey

$$e^{ip_6(s+2\pi R_6)} = e^{ip_6 s}, \qquad p_6 = \frac{n}{R_6}, \qquad n \in \mathbb{Z}. \tag{XIII.9.21}$$

For a neutral parent degree of freedom with mass m_6 to which free mode kinematics applies, the energy in the five-dimensional rest frame obeys

$$m_n^2 = m_6^2 + n^2\mu^2, \qquad m_n\big|_{m_6=0} = |n|\mu. \tag{XIII.9.22}$$

For example in one mass unit, take $m_6 = 3$, $\mu = 2$ and $n = 2$. The momentum contributes 4 in mass units; the rest mass is $\sqrt{3^2 + 4^2} = 5$. The pure massless-parent mode at the same n has scale 4. Charged fields can also have their allowed momenta shifted by a flavor holonomy. Figure XIII.9.2 plots the pure massless-mode scales of (XIII.9.22); the diagram does not enumerate normalizable particles or their multiplicities in the interacting E-string theory.

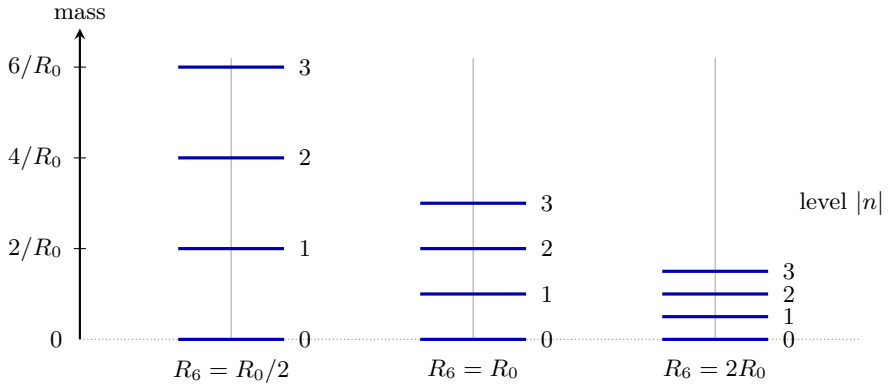


Figure XIII.9.2: The pure scales $|n|/R_6$ for $|n| = 0, 1, 2, 3$ at three spacetime radii, shown on the same vertical mass scale with R_0 a fixed reference radius. Increasing R_6 brings the levels closer; it does not increase the KK gap.

The finite-radius fiber period in (XIII.9.20) is positive. At energies $E_{\mathrm{probe}} \ll \mu$ one can omit the pure KK tower in a low energy description, provided the other conditions for a local effective sector hold. This hierarchy at a fixed radius does not remove the tower from the full compactification.

One can make the hierarchy quantitative without assigning a spectrum to the interacting parent. In the neutral massless Fourier example, the modes whose rest energy is at most a probe energy E_{probe} satisfy

$$|n|\mu \le E_{\mathrm{probe}}, \qquad |n| \le \lfloor E_{\mathrm{probe}}/\mu \rfloor . \tag{XIII.9.23}$$

At $\mu = 3/2$ and $E_{\mathrm{probe}} = 5$ in one mass unit, the allowed integers are $-3, -2, -1, 0, 1, 2, 3$. Lowering the probe energy to 1 keeps only $n = 0$ in this example; it has changed the energy window, not the compactification. At fixed positive probe energy the number of accessible Fourier labels instead grows without bound as $\mu \to 0^+$. This elementary test makes the order of operations visible. A low energy truncation at fixed radius discards high Fourier modes from the effective description. Decompactification lowers their spacing and defeats that truncation. Neither statement determines interacting multiplicities or normalizability. On the elliptic side we instead reach zero fiber area by taking

$$\mu \to 0^+, \qquad R_6 \to \infty. \tag{XIII.9.24}$$

This is the decompactification direction. It makes the KK scale light, with no claim here about an interacting six-dimensional scaling limit for the tensor vev. To remove that scale from the low energy construction we want the opposite direction, $\mu \to \infty$. To follow it with a chosen finite sector, we must first understand what happens when the section period reaches zero.

XIII.9.4 The flop moves the exceptional curve

A vanishing section in S_9 is a curve wall. What geometry is available on the other side? We will keep the threefold in view, so that we can account for the curve that replaces the section and determine what is left of the compact surface.

On S_8, let s_0, s_1 be the sections of k induced by G_1, G_0, respectively, with a common transverse zero at p. On the member $s_1 + ts_0 = 0$, their ratio is $[s_0 : s_1] = [1 : -t]$ away from p. This is our homogeneous coordinate on the pencil base. The total space B in (XIII.9.16) is the space of a vector $(u, v) \in \mathbb{C}^2$ lying in the line recorded by this coordinate. Its map to $\mathbb{C}^2$ collapses the zero section to the origin. Forgetting the line from the fiber product gives the threefold

$$Y_0 = \{(P, u, v) \in S_8 \times \mathbb{C}^2 : us_1(P) - vs_0(P) = 0\}. \tag{XIII.9.25}$$

Off p, a derivative in u or v is nonzero. At p with $(u, v) \neq (0, 0)$, the equation has nonzero differential $u\,ds_1 - v\,ds_0$ since ds_0, ds_1 are independent there. At $(p, 0)$, choose a local trivialization of k and coordinates $x = s_0$, $y = s_1$. The local equation is the conifold node

$$uy - vx = 0. \tag{XIII.9.26}$$

The four local derivatives of this quadratic vanish together only at the origin.

In the first resolution, record the common direction $[\xi : \eta]$ of (s_0, s_1) and (u, v). The two incidence equations are

$$\xi s_1 = \eta s_0, \qquad \xi v = \eta u. \tag{XIII.9.27}$$

The first graph is the blowup S_9 of the transverse base point. The second equation says that (u, v) is a vector in the tautological line over that graph. This is precisely X_9. Near the node on $\xi \neq 0$, with $\lambda = \eta/\xi$, the equations read $(y, v) = (\lambda x, \lambda u)$, with three free coordinates x, u, λ.

On the overlap, put $\kappa = \xi/\eta = \lambda^{-1}$. The second chart has free coordinates y, v, κ, and the transition is

$$\kappa = \lambda^{-1}, \qquad y = \lambda x, \qquad v = \lambda u. \tag{XIII.9.28}$$

Along the exceptional curve $x = u = 0$, both transverse fiber coordinates transform by the same factor. These are the two copies of the tautological line $\mathcal{O}(-1)$ over the projective direction $[\xi : \eta]$. This gives a local coordinate explanation of the normal bundle, independent of the extension argument below. On $\eta \neq 0$ the other chart exchanges the two pairs. Only above the node is the direction undetermined, giving the curve E rather than an exceptional divisor. Its two normal directions have bundle degrees -1:

$$N_{E/S_9} = \mathcal{O}_E(-1), \qquad K_9|_E = \mathcal{O}_E(-1), \qquad N_{E/X_9} \simeq \mathcal{O}_E(-1)^{\oplus 2}. \tag{XIII.9.29}$$

For the last equality, the normal extension of one $\mathcal{O}(-1)$ by the other splits because $H^1(\mathbb{P}^1, \mathcal{O}) = 0$.

For the second resolution let $[w : b]$ be the line coordinates of $\mathbb{P}(K_{S_8} \oplus \mathcal{O})$, the bundle of lines over S_8. The coordinate w takes values in K_{S_8}, so ws_i is scalar in the same line-coordinate convention as bu and bv. Now record the proportionality by

$$bu = ws_0, \qquad bv = ws_1. \tag{XIII.9.30}$$

If $b \neq 0$, the ratio $\rho = w/b$ is a coordinate in the canonical bundle and $(u, v) = \rho(s_0, s_1)$. In the local $w \neq 0$ chart, trivialize the bundle, put $w = 1$, and get $(x, y) = (bu, bv)$. These two charts are smooth near the exceptional curve.

Their overlap also describes the retained surface particularly simply. Put $\tau = b/w$ on the $w \neq 0$ chart, using a local trivialization near p. Then

$$\rho = \tau^{-1}, \qquad (x, y) = (\tau u, \tau v), \qquad E' = \{u = v = 0\} \quad (w \neq 0). \tag{XIII.9.31}$$

In the $b \neq 0$ chart the same curve is $x = y = 0$ with coordinate ρ. The surface S_8 is $\rho = 0$, so its intersection with E' is the point $\rho = 0$ on that projective line. The point $\tau = 0$ supplies the other end of the line and is outside the canonical-bundle chart. We therefore cannot identify the whole second resolution with $\operatorname{Tot} K_{S_8}$ at finite exceptional period. It contains the extra compact curve whose mass we must still send large. At every point of Y_0 off the node the ratio $[w : b]$ is fixed by the equations, including at p when $(u, v) \neq 0$. At the node the whole $\mathbb{P}^1$ remains. The two resolutions are small because each contracts just one curve. They are crepant, since the node is a Gorenstein

hypersurface and a small resolution introduces no exceptional divisor in the canonical class. The two graph choices resolve opposite rulings of the node, so their birational change is a flop. Denote the second smooth threefold by X_+.

We can now check where the curves lie. Over $(u, v) = 0$ in the $b \neq 0$ chart near p, the central ideal is

$$(\rho x, \rho y) = (\rho) \cap (x, y). \tag{XIII.9.32}$$

The first component is the zero section S_8 and the second is the affine part of the new curve over p. The locus $b = 0$ in the $w \neq 0$ chart contains the infinity point of that curve. Thus the central fiber is $S_8 \cup E'$, with $E' \simeq \mathbb{P}^1$ meeting S_8 transversely at p. The chart $b \neq 0$ is $\operatorname{Tot} K_{S_8}$, a proper open part of X_+. Figure XIII.9.3 follows the section through the two contractions.

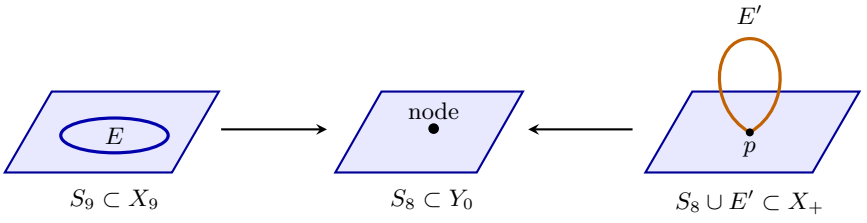


Figure XIII.9.3: The central fibers over $(u, v) = 0$ before, at and after the flop. The old curve E lies in S_9 and contracts to the node of Y_0. The new curve E' lies outside S_8 and meets it at one point. Both arrows pointing to Y_0 are small contractions of threefolds.

For fixed $(u, v) \neq 0$ the equations specify the pencil member $us_1 - vs_0 = 0$ in S_8, with a unique point over each P, including the point over p at $b = 0$. For example $(u, v) = (1, 0)$ gives $s_1 = 0$; in the $w = 1$ coordinates near p this is $y = 0$ and $x = b$. The local equation gives the missing point at $b = 0$ with multiplicity one. All these noncentral fibers are irreducible. Moreover, a complete irreducible curve in X_+ must map to one point of the affine (u, v) plane, because a regular function on a complete connected curve is constant. This leaves only three possibilities: a curve in S_8, the curve E', or an irreducible noncentral fiber. In the next section this list will let us check all compact-curve scales, including curves outside the retained surface.

There is a direct way to read the sign change. Blow up the exceptional curve to compare the two small resolutions on a common space. Its exceptional divisor is $Q = \mathbb{P}^1 \times \mathbb{P}^1$, with normal class $Q|_Q = (-1, -1)$ in the two ruling degrees. A class of signed degree e on the old curve pulls back with ruling degrees $(e, 0)$. The other resolution collapses the first ruling, so a class descending to it must have first degree zero. The required correction on the common blowup is

$$(e, 0) + e\, Q|_Q = (e, 0) + e(-1, -1) = (0, -e). \tag{XIII.9.33}$$

On the strict transform of S_9 the same correction adds eE. The restriction can descend to S_8 since its pairing with E changes by $eE^2 = -e$. Thus the signed degree e measures the old curve, and $-e$ measures the new one. Taking the absolute value of a single period would conceal the change in which curve is effective and where that curve sits.

XIII.9.5 A limit that leaves the daughter at finite scale

We want to send the KK scale μ large while keeping a five-dimensional sector accessible. The curve wall by itself only changes the chamber. To use it for this purpose we must specify what stays finite, prove that both classes lie in the claimed chambers, and follow the curves that might otherwise survive outside the daughter surface.

Let A be the pullback of k from S_8 to the graph models, and on X_9 let F pull back the pencil-base $\mathcal{O}(1)$. The positive period class before the flop is

$$\omega_- = \mu A + (a-\mu)F, \qquad 0 < \mu < a, \tag{XIII.9.34}$$

$$\omega_-|_{S_9} = \mu(f+E) + (a-\mu)f = af + \mu E. \tag{XIII.9.35}$$

The graph (XIII.9.27) is closed in the product of S_8, the pencil base and the affine (u,v) plane. Since k and $\mathcal{O}(1)$ are ample on the respective projective factors, their positive weighted sum is ample relative to the affine plane. Both coefficients in (XIII.9.34) are positive. This proves that the curve periods calculated from the class are attained within a chamber. At fixed μ its variation on the surface is $f = -K_9$, as required for the compact scalar. The period of the retained class $\pi^*k = f + E$ is a:

$$t_f = (af + \mu E)\cdot f = \mu, \qquad e := t_E = (af+\mu E)\cdot E = a - \mu, \tag{XIII.9.36}$$

$$t_{\pi^*k} = t_f + t_E = a, \qquad V_- := \tfrac{1}{2}\int_{S_9} \omega_-^2 = \tfrac{1}{2}(2a\mu - \mu^2) = a\mu - \tfrac{1}{2}\mu^2. \tag{XIII.9.37}$$

Here V_- is the geometric surface volume in squared mass units.

The choice of what to hold fixed is already visible in these formulas. The sum $t_f + t_E = a$ is constant on our path, whereas μ and the signed section period trade against one another:

$$\left.\frac{dt_f}{d\mu}\right|_a = 1, \qquad \left.\frac{dt_E}{d\mu}\right|_a = -1, \qquad \left.\frac{dt_{\pi^*k}}{d\mu}\right|_a = 0. \tag{XIII.9.38}$$

This is a variation of a background scale with the retained scale fixed. It differs from the compact-scalar variation at fixed μ, for which the fiber does not change. The two operations can cross the same wall, but they answer different physical questions. One varies the circle scale relative to a chosen sector; the other moves that sector in its Coulomb direction. A wrapped M5 interpretation of this normalization uses the relative tension convention of Chapter 2.

The wall is $\mu = a$. Its class aA pulls back a relatively ample class from $Y_0 \subset S_8 \times \mathbb{C}^2$, and its zero curve is precisely the small exceptional curve. The surface still has volume $a^2/2$. If μ increases further at fixed a, (XIII.9.36) would make the effective old section negative. We must move to X_+, where the new curve has period $-e$ by (XIII.9.33).

On the projective bundle of the second graph let L be the tautological dual class $\mathcal{O}(1)$ and retain A for the pullback of k. The new positive class is

$$M := \mu - a > 0, \qquad \omega_+ = aA + ML. \tag{XIII.9.39}$$

To check it, L is nef, meaning it has nonnegative degree on every complete curve. In the lines convention it is the tautological quotient of the dual bundle, $k \oplus \mathcal{O}$. On a curve this quotient line has a nonzero map from at least one of the two summands, both of nonnegative degree, so it has nonnegative degree. It also has degree one on each projective line fiber. For an irreducible positive-dimensional subvariety Z of dimension d in the projective bundle, the fibers of its projection to S_8 have generic dimension zero or one. In the first case $A^d \cdot Z > 0$ by ampleness of k on the image. In the second, intersect Z with $d-1$ pullback divisors from the base, leaving fibers on which L has positive degree. Thus

$$\begin{cases} A^d \cdot Z > 0, & \text{generic fiber dimension zero,} \\ A^{d-1} L \cdot Z > 0, & \text{generic fiber dimension one.} \end{cases} \tag{XIII.9.40}$$

Every other term in the expansion of $(aA + ML)^d \cdot Z$ is nonnegative because the factors are nef. The positivity criterion for ampleness gives the stated chamber for positive rational coefficients, and every positive real pair is a positive combination of such pairs. Restrict this relatively ample class from the product with the affine plane to X_+.

There is a global check that this class continues the old one. The coordinate w is a section of $L \otimes K_{S_8}$, written here as the line bundle of class $L - A$. Its zero locus on X_+ is S_8 with multiplicity one, since w/b is a normal coordinate there. On X_9 the zero section has class $-F$ by (XIII.9.16). The isomorphism off the small exceptional curves identifies the divisor classes, so

$$L - A = [S_8] \longleftrightarrow [S_9] = -F, \tag{XIII.9.41}$$

$$aA + (\mu - a)L \longleftrightarrow aA + (\mu - a)(A - F) = \mu A + (a - \mu)F. \tag{XIII.9.42}$$

At fixed μ the compact direction on X_+ is $A - L = -[S_8]$. This agrees with the common blowup: $af + \mu E + eE = a(f + E)$ restricts from ak on S_8.

On S_8 we have $A|_{S_8} = k$ and $L|_{S_8} = 0$ since b never vanishes there. On E' the two degrees are $(0, 1)$. On a noncentral cubic the A degree is $k^2 = 1$, while b, a section of L, vanishes simply at its point above p. For instance the $w = 1$ chart with $(u, v) = (1, 0)$ gives $x = b$. More generally $(x, y) = (bu, bv)$ with $(u, v) \neq 0$ makes b a parameter there. The noncentral degrees are therefore $(1, 1)$. It follows that

$$t_{E'} = M, \qquad t_f = a + M = \mu, \qquad t_C = a\, k \cdot C \quad (C \subset S_8), \tag{XIII.9.43}$$

$$V_+ := \tfrac{1}{2} \int_{S_8} \omega_+^2 = \tfrac{1}{2} a^2. \tag{XIII.9.44}$$

The curve E' grows on this side even though the compact surface stays the same size at fixed a. The period t_f continues to refer to a noncentral pencil fiber after the flop. It is the inherited KK scale of the deformation; the old elliptic map with its section over B is not kept unchanged.

For example, use $a = 3$ in one mass unit and increase μ from 2 to 7. At $\mu = 3$ the

period of the old curve vanishes, and V_- agrees with V_+:

μ	t_f	section or replacement period	V_S
2	2	$t_E = 1$	4
3	3	0	9/2
7	7	$t_{E'} = 4$	9/2

(XIII.9.45)

For example a retained curve of k-degree two has period 6 throughout the last chamber. Figure XIII.9.4 plots this distinction between increasing μ at fixed a and varying a at fixed μ.

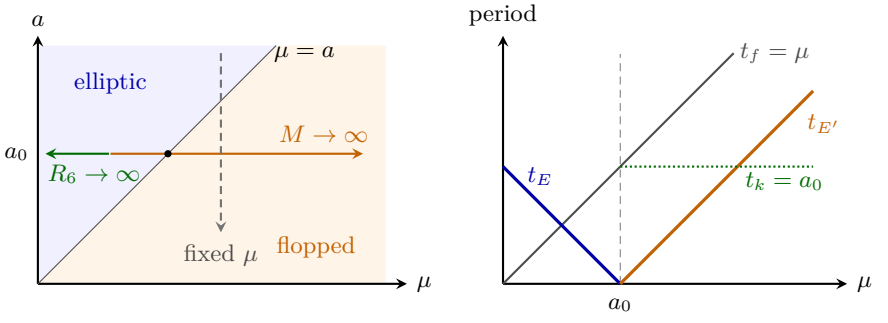


Figure XIII.9.4: The period plane with the wall $\mu = a$ (left) and its fixed-a slice (right). The horizontal path to increasing μ crosses the wall and sends M large. Its reverse on the elliptic side approaches decompactification. Varying a along the dashed vertical arrow crosses the same wall with no change in the background gap. The blue and orange lines in the right panel are periods of different effective curves.

Now follow the increasing-μ path at fixed positive a. For any effective compact cycle with a component outside S_8, the list of possible supports after (XIII.9.32) and the positive periods give

$$t_{\text{cycle}} \;\geq\; \min\{M, \mu\} \;\longrightarrow\; \infty, \qquad M = \mu - a \longrightarrow \infty. \tag{XIII.9.46}$$

Every fixed curve in S_8 has a finite period $a\,k \cdot C$. Thus an energy window can keep chosen finite scales accessible while satisfying

$$E_{\text{probe}}/M \longrightarrow 0, \qquad E_{\text{probe}}/\mu \longrightarrow 0. \tag{XIII.9.47}$$

The geometric bound controls compact-curve periods and their calibrated masses. To use this as a local quantum field theory limit we assume the required fixed asymptotic conditions, gravitational isolation, and decoupling of unwanted bulk and asymptotic modes. The bound itself gives no quantum or metric convergence theorem. Merely setting $R_6 = 0$ in the old chamber would give a negative section period. Taking both a and μ large can instead send the desired S_8 periods large as well. The finite scale is part of the specification of this daughter limit.

A changed numerical path illustrates the scale selection. Fix $a = 4$ and compare $\mu = 1, 4, 10$. The effective curve on either side of the wall and the surface volume are

μ	chamber	$t_{\text{exceptional}}$	V_S
1	elliptic	3	7/2
4	wall	0	8
10	flopped	6	8

(XIII.9.48)

At $\mu = 10$, a retained curve of k-degree three has period 12, while E' has period 6 and a noncentral fiber has period 10. A positive cycle with two E' components, one noncentral fiber and that retained curve has period

$$t_{\text{cycle}} = 2(\mu - a) + \mu + 3a = 3\mu + a = 34. \tag{XIII.9.49}$$

Following the same fixed-a path sends its exterior contribution large even though the degree-three part remains at 12. The positive coefficients are essential: an effective cycle is a sum with nonnegative integer multiplicities. A formal difference such as $f - E'$ has period a, but subtraction of an exterior component is not a counterexample to the bound on effective cycles. The compact-curve classification, together with positivity, is what makes the bound control every exterior component rather than only the named flopping curve.

The volume also distinguishes a curve wall from the later surface contraction. At fixed a, its first derivative in μ vanishes at the wall from either side, while the two chambers have different second derivatives:

$$\partial_\mu V_-|_{\mu=a} = \partial_\mu V_+ = 0, \qquad \partial_\mu^2 V_- = -1, \qquad \partial_\mu^2 V_+ = 0. \tag{XIII.9.50}$$

The nonzero value $a^2/2$ at this wall means the compact surface has survived. Only the subsequent $a \to 0^+$ step makes its area vanish. These statements concern the geometric area function along the chosen path; they do not identify it with a complete quantum observable.

The resolved daughter is $\operatorname{Tot} K_{S_8}$. To reach the point contraction, send $a \to 0^+$ on its slice with the eight flavor backgrounds set to zero. The order here specifies the chosen limit: first separate the heavy scales, then collapse the retained surface. A contraction at finite background can also yield a local infrared sector, while the full finite-radius compactification still retains its threshold. To construct the daughter contraction geometrically, evaluate sections of k^j on the jth power of a vector in K_{S_8}. These functions define

$$\operatorname{Tot} K_{S_8} \longrightarrow \operatorname{Spec} \mathcal{R}, \qquad \mathcal{R} = \bigoplus_{j \geq 0} H^0(S_8, k^j). \tag{XIII.9.51}$$

All positive-degree functions vanish on the zero section, giving the vertex. For an ample k the degree-zero localizations on distinguished opens of $\operatorname{Proj} \mathcal{R}$ recover the base S_8. Above such opens the nonzero line fibers are recovered by homogeneous ratios: choose nonvanishing sections in two consecutive sufficiently large degrees near a point. Their ratio, evaluated on a nonzero vector, gives a nonzero linear fiber coordinate in the corresponding local trivialization. The corresponding localized section rings describe

the nonzero line bundle, so (XIII.9.51) is an isomorphism off its zero section. This uses high powers of k, without needing the degree-one anticanonical pencil to embed S_8.

In the ordinary decoupled local del Pezzo construction, this particular contraction engineers the rank-one 5D E_8 fixed point. The smooth resolved threefold keeps one compact surface before the final contraction. The physical identification of the singular point comes from the local dP_8 construction, not from the vanishing curve at the flop wall. The $R_6 \to \infty$ direction on the elliptic side instead opens the original six-dimensional circle. We next compare the parameters that distinguish the two descriptions.

XIII.9.6 Which parameters survive?

The parent and daughter both have one compact surface. How can one retain an independent radius when the other does not? We count period directions first. The daughter in this comparison is the canonical bundle after the heavy curve scales have been removed, so it is $\operatorname{Tot} K_{S_8}$, rather than the full flopped threefold at finite M.

For $i = 9, 8$ write $X_i = \operatorname{Tot} K_{S_i}$. Retraction along the line fibers identifies $H^2(X_i;\mathbb{Z})$ with $H^2(S_i;\mathbb{Z})$. The pullback line class and the i exceptional classes give rank $i+1$. To identify the compact direction, use the Thom class of the complex line bundle. It generates $H_c^2(X_i;\mathbb{Z})$ and restricts to the Euler class of the line bundle on its zero section. Thus

$$H_c^2(X_i;\mathbb{Z}) \simeq H^0(S_i;\mathbb{Z}), \qquad \operatorname{im}(H_c^2 \to H^2) = \mathbb{Z}K_i. \tag{XIII.9.52}$$

In the basis of (XIII.9.9), the coefficient of each exceptional class in K_i is 1. The image is primitive and nonzero even for the null class K_9. The real quotient of periods by the compact direction has dimensions

$$\dim\left(H^2(X_i;\mathbb{R})/\mathbb{R}K_i\right) = \begin{cases} 10-1=9, & i=9, \\ 9-1=8, & i=8. \end{cases} \tag{XIII.9.53}$$

This quotient identifies changes that can be made by varying the compact class. It does not test the norm of any harmonic form.

Evaluate a representative η of the parent period space on f. The result is well defined on the quotient and can be varied independently. Indeed,

$$(\eta + \lambda K_9)\cdot f = \eta \cdot f, \qquad E \cdot f = 1. \tag{XIII.9.54}$$

For example, choosing the representative E adds one unit of fiber period. Its direction survives modding out by K_9. Holding this evaluation fixed leaves eight independent directions. Try the same construction with the smooth anticanonical curve in S_8. This time

$$(\eta + \lambda K_8)\cdot k = \eta \cdot k - \lambda. \tag{XIII.9.55}$$

In particular changing the compact scalar by one increases the k period by one. Evaluation on k does not define a separate background coordinate.

The eight fixed-radius directions can also be compared integrally in this marking. Let U be the span of f, E in the integral intersection lattice of S_9. Its Gram matrix

and determinant are

$$\mathrm{Gram}(f,E)=\begin{pmatrix}0 & 1\\ 1 & -1\end{pmatrix},\qquad \det\mathrm{Gram}(f,E)=-1. \tag{XIII.9.56}$$

The determinant is a unit, so subtracting the projection onto U uses integer coefficients.

To see those coefficients, let v be any integral class and write $v=\alpha f+\beta E+v_\perp$. Pairing successively with f,E determines the two coefficients without solving for all ten lattice coordinates:

$$\beta=v\cdot f,\qquad \alpha=v\cdot E+v\cdot f,\qquad v_\perp=v-(v\cdot E+v\cdot f)f-(v\cdot f)E. \tag{XIII.9.57}$$

Direct substitution gives $v_\perp\cdot f=v_\perp\cdot E=0$. Both coefficients are integers for an integral class, which explains why the determinant condition is stronger than a real-vector-space decomposition. For instance,

$$H=3f+3E+(H-3f-3E), \tag{XIII.9.58}$$

$$E_1=f+E+(E_1-f-E). \tag{XIII.9.59}$$

The expressions in parentheses are pullbacks from S_8. Replacing $f+E$ by π^*k, they are respectively the pullbacks of $H-3k$ and E_1-k. Their k pairings vanish because $H\cdot k=3$, $E_1\cdot k=1$ and $k^2=1$. This gives an explicit way to compare fixed-radius lattice directions across the blowdown. It is not an assignment of physical flavor charges to every lattice vector. A vector orthogonal to E is a pullback from S_8 by the blowup splitting. Its pairing with f is its pairing with k on S_8. This identifies

$$U^\perp=\pi^*(k^\perp),\qquad f^\perp=\mathbb{Z}f\oplus\pi^*(k^\perp),\qquad f^\perp/\mathbb{Z}f\simeq k^\perp. \tag{XIII.9.60}$$

For the middle equality a vector $xf+yE$ in U pairs with f to give y. As a concrete direction, E_1-E_2 on S_8 pairs to zero with k, since $k\cdot E_1=k\cdot E_2=1$. Its pullback pairs to zero with both f and E. The period classes on our path have zero evaluations on all eight such perpendicular directions. This explains which zero-background slice was used in (XIII.9.51).

Direction	Elliptic parent	Resolved daughter
Total periods	10	9
Compact image	1	1
Background quotient	9	8
Local flavor directions	8	8
Independent KK radius	1	0

Table XIII.9.1: Real period dimensions, with the last two rows interpreted using the specified local physical dictionary. The two bottom rows split the background quotient.

Under the local engineering prescription with the stated boundary conditions, the compact direction is the Coulomb direction. The eight fixed-radius backgrounds on

the E-string side are locally Cartan Wilson-line parameters. Globally holonomies are angles; an eight-dimensional real tangent space does not specify their identifications. On the daughter side the eight backgrounds are real flavor masses. Table XIII.9.1 makes the distinction: the ninth parent background is the radius, neither an additional flavor parameter nor an extra Coulomb scalar. The integral comparison in (XIII.9.60) concerns the marked surface lattice, without determining the global flavor or line lattice. In the next comparison, additional circles will be introduced explicitly in spacetime rather than read from a period of the internal threefold.

XIII.9.7 The same threefold on external circles

There is a second use of circle compactification in geometric engineering. Here take a canonical conical Calabi–Yau threefold singularity X for which both local constructions and the required infrared limits exist. Start with M-theory on X and two external spatial circles S^1_M, S^1_A. Reducing on the first gives ordinary massless IIA. Applying spacetime T-duality on the second gives IIB:

$$\mathrm{M}:\ X\times S^1_M\times S^1_A \xrightarrow{S^1_M\ \text{reduction}} \mathrm{IIA}:\ X\times S^1_A \xrightarrow{S^1_A\ \text{T-duality}} \mathrm{IIB}:\ X\times S^1_B. \tag{XIII.9.61}$$

The inverse of the first arrow is the M-theory lift. The circles are free, isometric and untwisted products with periodic spin structures. For the simple formulas below the background fields also have product form: there are no mixed circle components in the metric or B-field. The comparison is before any limit that would discard momentum or winding.

In the common units for the M/IIA dictionary, the first radius is $R_M = g_{s,A}\sqrt{\alpha'}$, where $\sqrt{\alpha'}$ is the string length and $g_{s,A}$ is the IIA coupling. For the second arrow take string-frame radii R_A, R_B. The reciprocal-radius rule and dilaton transformation give

$$R_A R_B = \alpha', \qquad \Phi_B = \Phi_A - \tfrac{1}{2}\log(R_A^2/\alpha'), \qquad g_{s,B} = g_{s,A}\sqrt{\alpha'}/R_A. \tag{XIII.9.62}$$

The signed charge n of a pure momentum mode on the IIA circle becomes signed winding on the IIB circle. With fundamental string tension $1/(2\pi\alpha')$, the static winding scale and the pure momentum scale agree:

$$m_{\mathrm{wind}} = \frac{2\pi|n|R_B}{2\pi\alpha'} = \frac{|n|}{R_A} = m_{\mathrm{KK}}. \tag{XIII.9.63}$$

For example if $R_A = 2$ and $\alpha' = 3$ in length and squared length units, then $R_B = 3/2$ and the pure level with $|n| = 2$ has mass 1 on both sides. The check is about the external circle scales.

The transformation can be reversed before taking a limit. A second T-duality on the dual product circle gives

$$R'_A = \frac{\alpha'}{R_B} = R_A, \qquad g'_{s,A} = g_{s,B}\frac{\sqrt{\alpha'}}{R_B} = g_{s,A}\frac{\alpha'}{R_A R_B} = g_{s,A}. \tag{XIII.9.64}$$

For a different input, take $R_A = 6$, $\alpha' = 9$ and $g_{s,A} = 1/3$. The dual data are $R_B = 3/2$ and $g_{s,B} = 1/6$. A pure mode with signed momentum number $n = -2$ has positive

rest mass 1/3, equal to the static winding scale on the dual circle. Dualizing again returns $R_A = 6$ and $g_{s,A} = 1/3$. Keeping the sign of n tracks orientation of momentum or winding; taking $|n|$ in the mass formula makes the energy positive. This reversibility checks the radius and coupling conventions together. Sending a radius to zero while discarding its winding or momentum sectors would change the comparison and would require a separate effective-theory argument.

The internal X is the same in every term of (XIII.9.61). In particular this operation does not replace X by a mirror Calabi–Yau or shrink a fiber inside X_9. The radii here are unrelated to R_6. The background arrows by themselves do not identify the bare three-dimensional electric reductions as mirror theories: their branch dimensions can differ, and proposals comparing the resulting electric and magnetic descriptions include gauging abelian flavor symmetries. Comparative three-dimensional dynamics are taken up in the planned SCFT atlas and the treatment of dualities. We do not apply the conical comparison to the nonconical X_9 as if it were already an isolated singularity.

Take-home message of this chapter

The elliptic fiber is effective, moves in a pencil, and is neutral under the compact divisor. In the ordinary M/F dictionary its background period is the KK scale. Sending that period to zero opens the six-dimensional circle. On the chosen fixed-a path, increasing the period instead flops the section and makes the exterior compact curves heavy. The retained degree-one del Pezzo surface can then contract to the local five-dimensional E_8 endpoint under the stated isolation assumptions.

XIII.9.8 Exercises

Use `benchmark/tasks.json` to find the question IDs and `benchmark/PROTOCOL.md` for submission. For Exercises 1–5, give one set of answer fields per question. Use exact integers or rational strings such as `"3/2"`. Lists follow the order in the question. Include each requested field exactly once and use exact numbers. Derivations and explanations are for a reader to assess.

1. **Recognize the compact-neutral elliptic class (`e1`).** Compute $(C^2, K \cdot C, p_a)$ for $H - E_4$, E_4 and f on S_9, then for k on S_8. Use these four rows as `data`. Give the one-based row number of the realized compact-neutral elliptic fiber as `candidate`, and its intersection with E_4 as `unit_pairing`. Explain why genus alone would not select the fiber.

2. **Change the pencil (`e2`).** Replace $3z^3$ in G_1 by $5z^3$. In the branch with $x, y \neq 0$, substitute into P_t and write it with denominator $27t^2(t-1)^2$. Give the numerator's six coefficients in descending order as `both_nonzero`. Also give the number of nodal finite members as `node_count`, and the four Hessian determinants in the order of (XIII.9.4) as `hessian_dets`. In your derivation check simplicity, distinctness, and the patch at infinity.

3. **Track a wall and two limits (`e3`).** Hold $a = 5/2$ and take $\mu = 3/2, 5/2, 9/2$, in that order. For each give a row consisting of the chamber label, the fiber period,

the effective exceptional period (zero at the wall), and V_S, under `rows`. Use `elliptic`, `wall` or `flopped` as the chamber label. Give the period of a retained curve of k-degree two as `retained_degree_two`. Use `heavy` or `light` for the limiting KK scale on the continued large-μ path and the original elliptic large-R_6 path, under `large_mu_direction` and `large_radius_direction`, respectively.

4. **Count periods before interpreting them (`e4`).** Under `parent` and `daughter`, give ordered lists of the total period-space dimension, compact-image dimension, quotient dimension, local flavor dimensions and independent KK radius dimensions. Give the ordered Gram matrix of (f, E) as `pair_gram` and the derivative of the daughter's k period with respect to a as `daughter_k_compact_change`. State which evaluation descends to the background quotient and why.

5. **Use the external circle dictionary (`e5`).** Set $R_A = 3/2$, $\alpha' = 4$, and $g_{s,A} = 1/8$. For the pure level $n = -3$ give `dual_radius`, `dual_coupling`, `kk_mass`, and `winding_mass`. Give `internal_space` as `same` or `mirror`, and `bare_mirror_identity` as `implied` or `not_implied`. Explain what additional comparison would be needed to identify mirror theories.

6. **Diagnose a proposed parent (written).** A resolved geometry contains a smooth genus-one curve of square zero. What else would you need to identify its period with a KK gap? Discuss a realized family and elliptic structure, compatibility with the boundary conditions and any twists or flux, intersections with the compact Coulomb directions, the positive background period and its physical identification, and an independent identification of a decoupled parent. Explain the two limits of R_6 and use the S_9 to S_8 path to give an example of the chamber and scale checks. This explanation has no automatic grade.

7. **Project a changed integral class (written).** For $v = 2H - E_1 - E_2$, use (XIII.9.57) to find its component in $\mathrm{span}_{\mathbb{Z}}(f, E)$ and its orthogonal component. Express the latter as a pullback from S_8 and check its pairing with k. Explain why this integral calculation does not determine global flavor holonomies.

8. **Choose a limiting path (written).** In the flopped chamber let $a = \epsilon$ and $\mu = \epsilon^{-1}$ for $0 < \epsilon < 1$. Compute the periods of E', a noncentral fiber and a retained curve of k-degree $d > 0$, together with V_S. Compare their ratios as $\epsilon \to 0^+$. Which algebraic scale separations occur simultaneously? Which isolation assumptions are still needed before interpreting this path as a quantum field theory limit?

Status and sources

§9.2: The pencil and its fibers. The affine and infinity calculations, blowup, and ampleness test in (XIII.9.1)–(XIII.9.15) give ([MATH]). For the marked blowup lattice see Jefferson et al. (2018, arXiv v3, §4.1, Eqs. (4.3)–(4.4)); for the two-cubic construction and rational ruling comparison see Douglas et al. (1996, arXiv v2, §§1.1 and 2.1). The pencil coefficients and branch computation are specific to this chapter. Equations (XIII.9.7), (XIII.9.8) and

(XIII.9.13) develop the same elliptic pencil calculation through local coordinates and integral normalization.

§9.3: Elliptic structure and the radius. The pullback, compact pairings and neutral Fourier kinematics are ([MATH]). The ordinary E-string identification ([GEO-E]) uses Bhardwaj and Jefferson (2018, arXiv v6, §4.3, Eq. (4.23)), Douglas et al. (1996, arXiv v2, §§1.1–1.2), and the fiberwise setting of Vafa (1996, §2 and §§4–4.1). The calibrated and metric-matched wrapping dictionary ([GEO-E]) uses the ordinary calibrated membrane mass and Schwarz (1995, arXiv v5, Eqs. (26)–(30)). Jefferson et al. (2018, arXiv v3, §4.2.4, before Eq. (4.20)) identifies the special anticanonical fiber and refers to zero volume. The zero-period degeneration here is defined by $\mu = 0$; the finite positive relation (XIII.9.20) uses Bhardwaj and Jefferson (2018, arXiv v6, §3.1) and Douglas et al. (1996, arXiv v2, §1.2, before Eq. (1.1)). The physical dictionary does not follow from adjunction. Equation (XIII.9.23) is a consequence of the finite-circle kinematics for neutral free Fourier modes.

§§9.4–9.5: The flop and the daughter path. The compact-curve list follows from the two graph models ([MATH]). The relative ample classes, common blowup and equality of wall volumes are geometric calculations ([MATH]); the relative volume normalization uses the relative period frame of Chapter 2 and Jefferson et al. (2018, arXiv v3, §2.2, Eq. (2.10)). The compact-curve bound and section-ring contraction are ([MATH]); the concrete path is calculated here. The chart overlaps, fixed-a derivatives, changed path and positive cycle calculation in (XIII.9.28), (XIII.9.31), (XIII.9.38) and (XIII.9.48)–(XIII.9.50) develop the local flop charts, wall volumes and contraction calculation. The geometric strategy of moving a curve off the compact surface is described by Bhardwaj and Jefferson (2018, arXiv v6, §5.1, Fig. 3 and case 2) and Douglas et al. (1996, arXiv v2, §§1.2 and 2). Sufficient isolation remains a premise ([DEC]). The ordinary local dP_8 endpoint ([GEO-X]) is the named construction in Douglas et al. (1996, arXiv v2, §1.2, Eq. (1.1)) and Jefferson et al. (2018, arXiv v3, Table 3), with independent probe evidence in Seiberg (1996, arXiv v2, §4, after Eq. (4.5)).

§9.6: Period directions. The compact-support image and lattice splitting (XIII.9.52)–(XIII.9.60) are ([MATH]). The explicit integral projection (XIII.9.57)–(XIII.9.59) uses the same Gram matrix and introduces no charge assignment. The background interpretation ([GEO-E]) uses Bhardwaj and Jefferson (2018, arXiv v6, §3.1 and Eq. (4.23)), Seiberg (1996, arXiv v2, §5), and, for the conical construction, Closset, Giacomelli, et al. (2020, arXiv v4, Eq. (1.3)). It is not a normalizability theorem.

§9.7: External circles. The pure scale match ([MATH]) follows from (XIII.9.62)–(XIII.9.63) in the isometric product-circle frame; (XIII.9.64) is its reversible product-circle check. The same-X background chain ([GEO-E]) uses the ordinary M/IIA lift and the isometric T-duality of Volume III, Chapter 8. See Closset, Schäfer-Nameki, et al. (2020, arXiv v5, §2.5, Eq. (2.33) and the following paragraph) and Closset, Giacomelli, et al. (2020, arXiv v4, Fig. 1 and Eqs. (1.7)–(1.8)) for the distinction from the proposed three-dimensional relations. No new QFT transfer is asserted.

References

Bhardwaj, L. and P. Jefferson (2018). "Classifying 5d SCFTs via 6d SCFTs: Rank one". In: arXiv: `1809.01650 [hep-th]`.

Closset, C., S. Giacomelli, et al. (2020). "5d and 4d SCFTs: Canonical Singularities, Trinions and S-Dualities". In: arXiv: `2012.12827 [hep-th]`.

Closset, C., S. Schäfer-Nameki, and Y.-N. Wang (2020). “Coulomb and Higgs Branches from Canonical Singularities: Part 0”. In: arXiv: 2007.15600 [hep-th].

Douglas, M. R., S. Katz, and C. Vafa (1996). “Small Instantons, del Pezzo Surfaces and Type I’ Theory”. In: arXiv: hep-th/9609071.

Jefferson, P. et al. (2018). “On Geometric Classification of 5d SCFTs”. In: arXiv: 1801.04036 [hep-th].

Schwarz, J. H. (1995). “An SL(2,Z) Multiplet of Type IIB Superstrings”. In: arXiv: hep-th/9508143.

Seiberg, N. (1996). “Five Dimensional SUSY Field Theories, Non-trivial Fixed Points and String Dynamics”. In: arXiv: hep-th/9608111.

Vafa, C. (1996). “Evidence for F-Theory”. In: arXiv: hep-th/9602022.

Chapter XIII.10

Frozen singularities and discrete background data

XIII.10.1 Returning to the ALE singularity

In ordinary ALE engineering, the same curves that describe a resolution also explain gauge enhancement. The intersection matrix of the exceptional spheres is the negative Cartan matrix. When their areas vanish, M2-branes wrapped on the root cycles give the charged gauge bosons. This is the starting point of Chapter 1. We return to the local seven-dimensional system because it lets us vary a background field while holding the transverse singularity fixed.

Take the surface singularity of type E_6. Its metric geometry does not tell us whether the localized gauge algebra is $\mathfrak{e}_6$, $\mathfrak{su}(3)$, or zero. What distinguishes these possibilities is a phase of the M-theory three-form measured on a small three-sphere quotient surrounding the singular point. The phase changes which gauge bosons and resolution parameters are available. We shall calculate the size of the surviving gauge sectors and follow the same phase into an elliptic description, where it becomes part of the identification around a spacetime circle.

The local M-theory setup has sixteen supercharges and seven uncompactified directions. Only the degrees of freedom localized at the singularity enter our gauge counts. In particular, these counts do not include bulk fields or specify the global form of a gauge group.

XIII.10.2 Measuring the three-form on the link

How can a field whose curvature vanishes outside the singularity still affect the physics there? The exterior contains a closed cycle on which its potential can have nontrivial holonomy. For a finite subgroup $\Gamma \subset SU(2)$, let U be a small punctured neighborhood of the apex of $\mathbb{C}^2/\Gamma$. At a fixed radius ρ the link is

$$L_\rho = S^3_\rho/\Gamma, \qquad U \simeq (0,\epsilon) \times (S^3/\Gamma). \tag{XIII.10.1}$$

Orient L_ρ as the outward boundary of the small neighborhood of the apex. For E_6, Γ is the binary tetrahedral group of order 24. The link encloses the apex even as we move the measuring surface to a smaller radius.

A unit electrically charged membrane on a closed three-dimensional world volume measures a phase. In local units in which an integer period of the three-form gives phase one, define

$$H(L_\rho) = \exp(2\pi i r), \qquad r = \int_{L_\rho} C_3 \pmod 1. \tag{XIII.10.2}$$

Here the integral is shorthand for the normalized holonomy, with one choice of local reference field used throughout. It can be defined with patchwise potentials. If C_3^{phys} denotes the potential in the membrane action with coefficient T_{M2}, the same normalization reads $T_{\mathrm{M2}} \int C_3^{\mathrm{phys}} = 2\pi \int C_3$ for the local phase. The number r and the exponent in (XIII.10.2) are dimensionless.

Let W_{12} be the shell between L_{ρ_1} and L_{ρ_2}, with $\rho_1 < \rho_2$. Its inner boundary enters with a minus sign. The boundary rule for the holonomy, with normalized curvature G_4, gives

$$\partial W_{12} = L_{\rho_2} - L_{\rho_1}, \tag{XIII.10.3}$$

$$\frac{H(L_{\rho_2})}{H(L_{\rho_1})} = \exp\left(2\pi i \int_{W_{12}} G_4\right) = 1 \quad \text{if } G_4|_{W_{12}} = 0. \tag{XIII.10.4}$$

Thus r is measured in a flat exterior and is independent of the radius used to measure it. There is a further test if we ask whether the same background can extend over a smooth filling. If a smooth cap W has $\partial W = L$ and the field extends flat over it, then

$$H(L) = \exp\left(2\pi i \int_W G_4\right) = 1. \tag{XIII.10.5}$$

A nontrivial phase obstructs this particular flat extension. If we allow curvature in the cap, the last equality is no longer available. Likewise, $H(L) = 1$ removes this obstruction without constructing a smooth physical vacuum.

The shell calculation compares two measurements of one background. Its boundary orientation matters even when the answer is one. If we instead write both links with their outward orientations from the apex, the inner contribution must be moved to the other side of the boundary formula. More generally, put $\gamma = \int_{W_{12}} G_4$ in the same normalized units. Then the relation before imposing flatness is

$$r_{\rho_2} - r_{\rho_1} = \gamma \pmod 1. \tag{XIII.10.6}$$

For example, an inner period $1/2$ and a shell integral $1/6$ would give an outer period $2/3$. This is a conditional evaluation of the boundary rule. It does not construct a shell solving the M-theory field equations, or a path between frozen vacua. It explains exactly why flatness is needed when a period is carried from one measuring surface to another.

A nonzero flat period is possible on the punctured region because there is no cap in that region. The radial interval in (XIII.10.1) moves the link without contracting it

through the missing apex. Asking for a flat smooth cap changes the topology of the region on which the field is defined. The additional boundary relation (XIII.10.5) is the resulting constraint. Thus zero local curvature and trivial link holonomy answer different questions.

One can change the representative of r by an integer, or change the orientation of the measurement. These are different operations:

$$H(r+k) = H(r) \quad (k \in \mathbb{Z}), \qquad H(-L) = H(L)^{-1}. \tag{XIII.10.7}$$

For example, $-1/3$ and $2/3$ represent the same period on the oriented link. The phase at $2/3$ is the inverse of the phase at $1/3$. The half-period is its own inverse. In these examples,

$$H(1/2) = -1, \qquad H(1/3) = \exp(2\pi i/3), \qquad H(2/3) = \exp(-2\pi i/3). \tag{XIII.10.8}$$

The half and thirds in (XIII.10.8) have orders two and three. Phase multiplication in $U(1)$ need not preserve admissibility: the local E_6 classification permits $1/2$ and $1/3$, but not $5/6$. Nor does the order of Γ determine the allowed set.

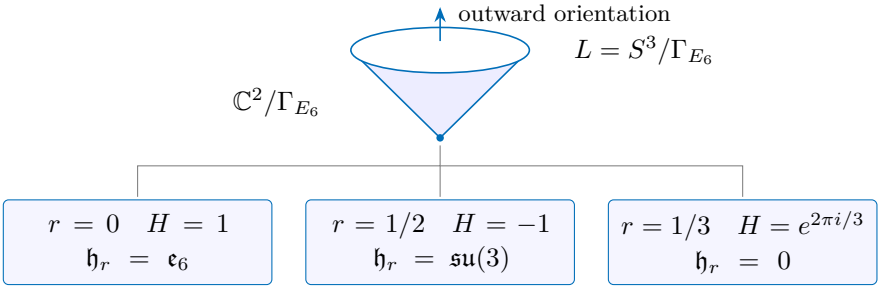


Figure XIII.10.1: One E_6 cone, with outward-oriented link L, and three choices of its local three-form period. The three boxes label separate backgrounds. The connectors compare them at fixed geometry and do not denote paths in moduli space. The period $2/3$ is the orientation inverse of $1/3$ and has the same zero gauge algebra.

The alternatives in Figure XIII.10.1 have the same link and the same algebraic surface germ. To predict the gauge sector we need the physical classification of the pair consisting of the germ and its phase.

XIII.10.3 Gauge algebra and allowed deformations

What changes in the localized gauge theory when only the link period changes? For this question we use the local frozen ADE classification. The construction behind the classification associates the period to the Chern–Simons invariant of a flat bundle on T^3 with simply connected compact structure group G of the original ADE type. Parallel transport around the three generators of $\pi_1(T^3)$ gives a commuting triple, up to simultaneous conjugation. The centralizer algebra of a triple consists of the generators

fixed by all three holonomies. The Chern–Simons invariant is constant on a connected component of the flat-connection space, even when the centralizer changes within that component. For example, switching on ordinary Cartan holonomies can reduce the centralizer while keeping $r = 0$. The frozen table uses the centralizer at the distinguished enhancement point of each selected component. In the ordinary component that point has three trivial holonomies. The M-theory correspondence takes the Langlands dual of the enhanced centralizer, exchanging roots and coroots. Here T^3 describes the bundle used in the classification, while L is where we measure C_3.

For the fixed E_6 germ the input is the assignment

r	0	$1/2$	$1/3$	$2/3$
$\mathfrak{h}_r$	$\mathfrak{e}_6$	$\mathfrak{su}(3)$	0	0

(XIII.10.9)

At zero holonomy this reduces to the ordinary ALE dictionary. At $1/2$ the singularity is partially frozen; at either third it is completely frozen, meaning that there is no localized gauge algebra. We use (XIII.10.9) as physical input and now work out what it implies. Counting roots in the resulting algebra cannot establish the table itself.

For $\mathfrak{e}_6$, use the realization inside the Euclidean E_8 root system. In terms of orthonormal basis vectors e_i of $\mathbb{R}^8$, the latter consists of

$$\{\pm e_i \pm e_j : i < j\} \quad \cup \quad \left\{ \tfrac{1}{2}(s_1, \ldots, s_8) : s_i = \pm 1,\ \prod_i s_i = 1 \right\}. \tag{XIII.10.10}$$

The E_6 subsystem is the intersection with the subspace $v_6 = v_7 = -v_8$. The three last coordinates of an integral root must all vanish, since an integral root has only two nonzero entries. For a half-integral root the last three signs are either $(+,+,-)$ or $(-,-,+)$. In the first case the first five signs must have odd parity of minus signs, in the second even parity. In either case choosing the first four signs determines the fifth. Consequently

$$N_{\text{integer}} = 4\binom{5}{2} = 40, \qquad N_{\text{half-integer}} = 2 \cdot 2^4 = 32, \tag{XIII.10.11}$$

$$|\Phi(E_6)| = 40 + 32 = 72, \qquad \operatorname{rank} E_6 = 5 + 1 = 6. \tag{XIII.10.12}$$

For the last equality, the integral roots span the first five coordinates and any half-integral root adds the direction with nonzero last coordinates. Both counts include positive and negative roots.

The root count also tells us which generators are being counted. In a Cartan decomposition, each root labels a one-dimensional complex root space. A compact real form has the same real dimension as the complex algebra has complex dimension. A pair $\alpha, -\alpha$ therefore contributes two real compact generators, rather than two additional Cartan directions. For E_6 this gives

$$\mathfrak{e}_6^{\mathbb{C}} = \mathfrak{t}^{\mathbb{C}} \oplus \bigoplus_{\alpha \in \Phi(E_6)} \mathfrak{g}_\alpha, \qquad 6 + 2\left(\frac{72}{2}\right) = 78. \tag{XIII.10.13}$$

This is the dimension of the enhanced algebra, where the root states can supply gauge generators. Moving to a generic Cartan expectation value changes which generators

are unbroken. It does not change the list of roots used to specify the algebra at the enhanced point.

At the half-period the algebra in (XIII.10.9) is of type A_2. Its roots are differences of basis vectors in $\mathbb{R}^3$. They span the plane in which the coordinates sum to zero, and every ordered pair of distinct coordinates supplies one root:

$$\Phi(A_2) = \{e_i - e_j : i \neq j,\ 1 \leq i, j \leq 3\}, \qquad |\Phi(A_2)| = 3 \cdot 2 = 6, \qquad \operatorname{rank} A_2 = 2. \tag{XIII.10.14}$$

At the completely frozen point there are no roots or Cartan generators in the localized gauge sector. Adding the rank to the root count gives the dimension of each algebra. The three outputs for $r = 0, 1/2, 1/3$ are

r	$\operatorname{rank} \mathfrak{h}_r$	$\lvert\Phi(\mathfrak{h}_r)\rvert$	$\dim \mathfrak{h}_r$
0	6	72	78
1/2	2	6	8
1/3	0	0	0

(XIII.10.15)

In particular the two nonzero ranks do not count exceptional curves of two different original cones. The cone is fixed. The numbers refer to the algebras appropriate to the different backgrounds.

There is a geometric way to see what the rank change asks of a resolution. At a generic point of the localized Coulomb branch the three real adjoint scalars of a seven-dimensional vector multiplet lie in a common Cartan subalgebra. Thus, locally and up to Weyl identification, the number of real scalar parameters is

$$\dim_{\mathbb{R}} \mathcal{M}_{\text{Cartan}} = 3 \operatorname{rank} \mathfrak{h}_r \in \{18, 6, 0\} \quad \text{for } r \in \{0, 1/2, 1/3\} \text{ respectively.} \tag{XIII.10.16}$$

At $r = 0$ the three numbers per Cartan direction have their familiar interpretation as periods of the hyperkähler forms over the exceptional curves. The underlying geometric intersection matrix still exists as a property of the bare resolution at nonzero r. It cannot tell us which of those deformations is available when the C-field is kept fixed. At $r = 1/3$ even the localized Cartan deformations are absent. This statement does not count spectator or bulk moduli.

For the half-period, the physical classification permits a partial branch with a fully frozen D_4 singularity left over. Its link can carry the same half-period. An elliptic model makes the proposed residual singularity concrete. Write an elliptic surface over a local base coordinate w with Weierstrass coefficients f, b_W and $\Delta = 4f^3 + 27b_W^2$ (the discriminant up to a constant). Start from

$$y^2 = x^3 + aw^2x + w^4, \qquad \Delta = w^6(4a^3 + 27w^2). \tag{XIII.10.17}$$

At $a = 0$, the orders of f, b_W, Δ at the origin are $(\infty, 4, 8)$, giving the IV^* fiber of the original E_6 model. For fixed $a \neq 0$ they become $(2, 4, 6)$. The leading cubic, found by writing $x = w\xi$ and dividing the right-hand side by w^3, is

$$\xi^3 + a\xi = \xi(\xi^2 + a). \tag{XIII.10.18}$$

It has three distinct roots over $\mathbb{C}$, giving a split I_0^* fiber and a residual D_4 surface singularity at $w = 0$. This Weierstrass calculation identifies the geometric endpoint

along one complex slice, parametrized by a. The six real parameters in (XIII.10.16) count the localized Cartan branch as a whole. The physical classification supplies a branch that can carry the original half-period to the D_4 point, where the remaining singularity contributes no enhanced gauge algebra.

We can examine how local this geometric comparison is by locating the other zeros of its discriminant. For $a \neq 0$, choose either square root w_* satisfying $w_*^2 = -4a^3/27$. Then

$$\Delta = 27w^6(w - w_*)(w + w_*), \qquad \left.\frac{d\Delta}{dw}\right|_{w=w_*} = 54w_*^7 \neq 0. \tag{XIII.10.19}$$

The central zero has order six and the other two zeros are simple. The assertion about the germ at $w = 0$ uses a disk smaller than $|w_*|$. It should not be read as a description of every fiber of the polynomial model. For two explicit choices of the existing parameter, the factors are

$$\begin{aligned} a = -3: &\quad \Delta = 27w^6(w^2 - 4), && w_* = 2, \\ a = -\frac{3}{4}: &\quad \Delta = 27w^6\left(w^2 - \frac{1}{16}\right), && w_* = \frac{1}{4}. \end{aligned} \tag{XIII.10.20}$$

Both nonzero choices have the same vanishing orders at the origin, but the second requires a smaller isolating disk. At $a = 0$ all eight orders of the discriminant coincide at the origin. This gives a concrete reason that the limit $a \to 0$ cannot be studied using one fixed disk that excludes the other zeros for every nonzero a. It also clarifies the hypothesis in the next construction: when we compare two enclosing cycles, we must know which singular points lie between them. No new gauge sector is being assigned to the additional zeros by this calculation.

XIII.10.4 From a link period to a circle identification

What becomes of the link period when the ALE singularity is placed in an elliptic surface? Take a local elliptic fibration $\pi : X_g \to \mathbb{C}_w$ with the relevant singularity over $w = 0$. Write $g \in SL(2, \mathbb{Z})$ for the action on elliptic one-cycles around a full positive loop in the w-plane, in a fixed basis. In the ordinary description, on a smooth torus patch one can reduce on one fiber circle and T-dualize the other. The local operation relates the elliptic fibration to a type IIB seven-brane on a spacetime circle. The choice of a fiber cycle is patchwise because the cycles can mix around $w = 0$. A nonzero C-field changes the identification along the spacetime circle.

To transport the period, take a small circle S^1_w enclosing the origin and its preimage $T = \pi^{-1}(S^1_w)$. This is a three-cycle, generally a torus bundle rather than a product. Assume that the exterior between T and the small link L is flat for the normalized C-field, and that no other link contributes to its period. Then

$$\partial W = T - L, \qquad \int_T C_3 = \int_L C_3 = r \pmod 1. \tag{XIII.10.21}$$

The three-cycle T is adapted to the elliptic duality because two of its directions lie in the fiber.

The local frame dictionary can be motivated by adding an auxiliary spacetime circle. Reducing on this circle leaves the period on T in the type IIA Ramond–Ramond three-form, since all legs of the period are on X_g. On each smooth torus patch, one T-duality along each of the two fiber circles removes the two fiber legs. This gives type IIA on the dual elliptic frame $\widehat{X}$ over the same w-plane, with a Ramond–Ramond one-form along the enclosing base circle. The normalized periods are

$$\int_T C_3^{\mathrm{M}} = r \;\longmapsto\; \int_T C_3^{\mathrm{IIA}} = r \;\longmapsto\; \oint_{S^1_w} C_1^{\mathrm{IIA}} = r \qquad \text{in } \mathbb{R}/\mathbb{Z}. \tag{XIII.10.22}$$

On these patches the lift of $\widehat{X}$ uses C_1^{IIA} as the connection of the new M-theory circle. Its Wilson period r is a translation in units of the circle circumference. This argument uses smooth fibers. At the central fiber we use the local M/F dictionary, which supplies a covering elliptic surface Y over the z-plane and a simultaneous identification of fiber, base and circle.

Let $r = n/d$ be the representative in $[0, 1)$ in lowest terms, including $(n, d) = (0, 1)$ for the trivial period. Winding d times around $w = 0$ makes the circle translation integral. On the degree d cover $w = z^d$, the resulting description uses a covering spacetime circle S^1_{cov} with coordinate $t \in \mathbb{R}/\mathbb{Z}$. The total lifted space is $(Y \times S^1_{\mathrm{cov}})/\mathbb{Z}_d$. Quotienting Y by the surface action alone gives the dual frame $\widehat{X}$. To obtain the F-theory description we shrink the generic elliptic fiber of Y in the total quotient, retaining the spacetime circle and its gluing. Write $\zeta = \exp(2\pi i/d)$. A positive base generator on the cover can be written in the active convention as

$$s : (z, t) \longmapsto (\zeta z, t + n/d). \tag{XIII.10.23}$$

For the nonzero periods in this chapter $d = 2, 3, 4$, and every relevant unit n obeys $n^2 \equiv 1 \pmod{d}$. The generator s^n of the same quotient shifts the circle by $1/d$. In these cases the active identification with the short circle step is therefore

$$A : (z, t) \longmapsto (\zeta^n z, t + 1/d), \qquad \lambda = \zeta^n. \tag{XIII.10.24}$$

For the selected inverse phases it is useful to see this change of generator without suppressing the arithmetic. At $r = 2/3$ the base positive generator s shifts the circle by $2/3$. Its square has

$$s^2 : (z, t) \longmapsto (e^{4\pi i/3} z, t + 4/3) = (e^{4\pi i/3} z, t + 1/3). \tag{XIII.10.25}$$

The equality of circle coordinates is modulo one. For $r = 3/4$, s^3 similarly rotates by $3/4$ of a turn and shifts by $9/4 = 1/4 \pmod 1$. The short positive circle step thus retains the numerator in its transverse rotation. Replacing it by $1/d$ in both entries would identify the wrong points for an inverse phase.

The action on the fiber data must accompany the action on the base; we will compute a lift in the next section. For $r = 0$ there is no quotient. When the end of a path at fixed covering z is described back at its initial circle coordinate, the identification acts by A^{-1} instead. The active formula specifies which way the two ends of the strip in Figure XIII.10.2 are identified.

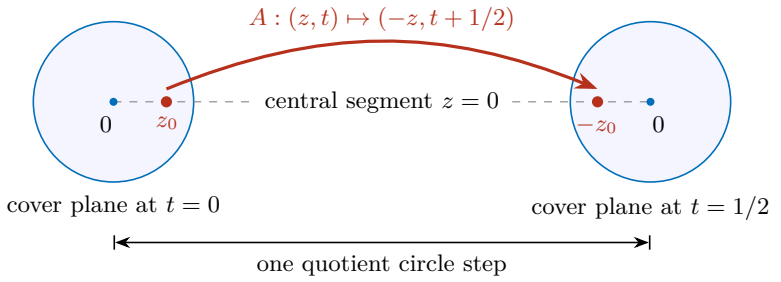


Figure XIII.10.2: The active diagonal action for the half-period, shown on one strip of the covering circle. The points z_0 at $t = 0$ and $-z_0$ at $t = 1/2$ are identified; their common image on the original transverse base is $w = z_0^2$. The marked segment over $z = 0$ has half the length of the covering circle. The transverse rotation shown here is the action on z; the elliptic coordinates transform as well.

The two parts of the action have different jobs. On the k-th step,

$$A^k(z,t) = (\lambda^k z, t + k/d), \qquad A^d(z,t) = (z,t). \tag{XIII.10.26}$$

For $1 \le k < d$ the shift is nonzero on the covering circle. The product action is therefore free even where the rotation fixes the base origin. If the covering circle has radius R_{cov}, the circumference over $z = 0$ becomes $2\pi R_{\mathrm{cov}}/d$ in the quotient. It is this circle that the seven-brane wraps in the compactified F-theory description. It is not the auxiliary circle used to explain (XIII.10.22).

The rotation selects $w = z^d$ as the first invariant positive power of z: the monomial z^p is invariant precisely when np is divisible by d. Write $z = \rho_z e^{i\varphi}$ on the punctured cover. A full positive loop $\varphi \mapsto \varphi + 2\pi$ winds w positively d times, so that the monodromy on this full cover loop is

$$g_{\mathrm{cover}} = g^d. \tag{XIII.10.27}$$

This full loop does not follow the compactification circle. Neither it nor its matrix specifies the active deck identification or parallel transport along an open path between its two base points. For example, if the original finite-order E_6 cone has opening angle $4\pi/6$, the base covering angle is

$$\Theta_{\mathrm{cover}} = d\,\Theta_{\mathrm{base}} = 4\pi/6,\ 8\pi/6,\ 12\pi/6 \qquad \text{for } d = 1, 2, 3 \text{ respectively.} \tag{XIII.10.28}$$

At $d = 3$ the base of the cover opens out to a plane. The quotient identification can still be nontrivial there.

A test field makes the identification visible without looking at any gauge bosons. Consider a scalar mode proportional to $e^{iq\varphi}e^{2\pi imt}$ on the punctured covering product, where q and m are integers. Under (XIII.10.24),

$$e^{iq\varphi}e^{2\pi imt} \longmapsto e^{2\pi i(nq+m)/d}\, e^{iq\varphi}e^{2\pi imt}, \tag{XIII.10.29}$$

$$\text{invariance} \quad \Longleftrightarrow \quad m + nq \equiv 0 \pmod{d}. \tag{XIII.10.30}$$

For the half-period, an angular mode with $q = 1$ descends only with odd m. A mode with $q = 0$ descends with even m, including the circle zero mode. The numerator matters as well: at $q = 1$, $r = 1/3$ selects $m = 2 \pmod 3$ while $r = 2/3$ selects $m = 1 \pmod 3$. This is a kinematic test of the quotient. A field carrying extra fiber or gauge quantum numbers must also transform by their action.

We can make the numerator test more systematic while remaining within the same scalar calculation. For $q = 0, 1, 2$, solving $m \equiv -nq \pmod 3$ gives

$$\begin{array}{c|ccc} & q=0 & q=1 & q=2 \\ \hline r=1/3 & m\equiv 0 & m\equiv 2 & m\equiv 1 \\ r=2/3 & m\equiv 0 & m\equiv 1 & m\equiv 2 \end{array} \qquad (\mathrm{mod}3). \tag{XIII.10.31}$$

For example, the $q = 2$ mode at $r = 1/3$ can have covering momentum $m = 1 + 3\ell$ with $\ell \in \mathbb{Z}$. Its angular phase contributes $2/3$ of a turn, while the circle phase contributes $1/3$ modulo one, so their product is one. At $r = 2/3$ the same angular mode requires $m = 2 + 3\ell$. The two phases have identical cover degree and identical full-loop monodromy, but different correlations between transverse angular dependence and circle dependence. Equation (XIII.10.31) is a test on the punctured cover. Smoothness at the transverse origin and any additional fiber transformation are separate conditions on an actual field.

XIII.10.5 Two different lifts over the same type IV fiber

Can two backgrounds have the same covering monodromy but different identifications of the resolved gauge cycles? To find out, we must retain the coordinate change used to make the base change minimal. Start from the monomial model $y^2 = x^3 + w^p$. At the origin the E_6 model uses $p = 4$. After $w = z^d$, write

$$e = \left\lfloor \frac{pd}{6} \right\rfloor, \quad b = pd - 6e, \qquad x = z^{2e}X, \qquad y = z^{3e}Y. \tag{XIII.10.32}$$

These powers remove the largest z^{6e} allowed by the simultaneous rescaling of x and y. On $z \neq 0$ the change of variables gives

$$z^{6e}\left(Y^2 - X^3 - z^b\right) = 0, \qquad Y^2 = X^3 + z^b \tag{XIII.10.33}$$

as the equation in the minimal coordinates. The discriminant is proportional to z^{2b}. For $p = 4, d = 2$ we get $e = 1, b = 2$ and Kodaira type IV. At $d = 3$ we get $e = 2, b = 0$, with smooth fiber $Y^2 = X^3 + 1$ of type I_0. The loop calculation agrees. In the chosen cycle basis it gives

$$g = \begin{pmatrix} -1 & -1 \\ 1 & 0 \end{pmatrix}, \qquad g^2 = \begin{pmatrix} 0 & 1 \\ -1 & -1 \end{pmatrix}, \qquad g^3 = \begin{pmatrix} 1 & 0 \\ 0 & 1 \end{pmatrix}. \tag{XIII.10.34}$$

Here g^2 is the full cover-loop matrix of type IV. The identity matrix at $d = 3$ is consistent with the explicitly smooth cover.

The number e is fixed by the weights of the Weierstrass equation. Removing one common factor of z^6 requires dividing x by z^2 and y by z^3. We can repeat this only while the exponent of the remaining constant term is nonnegative. In the two E_6 examples, the calculation is

$$\begin{array}{c|ccc} d & pd & 6e & b \\ \hline 2 & 8 & 6 & 2 \\ 3 & 12 & 12 & 0 \end{array}. \tag{XIII.10.35}$$

The coordinate substitution is invertible away from $z = 0$. At the central fiber it is a change to a minimal model, not an invertible coordinate chart on the original nonminimal equation. This distinction is why we examine its central singularity in the new variables, and why the induced deck phases must be recomputed in those variables. The residual exponent determines the equation; it does not determine the lift.

The active transformation $z \mapsto \lambda z$ leaves $w = z^d$ fixed. If we keep the original x, y fixed, their expressions in (XIII.10.32) force the minimal coordinates to move:

$$(z, X, Y) \longmapsto (\lambda z, \lambda^{-2e} X, \lambda^{-3e} Y). \tag{XIII.10.36}$$

In (XIII.10.33), all three monomials acquire the common factor λ^{-6e}, since $b + 6e = pd$. The local holomorphic two-form on the cover transforms as

$$\Omega = \frac{dz \wedge dX}{2Y} \quad \longmapsto \quad \lambda^{1+e}\Omega. \tag{XIII.10.37}$$

The phase is one for the covers considered here. These are calculations of a lift in the indicated algebraic charts. They are separate from assigning a transport matrix to the elliptic one-cycles along an open path.

For the E_6 half-period, (XIII.10.36) is $(z, X, Y) \mapsto (-z, X, -Y)$. To see its effect on the resolving curves of the type IV model, put

$$u = Y + z, \qquad v = Y - z, \qquad uv = X^3. \tag{XIII.10.38}$$

Blow up the origin. In the chart where X is the exceptional coordinate, write $u = Xu'$, $v = Xv'$. In the other charts, use u or v as the exceptional coordinate. The strict transforms are

$$u'v' = X \quad (X \text{ chart}), \qquad v' = u(X')^3 \quad (u \text{ chart}), \qquad u' = v(X')^3 \quad (v \text{ chart}). \tag{XIII.10.39}$$

Each equation solves for one coordinate, so the charts are smooth. The tangent-cone equation in the exceptional projective plane is $uv = 0$. Its two lines meet at one point and resolve the A_2 surface singularity. The half-period lift sends (u, v) to $(-u, -v)$, preserving both lines. A rotation of z alone with Y held fixed would send (u, v) to (v, u), interchanging them. It would also negate Ω. Thus it is possible to preserve the polynomial equation but get the wrong action on the resolution. The X chart also displays the intersection and the pointwise action explicitly. On the exceptional divisor $X = 0$, the strict transform is $u'v' = 0$. The two axes $u' = 0$ and $v' = 0$ meet at $u' = v' = 0$, and the differential of the defining equation $F = u'v' - X$ has

$$dF = v'\,du' + u'\,dv' - dX \neq 0. \tag{XIII.10.40}$$

Thus the crossing of the exceptional curves is a crossing inside a smooth surface. For the half-period, X is unchanged and $(u', v') \mapsto (-u', -v')$. A point on either axis usually moves along that axis. The component label is fixed because the axis is preserved as a set. This is the precise information that the diagram action records.

The component permutation detects the action on the Dynkin diagram. To obtain the gauge zero modes, we also need the specified gauge gluing. A circle-independent generator survives exactly when it returns to itself under the full gluing automorphism. Preserving the components alone would still allow an inner Wilson line. For the selected E_6 half-period the M/F dictionary specifies identity gauge gluing at the enhanced point, so the invariant algebra is $\mathfrak{su}(3)$. The lift verifies the associated trivial diagram action.

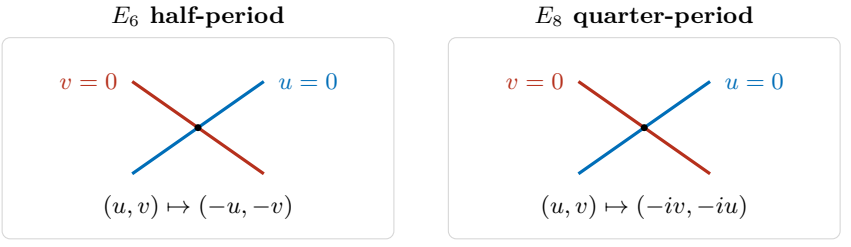


Figure XIII.10.3: The exceptional divisor in the type IV surface model $uv = X^3$ consists of the lines $u = 0$ and $v = 0$ in the blowup. Both panels use the same divisor. The lifted E_6 half-period fixes the labels of the lines; the lifted E_8 quarter-period exchanges them. Fixing a line as a component does not mean fixing each point on it.

The quarter-period of E_8 provides a comparison in the same covering geometry. In the source model take $p = 5, d = 4, n = 1$. Then $(e, b) = (3, 2)$, again of type IV. The chosen monodromy representative for the original II^* fiber gives

$$g_8 = \begin{pmatrix} 0 & -1 \\ 1 & 1 \end{pmatrix}, \qquad g_8^2 = \begin{pmatrix} -1 & -1 \\ 1 & 0 \end{pmatrix}, \qquad g_8^4 = \begin{pmatrix} 0 & 1 \\ -1 & -1 \end{pmatrix}. \tag{XIII.10.41}$$

The cover matrix is the same as g^2 in (XIII.10.34). But now $\lambda = i$, so the active lift is $(z, X, Y) \mapsto (iz, -X, -iY)$. Its action on the resolving lines is

$$(u, v) \longmapsto (-iv, -iu). \tag{XIII.10.42}$$

In the same X chart, the quarter-period sends

$$(X, u', v') \longmapsto (-X, iv', iu'), \qquad A^2 : (X, u', v') \longmapsto (X, -u', -v'). \tag{XIII.10.43}$$

The full geometric lift has order four, whereas the permutation of the two components has order two. These orders need not be equal. Changing to the inverse quarter $r = 3/4$ gives $\lambda = -i$, $X \mapsto -X$ and $Y \mapsto iY$, hence

$$(u, v) \longmapsto (iv, iu), \qquad (u', v') \longmapsto (-iv', -iu'). \tag{XIII.10.44}$$

The permutation remains an exchange even though the phases along the components reverse. This comparison uses the already selected quarter-period covers and does not select an allowed period from the equation.

The exchange in Figure XIII.10.3 verifies the nontrivial diagram action. For this background the physical dictionary supplies an outer involution as gauge gluing.

On traceless anti-Hermitian matrices a representative of this involution is $A \mapsto -A^{\mathsf{T}}$. Its fixed matrices satisfy both $A^{\mathsf{T}} = -A$ and $A^{\dagger} = -A$, so they are real antisymmetric 3×3 matrices. Thus the invariant algebra is $\mathfrak{so}(3) \cong \mathfrak{su}(2)$.

The dimension reduction under this particular involution can be seen without referring to a diagram. Let E_{ij} be the real matrix with a single unit entry. A real basis for $\mathfrak{su}(3)$ is formed by

$$\begin{aligned} L_{ij} &= E_{ij} - E_{ji}, & S_{ij} &= i(E_{ij} + E_{ji}) \quad (i < j), \\ H_1 &= i(E_{11} - E_{22}), & H_2 &= i(E_{22} - E_{33}). \end{aligned} \tag{XIII.10.45}$$

There are three L_{ij}, three S_{ij} and two H_a. Under $\sigma(A) = -A^{\mathsf{T}}$ they obey

$$\sigma(L_{ij}) = L_{ij}, \qquad \sigma(S_{ij}) = -S_{ij}, \qquad \sigma(H_a) = -H_a. \tag{XIII.10.46}$$

The fixed space has dimension three and the other eigenspace has dimension five. The first is a subalgebra, as the concrete brackets

$$[L_{12}, L_{23}] = L_{13}, \qquad [L_{12}, S_{12}] = 2H_1, \qquad [S_{12}, S_{23}] = -L_{13} \tag{XIII.10.47}$$

illustrate. In general the bracket of eigenspaces with signs ϵ, η lies in the eigenspace with sign $\epsilon\eta$, because σ preserves the bracket. The three fixed antisymmetric generators close as $\mathfrak{so}(3)$. Their complexification has rank one and two roots, reproducing the A_1 count for the sourced quarter-period algebra. This is an algebraic calculation once the gluing involution is specified; the component exchange by itself would not fix an arbitrary additional inner gluing.

This comparison explains why the gauge action cannot be read from the IV label or its full loop matrix alone. It does not replace the physical classification of allowed periods.

For the E_6 third-period there are no exceptional gauge curves on the cover. Nevertheless, for $r = 1/3$ and $\lambda = \exp(2\pi i/3)$, the same formula gives

$$(z, X, Y, t) \longmapsto (\lambda z, \lambda^2 X, Y, t + 1/3). \tag{XIII.10.48}$$

The circle gluing rotates the transverse coordinate and acts on the smooth elliptic fiber. Its existence is compatible with the trivial full-loop monodromy $g^3 = 1$. The case $r = 2/3$ reverses the two rotation phases while retaining the active $1/3$ circle shift.

XIII.10.6 The same monodromy with two orientifold signs

The frozen E_6 background led to an ordinary covering fiber with a nontrivial compactification. A different question arises for F-theory itself: can a seven-brane already be

frozen before it is compactified? To distinguish the two situations, consider a local I_4^* fiber. An ordinary realization is an $O7^-$ plane with eight coincident D7-branes. A frozen realization is a bare $O7^+$ plane. Here we count full D7-branes on the orientifold quotient, without counting a second copy of each image. One such D7-brane has charge $+1$ and the orientifold charges are ± 4. The two totals are

$$Q_- = (-4) + 8 = 4, \qquad Q_+ = 4 + 0 = 4. \tag{XIII.10.49}$$

They agree, but the sources of the charges differ.

For these configurations use the same monodromy convention as above. In a basis where one D7 contributes the unipotent matrix $T_7 = \left(\begin{smallmatrix} 1 & 1 \\ 0 & 1 \end{smallmatrix}\right)$, the orientifold factor includes the central sign on elliptic one-cycles. The product is

$$(-T_7^{-4})T_7^8 = -T_7^4 = \begin{pmatrix} -1 & -4 \\ 0 & -1 \end{pmatrix}, \tag{XIII.10.50}$$

which is also the monodromy of the bare positive orientifold. A local Weierstrass model exhibits the common Kodaira type. With z the local coordinate normal to the seven-brane, take

$$f = -3z^2, \qquad b_W = 2z^3(1 + z^4), \tag{XIII.10.51}$$

$$\Delta = 108z^6\big((1 + z^4)^2 - 1\big) = 108z^{10}(2 + z^4). \tag{XIII.10.52}$$

The orders are $(2, 3, 10)$. This calculation reads the common Kodaira data. It does not distinguish the orientifold projections.

For the negative orientifold, the coincident D7-branes have the orthogonal projection and support $\mathfrak{so}(16)$. Pulling the D7-branes away gives deformations of this configuration. In the positive case there are no D7-branes to move and no local D7 gauge algebra. The bare positive plane is a completely frozen F-theory seven-brane. The hat in $\widehat{I}_4^*$ distinguishes its physical background from the ordinary I_4^* background, without changing the monodromy in (XIII.10.50).

How does this genuinely frozen F-theory object look on an untwisted circle? T-duality along that circle produces two $O6^+$ planes at the two fixed points of the dual interval. The M-theory lift has two completely frozen D_4 points on the same elliptic fiber. Call the outward-oriented links of the two points L_1, L_2. The period around each point is a half-turn:

$$r_1 = r_2 = \tfrac{1}{2}, \qquad H(L_1) = H(L_2) = -1. \tag{XIII.10.53}$$

Now the outer elliptic three-cycle T surrounds both links. On the flat exterior W between them the oriented boundary is $\partial W = T - L_1 - L_2$. The same boundary rule used in (XIII.10.21) gives

$$H(T) = H(L_1)H(L_2) = 1, \tag{XIII.10.54}$$

$$r_T = r_1 + r_2 = 1 = 0 \pmod 1. \tag{XIII.10.55}$$

This vanishing agrees with the untwisted compactification. It does not make either interior period vanish. Nor can we replace both points by a single D_8 point with $r = 1/2$: that different local background has residual algebra of type C_4.

The boundary sum discards information in a way that can be stated precisely. It maps a pair of oriented link periods to one exterior period:

$$\mathcal{B} : (\mathbb{R}/\mathbb{Z})^2 \longrightarrow \mathbb{R}/\mathbb{Z}, \qquad \mathcal{B}(r_1, r_2) = r_1 + r_2. \tag{XIII.10.56}$$

Both $(0, 0)$ and $(1/2, 1/2)$ map to zero. This is a comparison of possible holonomy measurements, not an assertion that every pair in the domain is a physical frozen background. In the actual two-D_4 lift, a membrane phase measurement enclosing just one link still gives -1. A measurement enclosing both gives $+1$. Shrinking the latter surface onto just one point would cross or exclude the other boundary component and would not be the same comparison through a flat shell with no other contribution. The individual periods therefore remain necessary even when the exterior observer measures a trivial phase.

We can now separate the data that belong in a specification of the background. The ADE germ describes the geometry; the individual link periods specify the additional local M-theory data. In an elliptic frame the full-loop monodromy and the action used to glue a circle compactification answer different questions. Chapter 11 uses the pair of germ and period to index the three E_6 examples. Whether local choices extend to a consistent compact model is a separate problem.

XIII.10.7 Exercises

The first four exercises have exact answer checks. Give periods and phase angles as rational numbers of turns in $[0, 1)$, integer counts as integers, and monodromies in the displayed cycle bases. The remaining exercises ask for a written argument.

1. **An oriented link.** On the E_6 link, a local convention gives the representative $-4/3$ for the period. Find its representative in $[0, 1)$ and the representative on the oppositely oriented link. Use (XIII.10.9) to find the residual rank and number of roots for the original orientation.

2. **The inverse quarter-period.** In the E_8 model take $r = 3/4$, $p = 5$ and g_8 from (XIII.10.41). The local classification gives type A_1 at this period. Compute the residual exponent b of the minimal model, the full cover-loop matrix, and the permutation of the two lines of $uv = 0$, numbered 1 for $u = 0$ and 2 for $v = 0$. Give the rank and number of roots of A_1.

3. **Circle momentum and the numerator.** For E_6 at $r = 2/3$, compute the active transverse rotation, the active circle shift, and the phase of X in the minimal chart. With $q = 1$ in (XIII.10.30), state which of the residue classes $m = 0, 1, 2$ are invariant. Give the rotation, circle shift and X phase in units of a full turn.

4. **Exterior period of a frozen seven-brane.** For $O7^- + 8$ D7-branes and bare $O7^+$, give both net D7 charges and the common monodromy. Compute the order of the discriminant of the model (XIII.10.51). In the untwisted M-theory lift of the second configuration, compute the period on the outer cycle enclosing both D_4 points.

5. **Why the resolution matrix is insufficient.** Explain why the ordinary E_6 resolution matrix cannot choose among the residual algebras of (XIII.10.9). Use the flat-cap relation to specify a genuine obstruction and explain what additional information would be needed if the cap were allowed to carry curvature.

6. **Two tests of a seven-brane.** Compare the gauge algebras and available D7 motions in the two I_4^* realizations. Explain why the trivial exterior period of the frozen realization's untwisted lift does not allow one to remove the frozen data at the two points. Identify the assumption needed to use the boundary sum.

7. **Choosing the measuring disk.** In the family (XIII.10.17), determine the noncentral discriminant zeros for $a = -3/4$. Explain which radii isolate the central germ and why no fixed positive radius excludes the other zeros for every sufficiently small nonzero a. State which part of this conclusion is polynomial geometry and which physical conclusion about a fixed-period branch still needs the classification.

8. **Fixed generators and moving points.** Use (XIII.10.43) to compare the order of the geometric action with the order of its component permutation. Then use (XIII.10.46) to identify the fixed and anti-invariant real dimensions. Explain why knowing the component permutation would leave additional inner gluing undetermined.

Status and sources

§10.1–10.2: Ordinary ALE and normalized holonomy. Ordinary ADE enhancement ([GEO-X]) uses the zero-holonomy case only. See Chapter 1 and Tachikawa (2016, §1), and the resolved-to-singular comparison in Cvetič et al. (2025, §II A, Eqs. (2.1)–(2.8)). Equation (XIII.10.2) follows the period-one convention of Tachikawa (2016, Eq. (1.1)) and Cvetič et al. (2025, Eq. (2.9)); de Boer et al. (2002, Eq. (194)) put the factor of 2π in the potential used in their phase. Orientation, periodicity and the flat boundary relation ([MATH] conditional on this local reference holonomy) are shown in (XIII.10.4)–(XIII.10.7). See de Boer et al. (2002, §4.6.3) for the flat-field relation. No global shifted quantization assertion is used.

§10.3: Classification and deformations. The nonzero entries of (XIII.10.9) and the transfer rows for D_4, D_8, E_8 are imported physical classification ([GEO-E], with the stated limits on the frozen sector). See Tachikawa (2016, Eq. (1.1), Table 1 and §2) for the periods, centralizer description and partial freezing, and de Boer et al. (2002, Eq. (1) and §2.1.3) for the normalized Chern–Simons invariant of a component. The E_6 half-period row uses the A_2 algebra in Tachikawa's arXiv v2 Tables 1 and 3 and Cvetič et al. (2025, Tables I, II and VII). De Boer et al.'s Table 14 instead prints C_2 in that row. This is a different algebra: it has eight roots at rank two. The later row governs our calculation; no published correction to the older table is assumed. The root counts and real Cartan parameter arithmetic ([MATH]) use (XIII.10.11)–(XIII.10.16); the physical identification of the surviving parameters uses Cvetič et al. (2025, Appendix C, Eq. (C7)). The permitted half-period branch with a minimal frozen D_4 point is part of the local

classification ([GEO-E]); the geometric calculation (XIII.10.17) is separate ([MATH] with the Kodaira lookup of Tachikawa's Table 2).

§10.4–10.5: Elliptic frame and circle. The single-link M/F description ([GEO-E] in the specified local elliptic frame) follows Tachikawa (2016, §§1–2 and 4, Table 3) and Cvetič et al. (2025, §IV B, Eqs. (4.43)–(4.50)). The latter source distinguishes X_g, $\widehat{X}$, and Y in the dual-frame and quotient steps of Eqs. (4.46)–(4.49). The quotient and scalar-mode calculation (XIII.10.24)–(XIII.10.30), cover and monodromy calculations, and lifted action on exceptional lines ([MATH] within these models) are distinct from this frame input. The loop matrices and cone angles are Tachikawa's Tables 2–3; the sourced algebra actions used for interpretation are in the discussion following Table 3 and in Cvetič et al., Table VII and Appendix C. In particular, Tachikawa uses the known frozen algebras as input to select the outer actions in Table 3. The coordinate calculation tests the indicated actions on exceptional components; it supplies no new physical classification or general duality proof.

§10.6: The local frozen seven-brane. The two I_4^* realizations (sourced local physical comparison, [GEO-E] for the frozen extension of the ordinary dictionary) are in Tachikawa (2016, §1 and Table 2) and Bhardwaj et al. (2018, §§1, 2.1–2.2, Eqs. (2.2)–(2.6)). The charge, discriminant and monodromy arithmetic in (XIII.10.49)–(XIII.10.52) is [MATH] in that convention. The two-point M-theory lift (sourced local frame input, [GEO-E]) is the warm-up example of Tachikawa (2016, §3). Its exterior period is the conditional flat boundary calculation (XIII.10.54)–(XIII.10.55), tagged [MATH].

Expanded conditional calculations. Equations (XIII.10.6), (XIII.10.19)–(XIII.10.20), (XIII.10.25), (XIII.10.31), (XIII.10.35) and (XIII.10.40)–(XIII.10.47) give the blowup, discriminant and local root calculations under the stated geometric hypotheses ([MATH]). Equation (XIII.10.13) counts the local roots and Cartan directions; (XIII.10.56) develops the flat boundary calculation in the stated relative period frame. These computations add no physical classification row or stronger M/F claim. The discriminant zeros, quotient phases, blowup charts, compact-algebra eigenspaces and brackets have separate exact checks; the original bounded exercise contracts and their malformed/wrong-answer checks are retained.

References

Bhardwaj, L. et al. (2018). "The frozen phase of F-theory". In: *JHEP* 08, p. 138. DOI: 10.1007/JHEP08(2018)138. arXiv: 1805.09070 [hep-th].

Cvetič, M. et al. (2025). "Frozen generalized symmetries". In: *Phys. Rev. D* 111, p. 026018. DOI: 10.1103/PhysRevD.111.026018. arXiv: 2410.07318 [hep-th].

De Boer, J. et al. (2002). "Triples, Fluxes, and Strings". In: *Adv. Theor. Math. Phys.* 4, pp. 995–1186. DOI: 10.4310/ATMP.2000.v4.n5.a1. arXiv: hep-th/0103170.

Tachikawa, Y. (2016). "Frozen singularities in M and F theory". In: *JHEP* 06, p. 128. DOI: 10.1007/JHEP06(2016)128. arXiv: 1508.06679 [hep-th].

Chapter XIII.11

Atlas of M-theory engineering backgrounds

XIII.11.1 What an atlas entry specifies

What must agree before two constructions can be identified? The total spaces of the canonical bundles of $\mathbb{F}_0$ and $\mathbb{F}_1$ give the same signed cubic in a common gauge frame, yet their sections carry different electric charges and the theories have different discrete theta angles. Conversely, the very same E_6 surface germ can support several seven-dimensional gauge sectors. The extra information in that comparison is a three-form phase on the link. Neither the cubic nor the name of a singularity specifies all the data.

For a threefold X, we use ω for the class with positive periods on effective curves and $A = -\omega$ for the signed divisor class. We quote masses and tensions in common geometric units, suppressing the overall M2 and M5 tensions. A compact effective curve C and a compact effective surface S give the mass and string tension

$$t_C = \int_C \omega, \qquad T_S = \frac{1}{2}\int_S \omega^2, \qquad \mathcal{F} = \frac{1}{6}A^3. \tag{XIII.11.1}$$

On a noncompact X, the last expression means its terms with at least one compact divisor, with a purely background term fixed separately if two representatives are compared. A chamber records which curves are effective. A physical interpretation also specifies the spacetime dimension, which parameters are dynamical, which backgrounds are fixed, and which observable is being matched. Global charge and operator data require a choice at infinity beyond these local comparisons.

The atlas follows three tests. First compute positive periods and the intersection polynomial independently. Then state what operation relates two entries, if there is one. Finally match an observable in specified variables and state the range of the match. The same tests will distinguish a flop from a mass flow and an inherited Kaluza–Klein scale from an external spacetime circle.

The reader should already be able to evaluate a curve period, restrict an intersection to a compact surface, and differentiate a prepotential with its backgrounds fixed. We

shall use those operations to answer a more demanding question: which comparison should be made? A useful entry must let us recover the experiment as well as its result. For a particle mass this means specifying the effective curve and the parameters in its period. For a string it means specifying the primitive surface and the direction of differentiation. For a protected trace it also means specifying the circle, rotations and normalization.

The fixed inputs matter even when two results are numbers. An equality of string tensions at one point is weaker than equality of the tension functions in the same coordinates. Equality of those functions is still weaker than equality of the effective curve periods or of the boundary conditions. We will compare complete functions when they are available, and use selected numerical points to make the lost information visible. In particular, a comparison at equal inverse coupling need not agree with a comparison at equal instanton mass. Deciding what is held fixed is the first calculation, rather than a choice to be made after the answers have been obtained.

XIII.11.2 Equal cubics on different ruled surfaces

Can the prepotential determine the charge of an effective section? Let $S = \mathbb{F}_n$, with section s and fiber f. Choose the noncompact divisor D with $D|_S = f$, and put $\omega = -aS + m_0 D$. Here a is the compact Coulomb coordinate and m_0 the background inverse coupling in the gauge frame. For the local canonical bundle, adjunction gives $S|_S = K_S$. The ruled intersection matrix and canonical pairings are

$$s^2 = -n, \qquad s \cdot f = 1, \qquad f^2 = 0, \tag{XIII.11.2}$$

$$K_S \cdot s = n - 2, \qquad K_S \cdot f = -2, \qquad K_S = -2s - (n+2)f. \tag{XIII.11.3}$$

Indeed both curves are rational, so $K_S \cdot C = -2 - C^2$. Solving these pairings gives the last formula. Squaring it cancels the n dependence, and intersecting with f gives the mixed term. Thus

$$(S^3, S^2 D, S D^2) = (K_S^2, K_S \cdot f, f^2) = (8, -2, 0), \tag{XIII.11.4}$$

$$\mathcal{F}(a, m_0) = m_0 a^2 + \frac{4}{3} a^3, \tag{XIII.11.5}$$

$$T_S = \partial_a \mathcal{F} = 2m_0 a + 4a^2, \qquad \partial_a^2 \mathcal{F} = 2m_0 + 8a. \tag{XIII.11.6}$$

Here ∂_a inserts the primitive compact divisor at fixed m_0. In the pure $SU(2)$ gauge frame use the Cartan generator $H_{\mathrm{g}} = \mathrm{diag}(1, -1)$, with $\mathrm{Tr}_{\mathbf{2}}\, H_{\mathrm{g}}^2 = 2$. The classical quadratic is $m_0 a^2$, and the two roots ± 2 give $2(2a)^3/12$. This reproduces the geometric result at $a > 0$.

The periods retain precisely the information lost by squaring K_S. Write (q, I) for the coefficients of (a, m_0) in a curve period, so the two columns in the following matrix are the two marked charge vectors.

$$t_s = m_0 + (2-n)a, \qquad t_f = 2a, \qquad \begin{pmatrix} q_s & q_f \\ I_s & I_f \end{pmatrix} = \begin{pmatrix} 2-n & 2 \\ 1 & 0 \end{pmatrix}. \tag{XIII.11.7}$$

For $n = 0$, every integral combination has even q; for $n = 1$, the section itself has odd q. Both charge matrices have determinant -2. An index alone would therefore miss the way each lattice sits in the fixed gauge frame. The compact pairing is even on $\mathbb{F}_0$, since $(bs + cf)^2 = 2bc$, and odd on $\mathbb{F}_1$, since $s^2 = -1$. This parity survives an integral change of basis. At $a = 2$ and $m_0 = 4$ the section masses are 8 and 6, the fiber mass is 4, and both string tensions are 32. The half-area and the period see different parts of the geometry.

In the weak gauge region $m_0 \gg a > 0$ the section is the chosen unit-instanton generator and $q/2$ is its electric charge in units where the W has charge one. The web dictionary identifies $\theta = 0$ on $\mathbb{F}_0$ and $\theta = \pi$ on $\mathbb{F}_1$, with endpoints E_1 and $\widetilde{E}_1$ and flavor algebras A_1 and $\mathfrak{u}(1)$, respectively. This matching uses a separate identification of the instanton. The cubic has no coefficient that gives the discrete angle.

The Kähler inequalities are $a > 0$ and $m_0 + (2 - n)a > 0$. For example, substituting $(a, m_0) = (2, -3)$ for $\mathbb{F}_1$ gives $T_S = 4$ and $\partial_a^2 \mathcal{F} = 10$, but $t_s = -1$. Positive tension and kinetic coefficient do not certify a chamber. At fixed $m_0 > 0$, taking a to zero collapses the ruling while a section has positive area. Along $m_0 = 0$, both generators on $\mathbb{F}_0$ or $\mathbb{F}_1$ shrink. The toric contraction of the compact surface then gives a point. The distinction can be seen in the height-one polygons. The four rays for $\mathbb{F}_n$ can be projected to $(0, 1), (1, 0), (0, -1), (-1, n)$, with the compact ray at the origin. Deleting this ray coarsens its smooth star to a single cone for $n = 0, 1$; for $n = 2$ the outer boundary has collinear marked points and the period of the section is already zero on the proposed $m_0 = 0$ slice.

We can now change the comparison itself. Suppose the W mass and the marked section mass are prescribed, rather than a and m_0. Put the common section mass equal to σ, retaining $a > 0$. The two entries then require different background values:

$$m_0^{(0)} = \sigma - 2a, \qquad m_0^{(1)} = \sigma - a, \qquad t_s^{(0)} = t_s^{(1)} = \sigma, \qquad t_f^{(0)} = t_f^{(1)} = 2a. \tag{XIII.11.8}$$

Thus matching the two displayed particle masses has used up a change of coupling. Substituting these values into the already calculated string tensions gives

$$T_0 = 2a\sigma, \qquad T_1 = 2a\sigma + 2a^2, \qquad T_1 - T_0 = 2a^2. \tag{XIII.11.9}$$

For $a = 2$ and $\sigma = 8$, the two backgrounds are 4 and 6. The two section masses are eight and the two fiber masses are four, but the tensions are 32 and 40. Matching the masses of the marked generators therefore does not match the intersection pairing that computes the surface area. The two comparisons answer different questions: the earlier one fixed the gauge-frame coordinates and exposed the section charge; this one fixes the two periods and exposes the compact pairing.

A derivative along a path must be distinguished from the fixed-background derivative. As a separate example, take $\mathbb{F}_1$ with $m_0 = b + a$ and b constant. This differs from the fixed-section-mass path $m_0 = \sigma - a$. Along the former path, the chain rule gives

$$\frac{d}{da}\mathcal{F}(a, b + a) = \partial_a \mathcal{F}|_{m_0 = b+a} + \partial_{m_0}\mathcal{F}|_{m_0 = b+a} = 2ba + 6a^2 + a^2. \tag{XIII.11.10}$$

The primitive tension is the first term, $2ba + 6a^2$. The additional a^2 comes from varying the noncompact background while moving along the path. A table of tensions must

therefore retain its fixed-background prescription even when its coordinates are later replaced by measured periods.

The projective plane gives a useful control. For the line H, $H^2 = 1$ and $K_S = -3H$, so that $S^3 = 9$ and $t_H = 3a = t$. The normalized line coordinate does not change the primitive compact divisor:

$$\mathcal{F} = \frac{9}{6}a^3 = \frac{t^3}{18}, \qquad T_S = 3\partial_t \mathcal{F} = \frac{t^2}{2}. \tag{XIII.11.11}$$

Its outer rays over $(1,0), (0,1), (-1,-1)$ have determinant of absolute value three, with their average the deleted ray. The resulting scalar $\mathbb{Z}_3$ quotient is the point contraction associated with E_0. There is no ordinary ruling gauge chamber in this example. Table XIII.11.1 makes explicit which columns still differ after two cubics agree. The next comparison explains how either ruled surface can arise from a common geometry.

Local space	$\mathcal{F}$	Periods	q	$\theta/(2\pi)$	Endpoint
$K_{\mathbb{F}_0}$	$\frac{4a^3}{3} + a^2 m_0$	$2a + m_0$, $2a$	2, 2	0	E_1
$K_{\mathbb{F}_1}$	$\frac{4a^3}{3} + a^2 m_0$	$a + m_0$, $2a$	1, 2	$\frac{1}{2}$	$\widetilde{E}_1$
$K_{\mathbb{P}^2}$	$\frac{t^3}{18}$	t	3	not assigned	E_0

Table XIII.11.1: On a ruled surface the entries are in section, fiber order. The projective plane has just the line generator.

XIII.11.3 A flop followed by a mass flow

What remains after crossing a mass wall at finite parameters, and what leaves only at large mass? Blow up one point of $\mathbb{F}_0$ and write B, F for the pulled-back rulings and E for the exceptional curve. The intersection numbers are $B^2 = F^2 = B \cdot E = F \cdot E = 0$, $B \cdot F = 1$, and $E^2 = -1$. Let $R = F - E$ and $L = B - E$. The canonical class is $K_S = -2B - 2F + E$. Restrict the coupling and mass divisors by $D_0|_S = F$ and $D_m|_S = E - F/2$. Intersecting $\omega|_S = -aK_S + m_0 F + m(E - F/2)$ with the three generators then gives

$$t_E = a - m, \qquad t_R = a + m, \qquad t_L = a + m_0 + \frac{m}{2}. \tag{XIII.11.12}$$

All three periods must be positive in the central chamber. For instance $F \cdot R = 0$ and $(E - F/2) \cdot R = 1$. The signed weights on $R, -E$ have values $m + a, m - a$, the two weights of the selected full fundamental hypermultiplet. Since $K_S^2 = 7$, $K_S \cdot F = -2$, $K_S \cdot (E - F/2) = 0$, and $(E - F/2)^2 = -1$, the supported intersections give the central polynomial

$$\begin{aligned} \mathcal{F}_{\text{mid}} &= m_0 a^2 + \frac{7}{6}a^3 - \frac{1}{2}am^2 \\ &= m_0 a^2 + \frac{4}{3}a^3 - \frac{|m+a|^3 + |m-a|^3}{12}, \quad |m| < a. \end{aligned} \tag{XIII.11.13}$$

Terms depending only on the background are matched with the same representative across the walls.

At the isolated wall where $C = E$ or R vanishes, the other two periods stay positive. The two normal directions to C in the threefold are both of degree -1. The flop exchanges the two rulings of the exceptional quadric P in the common blowup. Write u, v for the two blowdowns and $d = A \cdot C = -t_C$. To descend along the other ruling one needs $v^*A' = u^*A + dP$, since u^*A has degree d and P has degree -1 on that ruling. The restrictions to P give $P^3 = 2$, $u^*A \cdot P^2 = -d$, and $(u^*A)^2 \cdot P = 0$. Expansion therefore gives

$$\mathcal{F}' - \mathcal{F} = \frac{1}{6}\big(3d^2(-d) + 2d^3\big) = -\frac{d^3}{6} = \frac{t_C^3}{6}. \tag{XIII.11.14}$$

The new exterior curve has period $-t_C$. The cubic change is negative on the outer side and leaves the first two Coulomb derivatives continuous at the wall. Its third Coulomb derivative raises 7 to 8 on either side. The effective triples follow from blowing down C on the compact surface. If J survives and $\overline{J}$ is its image, its pullback must pair to zero with C. Since $C^2 = -1$, the two pullback calculations give

$$\pi_C^*\overline{J} = J + (J \cdot C)C, \tag{XIII.11.15}$$

$$L \cdot E = 1, \qquad F \cdot E = L \cdot R = F \cdot R = 0, \tag{XIII.11.16}$$

$$\big(\pi_E^*\overline{L}, \pi_E^*\overline{F}\big) = (L + E, F), \qquad \big(\pi_R^*\overline{L}, \pi_R^*\overline{F}\big) = (L, F). \tag{XIII.11.17}$$

The transported class has the same degree on each displayed pullback as the continuation of ω in the old marking. The section periods are therefore $t_L + t_E$ and t_L, and either fiber has $t_F = t_R + t_E = 2a$. With $-t_C$ for the new exterior curve, the periods in section, fiber, exterior order are

$$m > a \qquad (2a + m_0 - m/2,\ 2a,\ m - a), \tag{XIII.11.18}$$

$$m < -a \qquad (a + m_0 + m/2,\ 2a,\ -m - a). \tag{XIII.11.19}$$

Since $L + E = B$, the first image has square zero. The second image retains $L^2 = -1$. These classes and the new exterior curve must all have positive period.

For example, take $a = 1$, $m_0 = 4$ and compare $m = 2$ and $m = -2$. Both exterior curves have period 1 and both signed changes relative to the continued central polynomial are $-1/6$. The remaining periods are $(5, 2)$ and $(4, 2)$. A wall crossing therefore changes the chamber while leaving a curve of finite mass. Taking its absolute mass in the old geometry would lose this information.

The mass flow is a subsequent operation. With $M = |m| > a$, expand the two absolute cubes in the gauge expression:

$$\mathcal{F}_{\text{out}} = \left(m_0 - \frac{M}{2}\right)a^2 + \frac{4}{3}a^3 - \frac{M^3}{6}. \tag{XIII.11.20}$$

The last term is purely background. At fixed $\widehat{m}_0 = m_0 - M/2$ and a, the two periods on the surviving surface stay finite and the exterior period $M - a$ diverges. With

the finite sector isolated, the positive branch gives $K_{\mathbb{F}_0}$ and the negative branch $K_{\mathbb{F}_1}$. Figure XIII.11.1 distinguishes these limiting operations from the flops and from adding an external circle. The elliptic example will use the same order of operations to separate an inherited circle scale.

For a concrete use of the mass-flow relation, choose $a = 2$ and $\widehat{m}_0 = 3$. Along the positive and negative paths take $m = \pm M$ and $m_0 = 3 + M/2$. Substitution into (XIII.11.19) gives

$$(t_s, t_f, t_{\text{ext}})_+ = (7, 4, M-2), \qquad (t_s, t_f, t_{\text{ext}})_- = (5, 4, M-2), \qquad M > 2. \tag{XIII.11.21}$$

At $M = 3$ the exterior particle has mass one in either branch. It has crossed the wall but is still lighter than the selected fiber particle. At $M = 9$ it has mass seven, while both compact periods have kept their original values. Only the latter direction of change can make the exterior object parametrically heavy relative to every fixed compact period. Its mere presence outside the compact surface does not remove it from the theory.

An energy window makes this distinction usable. Choose a fixed comparison scale Λ large enough to include the finite sector of interest, and then increase M so that

$$a,\ |\widehat{m}_0| \ll \Lambda \ll M - a, \qquad a, \widehat{m}_0, \Lambda \text{ fixed as } M \longrightarrow \infty. \tag{XIII.11.22}$$

These inequalities describe which threshold leaves the chosen local window. The isolation conditions of the construction remain needed to neglect bulk sectors. At fixed $m_0 = 5$, by contrast, the two section periods at $a = 2$ would be $9 - M/2$ and $7 - M/2$. They reach zero at $M = 18$ and $M = 14$, respectively. The naive large-mass path would leave both selected positive chambers before reaching infinity. Renaming $m_0 - M/2$ after that failure would not repair the path.

The surviving prepotential can also be compared before and after subtracting its background piece. On the prescribed path,

$$\mathcal{F}_{\text{out}} + \frac{M^3}{6} = \widehat{m}_0 a^2 + \frac{4}{3}a^3, \qquad \partial_a \mathcal{F}_{\text{out}}|_{m_0, M} = 2\widehat{m}_0 a + 4a^2. \tag{XIII.11.23}$$

A background-only subtraction changes neither this tension nor the kinetic coefficient. It changes the representative of the full polynomial, which is why the wall jump was compared before making that subtraction. The relation table must retain both prescriptions: a continuous representative for the finite flop, and a specified finite sector for the subsequent limit.

XIII.11.4 A KK scale and a five-dimensional point

When does a geometry with a finite elliptic period give an isolated five-dimensional fixed point? On the rational elliptic surface S_9 of Chapter 9, let $f = 3H - \sum_{i=1}^{9} E_i$ be the fiber and E a section of self-intersection -1. Since $H^2 = 1$ and the exceptional classes have square -1, $f^2 = 0$. The section meets the fiber once. Take the displayed

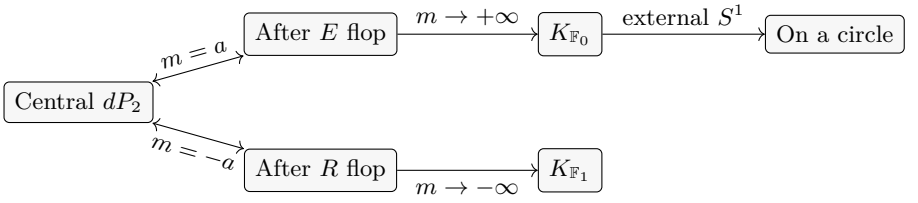


Figure XIII.11.1: The finite walls change the small resolution. The following limits remove the exterior curve at fixed $\widehat{m}_0$. The circle in the last step is introduced in spacetime.

zero flavor mass slice with $\omega_- = af + \mu E$ on the surface. Direct intersection gives

$$f^2 = 0, \qquad f \cdot E = 1, \qquad E^2 = -1, \tag{XIII.11.24}$$

$$(t_f, t_E, T_{S_9}) = \left(\mu,\ a - \mu,\ a\mu - \frac{\mu^2}{2}\right), \qquad 0 < \mu < a. \tag{XIII.11.25}$$

In the E-string construction the neutral fiber period measures the KK gap, $\mu = 1/R_6$ in common units. Its vanishing Coulomb charge is visible directly from $f^2 = 0$. A finite period by itself gives no enumeration of the KK spectrum.

It is impossible to send μ to infinity at fixed a while remaining in this chamber. At $\mu = a$ the section has normal bundle $\mathcal{O}(-1) \oplus \mathcal{O}(-1)$. Its blowdown has local equation $uy - vx = 0$. Resolving the projectivized ratio of the columns of the matrix $\left(\begin{smallmatrix} u & v \\ x & y \end{smallmatrix}\right)$ or the ratio of its rows gives the two small resolutions. On the flopped side the compact surface is $S_8 = dP_8$ and the new curve E' is exterior. If $\pi : S_9 \to S_8$ blows down E and $k = -K_{S_8}$, the canonical divisor formula gives

$$f = \pi^* k - E, \qquad \omega_- = a(\pi^* k - E) + \mu E = a\pi^* k + (\mu - a)E. \tag{XIII.11.26}$$

Transport of the curve degrees through the two resolutions then gives

$$\omega_+|_{S_8} = ak, \qquad k^2 = 1, \qquad t_{E'} = \mu - a, \tag{XIII.11.27}$$

$$t_k = a, \qquad t_{k+E'} = a + (\mu - a) = \mu, \qquad T_{S_8} = \frac{a^2}{2}. \tag{XIII.11.28}$$

The transported total fiber is $k + E'$. The curve class k in the compact surface alone does not measure the original circle radius.

For example, at $a = 2$, $\mu = 1$ the triple of total fiber period, current section period, and compact half-area is $(1, 1, 3/2)$. At $\mu = 4$ the appropriate triple is $(4, 2, 2)$, where the middle entry is now the exterior curve born from the section flop. The old section period would be -2. Taking its absolute value would happen to give the new exterior period, but would not give the new compact half-area or identify the two pieces of the total fiber.

One can now hold $a > 0$ fixed and send μ to infinity. The exterior curve becomes heavy, while every fixed effective curve class C on the compact surface retains period

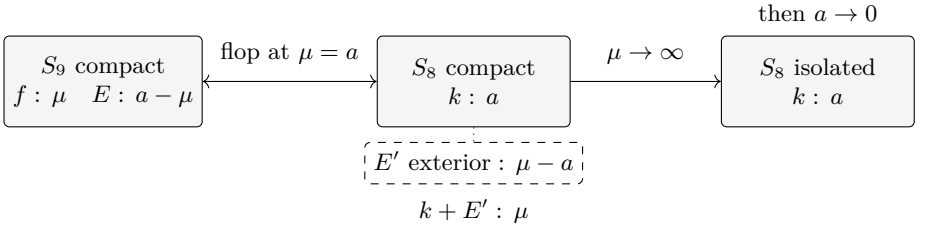


Figure XIII.11.2: At the wall the section moves outside the compact surface. Its new period adds to the period of the compact class k to give the period of the total fiber.

$a\,k \cdot C$. Here k is ample, and the local limit isolates K_{S_8}. A second operation sends a to zero. The section ring of the ample class contracts this zero section to its vertex. This selected contraction gives the ordinary rank-one E_8 fixed point. Its zero flavor mass cubic is

$$\mathcal{F}_{S_8} = \frac{a^3}{6}. \tag{XIII.11.29}$$

The flopped geometry already has compact cube one, before it loses the independent KK scale. A positive compact cube cannot replace the two operations.

The compact area gives a particularly instructive comparison across these entries. At fixed a, its derivative with respect to the inherited scale on the two sides of the wall is

$$\partial_\mu T_{S_9}|_a = a - \mu, \qquad \partial_\mu T_{S_8}|_a = 0, \qquad T_{S_9}|_{\mu=a} = T_{S_8} = \frac{a^2}{2}. \tag{XIII.11.30}$$

The area and this first response agree at the wall. Beyond the wall the area has lost all dependence on μ, although the full construction still has that parameter. At $a = 3$ two post-flop backgrounds give

μ	$t_{k+E'}$	$t_{E'}$	T_{S_8}
5	5	2	9/2
8	8	5	9/2

(XIII.11.31)

The two compact surfaces have identical periods on every fixed compact class, since $\omega_+|_{S_8} = ak$ in both cases. A particle on the exterior curve distinguishes them immediately. Thus even equality of all compact periods in this slice does not discard a background threshold. The isolated daughter is obtained by sending that threshold out of the retained window, rather than by observing an equality of compact areas.

This comparison also locates the two limits physically. Sending $\mu \to \infty$ at fixed a sends $R_6 \to 0$ in the inherited radius interpretation. It removes a compactification scale while the compact surface remains finite. Sending $a \to 0$ after isolating the daughter collapses that surface. Reversing the order would encounter the boundary of the selected local description with a finite independent scale still present. The local area formulas determine which objects shrink or become heavy; the named E_8 endpoint uses the ordinary contraction dictionary already specified above.

The background counts give another test. On either local canonical bundle, real divisor classes retract to the compact surface; quotient by the one compact divisor

class. The elliptic surface has rank ten before this quotient and the degree-one del Pezzo has rank nine. On the elliptic side the period functional of f descends to the quotient because $f \cdot K_{S_9} = -f^2 = 0$. The analogous functional of k does not descend since $k \cdot K_{S_8} = -1$. The remaining ranks on the two sides are therefore organized as

$$10 - 1 = 8_{\text{flavor}} + 1_{\text{KK}}, \qquad 9 - 1 = 8_{\text{flavor}} + 0_{\text{KK}}. \tag{XIII.11.32}$$

These are ranks for the stated local parameter problem; no integral global form is inferred. Table XIII.11.2 shows why the intermediate and isolated geometries must stay separate even though their compact areas agree. In the next comparison the circle is an extra spacetime input, so there is no analogous change of internal chamber.

Geometry	S^3	T_S	Backgrounds	Flavor	KK
Rational elliptic dP_9	0	$a\mu - \frac{\mu^2}{2}$	9	8	1
Flopped E-string geometry	1	$\frac{a^2}{2}$	9	8	1
Isolated K_{dP_8}	1	$\frac{a^2}{2}$	8	8	0

Table XIII.11.2: The new compact surface has the same cube and tension before and after the inherited KK scale is removed. The last three columns count background, flavor, and KK directions.

XIII.11.5 A protected coefficient on an external circle

What changes when the same internal threefold is used on a spacetime circle? Take local $\mathbb{F}_0$ and an external circle of circumference $\beta = 2\pi R$, as in Figure XIII.11.3. Let w be the positive root mass, so $w = 2a_5$ in the earlier five-dimensional normalization and $w = \sqrt{2}a_{\text{SW}}$ in the indicated four-dimensional normalization. Work in the positive electric chamber with periodic fermions around the circle. The two plane rotations, with equivariant parameters e_1, e_2, preserve the supercharge used in the trace. The continued fugacities are

$$q = e^{-\beta e_2}, \qquad t = e^{\beta e_1}, \qquad X = e^{-\beta w}. \tag{XIII.11.33}$$

Let Q_b count base degree. Divide the refined vertex series by its base-degree-zero, pure fiber factor. Thus V_1 is the coefficient of Q_b in $1 + Q_b V_1 + O(Q_b^2)$. The two internal Young diagrams label the two base edges of the local $\mathbb{F}_0$ square. At base degree one they have one box in total. In the framing of the normalized products from Chapter 8, the common factor $\sqrt{qt}$ is multiplied by $(t/q)^{1/2}$ or $(t/q)^{-1/2}$, giving the weights t and q:

$$\begin{aligned} V_1 &= \frac{1}{(1-q)(1-t)(1-X)} \left(\frac{t}{1-Xt/q} + \frac{q}{1-Xq/t} \right) \\ &= \frac{q+t}{(1-q)(1-t)(1-Xt/q)(1-Xq/t)}. \end{aligned} \tag{XIII.11.34}$$

In the common denominator the numerator in parentheses is $t(1-Xq/t)+q(1-Xt/q) = (q+t)(1-X)$, so the apparent $1-X$ pole cancels.

On the gauge side I_{AK} is the instanton fugacity of the framed index. After its degree-zero normalization, Z_1 is the coefficient of I_{AK}. The independent one-instanton expression is

$$Z_1 = \frac{1}{(1-1/q)(1-t)}\left(\frac{1}{(1-t/(qX))(1-X)} + \frac{1}{(1-1/X)(1-tX/q)}\right). \quad \text{(XIII.11.35)}$$

Using $1-u^{-1} = -(1-u)/u$ in both terms gives

$$Z_1 = \frac{qX/t}{(1-q)(1-t)(1-X)}\left(\frac{q}{1-Xq/t} + \frac{t}{1-Xt/q}\right), \quad \text{(XIII.11.36)}$$

$$Q_b V_1 = I_{\mathrm{AK}} Z_1, \qquad I_{\mathrm{AK}} = \frac{t}{q}\frac{Q_b}{X}. \quad \text{(XIII.11.37)}$$

For example, at $(q,t,X) = (1/2, 1/4, 1/8)$, the two rotation-dependent denominator factors are $15/16$ and $3/4$. The coefficient is $128/45$, and the fugacity multiplier I_{AK}/Q_b is 4. Dropping the rotation factor would give 8 for the multiplier even though the base degree had been counted correctly.

There is a second comparison that would be invisible in an unrefined specialization. Interchange q and t at fixed X. The two rotation-dependent denominator factors exchange places, so that

$$V_1(t,q,X) = V_1(q,t,X), \qquad \frac{(I_{\mathrm{AK}}/Q_b)(t,q,X)}{(I_{\mathrm{AK}}/Q_b)(q,t,X)} = \frac{q^2}{t^2}. \quad \text{(XIII.11.38)}$$

For the preceding values the common coefficient remains $128/45$. After the interchange the fugacity multiplier is sixteen rather than four. This is compatible with equality of the two protected expressions, since the independently normalized Z_1 changes along with its multiplier. A comparison that recorded only the symmetric coefficient would lose how its base-degree variable is translated to the gauge instanton variable. At $q=t$ the extra factor is one and this loss cannot be detected. Keeping two independent rotations is therefore part of the test, even though the final vertex coefficient is symmetric in them.

To take the additive limit set $Q_b = X\beta^4 P$ with P fixed and let β go to zero. The four denominator factors of V_1, divided by β, tend to $e_2, -e_1, w-e_1-e_2, w+e_1+e_2$, respectively. The numerator tends to two. Away from these poles one obtains

$$\lim_{\beta\to 0} Q_b V_1 = -\frac{2P}{e_1 e_2\big(w^2-(e_1+e_2)^2\big)}. \quad \text{(XIII.11.39)}$$

The scaling is fixed by counting the four vanishing factors, not by identifying Q_b with a four-dimensional parameter at finite radius. For small β their leading terms are

$$1-q = \beta e_2 + O(\beta^2), \qquad 1-t = -\beta e_1 + O(\beta^2), \quad \text{(XIII.11.40)}$$

$$1-Xt/q = \beta(w-e_1-e_2)+O(\beta^2), \qquad 1-Xq/t = \beta(w+e_1+e_2)+O(\beta^2). \quad \text{(XIII.11.41)}$$

Thus V_1 has leading order β^{-4} away from the four indicated poles. The prescribed Q_b supplies the compensating four powers. The factor X tends to one, while $q+t$ tends to two. If $w = e_1 + e_2$, one denominator loses its nonzero linear slope, and this derivation cannot be used at that point. Such a pole is a change in the stated meromorphic limit, not an error to remove by taking an absolute value.

The minus sign is in the stated continued equivariant frame. At $(e_1, e_2, w) = (2, 1, 4)$ the coefficient of P is $-1/7$. This matches one protected degree with fixed normalization. It does not identify every protected sector or establish equivalence of the full theories at finite radius. The internal threefold remained fixed throughout. A fixed internal germ can also hide a different kind of physical input, which we consider next.

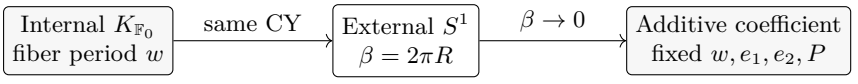


Figure XIII.11.3: The radius in this comparison belongs to an added spacetime circle. The second arrow compares one finite-circle coefficient with its additive limit.

XIII.11.6 A frozen phase needs a background

Does fixing the bare E_6 germ fix its gauge algebra? Its oriented link is $L = S^3/\Gamma_{E_6}$, where Γ_{E_6} is the binary tetrahedral subgroup of $SU(2)$. Write C_3 for the flat three-form potential normalized so that a unit membrane acquires phase one from an integer period. Its holonomy on L is

$$\exp\left(2\pi i \int_L C_3\right) = e^{2\pi i r}, \qquad r \in \mathbb{R}/\mathbb{Z}. \tag{XIII.11.42}$$

The orientation is outward. Reversing it takes r to $-r$. For instance $4/3$ represents $1/3$, and the reversed class is $2/3$. The phases of the two representatives are complex conjugate. Both choices can be assigned to the same oriented bare link. The lattice of the ordinary resolution is unchanged as a geometric invariant of the bare germ.

The frozen classification for this germ gives the residual algebras shown in Table XIII.11.3. The ordinary intersection lattice cannot derive this assignment. One can, however, check its numerical consequences. With simple roots α_i of square length two, write v for the vector of root coefficients and $\mathbf{e}_i$ for the unit vector representing α_i. With Cartan matrix $C_{\mathfrak{h}}$, reflection in α_i gives

$$s_i(v) = v - (C_{\mathfrak{h}} v)_i \, \mathbf{e}_i. \tag{XIII.11.43}$$

At half-period the two A_2 simple roots pair to -1, so $s_1(\mathbf{e}_2) = \mathbf{e}_2 + \mathbf{e}_1$ represents $\alpha_2 + \alpha_1$. Closing under both reflections gives the six roots $\pm\alpha_1, \pm\alpha_2, \pm(\alpha_1 + \alpha_2)$ of A_2, so its dimension is $2 + 6 = 8$. The older C_2 assignment would give eight roots and dimension ten. At zero period the D_5 subsystem of E_6 contributes 40 roots and the two sets of sixteen outside it give 72 in all, so the dimension is $6 + 72 = 78$. With three

r	Gauge algebra	Rank	Roots	Dimension	Minimal cover fiber
0	E_6	6	72	78	IV^*
$\frac{1}{2}$	A_2	2	6	8	IV
$\frac{1}{3}$	0	0	0	0	I_0
$\frac{2}{3}$	0	0	0	0	I_0

Table XIII.11.3: Changing the three-form phase leaves the bare E_6 germ fixed. Equal residual algebras do not identify the two oriented third-period entries.

real Cartan scalars per rank in a residual seven-dimensional gauge sector, the four rows have $18, 6, 0, 0$ such scalars. These counts concern the indicated gauge sector.

In the selected elliptic description of the same germ, choose the base monodromy g of the IV^* fiber. Write the phase as $r = n/d$ in lowest terms. A cover of order d maps one full cover loop to d base loops, hence monodromy g^d.

$$g = \begin{pmatrix} -1 & -1 \\ 1 & 0 \end{pmatrix}, \qquad g^2 = \begin{pmatrix} 0 & 1 \\ -1 & -1 \end{pmatrix}, \qquad g^3 = \mathbf{1}. \tag{XIII.11.44}$$

To see the fiber type on the cover, pull back the base coordinate by $w_{\mathrm{base}} = z^d$. The local Weierstrass equation becomes $y^2 = x^3 + z^{4d}$. Substituting $x = z^{2\ell}x'$, $y = z^{3\ell}y'$ cancels 6ℓ powers of z. The minimal exponent is

$$b = 4d - 6\ell, \qquad \ell = \left\lfloor \frac{4d}{6} \right\rfloor. \tag{XIII.11.45}$$

For $d = 1, 2, 3$ it is $4, 2, 0$, giving $\mathrm{IV}^*, \mathrm{IV}, \mathrm{I}_0$. The exponent on the cover detects the denominator here. In the local M/F-theory presentation the quotient on the cover coordinate z and normalized covering circle coordinate $\tau \in \mathbb{R}/\mathbb{Z}$ has generator

$$(z, \tau) \longmapsto \left(e^{2\pi i n/d} z,\ \tau + 1/d \right). \tag{XIII.11.46}$$

At $d = 3$ the monodromy on the cover is trivial but this combined rotation and translation still has order three. The denominator and the vanishing residual algebra cannot recover the numerator. This is why Figure XIII.11.4 compares backgrounds on the same germ, with the two thirds related by orientation reversal, without depicting a flow between them. Nor does a frozen gauge entry infer a five-dimensional fixed point. The ordinary threefold example below has an E_6 *flavor* algebra and illustrates a different use of the same name.

To use the two third-period entries, retain the first quotient action, not just its order. Write $\zeta = e^{2\pi i/3}$. Iterating the specified generator gives

$$(z, \tau) \longmapsto (\zeta^{nj} z, \tau + j/3), \qquad j = 0, 1, 2, 3, \qquad n = 1 \text{ or } 2. \tag{XIII.11.47}$$

For $n = 1$ the rotations have exponents $0, 1, 2, 0$ modulo three; for $n = 2$ they have exponents $0, 2, 1, 0$. At $j = 3$ the circle translation is an integer and the rotation is

trivial in both cases. Nevertheless the first rotation has a different phase. This is exactly the information retained by the numerator of r, after the cover and residual gauge algebra have forgotten it.

For example an outward period $7/3$ gives the $1/3$ entry, because its exponential is ζ. Reversing the orientation gives $-7/3 = 2/3 \bmod 1$ and exponential ζ^{-1}. Both have a smooth cover and zero residual continuous gauge algebra. Neither of those common properties licenses deleting the oriented phase column. At $r = 1/2$, on the other hand, the inverse phase equals the original one. Orientation reversal therefore acts differently on the half-period and third-period records, despite being the same operation on the link. This comparison uses the allowed backgrounds already specified; orbit arithmetic by itself would not decide which fractions are allowed on a different germ.

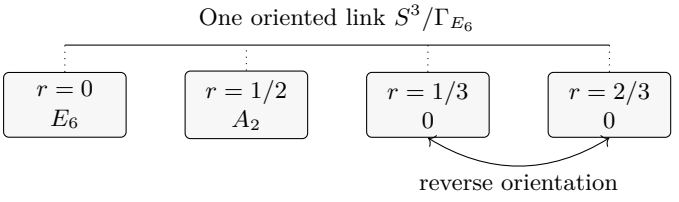


Figure XIII.11.4: The fixed link sits above four background choices. Only the orientation comparison is drawn as an arrow.

XIII.11.7 What the other ordinary lattices measure

When do the same root operations measure a kinetic term, a Coulomb chamber, or a flavor character? Consider three examples. On the ordinary A_2 ALE, choose the two compact spheres C_i over segments joining adjacent centers. As illustrated in Figure XIII.11.5, their charge roots can be written $\alpha_i = \mathbf{e}_i - \mathbf{e}_{i+1}$ in three orthonormal coordinates. Write C for the positive Cartan matrix and η_i for the compact Poincaré duals. The two sphere classes have

$$C = \begin{pmatrix} 2 & -1 \\ -1 & 2 \end{pmatrix}, \qquad C_i \cdot C_j = -C_{ij}. \tag{XIII.11.48}$$

Multiplying the duals by the inverse pairing gives

$$\lambda_i = -\sum_j (C^{-1})_{ij}\eta_j, \qquad \int_{C_j} \lambda_i = \delta_{ij}. \tag{XIII.11.49}$$

The square-integrable harmonic representatives are anti-self-dual. The Hodge inner product changes the sign of their intersection, and the change of basis introduces two inverse matrices. The result in the unit-period frame is

$$\int \lambda_i \wedge *\lambda_j = (C^{-1})_{ij}, \qquad C^{-1} = \frac{1}{3}\begin{pmatrix} 2 & 1 \\ 1 & 2 \end{pmatrix}. \tag{XIII.11.50}$$

For example the off-diagonal entry is $1/3$, while in the simple coroot frame it is -1. The six roots and ordinary enhancement describe a seven-dimensional gauge algebra, without a compact threefold cubic. Adding the external M-theory circle in the fixed string scale limit of Chapter 1 gives the indicated six-dimensional $(1,1)$ gauge effective theory. The link of the ALE is a different cycle from that circle.

A change of basis explains why the two kinetic matrices can both be correct. Regard the forms as a column vector. From (XIII.11.49) one has $\eta = -C\lambda$. If a two-form is written with coefficient vectors v and u in the two bases, then

$$\Omega = \sum_i v_i \eta_i = \sum_i u_i \lambda_i, \qquad u = -Cv, \qquad \|\Omega\|^2 = v^{\mathsf{T}} C v = u^{\mathsf{T}} C^{-1} u. \quad \text{(XIII.11.51)}$$

For $v = (2,1)^{\mathsf{T}}$ the unit-period coefficients are $u = (-3,0)^{\mathsf{T}}$, and both expressions give six. Using $(2,1)$ in the inverse matrix instead gives $14/3$. It is the norm of a different form. In a comparison of kinetic coefficients, transforming the matrix while retaining the old field coefficients changes the object being compared. The sign of one matrix entry is therefore not a test of equivalence between the two frames; the transformed quadratic expression is.

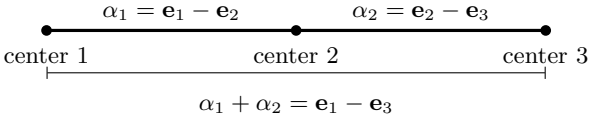


Figure XIII.11.5: Adjacent pairs give the two simple roots. Their sum corresponds to the outer pair, with the shared center canceled.

Now take the original rank-two gauge chamber of the $Y^{3,0}$ threefold. Name the height-one rays by their projected points, using the same letters for their toric divisors.

P	D_1	D_2	D_3	D_4	U_1	U_2
u	0	1	0	-1	0	0
v	3	0	0	3	1	2

(XIII.11.52)

Join each consecutive segment of the axis D_3, U_1, U_2, D_1 to each of D_2, D_4 and take the cones over these triangles. The compact divisors are $(S_1, S_2) = (U_2, U_1)$ and we choose $D = D_4$, so $A = pS_1 + qS_2 - hD$. The effective generators are the two ruling fibers f_1, f_2 and the common curve $C = S_1 \cap S_2$ over the edge U_1U_2. Their ordered divisor degrees and periods against $\omega = -A$ are

	D_1	D_2	D_3	D_4	U_1	U_2	period
f_1	1	0	0	0	1	-2	$x = 2p - q$
f_2	0	0	1	0	-2	1	$y = 2q - p$
C	0	1	0	1	-1	-1	$z = h + p + q$

(XIII.11.53)

For example, the opposite rays at U_1U_2 obey $v_{D_2} + v_{D_4} = v_{U_1} + v_{U_2}$, with $v_P = (u, v, 1)$. The corresponding row paired with $(0,0,0,h,-q,-p)$ gives z. The chamber has $x, y, z > 0$.

On each surface the other compact divisor restricts to the section C, the background divisor to f_i, and the surface itself to $K_i = -2C - 3f_i$. Since $C^2 = -1$, $Cf_i = 1$ and $f_i^2 = 0$, restriction gives the five compact degrees

$$(S_i^3, S_i^2 S_j, S_i^2 D, S_1 S_2 D, S_i D^2) = (8, -1, -2, 1, 0), \qquad i \neq j. \tag{XIII.11.54}$$

For instance $S_i^2 S_j = K_i \cdot C = -1$. Expanding $A^3/6$ gives the polynomial in the second line below. In the gauge calculation the eigenvalues $(p, q-p, -q)$ give positive roots $x, y, x+y$. Their cubes divided by six plus the classical quadratic give the first line, at bare nonabelian level zero.

$$\mathcal{F} = h(p^2 + q^2 - pq) + \frac{x^3 + y^3 + (x+y)^3}{6} \tag{XIII.11.55}$$

$$= h(p^2 + q^2 - pq) + \frac{4}{3}(p^3 + q^3) - \frac{p^2 q + pq^2}{2}, \tag{XIII.11.56}$$

$$\partial_p \mathcal{F} = x(z + x/2), \qquad \partial_q \mathcal{F} = y(z + y/2). \tag{XIII.11.57}$$

In particular, $(p, q, h) = (3, 2, 4)$ gives $(x, y, z) = (4, 1, 9)$ and tensions $(44, 19/2)$. Both derivatives hold h fixed. When $z = 0$ with $x, y > 0$, both tensions are still positive. A zero curve period does not imply a zero surface area, and this entry asserts no UV endpoint.

The curve periods also let us design a comparison without choosing new gauge coordinates by guesswork. Invert their first two relations:

$$p = \frac{2x + y}{3}, \qquad q = \frac{x + 2y}{3}, \qquad h = z - x - y. \tag{XIII.11.58}$$

Thus holding the two ruling periods x, y fixed and varying z holds the Coulomb point fixed while changing h. The two string areas respond linearly:

$$\partial_z T_1|_{x,y} = x, \qquad \partial_z T_2|_{x,y} = y. \tag{XIII.11.59}$$

For $(x, y) = (4, 1)$ we have $(p, q) = (3, 2)$. The inputs $z = 1$ and $z = 3$ correspond to $h = -4$ and $h = -2$ and give

$$(T_1, T_2)|_{z=1} = (12, 3/2), \qquad (T_1, T_2)|_{z=3} = (20, 7/2). \tag{XIII.11.60}$$

Both points obey the stated geometric chamber inequalities. The negative values of the background coefficient here are not a claim of a weak bare gauge description at negative inverse coupling. The period and area calculation remains a geometric comparison within that chamber. Letting z reach zero gives $(8, 1/2)$, with finite ruling periods and two finite surface areas. This is a direct witness for the distinction between a curve boundary and a point contraction: the calculation names the quantities that would still have to vanish.

In the ordinary local dP_6 entry the E_6 roots have another role. Use a generic marked blowup of the plane at six points, with no three collinear and no conic through all six. Let H be the pullback of a line and E_i the six exceptional curves. The canonical class

is $K_S = -3H + \sum_i E_i$. Write a candidate root as $U = dH - \sum_i b_i E_i$. The equations $K_S \cdot U = 0$ and $U^2 = -2$ become

$$\sum_i b_i = 3d, \qquad \sum_i b_i^2 = d^2 + 2, \qquad 9d^2 \le 6(d^2+2). \tag{XIII.11.61}$$

Thus $|d| \le 2$. To grade these roots, use $I = d - b_1$. At $d = 0$ the coefficients contain one 1 and one -1, so five vectors contribute to each of grades $1, -1$ and twenty to grade zero. At $d = 1$, three coefficients are 1, giving ten each at grades zero and one; $d = -1$ supplies the negatives. At $d = 2$ all six coefficients are 1 and the grade is one, with its opposite at $d = -2$. There are therefore $16, 40, 16$ roots in grades $-1, 0, 1$. Including the six neutral Cartan generators gives $16, 46, 16$ and total dimension 78, matching the selected x^2 index character. Here x in the index denotes the index fugacity, unrelated to the curve period in the preceding example.

To see the five-flavor gauge chamber in this marking, take the pencil of lines through the first point. Its generic fiber is $F = H - E_1$, with section $B = E_1$. For $i = 2, \dots, 6$, the line through the first and ith points splits into E_i and $R_i = F - E_i$. The coupling lift restricts to F and the mass lift for m_i restricts to $J_i = E_i - F/2$. Pairing the class $-aK_S + m_0 F + \sum_{i=2}^{6} m_i J_i$ with the curves gives

$$t_F = 2a, \qquad t_{E_i} = a - m_i, \qquad t_{R_i} = a + m_i, \quad i = 2, \dots, 6. \tag{XIII.11.62}$$

Each split fiber gives the two signed weights of one full fundamental in this gauge frame. For the supported cubic, $K_S^2 = 3$, $K_S \cdot F = -2$, $K_S \cdot J_i = F \cdot J_i = 0$, and $J_i \cdot J_j = -\delta_{ij}$. The result is

$$\mathcal{F} = m_0 a^2 + \frac{a^3}{2} - \frac{a}{2} \sum_{i=2}^{6} m_i^2. \tag{XIII.11.63}$$

What information would be lost if the mass column were replaced by the compact cubic alone? In this fixed lift the answer is explicit. Define $S_m = \sum_{i=2}^{6} m_i^2$. At fixed backgrounds,

$$T_S = 2m_0 a + \frac{3}{2} a^2 - \frac{1}{2} S_m, \qquad \partial_a^2 \mathcal{F} = 2m_0 + 3a. \tag{XIII.11.64}$$

Only S_m occurs in the fixed-background cubic and its first derivative, and the second derivative loses it. Compare the two mass vectors

$$(m_2, m_3, m_4, m_5, m_6) = (1,0,0,0,0), \qquad (3/5, 4/5, 0, 0, 0). \tag{XIII.11.65}$$

Both have $S_m = 1$. At $a = 2, m_0 = 4$ both therefore give $\mathcal{F} = 19$, $T_S = 43/2$, and kinetic coefficient fourteen. The two first split fibers, however, have periods

	(t_{E_2}, t_{R_2})	(t_{E_3}, t_{R_3})
$(1,0,0,0,0)$	$(1,3)$	$(2,2)$
$(3/5, 4/5, 0, 0, 0)$	$(7/5, 13/5)$	$(6/5, 14/5)$

(XIII.11.66)

All displayed split-fiber periods are positive. These selected inequalities alone are not a replacement for checking every effective generator of the chosen compact chamber. The

comparison shows what the polynomial forgets in its fixed real mass frame: it retains a quadratic mass combination while the marked particle periods resolve the individual masses. It does not claim that continuous rotations of the mass vector are physical flavor identifications.

The ordinary point contraction gives the E_6 flavor enhancement of the five-dimensional construction. The character check tests the grading of one coefficient. It gives neither the global flavor group nor a relation to the seven-dimensional gauge entry with the same algebra.

XIII.11.8 Read the entries with their relations

Table XIII.11.4 collects the examples used in the chapter. Its second column is the internal geometry and its third is the spacetime of the recorded sector. Distinct rows can have the same internal geometry. A missing determination, such as the line operators in one of the ruled surface examples, cannot be read as zero or as trivial global form. The comparisons are local and assume that unwanted bulk degrees of freedom are decoupled or can be neglected at the stated scales.

Entry	Internal geometry	Spacetime
Ordinary A_2 ALE	ALE surface	7D
$K_{\mathbb{F}_0}$	CY threefold	5D
$K_{\mathbb{F}_1}$	CY threefold	5D
Central dP_2 chamber	CY threefold	5D
After the E flop	CY threefold	5D
After the R flop	CY threefold	5D
$K_{\mathbb{P}^2}$	CY threefold	5D
$Y^{3,0}$ gauge chamber	CY threefold	5D
Ordinary K_{dP_6}	CY threefold	5D
Rational elliptic dP_9	CY threefold	5D
Flopped E-string geometry	CY threefold	5D
Isolated K_{dP_8}	CY threefold	5D
$K_{\mathbb{F}_0}$ on a circle	CY threefold	5D on a circle
E_6 link, $r = 0$	ALE surface	7D
E_6 link, $r = 1/2$	ALE surface	7D
E_6 link, $r = 1/3$	ALE surface	7D
E_6 link, $r = 2/3$	ALE surface	7D

Table XIII.11.4: The selected backgrounds. Separate chamber, circle and holonomy entries retain the data lost in a list of bare spaces.

In Table XIII.11.5, a flop exchanges small resolutions of an isolated curve wall with matched boundary data. A mass flow sends an actual scale to infinity while keeping the specified finite sector. Circle reduction adds a spacetime identification with its own scale. A background comparison holds the bare germ fixed and changes the phase, while the orientation comparison keeps track of its inverse. The last two rows of this type give comparisons of specified inputs, not motions through Kähler chambers.

Starting entry	Relation	Compared entry
Central dP_2 chamber	flop	After the E flop
Central dP_2 chamber	flop	After the R flop
After the E flop	mass flow	$K_{\mathbb{F}_0}$
After the R flop	mass flow	$K_{\mathbb{F}_1}$
$K_{\mathbb{F}_0}$	circle reduction	$K_{\mathbb{F}_0}$ on a circle
Rational elliptic dP_9	flop	Flopped E-string geometry
Flopped E-string geometry	mass flow	Isolated K_{dP_8}
E_6 link, $r = 0$	background comparison	E_6 link, $r = 1/2$
E_6 link, $r = 0$	background comparison	E_6 link, $r = 1/3$
E_6 link, $r = 1/3$	orientation comparison	E_6 link, $r = 2/3$

Table XIII.11.5: Each relation names the operation or comparison that justifies placing the two entries together.

For a proposed identification, first specify which data are matched. For example, two tensions may agree while the periods of the marked unit-instanton curves disagree. If the proposed identification concerns genuine line operators, the boundary conditions and charge lattice at infinity must be supplied. Agreement of one protected coefficient, a cubic, or a residual Lie algebra does not provide those inputs.

A practical route through the tables starts with an observable. Suppose we want a pure rank-one gauge comparison after removing one massive fundamental. Start at the central dP_2 row, select the sign of m, and follow the corresponding flop relation. Record which curve has become exterior. Then follow the mass-flow relation with $\widehat{m}_0$ fixed. The target surface is $\mathbb{F}_0$ or $\mathbb{F}_1$ according to that sign. Only after selecting this route should the equal pure cubics be compared. The distinct marked section charges and theta assignments stay in the target records. There is no step in this route that identifies the two targets.

Suppose instead the desired observable is the degree-one protected coefficient on a circle. Start with the $\mathbb{F}_0$ target and follow the external-circle relation. Supply β, the periodic spin structure, e_1, e_2, and the normalization of the trace. The finite comparison then uses the monomial map, and its additive limit uses $Q_b = X\beta^4 P$. This path changes spacetime and the observable, while the internal geometry stays the same. It cannot be substituted for the elliptic-parent route, whose inherited radius remains visible in $k + E'$ and is removed by a different mass-flow operation.

Table XIII.11.6 summarizes the information needed to perform these comparisons. The last column states what must still be supplied if the question is made stronger. It is useful when a common entry in the middle column tempts us to identify two backgrounds.

A blank determination is also informative. For example, the local period calculations do not specify which charged lines can end at infinity. The global-data field remains unresolved even in entries where every displayed period and cubic is known. Likewise a five-dimensional cubic is not applicable to the seven-dimensional ALE gauge entry; it is not a zero cubic. Keeping these two cases distinct prevents a missing answer from being used as evidence for an identification.

Question	Required comparison	Further input for a stronger claim
Same compact tension?	Primitive surface, Coulomb coordinate, fixed backgrounds and half-area	Effective particle periods and boundary conditions for a theory identification
Same finite sector after a flow?	Heavy threshold, held shifted coupling and surviving periods	Isolation of the retained sector from bulk modes
Same protected coefficient?	Degree, normalization, rotations and fugacity map	Other protected degrees and sectors for a full trace
Same gauge algebra on a link?	Bare germ, oriented three-form phase and residual-algebra assignment	Global completion and operator data

Table XIII.11.6: Choose the comparison by the quantity to be measured. An equality answers the stated question with these inputs.

Take-home message of this chapter

Match the observable and the conditions under which it was computed. Positive curve periods tell you which chamber is available, a mass limit tells you which degrees of freedom survive, and the background specifies which theory the geometry supports.

XIII.11.9 Exercises

Use `benchmark/tasks.json` to find the question IDs and `benchmark/PROTOCOL.md` for submission. Give exact values in Exercises 1–5. Exercises 6–10 are written transfer problems.

1. **Equal cubics and distinct records.** In the common ruled frame set $a = 3$, $m_0 = 5$. In $\mathbb{F}_0, \mathbb{F}_1$ order, compute the section periods, primitive tensions, section Coulomb charges q (the coefficient of a, with fiber charge two), and theta angles in turns. Decide whether the signed cubics agree and whether the two marked records should be identified. Explain which of the compared fields cannot be recovered from the cubic.

2. **A wall and a limit.** At $a = 2$, $m_0 = 5$, compare $m = 3$ with $m = -3$. On either side list the periods in section, fiber, exterior order. Give the signed cubic differences from the central continuation with its background terms retained, and the third Coulomb derivatives in the central and outer chambers. Name the operation at the wall and the operation at fixed shifted coupling as $|m|$ tends to infinity. Identify the two finite surfaces in positive, negative mass order.

3. **Two repairs on one link.** A raw outward period of the E_6 link is $-4/3$. Reduce it to $[0, 1)$, and then reverse orientation. Give the shared algebra and minimal cover fiber. Repair a half-period entry that used the older C_2 assignment by

giving the adopted algebra and its root count. Can the two oriented entries be identified? Does this seven-dimensional row determine a five-dimensional fixed point?

4. **A KK scale through a flop.** At $a = 3$ calculate the total elliptic period, current section or exterior period, and compact half-area first at $\mu = 2$ and then at $\mu = 5$. What would the old section period be at $\mu = 5$? Compare the background ranks and number of KK directions in parent, isolated daughter order. Explain whether this supports the claim that every positive compact cube implies a five-dimensional fixed point.

5. **A finite coefficient.** At $(q, t, X) = (1/4, 1/2, 1/32)$ compute V_1 and I_{AK}/Q_b. Separately take $(e_1, e_2, w) = (1, 2, 5)$ and give the coefficient of P in the additive limit. What base degree was checked, and does that comparison establish equivalence of the full finite-radius theories?

6. **A proposed identification.** A colleague identifies the two ruled entries because their cubics agree and the ordinary local dP_6 entry with a seven-dimensional entry because both have algebra E_6. Give a computed witness against each identification and identify the input needed for a comparison of genuine operators. Contrast the selected degree-one point contraction with the claim that positive compact cube is sufficient.

7. **Change what is matched.** Keep $a = 3$ and match the section masses of $\mathbb{F}_0$ and $\mathbb{F}_1$ to $\sigma = 12$. Find the two background couplings and primitive tensions. Explain why this result differs from Exercise 1, where the couplings were matched. Separately, consider $\mathbb{F}_1$ along the path $m_0 = b + a$ with b constant; this is not the fixed-section-mass path $m_0 = \sigma - a$. Distinguish its total derivative from the primitive tension.

8. **A threshold still outside the surface.** On each dP_2 outer branch take $a = 2$, $\widehat{m}_0 = 3$, $M = 6$, and then increase M. Give the three periods and identify which changes. Choose a fixed local energy window and explain when the exterior particle leaves it. Compare with increasing M at fixed $m_0 = 5$.

9. **Equal areas and unequal particles.** At $a = 4$ compare the post-flop elliptic backgrounds $\mu = 6$ and $\mu = 10$. Compute the compact area, exterior period and total fiber period in each. Then compare the two dP_6 mass vectors in (XIII.11.65) at $a = 3, m_0 = 5$. State what the equal areas determine in each example and give a particle period that distinguishes the entries.

10. **The record that a symmetric coefficient omits.** Interchange q, t in Exercise 5 while keeping X fixed. Determine which of V_1 and I_{AK}/Q_b changes and by what factor. Compare this loss of information with the two third-period entries, where the residual algebra and cover are equal. Write the first quotient action for each numerator, and state which information must remain in each comparison.

Status and sources

§11.1. Comparison data. The wrapped-brane and signed-cubic dictionary in (XIII.11.1) ([GEO-X]) uses Jefferson et al. (2018, arXiv v3, §2.2, Eqs. (2.9)–(2.15)). The fixed backgrounds, regime with calibrated wrapped cycles and isolation from unwanted bulk sectors remain premises ([DEC]). An absolute global form or line-operator lattice is undetermined.

§11.2. Ruled cubics and the plane. The supported tensor, marked periods, lattice parity and point contractions ([MATH]) use the local geometry of Chapters 2 and 5. For the root term see Intriligator et al. (1997, arXiv v2, §2.3, Eq. (2.22)); for the ordinary boundaries see Morrison and Seiberg (1997, arXiv v2, §§3.2–3.3, Eqs. (3.3)–(3.13)). The separate instanton and theta assignments ([GEO-E]) use Aharony et al. (1998, arXiv v3, §§II.E, III.F–H). The matched-section comparison and the path derivative in (XIII.11.8)–(XIII.11.10) are algebraic consequences of the period and contraction calculations ([MATH]); they add no identification of charge or boundary data. The ordinary E_0 endpoint ([GEO-X]) uses Morrison and Seiberg (1997, arXiv v2, §3.3) and the local isolation premise.

§11.3. Flop and mass flow. The chamber periods, pullbacks, wall jump and heavy limit ([MATH]) specialize the marked blowup and common-resolution calculations of Chapters 3 and 4. The weak gauge matter dictionary ([GEO-X]) uses Intriligator et al. (1997, arXiv v2, §2.3, Eq. (2.22)) and Morrison and Seiberg (1997, arXiv v2, §§3.2–3.3). The fixed-shifted-coupling examples and derivative comparison in (XIII.11.21)–(XIII.11.23) follow from the marked blowup and period data ([MATH]). The massive exterior state leaves the finite local energy window on the specified path ([DEC]).

§11.4. Inherited KK scale. The two resolution periods and quotient of period directions ([MATH]) use Chapter 9, including the anticanonical marking after the flop. The ordinary E-string parent and the radius interpretation ([GEO-E]) use Bhardwaj and Jefferson (2018, arXiv v6, §§3.1, 4.3, Eqs. (4.22)–(4.23)). The order of limits follows Douglas, Katz, et al. (1997, arXiv v2, §1.2). The isolated degree-one contraction gives the ordinary E_8 endpoint in the ordinary isolated local limit ([GEO-X]); see also the rank-one comparison of Seiberg (1996, arXiv v2, §4). The area response and equal-area examples in (XIII.11.30)–(XIII.11.31) follow from the geometry and periods of Chapter 9 ([MATH]). Isolation remains a separate premise ([DEC]).

§11.5. External circle coefficient. The finite comparison ([BPS:1/2|idx]) is one normalized coefficient with the Chapter 8 periodic spin structure, equivariant prescription and framing. The vertex input uses Iqbal et al. (2009, arXiv v2, §§5.5–5.6, normalized product after Eq. (81) and Eq. (90) at $m = 0$), and the framed gauge coefficient uses Awata and Kanno (2005, arXiv v3, Eq. (2.12)). The limiting denominator slopes and continued sign ([MATH]) are computed on the stated trajectory. The refinement interchange in (XIII.11.38) compares the same one-degree function and map; it does not add a protected sector.

§11.6. Frozen phases. The ordinary enhancement ([GEO-X]) and the nonzero-period residual classification ([GEO-E]) use Tachikawa (2016, arXiv v2, Eq. (1.1) and Table 1). The half-period A_2 identification in Cvetič et al. (2025, arXiv v1, §4.1.2, Eqs. (4.20)–(4.21)) differs from the earlier C_2 cell of de Boer et al. (2002, arXiv v3, §4.6.1, Table 14). The root counts, monodromy and cover exponents ([MATH]) follow from these inputs and the selected model of Chapter 10. Iteration of the third-period quotient in (XIII.11.47) is an arithmetic consequence of that same selected model ([MATH]). The local M/F rotation and shift ([GEO-E]) use Tachikawa (2016, arXiv v2, §2, Table 3 and accompanying text).

§11.7. Ordinary lattices. The ordinary cyclic ALE pairing and unit-period Gram ([MATH]) use Douglas and Moore (1996, arXiv v1, §2.1, Eqs. (2.1)–(2.2)) and Chapter 1. The ordinary

enhancement ([GEO-X]) and fixed string scale external-circle effective theory ([GEO-E]) use the distinct Chapter 1 limits. The rank-two tensor, periods and tensions ([MATH]) use Chapter 6 and Saxena (2020, §3.3, Eqs. (3.39)–(3.48)); the second tension follows from differentiating the cubic. The marked ruling and mass lifts, cubic and root grading ([MATH]) use Chapter 7. The basis change in (XIII.11.51), the fixed-period response in (XIII.11.58)–(XIII.11.60), and the equal-mass-norm comparison in (XIII.11.64)–(XIII.11.66) follow from the stated root and period calculations ([MATH]). The full fundamental per split fiber ([GEO-E]) is the weak matter dictionary in that chapter. The ordinary E_6 flavor endpoint uses the ordinary isolated local limit ([GEO-X]); the one-coefficient character match ([BPS:1/8|idx]) uses Kim et al. (2012, arXiv:1206.6781, Eqs. (4.22)–(4.23)).

§§11.8–11.9. Index and practice. The comparison rows use the earlier calculations and the isolation premise ([DEC]). The exercises apply those calculations with the same conventions and hypotheses.

References

Aharony, O., A. Hanany, and B. Kol (1998). "Webs of (p,q) five-branes, five-dimensional field theories and grid diagrams". In: *JHEP* 01, p. 002. DOI: 10.1088/1126-6708/1998/01/002. arXiv: hep-th/9710116.

Awata, H. and H. Kanno (2005). "Instanton Counting, Macdonald Function and the Moduli Space of D-Branes". In: *JHEP* 05, p. 039. DOI: 10.1088/1126-6708/2005/05/039. arXiv: hep-th/0502061.

Bhardwaj, L. and P. Jefferson (2018). "Classifying 5d SCFTs via 6d SCFTs: Rank one". In: arXiv: 1809.01650 [hep-th].

Cvetič, M. et al. (2025). "Frozen generalized symmetries". In: *Phys. Rev. D* 111, p. 026018. DOI: 10.1103/PhysRevD.111.026018. arXiv: 2410.07318 [hep-th].

De Boer, J. et al. (2002). "Triples, Fluxes, and Strings". In: *Adv. Theor. Math. Phys.* 4, pp. 995–1186. DOI: 10.4310/ATMP.2000.v4.n5.a1. arXiv: hep-th/0103170.

Douglas, M. R., S. Katz, and C. Vafa (1997). "Small instantons, del Pezzo surfaces and type I' theory". In: *Nucl. Phys. B* 497, pp. 155–172. arXiv: hep-th/9609071.

Douglas, M. R. and G. W. Moore (1996). "D-branes, quivers, and ALE instantons". In: arXiv: hep-th/9603167.

Intriligator, K. A., D. R. Morrison, and N. Seiberg (1997). "Five-dimensional supersymmetric gauge theories and degenerations of Calabi-Yau spaces". In: *Nucl. Phys. B* 497, pp. 56–100. DOI: 10.1016/S0550-3213(97)00279-4. arXiv: hep-th/9702198.

Iqbal, A., C. Kozçaz, and C. Vafa (2009). "The Refined Topological Vertex". In: *JHEP* 10, p. 069. DOI: 10.1088/1126-6708/2009/10/069. arXiv: hep-th/0701156.

Jefferson, P. et al. (2018). "On geometric classification of 5d SCFTs". In: *JHEP* 04, p. 103. DOI: 10.1007/JHEP04(2018)103. arXiv: 1801.04036 [hep-th].

Kim, H.-C., S.-S. Kim, and K. Lee (2012). "5-dim superconformal index with enhanced E_n global symmetry". In: *JHEP* 10, p. 142. arXiv: 1206.6781 [hep-th].

Morrison, D. R. and N. Seiberg (1997). "Extremal transitions and five-dimensional supersymmetric field theories". In: *Nucl. Phys. B* 483, pp. 229–247. DOI: 10.1016/S0550-3213(96)00592-5. arXiv: hep-th/9609070.

Saxena, V. (2020). “Rank-two 5d SCFTs from M-theory at isolated toric singularities: a systematic study”. In: *JHEP* 04, p. 198. DOI: 10.1007/JHEP04(2020)198. arXiv: 1911.09574 [hep-th].

Seiberg, N. (1996). “Five-dimensional SUSY field theories, nontrivial fixed points and string dynamics”. In: *Phys. Lett. B* 388, pp. 753–760. DOI: 10.1016/S0370-2693(96)01215-4. arXiv: hep-th/9608111.

Tachikawa, Y. (2016). “Frozen singularities in M and F theory”. In: *JHEP* 06, p. 128. DOI: 10.1007/JHEP06(2016)128. arXiv: 1508.06679 [hep-th].